



CARDIFF UNIVERSITY

School of Engineering

**A COUPLED PHYSICAL – COMPUTATIONAL
METHODOLOGY FOR THE INVESTIGATION OF SHORT
FALL RELATED INFANT HEAD IMPACT**

A Thesis submitted to Cardiff University for the

Degree of Doctor of Philosophy

By

Ghaidaa Abdulrahman Khalid

August 2018

DECLARATION

This work has not previously been accepted in substance for any degree and is not concurrently submitted in candidature for any other higher degree.

Signed:..... (candidate) Date:.....

Statement 1

This thesis is being submitted in partial fulfilment of the requirements for the degree of..... (Insert as appropriate PhD, MPhil, EngD)

Signed:.....(Candidate) Date:.....

Statement 2

This thesis is the result of my own independent work/investigations, except where otherwise stated. Other sources are acknowledged by explicit references.

Signed:..... (Candidate) Date:.....

Statement 3

I hereby give consent for my thesis, if accepted, to be available for photocopying, inter-library loan and for the title and summary to be made available to outside organisations.

Signed:..... (Candidate) Date:.....

ABSTRACT

Head injury in childhood is the single most common cause of death or permanent disability from injury. Little understanding exists of the response of a child's head to injurious loading, thus in clinical practice, head injured infants are difficult to assess. Developing an understanding of injurious events from practical experience and epidemiology alone is a significant challenge, since there are many age dependent and biomechanical variables that are poorly understood at the bedside. Without a comprehensive biomechanical characterisation of the primary injury mechanics, interpretation of the pathophysiological consequences will remain rudimentary. Experimentation on living infants is inconceivable and Postmortem-Human-Surrogates (PMHSs) rare. A further limitation is technological, since, researchers out of experimental necessity, typically derive impact acceleration data by calculation, dividing peak impact force by head mass, to produce a 'global' acceleration approximation. A need exists for a new experimental methodology, to provide specific regional and localised response data and characterisation of a range of biomechanical variables.

A coupled physical–computational methodology was developed. An infant 3D-CAD head model was created from high resolution CT and MR images, from which a physical and equivalent computational Finite-Element (FE) model was developed. The physical model was 3D-printed with tissue response matched co-polymers, a gelatin-brain and polyamide/latex-patch-scalp and validated against the PMHS impact response. Impact response, linear and angular velocities and accelerations, strains and strain rates, was optically measured by Digital-Image-Correlation. An infant FE head was subsequently developed and validated against impact response data, both 'regionally and locally' from the physical model and 'globally' against the PMHS,

showing good agreement with both. Fracture risk was investigated by FE simulation of injurious PMHS impacts; and a parametric analysis conducted to investigate the effects of fall height on maximum stress response and fracture risk probability. During impact of different regions of the coupled models, certain areas produced 'local' acceleration responses two to three times greater than the related global acceleration. Local translational acceleration was very different at different points on the skull and sensitive to impact location. In contrast, the global translational impact acceleration was not, providing justification for challenging the 'global' approach, a form of overall "averaging", and related injury thresholds. There were different local angular accelerations in different structures, at different times and significant variation at different impact heights and significant structural deformation during impact. Angular acceleration data is extremely valuable for quantifying local and regional deformational accelerations for determining both impact nature and injury risks. Strain was ten times greater in the suture and fontanelle areas than bone.

The coupled-methodology proved to be significant in characterising infant head impact injury mechanics and skull fracture risk, which is anticipated to inform clinical and forensic management and injury prevention strategies into the future.

ACKNOWLEDGEMENTS

I would like to convey my special appreciation to my supervisor Dr. Michael Jones, who has been a tremendous mentor for me. I wish to pass on many thanks for supporting my study and my related research. I believe that his advice and support have added significant value to my thesis. I will never forget these mornings working together on papers, not to mention the hard questions which inspired me to widen my research from various perspectives. I would like to thank my co-supervisor Dr. Peter Theobald for his priceless suggestions and comments, the continuous assistance, effort and advice during my PhD.

I am also grateful to the Higher Committee for Education and Development (HCED- Iraq), without their financial support, it would have been impossible to achieve this research. I would like to acknowledge the Middle Technical University, the Electrical and Electronic Technical Collage, Baghdad, Iraq for providing me with the opportunity to continue my study.

To my parents, you should know that your support and encouragement was worth more than I can express on paper. I am sorry to stay all this time away from you. I am also grateful to other family members, my sister and my brothers, my specialist and dearest aunts. Wafa rest in peace – you are missed!

To my beloved husband who was always my support in stressful times and my daughters, the reasons for me to breath, I love you all so much.

TABLE OF CONTENTS

DECLARATION..... II

ABSTRACT.....III

ACKNOWLEDGEMENTS.....V

TABLE OF CONTENTS.....VI

LIST OF FIGURES.....XIII

LIST OF TABLES.....XVI

LIST OF ABBREVIATIONS.....XXIII

1. INTRODUCTION..... 1

 1.1 Motivation..... 1

 1.2 Epidemiology of childhood head injuries 3

 1.3 The anatomy and development of the head..... 5

 1.4 Comparison of the anatomical configuration of the paediatric and adult head. .. 9

 1.5 Biomechanics of head injury. 11

 1.6 Severity coefficients and Head Injury Criteria (HIC). 15

 1.7 Material properties. 20

 1.7.1 Skull..... 21

 1.7.2 Sutures 26

 1.7.3 Scalp..... 29

1.7.4	Brain	30
1.8	Current tools used to understand head injury in children.	33
1.8.1	Postmortem Human Surrogates (PMHSs).....	33
1.8.2	Mechanical surrogates.....	39
1.8.3	Finite element (FE) models.....	41
1.9	Summary.....	52
1.10	Research aims and objectives	55
1.11	Scope of the work and Thesis layout (Chapter outlines).....	56
2.	MATERIALS AND METHODS	59
2.1	Paediatric head model development.	61
2.1.1	Data set and geometrical acquisition.....	61
2.1.2	Segmentation of paediatric head.....	62
2.2	Physical modelling of paediatric head surrogate.....	67
2.2.1	Bidirectional properties of paediatric bone.....	67
2.2.2	Material selection of bone and sutures.	70
2.2.2.1	Mechanical characterization of the Poly Jet printed materials.....	70
2.2.2.2	Specimen preparation and mechanical testing.	73
2.2.2.3	Mechanical Measurement	76
2.2.3	Manufacturing of the 3D printed physical head model.....	79
2.2.4	Modelling and material properties of brain and scalp.	81

2.3	Global validation and regional, local investigation of paediatric physical surrogate.	81
2.3.1	Digital Image Correlation	81
2.3.2	Subset correlation and speckle Patterns	82
2.3.3	High Speed Video.....	83
2.3.4	Experiential setup and procedures	85
2.3.5	Output variables and statistical analysis	92
2.4	Computational modelling.....	95
2.4.1	Finite element methods	95
2.4.2	Mesh generation.....	96
2.4.3	Bidirectional and material properties of the FE head model.	98
2.4.4	Analytical procedure and time integration.....	103
2.4.5	Boundary and loading conditions.....	105
2.4.5.1	First parametric model	105
2.4.5.2	Second parametric model	105
2.4.6	Mesh convergence	106
2.5	Global validation of the paediatric FE head model against PMHS data	109
2.6	Sensitivity analysis	111
2.6.1	Influence of the Impact location	111

2.6.2	Influence of the position of the occipital bone in relation to the parietal bones.....	112
2.7	Global, regional and local validation of the paediatric FE head model against physical model impact response.....	115
2.8	Investigating skull fracture from the literature.....	119
2.9	Output variables and Statistical analysis.....	122
3.	RESULTS	123
3.1	Mechanical characterisation of the Poly jet printed materials.....	123
3.2	Global validation of the paediatric physical model against PMHS data.....	128
3.2.1	Impact translational acceleration.	128
3.2.2	Duration of Impact	131
3.3	Regional and local investigation of the paediatric physical model.....	134
3.3.1	Impact translational and rotational accelerations.....	134
3.3.2	Head deformation	137
3.4	Global validation of the paediatric FE head model against PMHS data.	142
3.4.1	Impact translational acceleration.	143
3.4.2	Duration of Impact	146
3.5	Parametric study of the paediatric FE model.....	148
3.5.1	First parametric model.....	148
3.5.2	Second parametric model.....	149

3.6	Sensitivity analysis	149
3.6.1	Influence of the Impact location	149
3.6.2	Influence of the position of the occipital bone, in relation to the parietal bones.....	152
3.7	Global validation of the paediatric FE model against physical model data.....	154
3.7.1	Impact acceleration	154
3.7.2	Duration of Impact	157
3.8	Physical model regional and local validation of the FE head model.....	158
3.8.1	Impact acceleration	158
3.8.2	Sensitivity analysis	161
3.8.2.1	Influence of the Impact location	161
3.8.2.2	Influence of the position of the occipital bone in relation to the parietal bones.....	163
3.8.3	Duration of Impact	165
3.8.4	Head Deformation	166
3.9	Investigating skull fracture from the literature.....	168
4.	DISCUSSION.....	172
4.1	Introduction.	172
4.2	Mechanical characterisation of the Poly Jet printed materials.....	174
4.3	Global validation of the paediatric physical model against PMHS data.....	178

4.3.1	Impact translational acceleration.	178
4.3.2	Duration of Impact.	182
4.4	Regional and local investigation of the paediatric physical model.....	183
4.4.1	Impact translational and rotational accelerations.....	183
4.4.2	Head deformation.	185
4.5	Implications and limitations of the physical model.....	186
4.6	Global validation of the paediatric FE head model against PMHS data.	187
4.6.1	Impact acceleration.	190
4.6.2	Sensitivity analysis.	195
4.6.2.1	Influence of the Impact location.	195
4.6.2.2	Influence on impact response of the relative positions of the occipital and parietal bones.....	197
4.6.3	Impact time.	199
4.7	Global validation of the paediatric FE model against the physical model.....	199
4.7.1	FE model impact acceleration.	200
4.7.2	FE model impact time duration.	201
4.8	FE head model regional and local validation against the physical model.....	202
4.8.1	Impact acceleration.	203
4.8.2	Sensitivity Analysis	205
4.8.2.1	Influence of the Impact location	205

4.8.2.2	Influence of the position of the occipital bone in relation to the parietal bones.....	207
4.8.3	Duration of Impact.....	209
4.8.4	Head deformation.....	209
4.9	PMHS skull fracture reconstruction.....	210
4.10	Implications and limitations of the coupled physical - computational model.....	215
4.11	Study significance.....	219
5.	Conclusion and Future work.....	230
5.1	Conclusion.....	230
5.2	Future work.....	235
6.	References.....	237

LIST OF FIGURES

Figure 1.1. View of the new born skull showing cranial plates, sutures and fontanelles. The top left diagram is an anterior view, the top right is a posterior view, while the bottom is a superior view. The circled areas are the anterior and posterior fontanelles [15]..... 7

Figure 1.2. Diagram of the skull showing the location of the temporal bone (red) and the sphenoid bone (yellow). The sphenoid and the temporal bones form portions of the base of the skull (right) and the lateral walls (left) of the cranial cap [15]..... 8

Figure 1.3. Infant skull fibrous appearance due to the trabeculae shown the material orientation of cranial bones [18]. 8

Figure 1.4. Comparison between the paediatric head (left) and the adult head (Right) [38]. 11

Figure 1.5. Impulsive loading of head/neck in (a) rear loading and (b) front loading [39]. 13

Figure 1.6. The Wayne State Tolerance Curve (WSTC) [51] 17

Figure 1.7 Examples of acceleration - time profiles from two different impact simulations [50]. 19

Figure 1.8. paediatric head skull fracture pattern from Weber study [80, 81]. 35

Figure 1.9. Force time histories showing (a) the unimodal and (b) bimodal waveform [122] 38

Figure 1.10. Fracture risk curve graph from Coats study [71] showing maximum principal stress values in the occipital, right parietal, and left parietal bones. 46

Figure 2.1. Representation of major tissues within the head (a) CT scan (b) cranial bones (c) sutures (d) cranial bones and sutures (e) base of the skull (f) brain..... 67

Figure 2.2. The fibrous grooves of cranial bones of surrogate cranial bones model (a) Occipital bone (b) Right parietal bone (c) Left parietal bone (d) Frontal bones (e) Assembly of the cranial bone..... 70

Figure 2.3. Test specimen design as recommended by British Standards Institution (2012) [98], [99]. 74

Figure 2.4. 3D Printed specimens of (a) White and (b) Black materials. 75

Figure 2.5. Uniaxial Tensile testing of printed specimens (a) Black and (b) White materials 75

Figure 2.6. Calculation of elastic modulus of Grey and White materials. (Illustration of the relevant tensile stress-strain properties evaluated during this study). 77

Figure 2.7. Typical stress-strain curve of a rigid polymer [101]. 78

Figure 2.8. Method of calculating multiple tangent moduli for less stiff rubberlike materials (Illustration of the relevant tensile stress-strain properties evaluated during this study). 79

Figure 2.9. Physical 3D models produced by Rapid Prototyping technique. (a) Frontal view. (b) Side view (c) Coronal view (d) the base of the head..... 80

Figure 2.10. Head drop test orientation. (a) frontal bone impact with an arrow illustrating antero-posterior (AP) direction, (b) an occipital impact with an arrow illustrating postero anterior (PA) direction, (c) vertex impact with an arrow illustrating superior–inferior (SI) direction, (d) parietal impact with an arrow illustrating the left right (LR) direction..... 86

Figure 2.11. (a) Experimental setup of physical model for perpendicular drop onto force plate, (b) 3D printed physical model with speckle patterns..... 88

Figure 2.12. Physical head drop test orientation with the contrast of the speckle pattern (a) frontal bone impact, (b) occipital impact, (c) parietal impact and (d) vertex impact.. 89

Figure 2.13. (a,b-forehead, c,d-parietal, e-occipital and f-vertex) Digital Image Correlation of the physical model impact tests. 91

Figure 2.14. Abaqus/Explicit complete head mesh (a) side view (b) frontal view. 97

Figure 2.15. Material orientation of the cranial bones (a) paediatric head [18] (b) top view of FE head model (c) side view of FE head model..... 102

Figure 2.16. Fibrous appearance of the cranial bone in (a) physical model (b) FE model. 103

Figure 2.17. Profile of speed of analysis against the number of processors used..... 104

Figure.2.18. The error in the peak force against mesh density (number of elements). 108

Figure 2.19. The FE model impacted onto a rigid surface at (a) forehead region (b) occiput region (c) parietal region (d) vertex region. 110

Figure 2.20. The FE head model with different impact regions at the (a) Occiput (b) Parietal (c) Forehead cranial bones. 112

Figure 2.21. Comparison of the 3D CAD model with depressed occipital – parietal bone configuration (a-d) and with FE model have inline occipital – parietal bone configuration (e-h)..... 115

Figure 2.22. Comparison of the physical model head’s impact Digital Image Correlation tests (a - forehead, b-parietal, c-occipital and d-vertex) with FE numerical simulations of the FE mode (e-forehead, f-parietal, g-occipital and h-vertex). 118

Figure 2.23. Parietal-occipital impact simulating published paediatric PMHS from 0.82 m onto stone. 121

Figure 3.1. Stress-strain curves for the average of the six tension specimens of White material. 125

Figure 3.2. Stress-strain curves for the average of the six tension specimens of Black material. 126

Figure 3.3. Stress-strain curves for the average of the six tension specimens of Gray material. 126

Figure 3.4. Comparison of (a) Young’s modulus (MPa) (b) Tensile strength (MPa) and (c) Elongation at failure from test specimens White, Grey and Black with data sheet. 127

Figure 3.5. Peak acceleration and drop height for infant PMHS and physical model impact tests..... 131

Figure 3.6 Comparison of impact time duration between PMHS test and physical model from two different drop heights..... 132

Figure 3.7. Acceleration-time contact curve for the PMHS and physical model from a 0.30m height drop ($2.43 \text{ m}\cdot\text{s}^{-1}$) at the (a) forehead, (b) occiput, (c) parietal and (d) vertex regions. 133

Figure 3.8. Comparison between the physical model's global and local translational acceleration from the force plate and DIC system, respectively..... 136

Figure 3.9. Physical model maximum angular acceleration at different impact locations at two impact velocities. 136

Figure 3.10. Coronal view of physical head model deformation for a $2.43\text{m}\cdot\text{s}^{-1}$ impact onto a metal plate using HS-DIC (a) prior to impact - no head deformation, (b) 2ms post impact - 0.028mm deformation, (c) 3ms post impact - 0.032mm deformation, (d) 5ms post impact - 0.034mm deformation..... 140

Figure 3.11. Physical model comparison of max strain from different impact locations at two impact velocities. 141

Figure 3.12. Maximum strain and drop height from different impact locations of physical model at two impact velocities..... 141

Figure 3.13. Maximum strain rate at different impact locations of physical model at two impact velocities..... 142

Figure 3.14. The FE head model was impacted onto a rigid surface at the (a) forehead (b) occiput (c) parietal and (d) vertex regions at 2.43 m.s^{-1} 145

Figure 3.15. Peak acceleration and impact velocity for infant PMHSs and FE head model impact simulations..... 146

Figure 3.16. Comparison of impact - time durations, between the FE head model with the closest mass to PMHS. 147

Figure 3.17. Comparison of the peak acceleration response at the baseline and parametric FE head model at different impact regions at the impact velocity of 2.43 m.s^{-1} 151

Figure 3.18. Peak acceleration and drop height for infant FE ‘inline’ and FE ‘out of line’ (depressed) head model with infant PMHS impact tests. 153

Figure 3.19. Infant head acceleration - time contact response from different impact locations from the physical model experiments and FE simulations (a) forehead, (b) occipital, (c) parietal and (d) vertex, at 2.43 m.s^{-1} impact velocity. 155

Figure 3.20. Peak acceleration (global response) of the paediatric head in physical and computational simulations at two impact velocities. 156

Figure 3.21. Comparison of impact time duration with different impact velocity (drop height) between physical and numerical simulation experiments of paediatric head model. 158

Figure 3.22. Comparison of global acceleration and local acceleration response of the FE model. 160

Figure 3.23. Local response from the present FE simulation compared against the local response from physical model..... 160

Figure 3.24. Comparison of local peak acceleration response of the baseline and parametric FE head..... 162

Figure 3.25. Comparison of local acceleration response and drop height for infant FE 'inline' and FE 'out of line' (depressed) head model..... 164

Figure 3.26. Comparison of impact time duration between the physical model experiments and FE simulation. 165

Figure 3.27. Vertex impact illustrating strain zone in coronal sutures and fontanelles 167

Figure 3.28. Occipital impact illustrating strain zone in coronal sutures and fontanelles. 167

Figure 3.29. Maximum strain of the physical and FE models at different impact locations and two impact velocities. 168

Figure 3.30. Comparison of stress zone from the FE simulation (b, c and d) and the fracture pattern observed in the PMHS infant skull [80, 81] (a) at 0.82m drop height onto stone tile..... 170

Figure 3.31. Maximum principle stress from the FE model from the parametric study at different fall heights - 0.15, 0.3, 0.6 and 0.82m. 171

LIST OF TABLES

Table 1.1 Minimum-maximum stiffness (E) / MPa values of human infant cranial bone and sutures. (1) McPherson & Kriewall [64]; (2) Kriewall et.al. [65]; (3) Margulies & Thibault [37]; (4) Coats & Margulies [66]; (5) W Wang et al. [67] - (w=weeks, m=months).
 27

Table 1.2. Minimum-maximum σ_{uts} /MPa values of infant cranial bone and sutures. (1) Margulies & Thibault [37]; (2) Coats & Margulies [66]; (3) W Wang et al. [67]; (w=weeks, m=months). 28

Table 2.1 Head measurement of the Computed Tomography datasets compared to the Prange’s PMHS data series and the Root Mean Square. 63

Table 2.2 Material properties of White, Grey and Black, data from Stratasys (2016, 2016c) [96,97] 72

Table 2.3. . Dimensions in mm of type 1BA test specimen (BS EN ISO 527 2:2012) [99].
 74

Table 3.1. Mechanical properties (Mean \pm SD) of the White, Grey and Black materials at 1mm min⁻¹ strain rate. 124

Table 3.2. Comparison of the mechanical properties (mean \pm SD) tensile test specimens with supplier data sheet..... 125

Table 3.3. Comparison of mechanical properties from tensile test specimens with reported values. 128

Table 3.4. Output variables (global translational acceleration, duration of impact) from the physical model at two impact velocities..... 130

Table 3.5. Comparison of model performance between the PMHS and physical model experiments using the correlation score (CS) measured from CS_{N-phase}, CS_{N-amp} and CS_{N-shape} from a 0.30m height drop (2.43 m.s⁻¹). 130

Table 3.6. Physical model local translational impact acceleration and duration at two impact velocities. 135

Table 3.7. Physical model maximum rotational acceleration at different impact locations at two impact velocities. 135

Table 3.8 . Maximum strain produced by the physical model at different impact locations at two impact velocities. 138

Table 3.9. Maximum strain rate produced by the physical model at different impact locations at two impact velocities. 138

Table 3.10. Comparison of model performance between the PMHS and FE model experiments using the correlation score (CS) measured from CS_{N-phase}, CS_{N-amp} and CS_{N-shape} at 2.43 m.s⁻¹..... 143

Table 3.11. Global translational acceleration and duration of impact from the FE model at 1.72 m.s⁻¹ and 2.43 m.s⁻¹..... 144

Table 3.12. Comparison of global translational acceleration from the baseline and the parametric FE model at two impact velocities. 148

Table 3.13. Comparison of global translational acceleration from the baseline and the parametric FE model at two impact velocities. 149

Table 3.14. Peak acceleration response of the baseline FE head model and parametric FE model at different impact regions at the impact velocity of 2.43 m.s⁻¹..... 151

Table 3.15 Comparison of peak translational acceleration from the FE ‘inline’ and FE ‘out of line’ head model with infant PMHS impact tests at two impact velocities. 153

Table 3.16. Comparison of model performance between the physical model and FE model experiments using the correlation score (CS) measured from CS_{N-phase}, CS_{N-amp} and CS_{N-shape} at 1.72 m.s⁻¹ and 2.43 m.s⁻¹. 156

Table 3.17. FE model local translational impact acceleration and duration at two impact velocities. 159

Table 3.18 Peak acceleration response of the baseline FE head model and parametric FE model with different impact regions at a 2.43 m.s⁻¹ impact velocity. 162

Table 3.19. Output variables (local translational acceleration, duration of impact) from the FE model at two impact velocities. 164

Table 3.20. Maximum strain of FE model from different impact locations at two impact velocities. 166

Table 3.21. Maximum principle stress of FE model from the parametric study with different fall heights. 171

LIST OF ABBREVIATIONS

Symbol	Definition
PMHSs	Postmortem Human Surrogates
FE	Finite Element
ED	Emergency Department
TBI	Traumatic Brain Injury
ICI	Intracranial Injury
SDH	Subdural Haematoma
TAI	Traumatic Axonal Injury
ATDs	Anthropomorphic Testing Devices
WSTC	Wayne State Tolerance Curve
GSI	The Gadd Severity Index
ASDH	Acute Subdural Haematoma
DBI	Diffuse Brain Injury
HIC	Head Injury Criterion
NHTSA	National Highway Traffic Safety Administration
CRABI	Child Response Airbag Interaction
FEA	Finite Element Analysis
PMCT	Post Mortem Computer Tomography
CT	Computer Tomography
AM	Root Mean Square
RMS	Additive Manufacturing
PJP	PolyJet Printed
DIC	Digital Image Correlation
SI	Superior - Inferior
AP	Antero - Posterior
LR	Left - Right
PA	Posterior - Anterior
HS-DIC	High Speed-Digital Image Correlation

CS	Correlation Score
QPRT	Quality Preserving Reduce Triangles
CSF	Cerebro Spinal Fluid

1. INTRODUCTION

1.1 Motivation

Head injuries are one of the major causes of death or permanent invalidity, especially amongst the very young. Despite a natural tendency for parents and carers to protect infants and young children, a significant number suffer traumatic head injury. In England alone, around 35,000 children are admitted to hospital with head injuries each year, an incidence of 4 per 1000, of which 19% are younger than one year of age [1]. Many more children attend the Emergency Department with a head injury, accounting for 9% of all childhood attendances [2], of whom 5 – 10% will develop intracranial complications. The United Kingdom's 2015 National Confidential enquiry into child head injury, [3], confirmed a peak prevalence for child head injury in infants and young children at ≤ 2 years. At a time of rapid brain development, traumatic brain injury has the potential for life-long morbidity, including long-term disability, intellectual, personality and behavioural problems.

In medical practice, infants are difficult to assess, since clinicians are often presented with only a very brief third-party description of the causal event and a combination of the signs and symptoms of injury. Developing an understanding of the cause and effect relationship from such imprecise, epidemiological data, alone, is an enormous challenge, since many age-dependent and biomechanical variables exist, including geometry, tissue response, mass, velocity, angle, a location of head impact and surface characteristics. Also, despite national head injury guidelines [4], it is extremely challenging to know which injury mechanisms are associated with the greatest risk of morbidity and mortality in children.

Whilst training, anecdote, experience and epidemiology will continue to incrementally provide some general understanding of traumatic head injury cause and effect, which can inform the diagnostic and management process, without a comprehensive biomechanical characterisation and understanding of the primary injury mechanism, an understanding of the pathophysiological consequences of different and complex types of injury mechanisms will remain rudimentary. It is of course in forensic practice that causation is subject to the greatest scrutiny since practitioners are routinely faced with the challenge of trying to establish, out of the many thousands of traumatic head injury attendances, whether an explanation of the cause of a specific traumatic child head injury is accidental or non-accidental in origin.

A significant proportion of infant head injuries are a result of abuse, and it is currently difficult to diagnose with any confidence [5]. In consideration of the above-mentioned challenges associated with attempting to understand head impact injury cause and effect by anecdote, experience and epidemiology; this thesis presents a novel physical and computational modelling framework that can be used to improve the understanding of injury mechanisms, where modelling appears a logical way to advance understanding, since it offers significant potential to perform simulations and parametric and multivariate analyses.

1.2 Epidemiology of childhood head injuries

Head injury in children is a very significant problem, both in terms of morbidity and mortality [1]. Approximately 35,000 children are admitted to hospital in England each year with head injuries, of which 19% are younger than one year of age [1]. Many more will attend the emergency department (ED) with a head injury, accounting for 9% of all childhood attendances [2]. Falls are a leading cause of head injuries in most households [6] and a cause of significant variation in head injury severity as a result of the combination of the biomechanical loading environment, the primary biomechanical response of the head and the subsequent pathophysiological response. Additional complexity is a result of head geometry, developmental changes, increasing gross motor capability and mobility. The majority of such cases are non-life threatening, with only 4.8 % of children attending the hospital and <1% of falls resulting in either a concussion or skull fracture in infants [6]. Falls are, however, reported as the most common cause of minor head injury in children of less than one year of age (69.4%) and 2-4 years (62.7%) [5]. Head injury is further, reported as the commonest cause of TBI in the age group 0-4 years (38%) that are admitted to intensive care units following motor vehicle collisions (30%) and assaults (16%) [3]. However, considering only infants (age <1 years old), falls only account for 19% of TBI cases; the most common cause of TBI being suspected assault (52 %) [3].

The intentionally inflicted head injury is a further major cause of head injury in children. Predominantly occurring in the under 4 years [7], the rate of death is reported to be between 15% and 35% and the probability of long-term injury is between 50% to 78% [8]. The percentage of hospitalised children diagnosed with intentional head injury varies with age. However epidemiological studies report a frequency of between 25-30% [9].

Rates of inflicted head injury in under one-year are as high as 24.6 and 26.0 per 100,000 in the United Kingdom and the United States, respectively. However, these numbers must be viewed with caution, since an exact rate is difficult to determine in abuse cases, because it is difficult to properly distinguish accidental fall injuries from child abuse injuries [8, 6, 10, 11].

Hughes et al. [12] conducted a retrospective and prospective analysis of paediatric head injury related hospital admissions subjected to an exploratory CT scan, to investigate the correlation between head-injury severity and fall dynamics in children younger than or equal to 48 months, who were admitted to one hospital. The analysis focused on falls from <3m (10 ft) within a domestic environment, which were considered to be low height falls. The study considered those cases which presented with a skull fracture or intracranial injury (ICI) and compared them with those who had minor head injuries; evaluating the correlation between the fall characteristics (such as, the mechanism of injury, surface of impact, site of impact to the head and fall height) and skull fracture or ICI, identified from neuroimaging. This study indicated that skull fracture and or ICI were absent in falls below 0.6 m (2 ft) of the head centre of gravity, or with a parietal/temporal or occipital impact. Hughes et al, therefore, proposed 0.6m as a threshold for paediatric head injury. Highlighting that these variables should be documented when evaluating the likelihood of skull fracture/ICI.

1.3 The anatomy and development of the head

The human head is considered to be one of the most vulnerable parts of the human body when subjected to external impact from accidents or violence. To assist the understanding of the biomechanics of paediatric head injury, this section will introduce the basic knowledge of paediatric human head anatomy, the terminology and features of paediatric anatomy, which are relevant to the head and finally describing the major, distinguishing differences between the adult and paediatric head with respect to head injury vulnerability.

The scalp is an extracalvarial soft tissue cover over the cranium; consisting of five tissue layers, the skin, dense connective tissue, the galea, loose connective tissue and a periosteum (pericranium) . The skin and galea are bound to each other by a dense connective tissue layer, which contain the blood and nerve supply of the scalp. The galea and the periosteum are not firmly connected by loose connective tissue making a space where the blood and fluid can accumulate within this space [13]. Thickness of the scalp increases with age; initially this raises starts 1- 9 months of age with the mid sagittal line, then it will be consistent up to 3 - 4 years old, when the scalp starts to thicken again, persisting until adulthood [14].

The paediatric skull has two major sections: the neurocranium and the viscerocranium. The neurocranium, which is also called the calvarium or cranial vault, represents the superior part of the head, consisting of seven cranial plates that enclose and protect the brain. These cranial plates, from anterior to posterior, consist of two frontal bones, two parietal bones and one occipital bone in the posterior, as illustrated in Figure 1.1. The viscerocranium represents the inferior part of the head consisting of the face, the base of

the skull and the mandible [15]. The base of the skull is composed of two bones, the temporal bone and the sphenoid bone, which are also parts of lateral walls of the skull encapsulating the brain as shown in Figure 1.2. The paediatric cranial bone/plate appears as a classic lamellar structure, represented by a single cortical bone layer with a fine network of trabeculae, macroscopically emanating from ossification centers, shown in Figure 1.3. This single compact layer continues to develop into three layers: called an outer table of cortical bone, a middle spongy diploe layer and an inner table of cortical bone. The trabeculae has a fibre pattern, radially oriented from a centre of ossification, appearing very clearly in the paediatric skull, while not visible in the adult skull [16, 17]. For newborns, the cranial plates of the neurocranium are loosely connected by fibrous intersections: sutures, when joining only two cranial bones, and the fontanelles, when joining three or more cranial bones (Figure 1.1) [19]. Sutures are a membranous tissue comprised of collagen fibres which form flexible joints, which connect adjacent cranial bones [20]. The morphology of sutures is easily distinguishable from the paediatric skull. Both interdigitated sutures and straight edged sutures exist [20]. Interdigitated sutures exist between adjacent parietal bones and straight edged sutures between parietal and occipital bones [20]. The fontanelles appear as a junction at the back of the head, between the parietal bones and occipital bone, called posterior fontanelle and the anterior fontanelle between the frontal and parietal bones, positioned at the top of the head [21]. The sutures and fontanelles play a vital role during the child birth process by enabling the head to mold and deform to assist a safe passage through the birth canal [22, 23]. During development, the sutures provide a place of growth for the cranial bones [22] and growth and expansion of the brain [23] throughout infancy and childhood until the sutures and

fontanelles are ossified and obliterated by new bone [23]. The new bone is deposited within the joints to allow expansion of the bone plates continuing to be a region of growth until adulthood. Later in life, the sutures serve to connect the bone plates together to make the skull a solid continuum [24]. Furthermore, the sutures may act as dampers of forces to the skull during impact; theoretically to guard the brain against damage, as a result of compression or impact [25, 26].

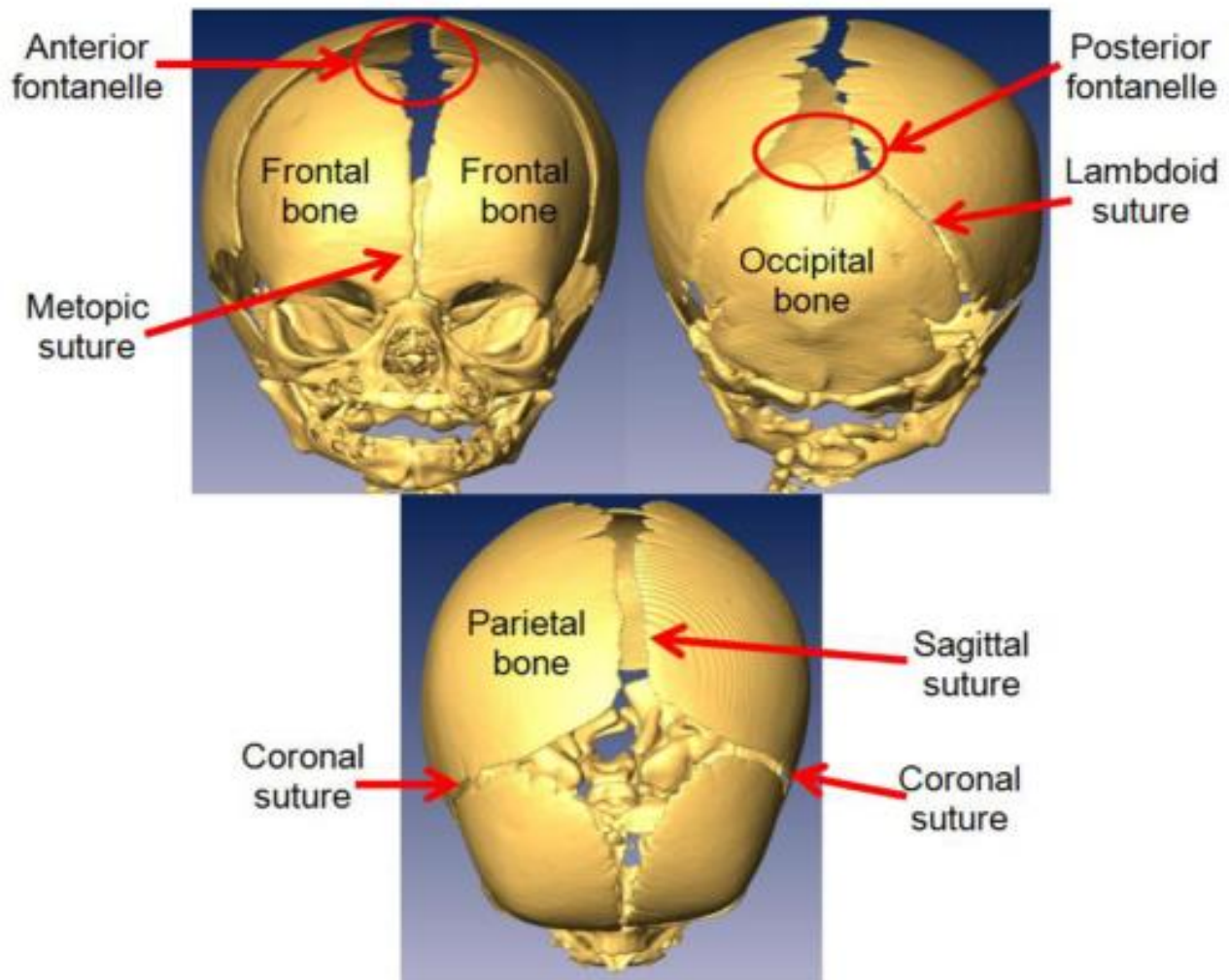


Figure 1.1. View of the new born skull showing cranial plates, sutures and fontanelles. The top left diagram is an anterior view, the top right is a posterior view, while the bottom is a superior view. The circled areas are the anterior and posterior fontanelles [15].

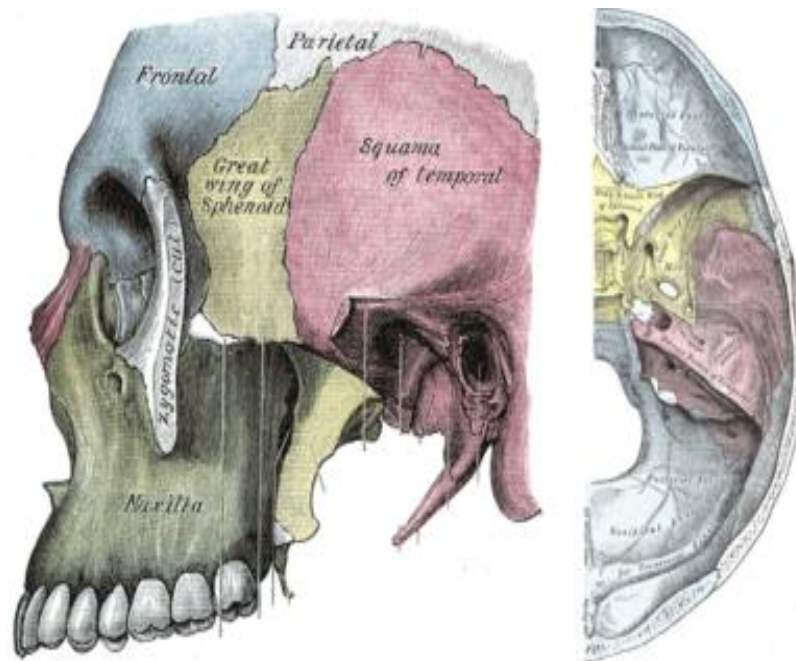


Figure 1.2. Diagram of the skull showing the location of the temporal bone (red) and the sphenoid bone (yellow). The sphenoid and the temporal bones form portions of the base of the skull (right) and the lateral walls (left) of the cranial cap [15].

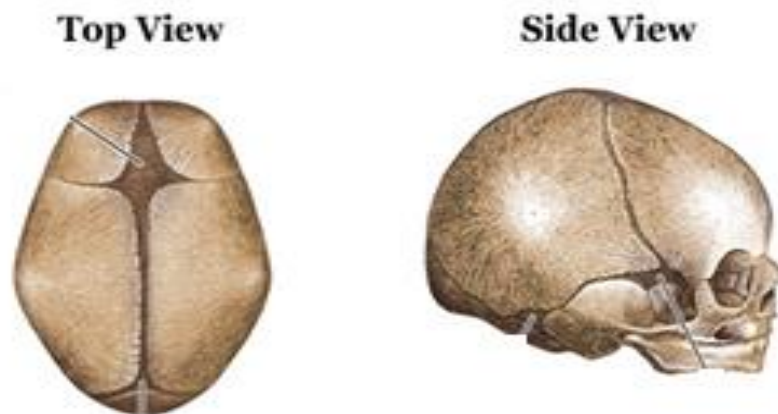


Figure 1.3. Infant skull fibrous appearance due to the trabeculae shown the material orientation of cranial bones [18].

1.4 Comparison of the anatomical configuration of the paediatric and adult head.

The paediatric head has different morphometric (size and shape) and anatomical structures from that of an adult, which affect the head impact response and structural integrity. The volume of the infant and child head is approximately 25% of the adult head [27]. With a mass of approximately 1 kg compared to approximately 4.5 kg for the 50th percentile adult male head [27, 28]. Head circumference increases markedly through the first year of life, as a result of the rapid and progressive growing of the brain [27], making the cranial cap, which encapsulates the brain, proportionally larger in the infant head than in the adult's (see Figure 1.4). Overall, the neonate head height constitutes 25% of the total body height, compared to 14% for the adult [27]. The skull is significantly compliant, due to the segmental development, arrangement and flexibility of individual bones [27], where the cranial bones are thin and pliable, not being fully ossified, since the bone is formed from intramembranous ossification [29]. Furthermore, the viscerocranial bones (temporal and sphenoid bones) are more prominent in the cranial cap of the adult head than the arrangement of its bones and the manner by which the bone plates are connected. The infant head has "soft spots" (sutures and fontanelles), which make the head pliable, as described above. The sutures between the bones are made of flexible collagen fibres and each cranial bone has only one thin cortical table (~1mm thick) [30]. However, the adult head has suture joints that are rigidly connected by interdigitated bone, which makes the skull rigid and not easily deformable [22, 31]. The fontanelle is absent from the cranium of the adult [22, 32]. The adult cranial bone comprises of a multi-layered structure (>5mm thick), having an inner and outer table [33], compared to the paediatric cranial bone, which is thin and has only a single layer of cortical bone.

These properties make the adult head structurally stiffer than the infant head [27, 34, 35, 36]. The different features of the relatively large head of the infant, including the shape and structure and relatively soft, pliable and elastic bones of the cranial vault and the fontanelles provide a very different impact response and biomechanical structural properties, compared to the adult. Resulting in the paediatric head being less resistant to impact trauma, paediatric skull response from an impact differs from the one of an adult skull, where the material, geometrical properties and the structural composition of the skull affect the biomechanical behavior [37]. These differences prevent a simple extrapolation of biomechanical properties, such as the overall stiffness and impact response from the adult head to the paediatric head. Likewise, the distinct morphologies of the adult and paediatric heads make it difficult to apply the mechanics of adult head injury to those of the paediatric head. All of these points must be considered in terms of proper head impact cases. Therefore, the head of an infant cannot be considered simply as a scaled down adult head [38].

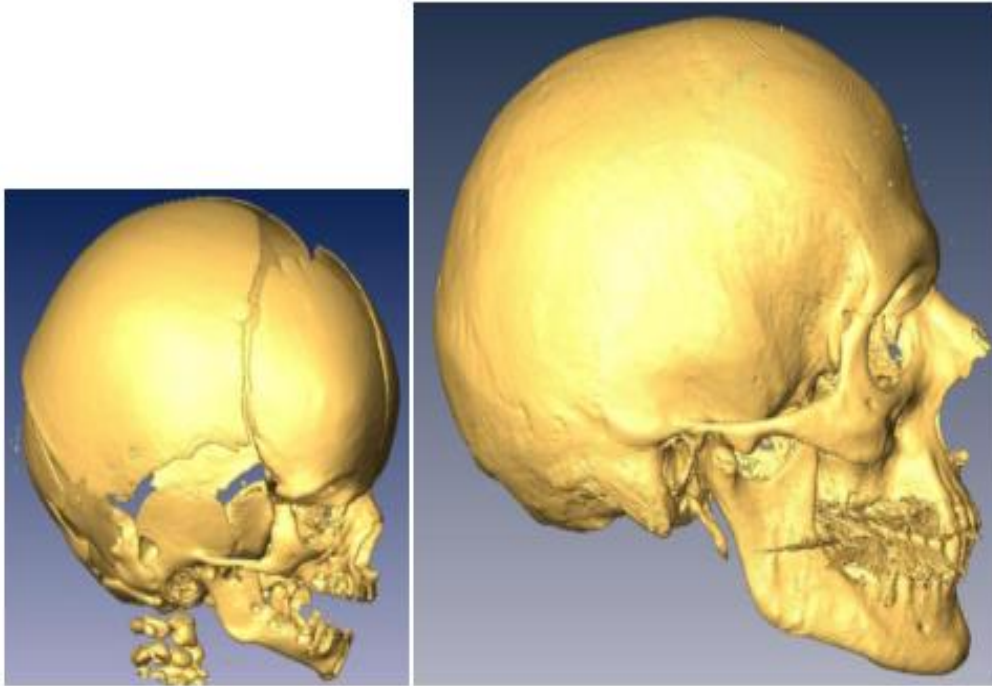


Figure 1.4. Comparison between the paediatric head (left) and the adult head (Right) [38].

1.5 Biomechanics of head injury.

Head injury in the paediatric and adult populations is caused by one of two types of dynamic mechanism; either by the movement of the head resulting from motion transmitted to some other part of the body called an inertial loading (shaking) ("whiplash", see (Figures.1.5a and 1.5b), or by impact loading, where the head either strikes a fixed object (see Figure.2.6a) or is struck by a moving object (see Figure 1.6b). These mechanisms of loading are completely different and have different consequences and may result in different head injury outcomes [39]. An impact between two objects, such as the head and a rigid surface, may result in one of two consequences: (a) some contact phenomena that occur with the colliding objects (one or both of the them), such as a scalp contusion, skull fracture, large local deformations, different types of fractures, bruising, etc. and (b) the transmission of loading effects (the elements of initial loading) to distal

parts of the system, known as 'wave propagation', whose indices often produce destructive effects at locations distant from the contact point, as illustrated by the coup and contre - coup phenomenon. This feature includes the generation and release of skull deformations at positions distant from the impact location [40, 41, 42, 43]. The interior structure of the skull plays a significant role in the localisation of the coup and contre - coup contusion with and without skull fracture [44, 45]. In cases where there is no contact phenomenon or wave propagation, the event is not an impact. During impact the scalp compresses, making the skull bend inwards and stress waves dissipate around the surface of the skull, whilst passing throughout the brain material. These events appear just before the head undergoes acceleration or deceleration to its maximum value; each event resulting in loading of the materials that form the head structure. While the scalp is compressed by the impact, the stresses are dependent on the magnitude of the impact force or pre impact velocity, the direction of the blow, the area of contact and properties of the impacting surface. All play a fundamental role in affecting the material response of the head. Subsequently, the head will be accelerated or decelerated; resulting in differential motion of the skull and brain, since, during impact, the skull will come to a stop and the brain will continue to move in the cranium, resulting in a differential motion. Tissues will be subjected to translational accelerations, producing compression and tension, whilst angular accelerations will produce additional shear stresses. Given TBI is a result of both skull mechanism and brain mechanism, This study has acknowledge that TBI is a consequence of skull mechanism but also has its brain mechanism of both translational and rotational brain motion that produce focal and rotational loading of the

brain and the blood vessels and all contribute to TBI. This study will focus on addressing skull mechanics which in turn contribute to address the TBI.

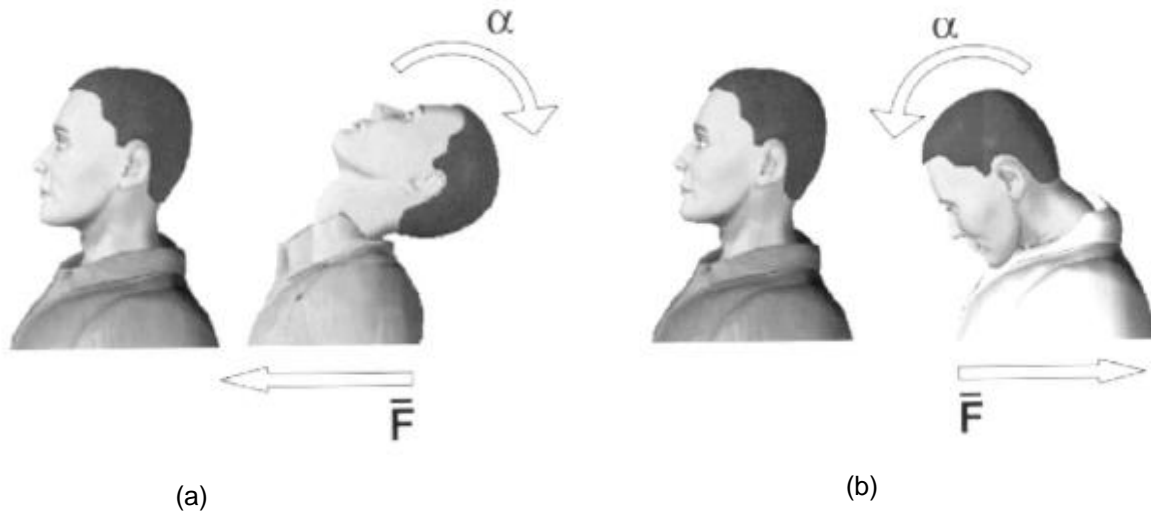


Figure 1.5. Impulsive loading of head/neck in (a) rear loading and (b) front loading [39].

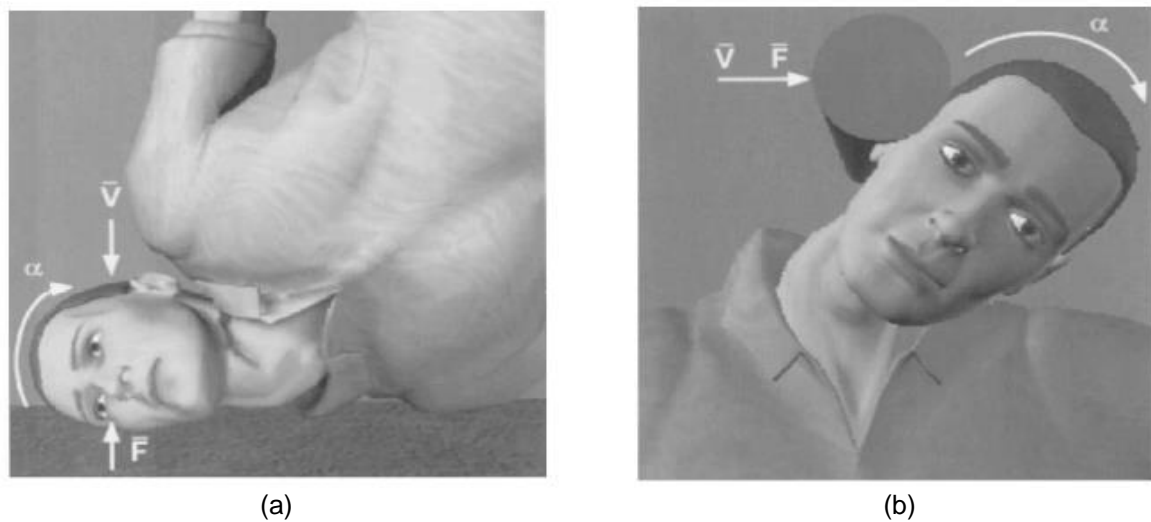


Figure 1.6. Impact loading of head/neck illustrating (a) impact from fall and (b) impact from object [39].

As outlined in the previous section, the skull of an infant is not a rigid shell as observed in the adult; the infant skull consists of curved plates, loosely connected by sutures that are unable to support bending loads during early development. During impact, the infant skull experiences large elastic deformations and even plastic deformations, resulting in different types of skull fracture. Due to this change in structure shape, even in the absence of skull fracture, large strains will be generated throughout the cranium and its contents. When fracture occurs, greater shape changes are demonstrated in the skull and brain. This phase of infant skull and brain injury requires further investigation [39, 46].

In contrast, inertial loading comprises of movement of the system's elements by an applied motion, at a position distant from the head, transmitted through the linkages of the neck. This type of loading does not have the two consequences of an impact loading. During the inertial loading, there will be acceleration or deceleration of the head without head contact, where the force is typically applied to the torso and or the neck structure, the force will be transmitted to the head causing acceleration and deceleration. With this type of loading, no contact injury occurs at the scalp or skull. As in the case of shaking a baby, under these conditions, the neck will be the first structure to experience loading and possibly an injury; this mechanism is commonly called "whiplash". During inertial loading, the brain freely moves within the cranial vault and the distortion of its shape generates stresses in its structures, leading to a risk of injury, induced by rotational accelerations. Inertial movement may have a cyclical element to it, produced by the head moving backwards and forwards. The subsequent relative displacement of the brain, skull, spinal cord and neck potentially produces rupture of the parasagittal bridging veins and contusions and haemorrhages of the brain [46, 47, 48]. Usually, sagittal plane

accelerations produce risks of subdural haematoma (SDH), compared to coronal plane accelerations which produce risks of traumatic axonal injury (TAI) [49].

1.6 Severity coefficients and Head Injury Criteria (HIC).

There are a range of variables that produce a risk of head injury during impacts, such as the kinetic energy of the body, the force transmitted to the body, the stress and strain of the structure and the whole acceleration of the body [50]. Each of these variables, either alone or in combination, may be produced during fall/impact scenarios. Head acceleration measurements are used as a key correlate to head injury which are applied to reducing the likelihood of a major head injury by testing acceleration mitigation products such as safety helmets, the interior structures of vehicles and playground surfaces. Head injury thresholds have been developed by subjecting adult human cadavers or primates to translational or rotational accelerations and evaluating any significant corresponding injuries. Observed injury patterns are correlated with accelerations to produce head injury threshold values, in terms of the kinematic variables, for example the peak linear accelerations (peak G). These thresholds have been further investigated, through the use of computational modelling and anthropomorphic testing devices (ATDs) in threshold testing and accident reconstruction. The thresholds have generally been expressed in terms of kinematic variables, to provide an indicator with which incidents can be assessed. The severity coefficients (thresholds) of head injury will be discussed generally in terms of translational accelerations and in particular those relating to infants. The fall/impact scenario results are represented graphically as a profile of acceleration on impact (expressed in units of gravity) over a period of time (t) called the g/time trace, which is used as a basis for measuring the head impact injury intensity in the head injury

models. A head injury threshold was developed, based on the original kinematic variables of the Wayne State Tolerance Curve (WSTC) proposed by Lissner et al. [51]. This curve, based on volunteer sled testing and experimental drop test of four human adult cadavers, with measurement and comparison of acceleration and structural damage, was used to estimate human tolerance. The WSTC, shown in Figure 1.6, considers the severity of head injury, dependent on both the magnitude of acceleration and the duration of an impact. The WSTC creates a relationship between a single point or value of linear acceleration for a duration of time and severity of injury. Impact response values, above the threshold curve imply a danger to life, whilst those values underneath the threshold curve are acceptable. Figure 1.6 illustrates that an impact response value of 100 g over a duration of 6 ms represents the same threshold of injury as 200 g for 3 ms, since they both lie on the curve. However, an impact force of 75 g for 10 ms would represent a danger to life, whilst 150 g for 3 ms would be tolerable. In reality, Collantes [50] deemed that the acceleration forces acting on the head rise and fall during the total duration of an impact, rather than producing a single value at any given duration. Thus, the WSTC has been considered by some [52, 53] to inadequately represent actual tolerances. However, the curve represents a valuable first step, both in defining the tolerance levels for head impact within the evaluation parameters and for developing injury criteria to estimate the different levels of head injury risk.

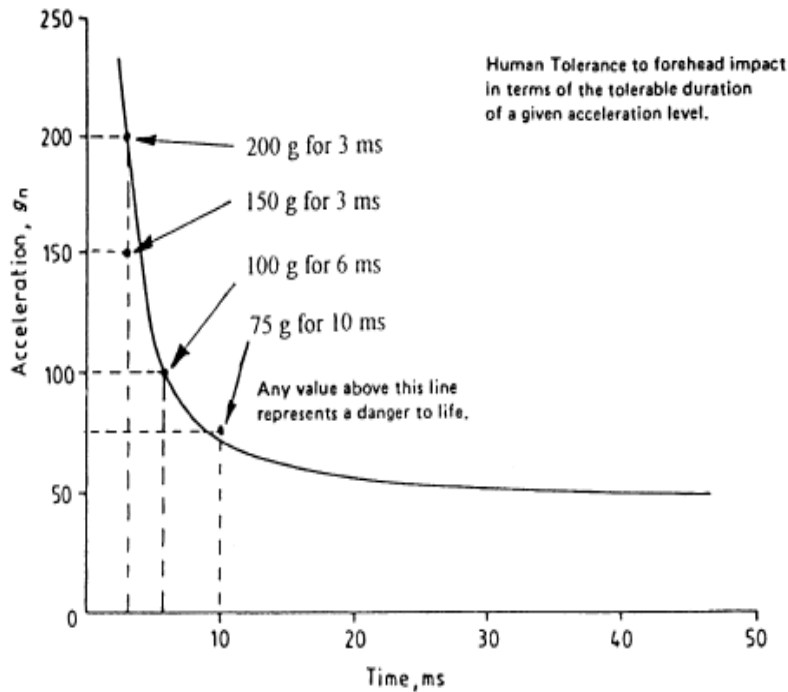


Figure 1.6. The Wayne State Tolerance Curve (WSTC) [51]

In general, a mathematical expression is required to quantify head injury risk and provide a standardised method, capable of estimating the severity of a head injury established on external data. The Gadd Severity Index (GSI) [54] provides a consideration of an acceleration - time relationship with injury risk and takes the form of a weighted factor (2.5) applied to the integral of the acceleration - time waveform experienced by the head. In this way, the GSI is able to improve upon the injury criterion of the WSTC by taking the waveform of the impact into account [55]. The GSI is defined as

$$\text{GSI} = \int_0^t a^{2.5} dt \quad (1.1)$$

where GSI is the function of acceleration and time of impact, a in a unit of gravity, is the acceleration on impact, t the time duration (s). The GSI was developed to be applied in the automotive industry for assessing the safety of various motor vehicle interior structures and injury mitigation strategies. Historically, the most frequent head injury in automotive collisions was acute subdural haematoma (ASDH), however, whilst injury mitigation strategies have reduced ASDH, the mortality rate remained fairly constant. Diffuse Brain Injury (DBI) [49] now predominates. For instance, if the occupant's head strikes the dashboard of a vehicle, the padded interior structure is designed to deform to increase the impact time duration, whilst increasing the stopping distance. This results in both of longer durations and softer impacts, increasing the probability of the occupant sustaining DBI. However, the source data used for the GSI was based on tolerance to severe concussion, DBI, rather than ASDH [18] and as the GSI value is calculated by the integration of the whole impact waveform. For example, the impact tests on two different surfaces produce similar GSI values, see Figure 1.7. This is in conflict with the observations of variance in the probability of DBI (low impact acceleration, long impact duration) and ASDH (high impact acceleration, short impact duration).

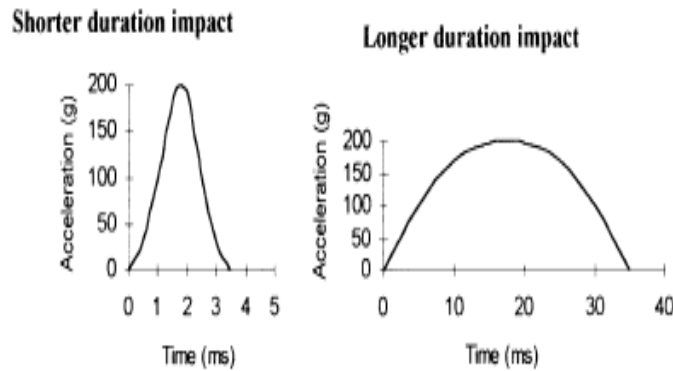


Figure 1.7 Examples of acceleration - time profiles from two different impact simulations [50]. Therefore, it is difficult to know the correlation between the GSI values and injury levels. This GSI was then updated by Versace [53] to investigate only the injurious region of the acceleration - time curve, irrespective of the waveform shape, resulting in the Head Injury Criterion (HIC), as defined in Equation (1.2).

$$HIC = \left| (t_2 - t_1) \left\{ \frac{1}{t_2 - t_1} \int_{t_1}^{t_2} a dt \right\} \right|_{\max}^{2.5} \quad (1.2)$$

where again, a (g) is acceleration on impact and $t_2 - t_1$ is considered to be the injurious portion of the acceleration - time waveform. The HIC is the most significantly adopted and commonly used severity coefficient [50, 56]. Prasad and Mertz [57] conducted a number of experimental studies on adult cadavers, presenting a collection of skull fracture and brain injury data with their corresponding HIC values to develop an injury risk curve. The study proposed that the HIC value of 1000 was associated with an 18% risk of severe or fatal head injury [57, 58], when the impact time duration was shorter than 15 ms [58]. Since the original National Highway Traffic Safety Administration (NHTSA) data was related to adults, a method was proposed for scaling the HIC for children, extending

research by using a family of child anthropomorphic testing devices. Original scaling methods were based on head measurement and skull stiffness properties [59], although this was later updated to be based on brain material properties. For children, they proposed that a HIC value of 800 was associated with a 5% or greater risk of sustaining a severe head injury, such as brain bleeding and/or skull fracture [60]. However, some authors suggest the HIC is oversimplified and a poor predictor of head injury severity. Of note, is Goldsmith's 1981 essay, wherein he expresses concerns, echoed by others in the field, that a single-parameter criterion such as the HIC, determined only by rigid-body linear acceleration of the head, is an unsatisfactory description of head injury with regard to assessing safety, particularly as the influence of angular accelerations (e.g. Whiplash) and stress waves through the brain, are not yet fully understood [61].

1.7 Material properties.

The impact response of either a physical or computational head model will be dependent on the material properties used to develop them. Consequently, for physical or computational models to work like appropriate biofidelic surrogates, their material response properties have to resemble those of a human. There has been extensive characterisation of the dynamic material properties of adult skull tissue [62, 63], but the dynamic properties of the paediatric infant skull and suture remain relatively unknown. The skull of the infant, as outlined previously, consist of thin, flexible plates composed of partially calcified bony tissue, joined at their margins by membranous sutures and fontanelles. Unlike, the stiff adult cranium, the infant skull is a pliant structure, capable of substantial deformation under external loading, further intimating that scaled down adult criteria are not applicable to children or infants [38]. A paucity of data in this field, due to

ethical, moral and limited access to the infant cadaver heads, means that further research is required. In addition to an absence of whole head response data, there are very few material response studies relating specifically to infants. To obtain a biofidelic physical or computational surrogate model response, this following section will outline a comprehensive overview of all the relevant reported mechanical testing and material properties of the different structures of the heads of infants and young children.

1.7.1 Skull

The cranial vault of a new born infant consists of soft pliable monolayer plates, connective sutures and fontanelles, which become increasingly mineralised and therefore, stiffer during the early years of life. When subjected to an appropriate force an infant skull will readily deform. This response has many advantages, since it allows the skull to deform and grow during a period of very significant neuro development. With advancing age the skull becomes increasingly mineralised, the sutures and fontanelles narrow and the monolayer becomes increasingly differentiated to produce a three - layer composite. By 6 months, the infant's skull is less pliant and increasingly shell - like in its structure, though still relatively deformable compared to an adult skull. Whilst readily deformable when subjected to compressive loading, the infant skull material stiffens when subjected to short duration (impact type) forces. This phenomenon is believed to be due to the fact that biological tissues are visco. Thus, their response and tolerance to impact is rate sensitive. The collagen matrix of infant bone contains many contacting protein fibres and a significant amount of fluid. If the structure is loaded slowly, much of the energy can be absorbed through movement of the fibres and re-distribution of fluid without tissue damage. When loaded rapidly, however, the structure cannot deform quickly enough and

rupture can occur before a change in shape. For a rupture to occur in tissue, an applied force must be of a sufficiently high loading (strain-rate) distribution to load the tissue to a critical level (strain energy density).

During impact loading the skull responds by deforming and thus extending the time period over which the force is applied. If a sub-fracture level of force is absorbed, the skull dissipates the impact energy by deforming and reforming, such that the energy is transmitted and spread throughout other areas of the skull. If no skull fracture occurs, then the integrity of the skull is maintained and it is able to again absorb subsequent impact loading at a sub fracture level. If however, a fracture level of force has been applied, producing a structural imperfection (e.g. linear fracture), the total mechanical strength of the skull is compromised (weakened). The ends of the crack serve to concentrate any subsequent stress, and can produce the further propagation of cracks. Alternatively, it has been demonstrated with the skulls of adults that rather than retaining the properties of a shell structure, i.e. deforming and reforming when loaded, a fracture can serve to destabilise the entire structure, such that additional loading can predispose the skull to injury distant from the original fracture. A fracture is produced when a force of sufficient magnitude produces strains within the bone that its material limits are exceeded. A skull fracture can be initiated as a small micro-fracture at a site of weakness, either an imperfection in the material structure of the bone or within the complex geometry of the bones of the skull. Therefore, fracture tolerance values can vary between individuals in a population and similar impacts can produce different injuries in different individuals. Other variables include the duration over which the force acts, the angle

through which the force is applied, the area over which the force is applied and the site of the skull which is impacted.

McPherson and Kriewall (1980) [64, 65] provided the first basic material properties for foetal cranial bone by using three-point bending tests at a quasi-static loading rate of 0.5 mm min^{-1} to examine the elastic modulus of foetal cranial bone on multiple parietal and frontal bone foetal cranial specimens. These specimens were excised from six different foetal calvaria (26-40 weeks gestation) and a specimen from a six-year-old head with the grain fibres of the bone running either parallel or perpendicular to the long axis of the specimen. The trabeculae are distributed in a radial pattern, emanating from the cranial bone ossification centers which provides the surface of the bone with a fibrous appearance, see Figure 1.3. The mechanical characteristics of cranial bone are reported in two groups: pre-term (26-30 weeks gestation) and term (36-40 weeks gestation). Fibre orientation is characterised as either parallel or perpendicular, which has a significant effect on the elastic modulus of the bone. The Young's modulus of elasticity increases with age and the parietal bone, across all ages, is nearly three times greater when grain fibres are oriented parallel to the long axis of the specimen. This variance in the elastic modulus between the parallel and perpendicular specimens confirms the significant anisotropic material properties (orthotropic appearance) in the immature cranial bone, as documented in Table 1.1.

This highlights the fact that for modeling and design purposes a surrogate model should require the bone stiffness properties to be represented as transverse isotropic and that age should be taken into consideration when defining material properties. McPherson and Kriewall [64, 65] is the only study to date which compares parallel and perpendicular

fibre orientations and shows a difference in stiffness of approximately three times between them. This is a very important value for infant head loading analyses, since adult cranial bone is not anisotropic in this manner. However, other mechanical characteristics, such as yield stress and yield strain were not informed; thus, making failure properties of foetal bone difficult to assess. Also, no specimens of infants (1-12 months) were investigated. Furthermore, since the study was an investigation of the deformation of the foetal head passing through the birth canal, low rates of loading (quasistatic) were investigated, this is a significant limitation of this study, when considering head impacts, since it provided only limited young's modulus values.

Margulies and Thibault (2000) [37] performed three-point bending tests on parietal bone specimens from four human infant cadavers (25 weeks gestation to 6 months) with fibres running perpendicular to the long axis of the specimen, at two different strain rates, 2.54 mm min⁻¹ and 2540 mm min⁻¹. The elastic modulus and ultimate stress of parietal bone from a 6-month-old infant were at least five times greater than those of the pre-term age group (25-40 weeks gestation), as shown in Tables 1.1 and 1.2. While the elastic modulus and ultimate stress increased with age, the ultimate strain decreased. The age of donor had a significant effect on the elastic modulus of the paediatric skull, which was comparable to McPherson and Kriewall [64]. However, the published data for the fibre - skull studies, tested at slow "crush" rates [64, 37] may not be suitable for understanding skull response to short height falls or inflicted impacts, which impose deflection rates of 2.4 m s⁻¹ or higher. Thus, to determine injury risk, and develop effective injury interventions for the infant during falls and inflicted impacts, it is important to obtain fibre material response properties at relevant rates.

In tandem to the human infant cranial bone testing, the authors carried out three point bending and tensile testing on cranial bone and suture samples, from 30 strips of immature porcine cranial bone with fibre directions perpendicular to the sample. The properties of the human and porcine samples were shown to be equivalent, however, due to the small sample size there were no statistical comparisons; so, it remains unknown whether this evaluation is valid. The immature porcine cranial bone showed strain rate dependency, with the elastic modulus, rupture modulus and energy to absorption increasing with strain rate, which is similar to adult material properties [63]. It is ambiguous whether this would be true for human infant bone.

To obtain material properties for infant cranial bone, at rates more appropriate to low height falls, Coats and Margulies (2006a) [66] assessed the effect of rate dependency of infant cranial bone, at higher strain rates, 1.58 and 2.82 m s⁻¹, respectively. A rate similar to the impact velocity of an unimpeded fall from 0.3 and 0.9 m, respectively, is shown in Tables 1.1 and 1.2. Material properties of 46 parietal and occipital bone specimens from 21 paediatric cadaver heads (36 weeks' gestation to one year of age) were derived by using three-point bending tests and an increasing elastic modulus and ultimate stress was shown with an increasing age. Furthermore, the location of the specimen (that is, parietal versus occipital) and age, significantly influenced the elastic modulus and ultimate tensile strength, with both properties increasing with age for the parietal specimens relative to occipital specimens. Thus, material properties continue to be age dependent past the infant stage of development (greater than one year). Which again, confirm the need for age-specific material properties [64, 37]. Comparing the effect of strain rate on other mechanical characteristic with previously reported data [64, 37], it appeared that

strain rate has no significant effect on the elastic modulus or the ultimate tensile strength. This illustrates a difference between the reported adult cranial bone and immature porcine samples [37]. Therefore, caution should be agreed before assuming that porcine or adult samples are a suitable surrogate for human infants. For fibres perpendicular to the long axis of the specimen, the findings of Margulies and Thibaut [37] suggest that the stiffness of the bone was not significantly different to the original data reported by McPherson and Kriewall [64]. However, Coats and Margulies [66] were unable to measure the material properties of fibres, which were parallel to the long axis of the specimen. Subsequently, the effect of strain rate and age on a specimen with a parallel fibres are different. This study was fundamental, since it provided age specific material properties for infants, which will be used by this present study for the development and justification of both physical and finite element infant head models

1.7.2 Sutures

There are very few studies on the material properties of paediatric cranial sutures in the literature. Coats and Margulies (2006 a) [66] measuring the mechanical properties of infant human cranial bone, measured the tensile properties of infant human suture. Tensile tests were conducted on 14 coronal suture specimens from 11 infant calvaria (21 weeks gestation to 1-year-old) at 1.20 and 2.38 m s⁻¹ impact velocities, comparable to the impact velocity from a fall of 0.3 and 0.9 m, respectively. No significant effect of age or strain rate on the modulus of elasticity, ultimate stress and ultimate strain of the coronal suture was reported. Though the elastic modulus was affected by the interaction between donor age and strain rate. The elastic modulus of a specimen from older donors increased with the strain rate, compared to younger donors, which tended to decrease

with strain rate. The limitation of this test was that there was no donor age–strain rate interaction reported for ultimate stress or ultimate strain, due to the samples being bone–suture–bone specimens rather than suture specimens, alone.

Table 1.1 Minimum-maximum stiffness (E) / MPa values of human infant cranial bone and sutures. (1) McPherson & Kriewall [64]; (2) Kriewall et.al. [65]; (3) Margulies & Thibault [37]; (4) Coats & Margulies [66]; (5) W Wang et al. [67] - (w=weeks, m=months).

Age	Study	Bone (Parallel)		Bone (Perpendicular)			Suture	
		Parietal	Frontal	Parietal	Occipital	Frontal	Coronal	Sagittal
25≤w<Term	(1)	530-4080	-	60-220	-	-		-
	(2)	731-4082	-	-	-	-		-
	(3)	-	-	44-619	-	-	-	-
	(4)	-	-	50-553	45-181		4.3-14.2	-
Term ≤m<3	(1)	2660-5290	1870-4000	430-2330	-		-	-
	(2)	1873-5158	2579-3999		-	910-2490	-	-
	(3)	-	-	821	-	-	-	-
	(4)	-	-	183-933	29-551	-	3.8-6.4	
3≤m<6	(1)	-	-	2112-3582		-	-	-
	(4)	-	-	552-1155	318-1318	-	-	-
11≤m<12	(4)	-	-	201-784	104-622	-	4.2-16.2	-
12≤m<24	(5)	-	-	990-1216	-	1145-1387	310-400	349-467

Table 1.2. Minimum-maximum σ_{uts} /MPa values of infant cranial bone and sutures. (1) Margulies & Thibault [37]; (2) Coats & Margulies [66]; (3) W Wang et al. [67]; (w=weeks, m=months).

Age	Study	Bone (Parallel)		Bone (Perpendicular)			Suture	
		Parietal	Frontal	Parietal	Occipital	Frontal	Coronal	Sagittal
25≤w<Term	(1)	-	-	3.1-17.0	-	-	-	-
	(2)	-	-	5.5- 81.1	3.3 - 31.4	-	4.2- 6.7	-
Term ≤m<3	(1)	-	-	10.6	-	-	-	-
	(2)	-	-	8.4- 53.7	3.1-18.5	-	2.2 - 7.2	-
3≤m<6	(1)	-	-	42.1- 71.7	-	-	-	-
	(2)	-	-	23.7- 69.7	16.4- 43.4	-	-	-
11≤m<12	(2)	-	-	15.1- 52.1	6.2- 37.6	-	3.5 - 4.1	-
12≤m<24	(3)	-	-	76.5- 97.7	-	88.7- 110.8	43.7- 61.15	34.6 - 54.9

Coats and Margulies (2006 a) [66] were the first to measure the material properties of infant human suture, thus providing essential material properties which are used in this present study for the development of both infant physical and computational head models. Prior to the above study, Margulies and Thibault [37] measured the mechanical properties of immature porcine suture and confirmed that the elastic modulus and ultimate strength of infant porcine suture increased with age and further, that rate dependency, rupture modulus and elastic modulus increased with strain rate. The elastic moduli were 22-80 times larger than those of human infant sutures reported by Coats and Margulies [66]. Again, this further illustrates that caution should be adopted prior to using porcine material properties as a surrogate for infant human sutures (<13 months old). Recently, Wang et al. [67] extracted two frontal bones, two parietal bones, two sagittal suture samples and

two coronal suture samples from each of the seven human infant cadavers aged 1-2 years old. The specimens were tested at a strain rate of 1.5 mm s^{-1} in a three-point bend setup. Significant differences in the mechanical properties were observed (ultimate stress, elastic modulus, or ultimate strain), as shown in Tables 1.1 and 1.2 between the specimens of frontal bones, parietal bones, cranial bones and sutures. However, there was no significant difference between the sagittal and coronal sutures.

1.7.3 Scalp

There is a lack of mechanical studies of the paediatric scalp tissue. The only mechanical study performed with adult human tissue, Raposio and Nordström [68] performed a tensiometric test on 20 samples of human scalp tissue. They reported an initial linear increase with load up to 500 g., after which the scalp exhibited an exponential growth in stiffness with load up to 5,000g. It is unknown if the paediatric scalp would respond in a similar manner [69]. Given that researchers incorporated scalp tissue in paediatric head injury models to mitigate head injury in impact scenarios [70, 71], there is a requirement that studies be conducted to investigate the rate dependency of the paediatric scalp tissue. Galford and Mc Elhaney (1970) [72] performed tensile and compressive tests using scalp samples from adult rhesus monkeys. They found the dynamic modulus of the scalp was 1.54 MPa compared to 1.03-1.38 MPa moduli from the quasistatic test, confirming the rate dependency of the scalp. Mechanical characterisation of the paediatric scalp to investigate the rate and age dependency are important factors to study the paediatric scalp impact response [69].

1.7.4 Brain

The development of child head models requires the mechanical behavior of brain tissue to be characterised. The mechanical properties of adult brain tissue have been extensively investigated across several species, however, there is a significant lack of data concerning the brain of paediatric population. Whilst no mechanical testing studies have been conducted on human infant brain samples, there are limited immature porcine studies. Thibault and Margulies (1998) [73] used porcine samples to study the age-dependent material properties of brain tissue. Using 2-3 day old and one year old samples, which correspond to human child ages of less than one month and greater than four years, respectively. Harmonic shear tests were conducted at strain amplitudes of 2.5% and 5.0% from 20-200 Hz.

This experiment outlined that both the storage and loss modulus significantly increased with age at 2.5% strain, while only the loss modulus significantly increased with age, at 5% strain. This study found that the shear modulus of porcine brain tissue has a significant age dependence. Further, the study found a difference between the relative magnitudes of the modulus for tested porcine samples and reported human brain tissue. However, the reported frequency dependent behaviour of adult porcine tissue matched that of published adult human tissue. Although their study analysis highlights a significant difference between immature and adult porcine samples, a study limitation is that the test were conducted at low strains and at only one location (independent of anisotropy) and oriented in one direction (independent of the inhomogeneous nature of the brain).

Consequently, Prange and Margulies (2002) [74] investigated the anisotropy, inhomogeneity and age dependent material properties of brain tissue at a high strain rate

from porcine sections of the white matter and grey matter. Age dependency was assessed from five-day-old and four-week-old porcine that have the equivalent composition and neurological development of a human newborn (less than one month old) and toddler (approximately one to three years), respectively. The samples consisted of mixture of grey and white matter. The results from the tests were compared with the mean values of the white and grey matter properties of adult porcine. Finally, fresh human grey matter samples were tested within three hours after excision and compared with porcine sample data.

The study confirmed that at large strain rates, up to 50%, a significant inhomogeneity exists between the grey and white matter and also between two regions of white matter. Where the properties of grey matter were 1.3 times stiffer than the corpus callosum (white matter). Also the grey matter was found to be isotropic; though, the tested white matter regions had a significant degree of anisotropy, which correlated with local neuroarchitecture. Prange and Margulies [74] confirm the age dependency of brain tissue properties, with infant tissue being approximately twice as stiff as adult tissue at high strain rates. Also, they stated that a non-linear modified 1st order Ogden hyperelastic model was appropriate for the brain shear and compressive loading results, and at large strains, the brain must be modeled as non-linear. They found that the reported properties of autopsy specimens in the literature are approximately four to ten times stiffer than the brain tissue testing results of fresh brain tissues (porcine and human).

Given there are limited studies of Traumatic Brain Injury (TBI) in infants, data on the material properties of infant brains is rare. Although, mechanical data is more commonly available from adult cadaver studies, there are vast differences in the proportions, injury

response and material properties between the infant and adult brain. Therefore, these reported large strain, regional, directional and age-specific data enhanced the computational models biofidelity and provide important information regarding the mechanisms of traumatic brain injury. The absence of paediatric human brain data leads to the use of infant porcine data in existing FE models [71, 75, 76, 77], based on the similarities reported by Thibault and Margulies [73] between both species, related to the compositional changes in brain tissue through maturation. Therefore, the implementation of child and infant head models often involves restrictive assumptions, like property scaling from adult or animal data.

A study by Chatelin. S, et al. (2011) [78] provided the first data on the human brain tissue at different ages and brain regions, including how infant brain tissue compares with adult. Using samples that were extracted from autopsy, with apparent brain damage, they compared the local mechanical properties of seven subjects whose age varied from 2 months to 50 years. The samples included the brain stem, grey matter (taken from the thalamus and not the cortex) and white matter (Corona radiata). Grey matter was not used from the cortex, which has been shown by Coats and Margulies (2006) [79] to have different mechanical properties to the thalamus in adult brain tissue. Viscoelastic properties in a linear strain range were investigated using an oscillatory rotational shear test using a dynamic shear rheometer (AR2000). The properties were investigated at strain (ϵ) equal 0.5% engineering strain between a static and rotating plate. The frequency range was 0.1 to 10 Hz. The tests were performed at non-destructive strain values, thus, limiting the accuracy of the data when constructing models for paediatric brain injury, as these injuries are likely to occur at high strain values. The specimens

were extracted at post mortem over a range of 24-48 hours; it is noteworthy that this time variance could lead to variations in brain matter degradation. Also, this study was constrained by the number of samples obtained, as there were only one or two samples, this means that it is unclear whether the samples are representative of the whole infant population. The testing results confirmed that brain tissue response was age dependent, since the adult brain samples were 3-4 times stiffer than a young child brain at a low strain rate. A 200% increase in stiffness and viscoelasticity was observed between the ages of 5 months and 22 months. However, at high strain rates it has been shown from the animal studies that the infant brain tissue is approximately twice as stiff as adult brain at high strains, as reported by Prange (2002) [74]. Further, this study found, from comparing the stiffness of the different regions, the brain stem appeared to be approximately 2-3 times stiffer than the grey and white matter.

1.8 Current tools used to understand head injury in children.

1.8.1 Postmortem Human Surrogates (PMHSs).

Postmortem Human Surrogates (PMHSs), are one of the most valuable tools used in the field of biomechanics for studying and investigating injuries; however, PMHSs have limited availability, particularly in paediatric populations [80, 81, 82]. A short fall series of experiments were conducted on infant cadavers by Weber (1984 [80] and 1985 [81]). Weber's studies were the first cadaveric infant head impact research attempted and provide a very valuable dataset for study in this field. Weber (1984) [80] carried out his study in an effort to distinguish between accidental and non-accidental injury to an infant who was alleged to have fallen from a changing table. In the 1984 study [80], fifteen infant cadavers (up to 8.2-months-old) were dropped in free fall from a height of 82cm

onto three types of flooring (stone, carpet and foam backed linoleum). The cadavers were checked for skull fractures before testing using both radiography and palpation. Weber (1984) stated 'all infants were dropped in a way that the body (in a horizontal position) and the skull (in the area of the parieto-occipital) dropped on the ground at the same time' [80]. In all cases skull fractures were reported, in three cases the fractures crossed sutures, leading to the conclusion that "fractures of the infant skull should be expected regularly in falls from the mentioned short fall heights" and "linear fractures can remain unrecognised not just by laypersons." Weber having completed his study in 1984 [80], extended the work in 1985 [81] using the same experimental protocol and two different soft impact surfaces. A further 35 cadaveric infants were dropped. Ten cadavers onto a rubber matt (2cm thick). A further 15 cadavers were dropped onto a double folded camel hair blanket (8cm thick). Fractures were not seen in all the drops onto these softer surfaces unlike that for the harder surfaces but, there was one infant cadaver which had a skull fracture in the rubber mat impact group (two linear fractures of the left parietal bone) and four cases of fracture on the camel hair blanket (in the left parietal bone). Unfortunately, the only data generated by Weber's study [80] [81], perhaps a result of a lack of technology were of a hand drawn representation of the fractures with associated descriptive text see Figure 1.8.

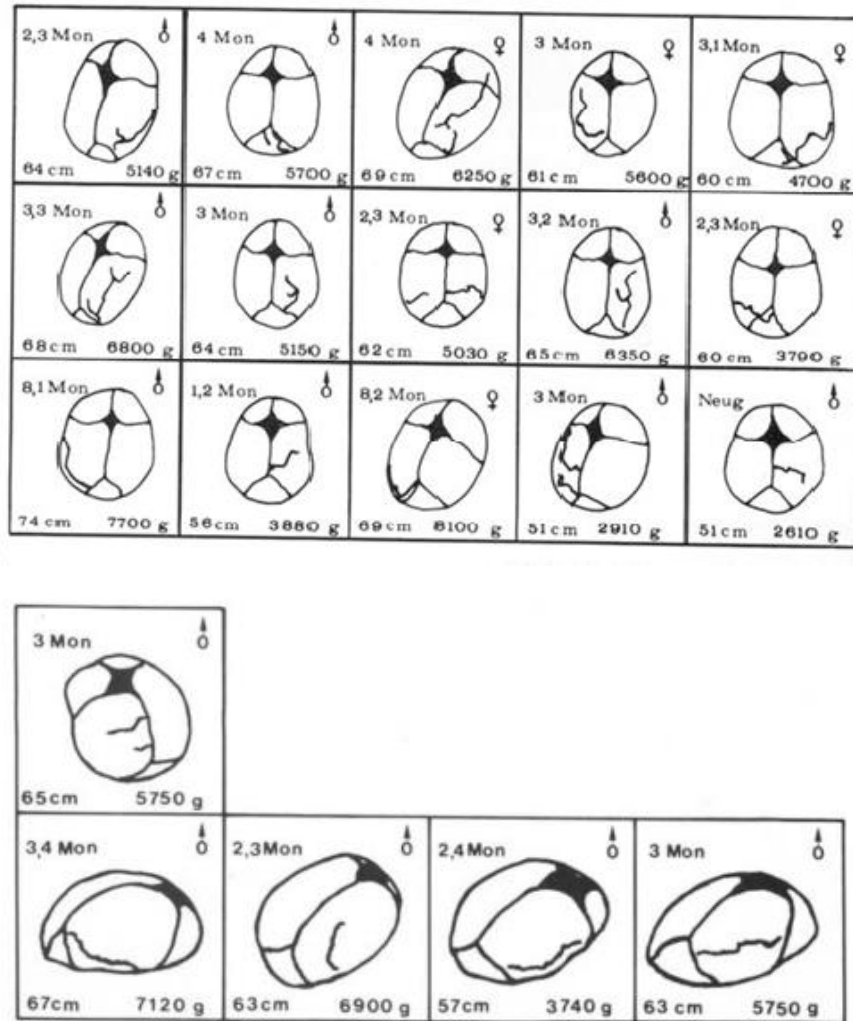


Figure 1.8. paediatric head skull fracture pattern from Weber study [80, 81]. The lack of numerical results makes it difficult to apply the results for precise validation of other work. As with all cadaveric studies, the response is not going to be the same as that of a living infant. In particular, Weber did not pressurise the venous or CSF systems prior to, or during, the drop. However, unlike all other cadaveric work, Weber dropped the whole body so there was the opportunity for CSF and brain to distribute internal pressures in a biofidelic manner. By increasing the number of subjects in his overall combined study to 50 infant cadavers, Weber provides the greatest number in any study to date. This makes it particularly unfortunate that as discussed above, it is difficult to

use it for precise validation purposes. To date only Prange et al., 2004 [82], have produced quantitative data. Thus, the majority of current infant head impact understanding is based on Prange's study, which investigated three infant postmortem human surrogate (PMHS) heads, impacted from two fall heights (0.15m and 0.30m), at an angle perpendicular to a single surface. Prange, out of experimental necessity, had to derive the current key correlate for head impact injury, acceleration by calculation, by dividing the impact force at the impact surface by the head mass. This limited "global approximation" provides only a single generalised head impact response curve, rather than specific regional or localised responses. Thus, current injury prediction strategies are incapable of considering the significant complexities associated with infant head impacts. Overriding limitations in deriving this information include the rarity of access to child PMHSs and the technical complexities of measuring localised head responses. The study has, however, a number of shortcomings, since it investigated only three infant PMHS heads (1, 3 and 11 days old), impacted multiple times, from only two fall heights (0.15m and 0.30m), at five different impact locations, generally described as the frontal bones, right and left parietal bones, occipital bone and vertex, at a single angle, perpendicular to a single surface (steel force plate).

Lloyd in 2011 [38] conducted cadaveric impact testing which was clearly modelled on Prange's study [82] with a very similar experimental protocol but a much larger sample size and with some additional research and tests included. Of the cadaveric heads studied, six were full term and under one month old and impact tested in the same way as Prange. Lloyd [38] also took advantage of developments in data collection and analysis in the interval since Prange's study. The sampling frequency of the force plate

used for the failure drop tests was significantly higher at 300 000Hz and photo target dots were used to track translation and rotation during drop tests with a 2000Hz video and a pressure sensitive film to analyse the impact contact area. However, despite this additional data collection there is very little reference or analysis of this in the study. Similar to Prange [82], Loyd [38] developed acceleration vs time plots for his drop tests by dividing the force time response of the force plate by overall mass, making the assumption that the head behaves as a rigid body. Loyd's conclusion, based on the above rigid body assumption, was that impact response is due to local, rather than global stiffness; suggesting that research and analysis of accelerations in 3D and at different points on the head, plus rotational accelerations, is the next step required to further the research. Work of this nature would remove the clearly inaccurate rigid body assumption.

A test series [122] was conducted using adult PMHSs to investigate factors affecting the creation of cervical spinal damage, from impact to the crown of the head. The kinematic data of the head and spine were gathered from a series of drop tests which impacted the head of a PMHS onto a load plate. The primary response characteristics investigated in this series of drop tests [122] were the force time histories of the impact and the acceleration response of the subjects. The results of the drop tests indicated that the force time histories were either unimodal or bimodal waveforms see Figure 1.9. The unimodal waveform was referred to as the inertial loading of the head during the inertial part of the pulse, with significant interaction of the cervical spine late in the event, see Figure 1.9 a. The bimodal waveform was attributed to an initial inertial loading of the head (with some coupling of the cervical spine), followed by a second peak force which is believed to be caused by an additional coupling between the head, neck and the whole

body, see Figure 1.9 b . Dynamically, the peak acceleration of the head precedes the first peak force and becomes negative while the force remains positive indicating a greater force exerted on the head from the neck and body in opposition to the action of the impact. It clearly demonstrates that the principal force is produced by the effective mass of the head.

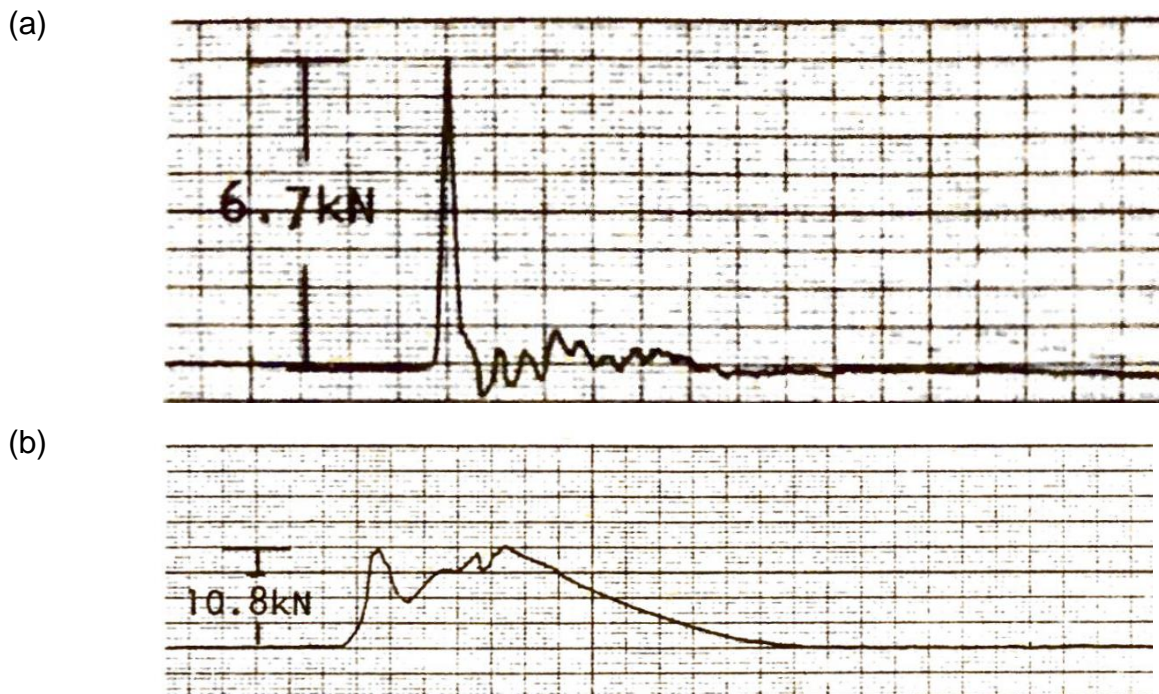


Figure 1.9. Force time histories showing (a) the unimodal and (b) bimodal waveform [122]

The lack of cadaveric studies is further complicated by variations in methodology. Weber [80, 81] performed experiments on whole bodies, rather than just the head and only recorded the results by the way of sketches, whereas Loyd [38] matched Prange's [82] methodology and collected numeric impact force data. Thus, Prange and Loyd's results can be combined for direct numeric validation, whereas Weber's can only be used for validation in an indicative manner.

Further, the rapid changes in anatomy of infants between birth and one year old, as discussed earlier and investigated in detail by Burdi [27] also significantly affect the number of available validation opportunities. By six months of age the structure of the skull has six sets of cadaveric numeric data available for head impact or quasi static compression in those infants who are under one month old. Faced with these restrictions, clinicians and researchers have often looked to models to help inform their opinions. Physical and computational modelling is an attempt to combine known anthropometry and material properties, with justified approximations for aspects which are not known.

1.8.2 Mechanical surrogates

The Weber [80, 81], Prange [82] and Loyd [38] studies concentrated on producing impact scenarios, which were predominantly perpendicular to the impact surface, that is, linear translational (straight line) loading. It is important to acknowledge, however, that certain other biomechanical scenarios occur, which produce more angular impact accelerations. Since there has been no opportunity to conduct cadaver experimentation in this area, biomechanical engineers have resorted to using instrumented biomechanical models (also known as) dummies or anthropometric test devices (ATDs). It is important to appreciate that an ATD's validity depends on the mechanical context/loading environment, and the data used to develop it. Both Prange [82] and Loyd [38] compared their cadaveric head results with those of appropriate ATDs and the results from these, highlight the variation in ATD validity from one situation to another. Loyd's data [38] shows statistically the same peak acceleration results for the Adult (Hybrid III) ATD, when compared to an adult cadaveric head. The child equivalent 6-month (CRABI) ATD was however, statistically different from a 5-month old cadaver in the majority of drop

orientations. Anthropomorphic test devices are often used to act as surrogates for post-mortem human surrogate (PMHS) testing, when assessing the possibility of an injury being a result of a given incident.

Infant and child head ATDs are, however, based on scaling animal and adult response data and since the paediatric head response is poorly characterised, their specific validity is ambiguous. It seems likely that the variety in quality of an ATD's performance, highlighted by Loyd [38], is due to the quality of the data used to develop it. The Hybrid III has been developed directly from cadaveric results, whereas by necessity, the CRABI has used values scaled from adult response data. Finite element studies have also raised concern over the validity of infant ATDs in certain scenarios. Furthermore, none of the commercially available ATDs, reported by Melvin (1995) [60] and Irwin and Mertz (1997) [83], represent the separate bone structures or the flexible/pliant nature of the infant skull, so there is no appropriate test device that properly represents the infant head impact response. In addition to the commercially available ATDs, researchers have developed physical models for the investigation of dynamic scenarios [84, 85].

Specific to short falls in young children, Prange et al., (2003) [84] developed a 1.5-month-old dummy to determine the rotational response of the infant head during low-height falls and inflicted head injury. A limitation of the study, however, was that the head of the dummy was represented by a simplified 2.25 mm thick homogenous plastic shell. No account was given to the anatomical complexity of the infant skull plates, sutures or fontanelles, such that it would likely have produced a stiffer response and concomitantly higher response values than an actual infant head. However, Prange et al. [84], out of experimental necessity, measured the head impact as if it were a 'rigid body,' such that

the angular acceleration sensor was attached to the top of the dummy head to measure rotation with axis perpendicular to the sagittal plane. The transducer measured the rotational velocity experienced by the head of surrogate during shaking, inflicted impact and short distance fall. However, this approach is incapable of providing localised specific details with respect to head response. Coats and Margulies (2008) [82] developed a 'more responsive' infant head constructed from copolymer plates, connected by silicon rubber, overlaid by latex to represent the bone, suture and scalp characteristics, respectively. This instrumented anthropometric infant was used to measure the forces and angular accelerations during a fall related impact. Again, localised response measurement was not possible, since the focus was on the global translational and rotational head response, measured by a nine-accelerometer-array and angular velocity transducer placed at the center of the surrogate head. Head response values were derived from a rigid body assumption.

1.8.3 Finite element (FE) models

Finite element (FE) analysis has become an effective method to investigate head injury mechanics and evaluate head injury risk. There is, however, a limited availability of paediatric FE head models to predict the presence of skull fractures and neurological injuries, compared to the number of FE adult head models [86, 87, 88]. Paediatric head FE model development is constrained by the limited availability of material property data, quantitative age-dependent anatomical data and paediatric impact response data. Ideally, the biofidelity of an FE head model, subjected to impact loading, requires validation from impact response data acquired from experimental impact testing on PMHSs, though this is also of limited availability.

To the author's knowledge, the earliest reported use of an FE head model, for investigating head trauma in infants was an investigation of head deformations during labour, to understand mechanical cranial birth injuries by McPherson and Kriewall [16] in 1980. An FE model of the parietal bones of a foetal skull was developed, utilising bone stiffness properties from material experiments on foetal parietal bone [64], to provide an understanding of the biomechanics of foetal skull deformation during the birth process and to specify the differences in skull bone stiffness between preterm and term infants during head deformation. They reported the FE model exhibited deformation, close to that in normal labour and that a parietal bone in preterm can withstand 2-4 times the deformations of a parietal bone in term with similar load distribution. Lapeer and Prager in 2001 [17] extended and improved the work of McPherson and Kriewall [16] by utilising FE analysis to further understand head moulding during the natural birth process. However, whilst their FE model was developed from scans of a foetal head and included the skull and sutures, no intracranial soft tissue structures were included. Deformation of the FE model showed good agreement against clinical deformation measurements from 319 birth deliveries, considering two parameter shape change and the degree of deformation, yet no statistical comparisons between the two were documented.

It was not until the study of Thibault and Margulies in 2000 [37], that an investigation was conducted into the effects of the infant cranium and sutures in protecting the brain during impact head injury by FE analysis. Their FE simulations incorporated the tissue response data from their experimental tests [37], which were performed on samples of human infant cranial bone and porcine bone suture. The authors assumed that the suture properties of infant porcine sutures would be the same as an infant. However, Coats and Margulies

(2006) [66] later proved this to be incorrect as an infant porcine suture was 22-80 times stiffer. Two FE head models were produced with different mechanical properties, a one-month old infant head and an adult head. An impact loading was applied to both, to investigate the influence of the cranial bone properties on the intracranial tissue deformation pattern. Two impact loadings were applied to the parietal area of the skull at 45 degrees, relative to the vertical axis. The impact loading was a half sinusoid, with a pulse duration of 10m.s and peak loading force of 1000N and 5000N, representing a minor and severe impact loading. The geometry of the FE mesh was simplified to 'half an ellipsoid' and the base constrained, to prevent displacement and rotation. The authors reported that deformation of the model was affected by stiffness of the cranium, increasing peak deformation from 2mm to 4mm at 1000N and from 4mm to 10mm at 5000N. Impacts to an FE model with the mechanical properties of the infant brain case (cranial bone and sutures) are associated with relatively large cranial shape changes and greater, diffuse brain distortion (bilateral and diffuse patterns of strains of the brain) than the FE head model having adult mechanical properties (brain strains being focal to impact). It was assumed that infant head impact force can produce diffuse brain injury; however, with the adult head, the same impact force can produce a focal injury. In reality, these results are restricted by the simple geometry of the FE head model and the application of infant porcine material properties for the sutures. This study [37] represented an initial step in understanding the mechanical response of cranial bones subjected to traumatic loading and head injury; hence, defining child head injury thresholds.

Subsequent to Coats and Margulies' (2006) [66] quantification of the material properties of human infant bone and sutures, Coats et al. (2007) [71] developed an FE model of a 5-week old infant head from CT and MRI scans with the corresponding material data implemented. This FE model was used to predict fracture from short height falls and the performance of a parametric study to investigate the change in impact response in terms of the material properties and anatomical variations. The brain was modelled using hyperelastic and viscoelastic material properties scaled from Prange and Margulies (2002) [74]. The authors concluded that changing brain compressibility, stiffness and suture, influences the outcome in terms of peak principal stress, peak force, contact area and duration of impact. By increasing the brain compressibility, brain stiffness by approximately 3 orders of magnitude increased the measured peak principal stress, peak force, contact area and duration of impact by greater than 15%. However, a 50% reduction in brain stiffness did not affect the measured outcomes by greater than 2%. Coats et al. [71] used the measured ultimate stress values from their paediatric PMHS material experimental tests [66] to create a parietal and occipital fracture risk curve graph, see Figure 1.10. This study [71] used maximum principal stress to predict skull fracture, utilising their ultimate tensile stress values from their mechanical experiment study [66]. The von Mises stress was used to evaluate the probability of skull fracture, based on their fracture risk probability graph of the parietal and occipital bones. The ability of the FE model to predict fracture was demonstrated to show a good agreement with the PMHS cases of Weber [80, 81]. The authors reported the parietal bone produced maximum principal stress values, which are associated with 99.8% risk of fracture, utilising the values of the ultimate tensile stress of the parieto-occipital area impacted from an 82cm

fall onto a rigid surface. Furthermore, and related to the fracture path, the simulation indicated a probability of fracture propagating from the lambdoid suture to the centre of the parietal bone was very high. This study represented a significant step forward in terms of understanding infant head injury biomechanics from a low height fall and highlights the importance of a biomechanical understanding of infant head injury from a short fall height. This model biofidelity, in terms of impact response, was unknown. The FE analysis reported a 29-35g impact response corresponding to a 50% risk of fracture, in contrast to the PMHS study [82] there were no appearances of skull fracture, average peak accelerations during 0.30 m drop tests were 55.3g and for 0.15 m were 38.9g.

Post publication of the material properties of the skull and suture by Margulies and Thibault [37], Roth et al. [76] in 2007, published the study of an FE model of a 6-month head constructed from CT images, to assess the relative dynamic response of the head during impact and shaking. The authors reported that the pressure and shear appearing on the brain, was significantly lower in shaking than impact scenarios. While, it appeared that strain on the bridging veins, in both scenarios, were comparable. However, it was ambiguous if the potential strain on the bridging veins was caused only by the relative brain - skull motion, since the veins were modelled as springs, without reporting the stiffness values. Also, Coats and Margulies [66] later reported that the material properties of the skull were stiffer than those applied by Roth, the implication being that Roth over-represented the strain applied to the bridging veins.

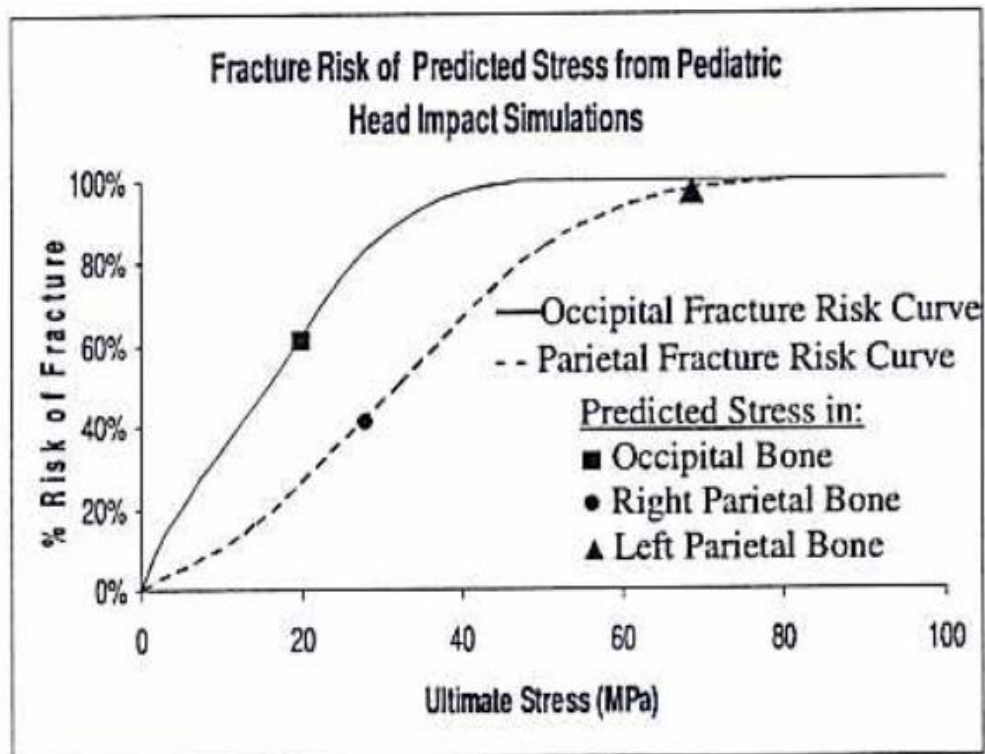


Figure 1.10. Fracture risk curve graph from Coats study [71] showing maximum principal stress values in the occipital, right parietal, and left parietal bones.

Using the 6-month FE model as a reference, Roth et al. [89] in 2008 reported the effect of scaling by comparing the original model with another 6-month model, developed from scaling down an adult FE model. Model conformity was assessed, in terms of the accuracy of head geometry, shape and thickness. The two models were subjected to three impact conditions; frontal, lateral and occipital impacts and produced a different pressure and stress response of the brain and skull between the scaled and original models. The authors attributed this difference to the variations in curvature between the skull and brain between the models, thus causing differences in deformation and therefore, pressure and stress. In addition, the cranial bone scaled model had a thickness greater than physiological, resulting in lower deformations and stress. Scaling of model geometry and shape for children less than 6 years old was inappropriate, and for bone thickness, was inadequate for children before the age of 10 years. In terms of the brain

shape, the authors reported that the scaling approach was not an accurate representation of the brain of a 6 month and 3-year-old child. The original and scaled models were applied to the replication of the fall accident scenarios of a 4.5-month-old child, reported to have sustained a fracture and the original model found to be more accurate in predicting fracture. The research further highlights that children's heads should not be considered as a scaled adult head, where the output stress has different values and locations. Like Roth et al.[77], this model was limited by skull material properties, which were later reported to be too stiff [66] and the fact this FE model was not validated against PMHS response data. In 2009, Roth et al. [90], reported a similar geometric analysis of a 3-year-old child, scaled FE head model and compared its impact response to the same aged model, accurately constructed from CT images. Similar results were reported to Roth et al. [89], except the values of the peak pressure on the brain was close between a 3-year-old child, scaled FE head and a 3-year-old child constructed from CT images. This article highlighted, again, a need for geometrically accurate FE models. The same researcher modelled a different FE head model of a 3-year-old child for reconstructing fall related accidental scenarios, to investigate neurological injury. Twenty five cases were investigated, composed of two groups of patients, those with no neurological lesions and those with severe lesions. Although, the model's von Mises stresses were a good predictor for neurological lesion, still the mechanical properties of the brain at this age and the biofidelity of the model were unknown.

Even though the paediatric FE head models provided encouraging results for investigating child head injuries, none of those found in the literature were validated against cadaver (PMHS) test data from a similar age group. Only the 17-day-old

(newborn) child head model developed by Roth et al. (2010) [77] and the 6-month old FE head model from Li et al. (2013) [91] were quantitatively validated against cadaver (PMHS) experimental data from corresponding age group. Roth et al. (2010) [77] created an FE model from 230 slices of a CT scan of the 17-day-old (newborn) child head model. Mean material properties from the Coats and Margulies' (2006) [66] were used to represent the suture and the skull. The brain was modelled as viscoelastic from Thibault and Margulies study [73]. Due to the very few experiments exist for paediatric brain tissues. The author's investigated this point using the mathematical model to know the influence of material law parameters on the model response. A parametric analysis was conducted to study the influence of the brain compressibility and stiffness values on the FE model's response for a forehead impact from 0.30 m fall height by varying the viscoelastic parameters (G_0 , G_∞ and bulk modulus) of the brain tissue. The parametric study results indicated that brain constitutive law have a small variations in the measured skull deformation and von Mises stress and peak acceleration for the reconstructed impact test. These results unlike from those reported by Coats et al. (2007) [71], potentially as a result of using different material models for the brain.

Li et al. (2013) [91], developed a 6-month old child head FE model that had the geometries of different components from the CT scan data used in Klinich's head model [70]. Data from the FE head simulations were compared with the 5-month-old child cadaver experimental data from Loyd [38], for validation purpose, based on the age similarity. The reported output values from the 6-month old child head model of Loyd [38], under compression and drop impact conditions, showed good biofidelic dynamic response behavior.

Subsequently, whilst these paediatric FE head models provide an understanding of head injury mechanics, they are limited, since their validity has not been assessed against experimental paediatric PMHS data. Roth et al. [77] and Li et al. [91] validated their models against PMHS test data from a similar age-matched group, which provided a valuable insight for investigating child head injuries. Both [77] and [91], however, represented the material properties of the infant cranial bone as homogeneous and isotropic using 'mean material properties' from the literature [66], rather than the heterogeneous, anisotropic material properties reported by McPherson and Kriewall [64]. Thus, because the cranial bones are a significant contributor to overall head impact response, to provide the greatest degree of biofidelity, it is deemed imperative that the material properties be accurately represented.

Recently, Xiaogai Li et al. (2017) [92] developed three paediatric FE head models representing a newborn, 5-month and 9-months old child. The cranial bones of these models incorporated the orthotropic appearance of skull bones. Further, this study presented a new nonlinear constitutive law for soft tissues (scalp, sutures and dura mater) for infant head modelling. The FE models were subjected to extensive drop tests, as in Loyds PMHS experiments, as well as compression tests [38]. During the impact test, the model's performance was assessed, based on the entire acceleration–time impact curve. Global head impact response coincide well with experimental data, for both drop and compression tests, highlighting that impact angle has a profound influence on the global head impact response. A subsequent parametric analysis was conducted to investigate the influence of the nonlinear constitutive models, compared to the linear elastic models for the soft tissue that are widely used in the existing infant head models. The improved

nonlinear models for the suture, scalp and dura, together with an accurate impact angle, enable the models to predict acceleration–time curves and impact surface area that are comparable with experimental findings at various impact locations, as well as force–deflection curves in compression simulations. The simulations show profound deformation of infant head, resulting a large deformation/strain at the interfaces between the bone and the sutures/fontanelles, unique to the infant head compared to older children and adults where the skull bones are fused. Further, whilst the newborn FE model was globally validated against Prange’s PMHS response data [82], no localised bone and suture response values were reported.

Skull fracture is one of the most common paediatric traumas. However, injury assessment tools for predicting paediatric skull fracture risk are not well established, mainly due to a lack of cadaver testing. Weber [80, 81] conducted 50 paediatric cadaver head impact tests for the forensic research of suspected child abuse. A shortcoming of the tests were, however, an absence of objective injury measurement (such as head acceleration and contact force and injury magnitude). Only skull fracture patterns were reported by way of sketches, limiting their direct application to the investigation of paediatric skull fracture risk. Li et al. [123] reported a method to predict the paediatric skull fracture risk using Weber’s data. Li et al. (2015) [123], also conducted a parametric study using different paediatric head FE models from 0 to 9 months old. Reconstructing Weber’s cadaver tests, matching physical characteristics associated with appropriate age and size to collect quantitative measurements, skull fracture risk curves were developed. The skull fracture risk curves for infants from 0 to 9 months old were developed based on the model predicted head injury measures, through logistic regression analysis. Li et al.

[123] considered the predicted responses of six models, representing different ages, as skull fracture predictors, including peak head acceleration, head injury criterion (HIC), maximal von Mises stress, maximal first principal stress and strain, and maximal shear stress. Age was considered as a covariate in each logistic regression; thus, the skull fracture risk curves for different ages could be illustrated. These parameters were assessed by comparing their distribution with the actual location and pattern of skull fracture in Weber's cadaver tests. Li et al. [123] found that the models predicting stress responses in the skull (maximal von Mises stress, maximal shear stress, and maximal first principal stress) were better than global kinematic based injury measures (peak head acceleration and head injury criterion (HIC)), in predicting paediatric skull fracture in terms of the goodness of fit and accuracy.

Recently, Coats et al. (2018) [124] utilised an integrated approach, consisting of case evaluation, anthropomorphic reconstruction and finite element simulation to identify biomechanical metrics for the prediction of skull fracture, determining threshold values associated with fracture and developing skull fracture risk curves for low-height falls in infants. Four biomechanical candidates were identified for predicting skull fracture (first principal stress, first principal strain, shear stress, and von Mises stress) which were evaluated against clinical well witnessed falls in infants (0–6 months). For the clinical cases with skull fracture, the distribution of stress and strain in the FE model was compared to the skull fracture location, to confirm that high values occurred in the elements located around the site marked as fractured by a neuro-radiologist. For each simulation, peak values of four fracture predictors (first principal stress, first principal strain, maximum shear stress, and von Mises stress) were extracted from every element

in the right and left parietal skull plates. The skull fracture risk curves derived from binary logistic regression analysis, for the four predictor candidates, which were assessed not only in terms of quality of fit of the corresponding developed risk curves and their prediction accuracy rates, but also by comparing the distribution of these parameters with the actual location and pattern of skull fracture in clinical real-world falls. Among the predictor candidates, first principal stress correlated best with the occurrence of skull fracture.

Although these studies significantly advance the paediatric head trauma literature by proposing new biomechanical fracture criteria (like von Mises stress and maximal first principal stress) to predict injury due to impact loading in low-height fall scenarios, the biomechanical fracture criteria are not accurately determined corresponding to the fracture mechanism, thus, this method may potentially lead to errors.

1.9 Summary

It is clear from the literature that the understanding of infant head response to loading is currently significantly behind that of adults. Effective clinical and forensic case management is difficult without a complete understanding of the cause and effect relationship to predict and mitigate the potential consequences of infant head injury. Since the development of a child head injury cause and effect relationship from experimentation with living children is certainly impossible, Post Mortem Human Surrogate (PMHSs) experimentation provides a reasonable alternative. However, with respect to infants, very limited access to child PMHSs mean that testing is extremely rare, due to moral and ethical considerations. Only the studies of Prange [82] and Loyd [38]

PMHS have ever quantitatively tested head response for short fall impacts and contributed to infant head impact understanding. However, these studies have limitations with their experimental methodology. In addition, out of experimental necessity, both studies had to derive the current key correlate for head impact injury - acceleration by calculation, by dividing the impact force at the impact surface by the head mass. This limited global approximation provides only a single generalised head impact response value, rather than specific regional or localised responses. As a consequence, any subsequent injury prediction strategies are incapable of considering the significant complexities associated with infant head impacts. In addition to the rarity of access to child PMHSs, the overriding limitation in deriving the necessary information, is the technical complexity of measuring localised head responses. Faced with these restrictions, clinicians and researchers have often looked to models to help inform their opinions.

Physical and computational modelling is an attempt to combine known anthropometry and material properties with justified approximations for aspects which are not known. With respect to physical modelling, often the limits of suitable materials and manufacturing technologies mean that compromises have to be made. Anthropometric test devices (ATDs) are often used to act as surrogates for PMHS testing, when assessing the possibility of an injury being a result of a given incident. Infant and child head ATDs are, however, based on scaling animal and adult response data and since, the paediatric head response is poorly characterised, their specific validity is at present largely unknown. None of the commercially available ATDs [60] [82] adequately represent the separate bone structures or the flexible nature of the infant skull, so there is no

appropriate test device that properly represents the infant head impact response. In addition to the commercially available ATDs, researchers have developed a range of physical models [84, 85] for the investigation of dynamic scenarios. However, each has limitations by either failing to adequately represent the anatomical complexity of the infant skull plates, sutures and fontanelles, or out of experimental necessity measuring the limited global approximation of the head, such that the impact force is measured only at the location of impact. The impact acceleration values, a correlate for head injury risk, are calculated in the same way as in Prange's study [82] where this approach is incapable of providing localised area specific details with respect to head response.

With respect to the computational model, there are relatively few biofidelic infant or child FE head models [77, 91] and to date, any developed FE models have been unsuccessful in representing the significant geometric and physical response complexities of the tissues. Preceding models represent cranial bone response as homogeneous and isotropic, however, at birth, cranial bones demonstrate a visible fiber orientation, due to trabeculae radiating from centralised growth centers [16, 17, 18], which published response data confirms as behaving orthotropically and inhomogeneously, with different cranial bones having different stiffness properties [64].

In response, this present study investigates the development and validation of a physical model and FE model, to study the biomechanics of infant head injury, with the capability to measure localised area specific metrics, allowing potential correlation with head injury. Such physical and FE surrogates are intended to be used to inform clinical, forensic practice, child safety prevention and mitigation strategies. Also these surrogates are

highly significant for investigation of both accidental and non-accidental infant head trauma.

1.10 Research aims and objectives

The primary goal of this thesis is to report the development of a coupled physical-computational modelling framework that can be used to improve the biomechanical understanding of paediatric head injuries during impact conditions. Application of this framework is intended to assist in the investigation of the causal mechanism of a presented injury; helping to distinguish between accidental and non-accidental head injuries in paediatric populations. Furthermore, it is intended that the modelling framework be subsequently applied to producing injury risk predictions for the purpose of developing injury risk mitigation strategies. The specific objectives of this research are:

- To verify the use of different commercially available digital-additively-manufactured rigid and rubber acrylate polymers in the construction of the 3D printed physical model.
- To justify that the co-polymer materials are most closely matched to the mechanical properties of paediatric specimen tissue.
- To develop a verified surrogate physical model of a paediatric human head that incorporates anatomical information obtained from high-resolution CT scans and manufactured using Poly Jet Printing (PJP) technology.
- To develop a verified computational model of a paediatric human head that incorporates anatomical information obtained from the same high-resolution CT scans used in the construction of the physical model and applied the verified material properties.

- To use the verified physical model to investigate the kinematic response of individual structures of the head in response to a variety of loadings of the head as a whole.
- To use the verified computational model to simulate and investigate infant fall-related head impacts.
- To use the verified computational model to simulate head kinematic responses in a localised area in the head during different impact scenarios and to compare the results to the individual structural response of the physical model.
- To use the verified computational model to investigate the occurrence of fracture, by replicating the PMHS experiments, and to address the ability of the model to predict the fracture and the fracture risk probability at different fall heights.

1.11 Scope of the work and Thesis layout (Chapter outlines)

Chapter one provides the background information and essential details about paediatric head injury, in terms of definitions, epidemiology, basic anatomy and the development of the paediatric human head, as well as comparison with that of the anatomy of adult head, mechanism and Head Injury Criteria (HIC). Other sections, include a review of the material properties and current tools used to understand head injury in the paediatric population, including Postmortem Human Surrogates (PMHSs), mechanical surrogates and computational models. In addition, important findings and limitations of previous research are summarised.

Chapter two describes the materials and methods used in the development of a 3D printed multi-material physical model. Included are the mechanical properties of the polymeric materials used in the manufacturing of a 3D printed physical model, through

uniaxial tensile testing, to investigate the mechanical properties of rigid and rubber additively manufactured acrylate polymers at low strain rates. Enabling an assessment of their suitability as materials to mimic infant cranial bones and sutures; and validation of the physical model against published PMHS data, providing the capability to measure localised area specific metrics and allowing potential correlation with head injury. Further, describe the development of a computational FE model of paediatric head, based on the infant polypropylene polymer physical surrogate used for head injury analysis from high-resolution CT scan data set through image processing tools and using reported material properties; and the validation process against published PMHS data response and using this FE model to address the limitation with Prange's PMHS experimental test. The validation process includes comparison of the global approximation response of experimental physical surrogate drop tests against the regional response data from FE simulations of the physical surrogate impact tests, which provided the experimental regional and local response data of the physical surrogate impact tests.

Chapter three, presented the results of the output variables obtained from the following sections: mechanical characterisation of the Poly Jet printed materials; global validation of the paediatric physical model against PMHS data; Regional and local investigation of the paediatric physical model; global validation of the paediatric FE head model against PMHS data; global validation of the paediatric FE model against physical model data; physical model regional and local validation of the FE head model; and finally investigating skull fracture from the literature.

Chapter four, presents a discussion of the results in chapter three from the following perspectives: mechanical characterisation of the Poly Jet printed materials; global

validation of the paediatric physical model against PMHS data; Regional and local investigation of the paediatric physical model; global validation of the paediatric FE head model against PMHS data; global validation of the paediatric FE model against physical model data; physical model regional and local validation of the FE head model; and finally investigating skull fracture from the literature.

Chapter five, summarises and concludes the work providing the insights obtained in this thesis. Methodological limitations are acknowledged and future directions suggested for research that address some of these limitations.

2. MATERIALS AND METHODS

Falls, in the paediatric population, are the most common cause of head injury from trauma; and head injury the single most common cause of death and permanent disability. Clinicians, however, often struggle to establish a sufficiently detailed understanding of a cause and effect relationship to predict and mitigate the potential head injury consequences. In addition, whilst the majority of head injuries are accidental in origin, clinicians also struggle to discriminate between accident and abuse. There is, therefore, an opportunity to develop head impact surrogates to establish a more informed understanding of the response of the infant head to potentially injurious scenarios. Previous attempts at conducting infant head injury physical modelling have failed to adequately address the necessary challenges of cranial geometry and the physical response complexities of the paediatric head tissues. Infants are particularly vulnerable to impact related injury, and since, infant head impact response is heavily dependent on the cranial bones, any absence of cranial bone biofidelity is a significant limitation. This present study section describes a new approach to characterising and understanding infant head impact mechanics by developing printed physical and computational FE head models, using high resolution clinical postmortem imaging, to provide the most complete anatomical representation currently available, and biological material response data-matched polypropylene polymers, to replicate the relative mechanical response properties of immature cranial bone, sutures and fontanelles.

Additive manufacturing technology was applied to creating a physical polymeric model of a newborn infant skull, using PolyJet printed materials. Infant skull materials responses, were matched by a response characterisation study, utilising uniaxial tensile testing (1

mm min⁻¹ loading rate), to determine: the stiffness, ultimate tensile strength and maximum strain of rigid and rubber additively manufactured acrylates.

A 3D physical model of an infant head was subsequently printed from the matched materials. The brain, represented as a lumped mass, comprised of an injected gelatin/water mix. Subsequently the physical model was validated against results obtained from a series of Post Mortem Human Surrogate (PMHS) tests. High-Speed Digital-Image-Correlation optically measured linear and angular velocities and accelerations, strains and strain rates. The “global approximation” was challenged by comparison with regional and local acceleration data. The methodology has proven a significant new step in characterising and understanding infant head injury mechanics.

FE Analysis was applied to the 3D CAD head model; the process by which a successful FE mesh has been developed and applied to the skull’s natural but complex structure; determination and application of appropriate material properties. To mimic the fibre orientation of immature cranial bone, radially orthotropic properties were applied to the FE cranial bone model, with elastic moduli representing the bone response, both parallel and perpendicular to the fibre orientation. Subsequently, the biofidelity of the computational model was assessed by global validation against published PMHS data, by replicating experimental impact tests with a series of computational simulations, in terms of the infant head’s kinematic response. Following the validation process of the FE head model against the PMHS’s impact response and consider the shortcoming of the limited global approximation reported in PMHS study [82]. Computational model was applied to replicating the physical model during a range of fall related impact scenarios onto a hard surface. Finally, the computational tool was to be employed to verify its

efficacy in the prediction of actual fracture patterns by replicating experimental PMHS impact cases reported in the literature.

This new step in the development of a coupled physical and computational modelling approach provides valuable insight into the biomechanical engineering understanding of how a child's head responds during injurious loading, and provides a significant contribution to addressing the internal structural complexities of the head, which will subsequently inform clinical and forensic management and injury prevention strategies.

2.1 Paediatric head model development.

2.1.1 Data set and geometrical acquisition.

To take advantage of improved 3D technology, high resolution skull and brain post mortem imaging was performed on a 10-day old infant for whom no cause of death was found. Parental consent was obtained for pre-autopsy imaging as part of an ethically approved study, with institutional research ethics approval. Post mortem computer tomography (PMCT) imaging was performed with a 64-slice multidetector system (Siemens SOMATOM Definition; Siemens Healthcare, Erlangen, Germany). Volumetric brain PMCT imaging was performed at 120 kV with variable mAs, a pitch of 1, and 0.625 mm collimation. Images were reconstructed with bone algorithms to provide 1.25 mm slices. These images provide the highest resolution acquisition currently obtainable using conventional clinical scanners, although the dose may have been higher than currently in clinical use. Post mortem imaging clearly does not encounter the movement artefacts caused by patient movement, cardiac or respiratory variation and can be conducted until the scans are optimised.

2.1.2 Segmentation of paediatric head.

The high-resolution Computer Tomography (CT) data set was imported into Mimics 3D Medical Image Processing software (Materialise; Leuven, Belgium), aligned relative to the Frankfurt Plane, to measure the head dimensions from the CT images, by aligning a vector from the left to the right external acoustic meatus to be parallel with x axis. Then a vector from left external acoustic meatus to the inferior aspect of the left orbit was aligned to be parallel with the y axis. Markers were then placed at the most distal aspects of the head anteriorly (A), posteriorly (P), lateral (left), lateral (right), vertex and finally at the external acoustic meatus, using Mimics Package. The local coordinates for these markers were then exported from Mimics into Excel format. The head length, width and height for of the CT data set was calculated using (2.1 - 2.3) [93].

$$\text{Paitent Head Length (PHL)} = A_X - P_X \quad (2.1)$$

$$\text{Paitent Head Width (PHW)} = LL_y - LR_y \quad (2.2)$$

$$\text{Paitent Head Height (PHH)} = V_z - LEAM_z \quad (2.3)$$

where A_X is the X coordinate of anterior marker, P_X is the x coordinate of posterior marker, LL_y is the y coordinate of left lateral marker, LR_y is the y coordinate of right lateral marker, LR_z is the z coordinate of vertex marker and $LEAM_z$ z coordinate of left external acoustic meatus. The head length, width and height measurements from the

scan are presented in Table 2.1. The Root Mean Square (RMS) error for the three dimensions was then calculated, between the head dimensions measurement from CT dataset in this study and each of the three PMHS heads from Prange’s study using (2.4) [93]

$$RMS = \sqrt{\frac{(P_rHL- PHL)^2 + (P_rHW- PHW)^2 + (P_rHH- PHH)^2}{3}} \quad (2.4)$$

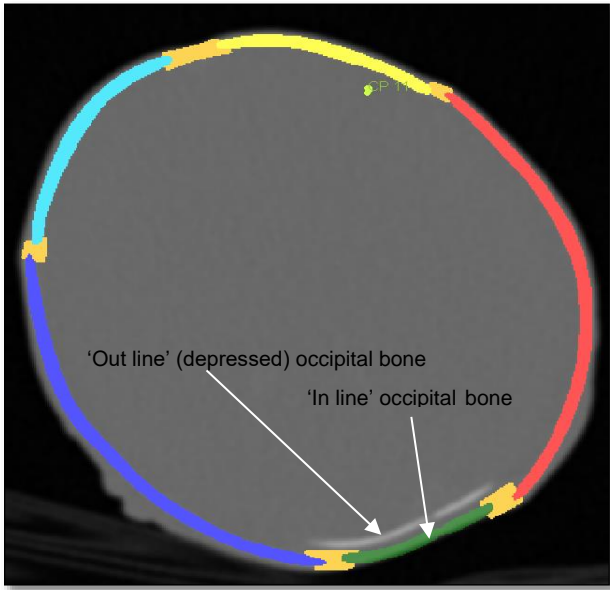
where PHL is the head length, PHW is the head width, PHH is the head height from CT data set, while P_rHL is the head length, P_rHW is the head width and P_rHH is the head height from Prange et al.[82] data series. From Table 2.1, the lowest RMS error (2.7) classified the chosen CT dataset of a 10-day old child as close to the 3-day old PMHS from Prange’s data series, further, both have the most similar masses.

Table 2.1 Head measurement of the Computed Tomography datasets compared to the Prange’s PMHS data series and the Root Mean Square.

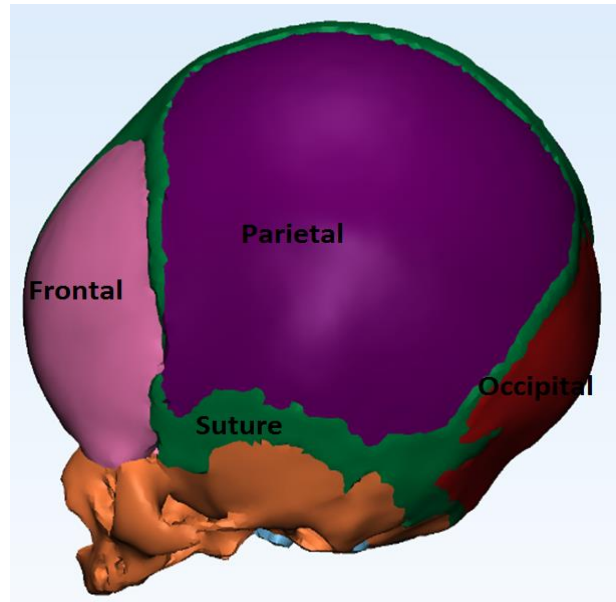
Parameters	Head model	Prang et al.[82]		
Age/days	10	1	3	11
Head Length/mm	100	108	103	112
Head Width/mm	83	88	85	104
Head Height/mm	72	88	75	92
Head Mass/g	460	666.5	491.5	701.9
RMS	-----	8.7	2.7	18.11

Initial development of the model was by subdividing the infant skull into four cranial segments: the parietal, occipital and frontal bones and the skull base, which demonstrates an intricate geometry, including, the multiple foramina, processes, internal cavities and branching structures. The frontal bones and skull base were grouped, and are subsequently referred to collectively as the 'frontal bones'. Within the software there are a wide range of thresholding techniques, which can be applied to differentiating between skeletal and soft tissue structures. This requires careful use of 'thresholding', supported by the manual editing of irregular, "awkward", areas. Greyscale thresholding was applied and those pixels within the upper and lower threshold of greyscale were defined as a 'region of interest' and regarded as a cross section of 3D geometry. A soft tissue mask was segmented to include the whole head, to ensure that pixels that were unclassified, were classified as soft tissue. The mask, which was thresholded to include all the pixels in the head was then subjected to 'morphological closing', to seal off any small cavities, for example the internal nasal cavities. Then 'minor manual editing' was applied to ensure there were no holes in the mask. The brain and cranial bones have distinguishable thresholds, which were segmented using the threshold filter to differentiate those tissues from the soft tissue structures as shown in Figure 2.1. The cervical vertebrae and the mandible were removed to replicate Prange et al's PMHS [82]. The bones were separated and each one smoothed to improve the definition of the 3D CAD model, reduce complexity and assist further computational operations. The infant CT scan image showed the occipital bone significantly depressed, (see Figure 2.1a). This is a normal physiological phenomenon, due the passage of the head through the birth canal during natural birth and normally reverses during the first few weeks of life. Since, cranial

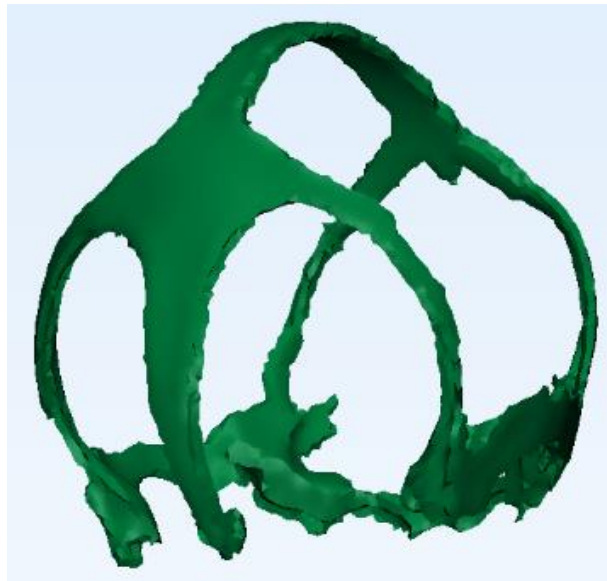
development at around the time of birth is subject to wide variation, as a result of gestational age at the time of birth (+/- 18.5 days [94]), to represent a wider infant population, the occipital bone was moved outwards to align with the edges of the parietal bones on each side (see Figure 2.1a). Many unsatisfactory attempts were made to separate the sutures from the cranial bones and other soft tissues using the 'usual' Materialise 3-matic segmentation tools, since their pixel greyscale values in the CT scans were so close to that of the surrounding tissues. In response, different 3-matic tools, including wrapped, Boolean operations and manual editing tools were applied to achieve the final suture model. Figure 2.1 shows the infant head parts after applying different thresholds values, using different segmentation tools and morphological operations. Communal borders, between adjacent parts, were created to allow the application of boundary conditions. The 'non-manifold' tool in Mimics was employed for this purpose, to remove any gaps between the adjacent parts and to create a 'non-manifold assembly' of the surfaces for the 3D "boney" and soft tissue models. This method was effective for structures with complex and irregular geometries, such as the paediatric head model. When creating the head assembly, intersecting surfaces were either deleted or smoothed for proper surface-to-surface contact and then boundary surfaces created for the contacts. This procedure was repeated until all parts, comprising the head model, were included and the final 3D CAD model produced (see Figure 2.1).



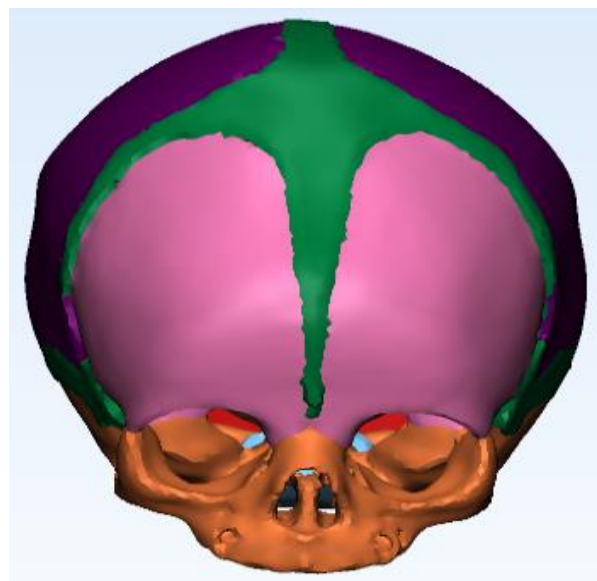
(a)



(b)



(c)



(d)

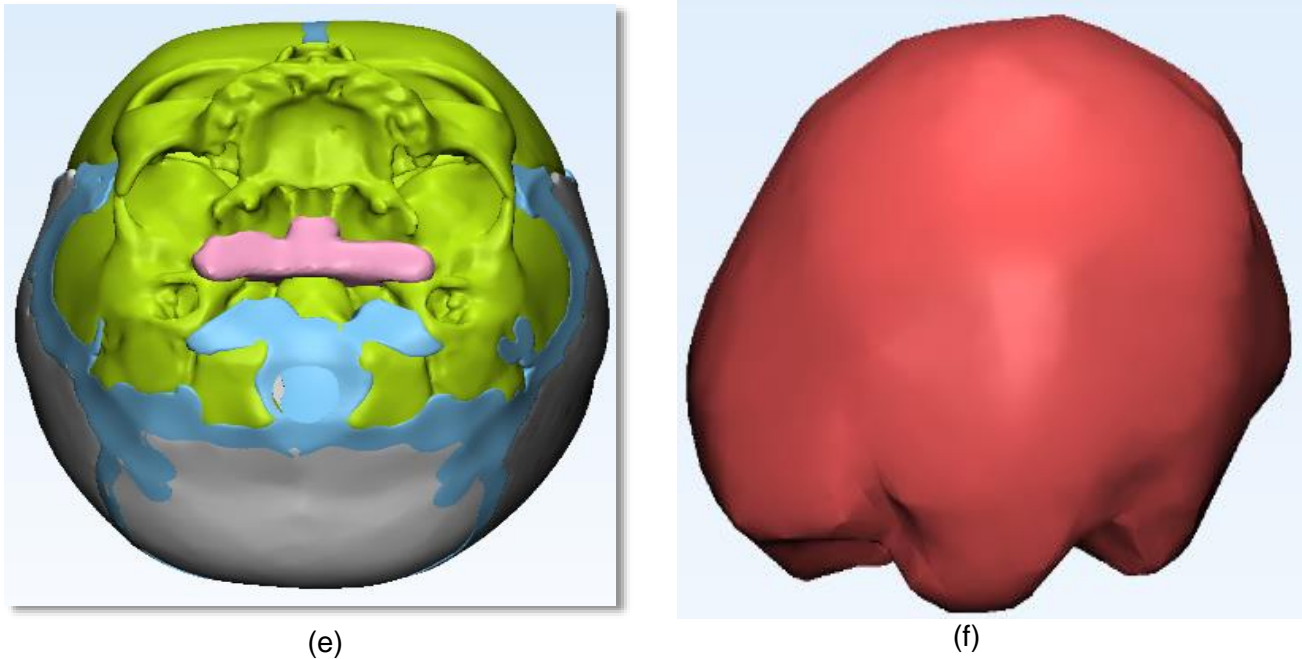


Figure 2.1. Representation of major tissues within the head (a) CT scan (b) cranial bones (c) sutures (d) cranial bones and sutures (e) base of the skull (f) brain.

2.2 Physical modelling of paediatric head surrogate.

2.2.1 Bidirectional properties of paediatric bone.

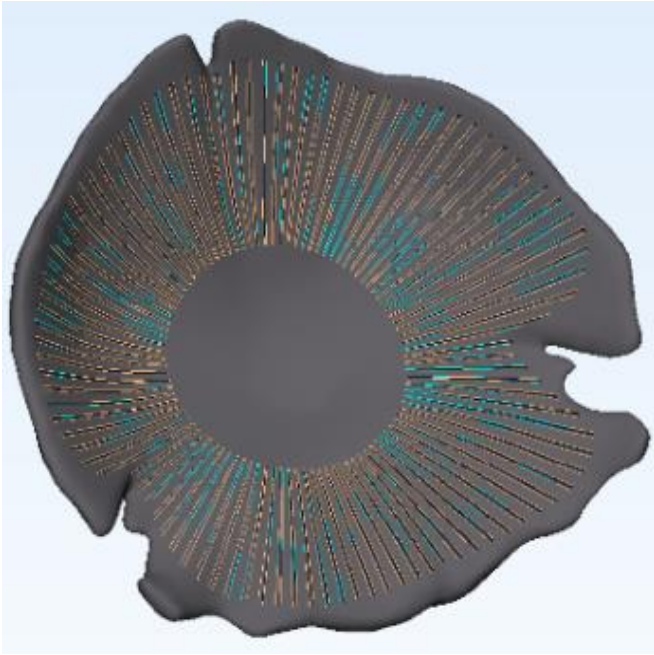
McPherson and Kriewall [64] determined that infant skull bone is approximately four times stiffer in line with its radial trabeculae, identified as having a fibrous appearance, compared with the perpendicular orientation. To improve the biofidelity of the model bones, during impact, an attempt was made to mimic their anisotropic properties. This anisotropic nature could not be directly replicated by the printed materials, however, a solution to this problem was instigated during the development of the 3D data. To mimic the anisotropy a material was selected, which reproduced stiffness in line with the radial direction and very fine radial grooves, emanating from estimated centres of ossification, were designed into the model. The depth of these grooves was determined, such that

the second moment of inertia (I), for the circumferential direction was a 1/4th of that for the radial, using the equation (2.5) [95]:

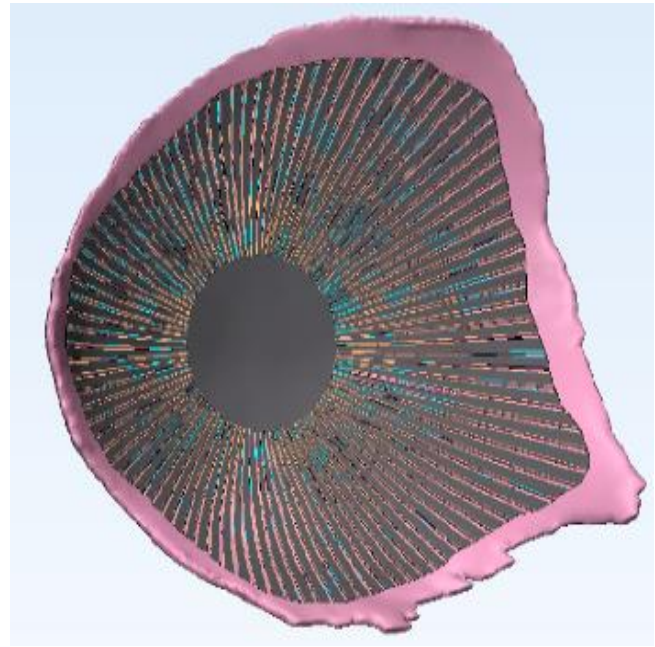
$$I = \frac{bd^3}{12} \quad (2.5)$$

where the breadth, b , was taken as constant and the original thickness of the bone, d , was determined as the mean of the thickness, taken at a number of different points. There is no breadth (b) to the skull bone and the shape overall is very complex, thus to solve/simplify this problem, this study considered a very small section of material as a simple beam. The equation 2.5, provides a quantity, that is the second moment of area, which is directly related to the stiffness of a standard rectangular beam of cross sectional dimensions (b) and (d); from which the stiffness of the skull was reduced by a factor of 4 in the circumferential direction, to allow it to behave anisotropically like the paediatric bone in the reported paper by Kriewall [64].

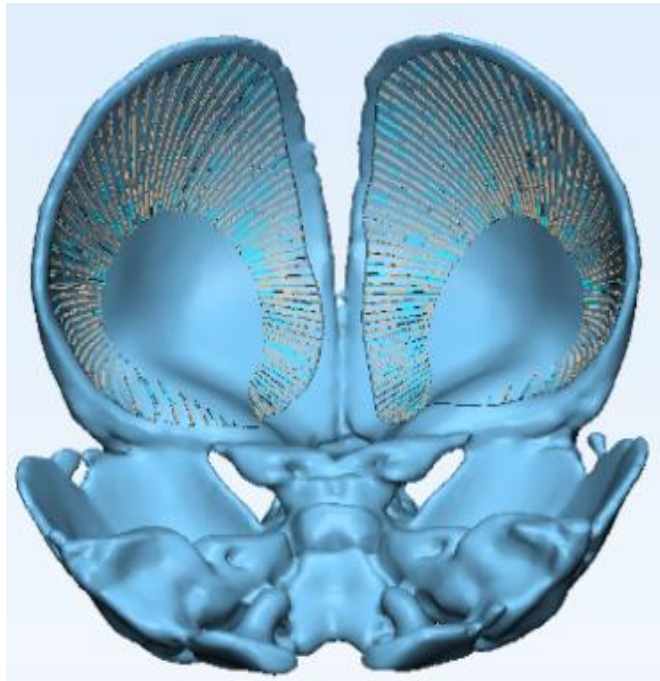
The stiffness of the 'simplified element' is proportional to $D^3/12$. The stiffness in the circumferential direction needed to be a quarter of that of full skull thickness, so D was changed to make $D^3/12$ a quarter of the size. The breadth, in this study, is irrelevant because it is the same for both the full D and reduced D situations. The groove was created and cut based on this equation in the whole bone to the same depth, so the depth of the grooves did not vary within any skull bone. The representation of anisotropic properties for cranial bones is shown in Figure 2.2.



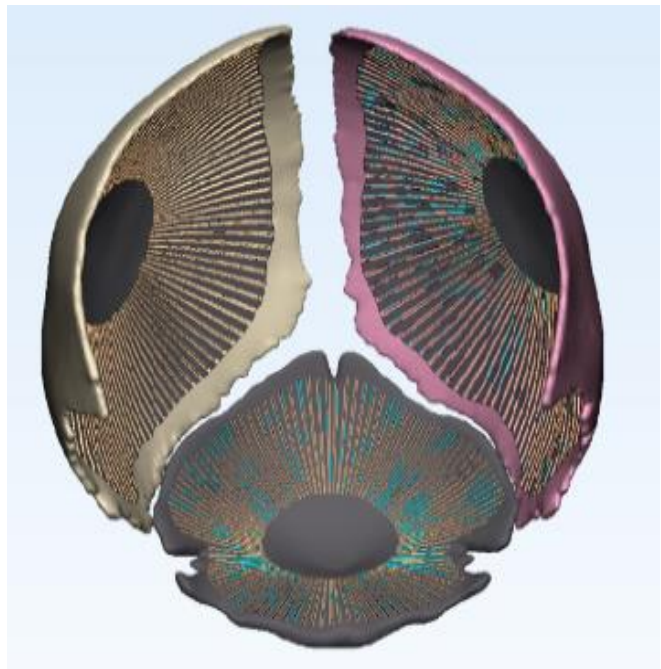
(a)



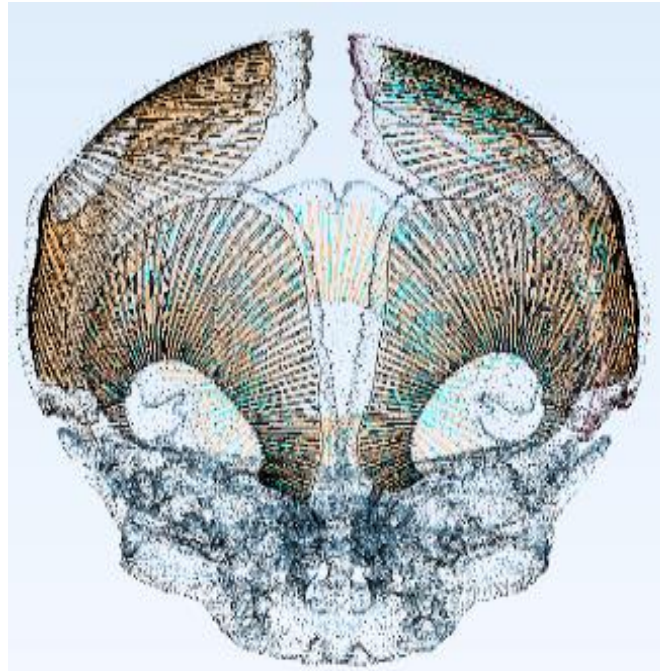
(b)



(c)



(d)



(e)

Figure 2.2. The fibrous grooves of cranial bones of surrogate cranial bones model (a) Occipital bone (b) Right parietal bone (c) Left parietal bone (d) Frontal bones (e) Assembly of the cranial bone.

2.2.2 Material selection of bone and sutures.

2.2.2.1 Mechanical characterization of the Poly Jet printed materials.

Opportunities to investigate human infant tissues are rare, either as a result of ethical or moral reasons and once tested to failure, cannot be retested. Additive manufacturing (AM) could potentially solve these issues since material matched materials can be printed to reproduce the complex geometry of the infant skull as many times as is required, quickly and to micrometer accuracy. Therefore, if suitable materials can be found and validated, it is feasible to produce realistic models (physical / computational) of the infant skull to facilitate testing of different impact scenarios. To rectify the previous issues and benefit from the AD technology, a physical polymeric model of a 10-day-old infant skull was produced, using the reported Poly Jet printed polymeric materials from the

manufacturer data sheet, see Table 2.2 [96, 97]. Hence this physical model can be used to investigate the biomechanics of different impact scenarios, injury thresholds and the validation of computational models. As outlined in the literature, there has been extensive characterisation of the dynamic material properties of adult skull tissue [62, 63]. However, the dynamic properties of the paediatric skull and suture remain relatively limited/unknown. The skull of the infant consists of thin, flexible plates, composed of partially calcified bony tissue joined at their margins by membranous sutures. In contrast to the stiff adult cranium, the infant skull is a compliant structure, capable of substantial deformation under external loading [37]. Meaning that scaled down adult criteria are not applicable to children or infants. The paucity of data in this field, means that further research is required.

Furthermore, there are very few studies on the material properties of paediatric cranial bone and sutures that exist in the literature or their minimum-maximum stiffness values and tensile strength values of infant cranial bone and sutures, as in Tables 1.1 and 1.2, respectively. These polymeric materials from the Stratasys data sheet [96, 97] were matched to the few mechanical properties values of the infant cranial bones and sutures available in the literature, as shown in Tables 1.1 and 1.2, including the variation of different bones in the infant head. The polymeric materials that will constitute the infant physical model are VW "RGD835 Vero White Plus" (hereinafter known as White); replicating frontal and parietal bones, 25 "RGD8510-DM RigidLightGrey25" (hereinafter known as Grey); replicating occipital bone and 70 "FLX9870-DM" (hereinafter known as Black) replicating the sutures. However, regarding the digital materials, whilst the Poly Jet technology allows a wide range of material properties to be printed, there is no

numerical data available which defines their specific material properties, hence there is a requirement for this work.

For printing purposes, the manufacturer provides a range of material response properties, to describe the PJP materials used in the construction of the physical model, rather than discrete values, as shown in Table 2.2. Hence, investigation and validation of these polymeric materials, against reported mechanical properties of infant cranial bones and suture, is required.

Table 2.2 Material properties of White, Grey and Black, data from Stratasys (2016, 2016c) [96,97]

Material	Tensile strength (σ_{uts})/MPa	Elongation at failure (ϵ_{max})/%	Modulus of elasticity (E) /MPa
RGD835VeroWhitePlus (White)	50-65	10-25	2000-3000
RGD8510-DMRigdLightGrey (Grey)	40-60	15-25	1700-2300
FLX9870-DM (Black)	3.5-5.0	65-80	none given

The possible types of injuries, resulting from low height falls, are more likely to be identified if the dynamic material properties of the paediatric suture and cranial bones are known. Material properties, such as elastic modulus, ultimate stress and ultimate strain dictate the response and failure of a material to loading. The elastic modulus is an indication of the stiffness or resistance to deformation, of a material. The ultimate stress and strain are indications of the maximum force and deformation, which the material can undergo before it fails. Determining the material properties of paediatric skull, suture and fontanelles will not only provide insight into the reaction of the paediatric cranial cavity to

loading, but will also improve the accuracy of computational and experimental models simulating falls or impacts to a paediatric head.

To create a physical polymeric model of a newborn infant skull, using Poly Jet printed materials, infant skull materials responses, were matched by a response characterisation study, utilising uniaxial tensile testing (1 mm min^{-1} loading rate), to determine: the stiffness, ultimate tensile strength and maximum strain of rigid and rubber additively manufactured acrylates (White, Grey, and Black). Comparisons were made between the mechanical output values with reported material properties of tissue samples and supplier data, to justify the use of these materials in the construction of the physical model to ensure they were close to reality.

2.2.2.2 Specimen preparation and mechanical testing.

The experimental work involves producing “dog bone” specimens of Grey, White and Black materials and testing them for structural strength. A CAD model of the dog bone specimen is designed, using SolidWorks software 2017 following the British Standard for Additive Manufacturing [98 to comply with type 1BA of BS EN ISO 527-2:2012 [99, 100], see Figures 2.3 and the dimensional details in Table 2.3. Six test specimens of each material were printed in an XYZ orientation, via additive manufacturing, see Figure 2.4. Once the test specimens were designed and printed, uniaxial tensile tests are performed on these specimens for structural response, see Figures 2.5. The recommended velocity of testing for 1BA specimens is dictated by BS EN ISO 527-2:2012 [102, 103], as “the ratio of the speed of testing ... versus the initial distance between the grips ... recommended to correspond to $1\% \text{ min}^{-1}$, where this value is compared to Table 2.3 of BS EN ISO 527-1:2012, to find the closest applicable rate. In this case 1%

$\text{min}^{-1} = 0.78\text{mm min}^{-1}$, which corresponds to 1mm min^{-1} in Table 2.3. The mechanical test conducted to investigate the mechanical properties of the Grey, White and Black materials that will comprise the infant physical skull model at an ambient temperature. The materials were tested using the uniaxial tensile test machine Zwick 100 at a cross head speed of 1mmmin^{-1} , see Figure 2.5.

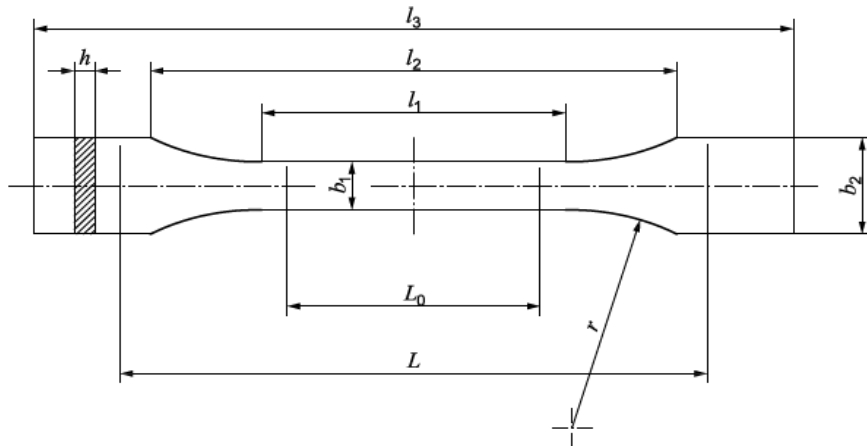


Figure 2.3. Test specimen design as recommended by British Standards Institution (2012) [98], [99].

Table 2.3. . Dimensions in mm of type 1BA test specimen (BS EN ISO 527 2:2012) [99].

	Description	Type 1BA
l_3	Overall length	≥ 75
l_2	Distance between broad parallel-sided portions	58 ± 2
l_1	Length of narrow parallel-sided portion	30 ± 0.5
r	Radius	≥ 30
b_2	Width at ends	10 ± 0.5
b_1	Width at narrow portion	5 ± 0.5
h	Preferred thickness	$\geq 2 \pm 0.1$
L_0	Gauge length	25 ± 0.5
L	Initial distance between grips	$l_2 + 20$

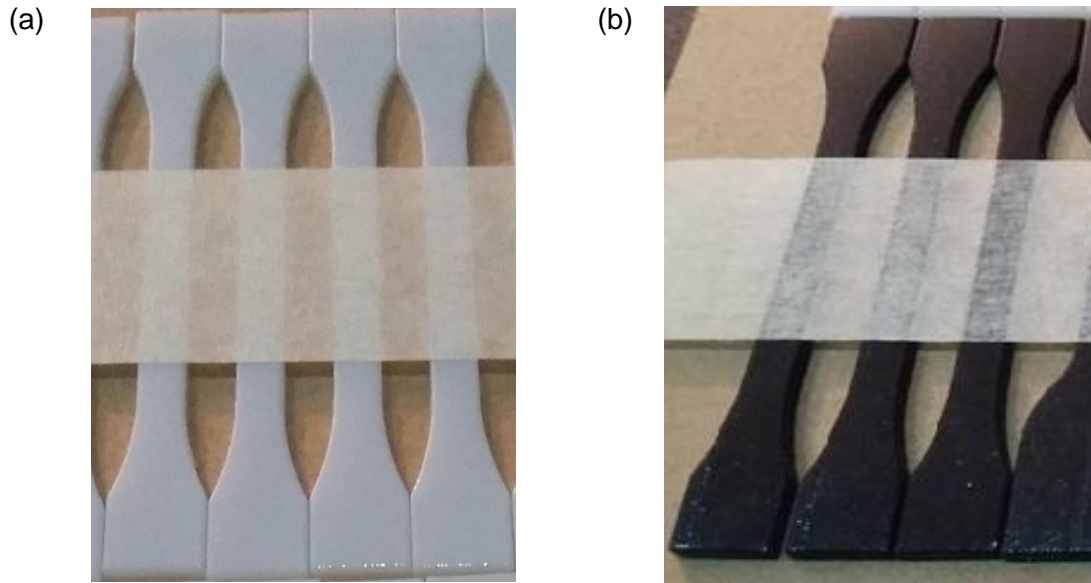


Figure 2.4. 3D Printed specimens of (a) White and (b) Black materials.

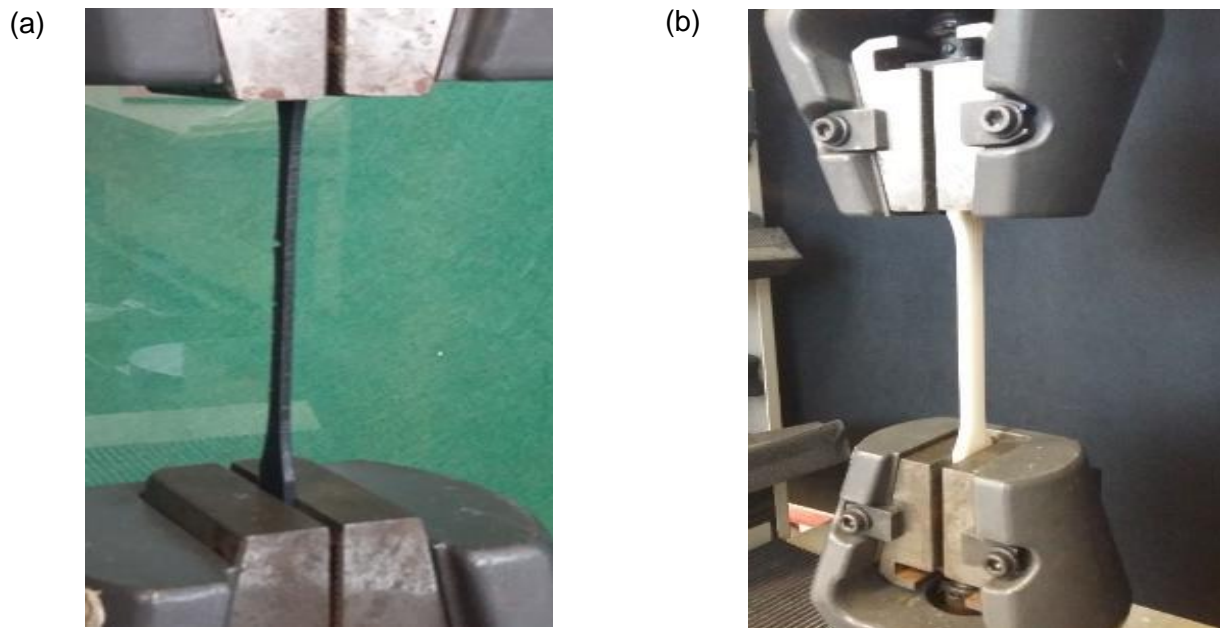


Figure 2.5. Uniaxial Tensile testing of printed specimens (a) Black and (b) White materials

2.2.2.3 Mechanical Measurement

Stress, σ , is defined as the force, F , applied per unit area; strain, ϵ , as the deformation (change in length, dL/L) under that load. Engineering stress is given with respect to original cross-sectional area, A_0 , as in equation (2.6). Engineering strain, is strain with respect to original length, L_0 as in equation (2.7). Deformation occurs elastically (temporarily) or plastically (permanently). A measure of a material's elastic deformation is its elastic modulus (E), as in equation (2.8). In tension, this is obtained from a tangent to the slope of the initial linear aspect of a stress-strain curve, as an example of Grey and White materials see Figures 2.6.

$$\sigma_{eng} = \frac{F}{A_0} \quad (2.6)$$

$$\epsilon_{eng} = \frac{dL}{L_0} \quad (2.7)$$

$$E = \frac{\delta}{\epsilon} \quad (2.8)$$

During a linear elastic deformation, a material deforms elastically and returns to its original dimensions upon removal of the load. As an example, see Figure 2.7, which represents the typical stress-strain curve of a rigid polymer. The proportional limit is the point at which elongation is no longer linearly proportional to stress, however, though the material would still return to its original dimensions on removal of the load. The maximum load a material can sustain, while deforming elastically, is the yield stress (σ_{yield}). Further

loading past this point, results in plastic deformation and the material not returning to its original dimensions on removal of the load. Ultimate tensile strength (σ_{uts}) is the maximum stress a material can sustain. The area under the graph gives the energy absorbed to failure, a measure of toughness. Engineering (σ_{uts}), (ϵ_{max}) and the modulus of elasticity (E) have been calculated as these are the measures reported in the literature for infant cranial bones and sutures, see Tables 1.1 and 1.2. Plastic deformation, in even the most rigid of the rubberlike materials was negligible in contrast to elastic. Depending on the material, the method of calculating the moduli differed. For the materials White and Grey a single tangent modulus was sufficient to describe the behaviour of the whole curve, see Figure 2.6. For Black material, (E) varied with % strain, thus multiple tangent moduli have been given and corresponding strains specified see Figure 2.8.

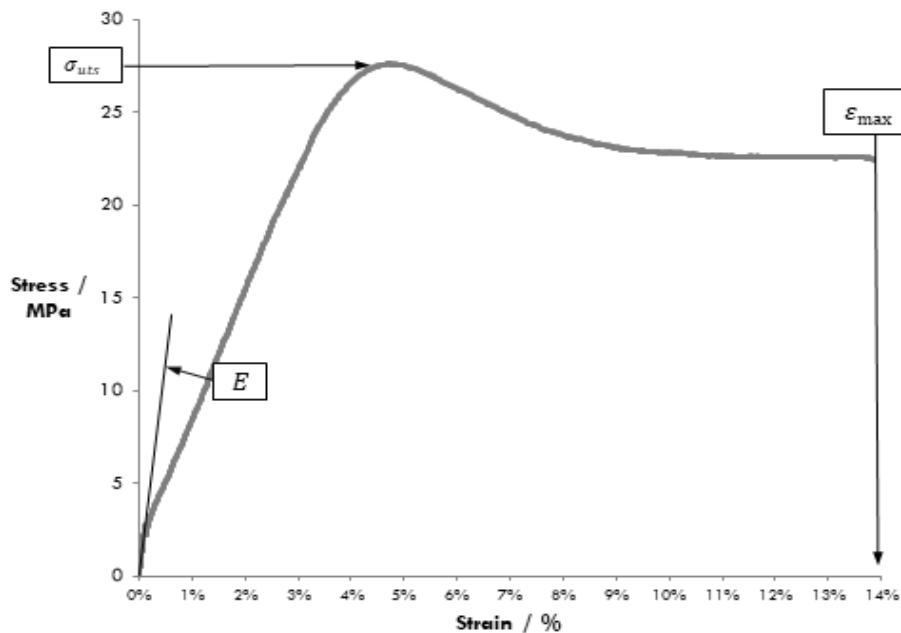


Figure 2.6. Calculation of elastic modulus of Grey and White materials. (Illustration of the relevant tensile stress-strain properties evaluated during this study).

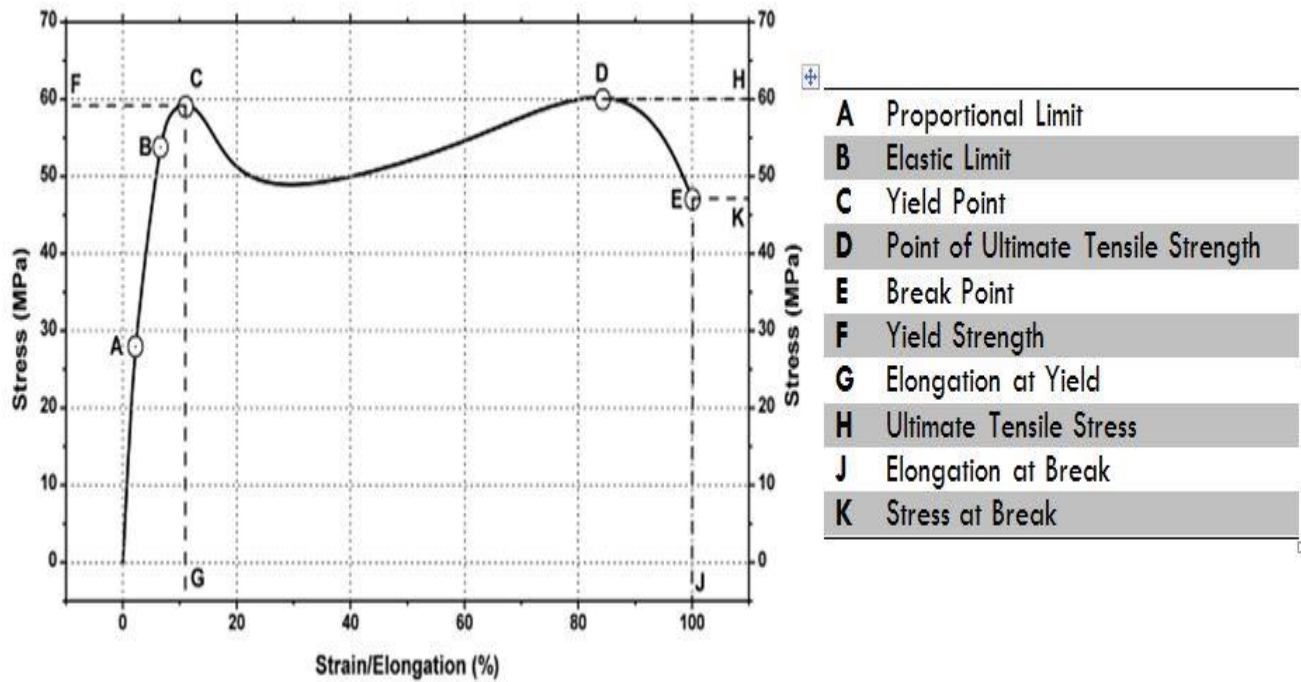


Figure 2.7. Typical stress-strain curve of a rigid polymer [101].

During the mechanical testing, the force – displacement curves of the specimens were recorded. Once the testing of the materials specimens were finished, the raw output data (force and extension) were zeroed and used in equations (2.6 – 2.8) to calculate engineering ultimate tensile stress (σ_{uts}), engineering ultimate strain (ϵ_{max}) and engineering elastic modulus (E) to 0.1% strain of the White, Grey and the Black materials. Further engineering elastic modulus (E) to 1%, 10%, 20% and break point strain were calculated. Where F is the measured force, A is calculated from the width (w) and thickness (t) of the specimen. The data are presented as mean \pm SD.

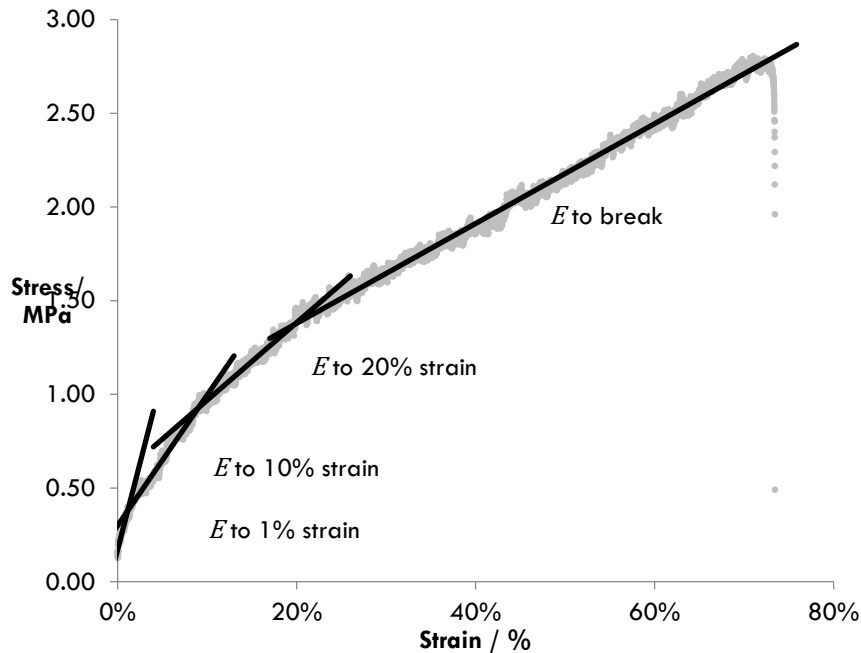


Figure 2.8.

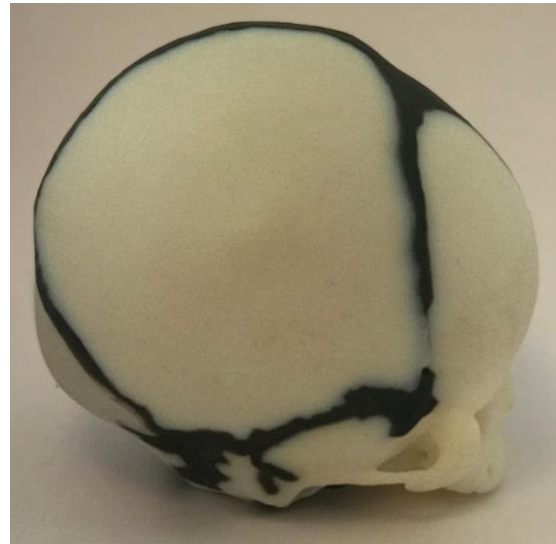
Method of calculating multiple tangent moduli for less stiff rubberlike materials (Illustration of the relevant tensile stress-strain properties evaluated during this study).

2.2.3 Manufacturing of the 3D printed physical head model

The physical infant head model was manufactured using Poly Jet 3D printing technology, since it allowed the production of a model with more than one material and therefore, more than one material property. The final 3D CAD design of the head was imported to the 3D printer to produce the physical head model of a 10-day-old child, shown in Figure 2.9. During printing, two different materials, with different material properties, were combined in different proportions to produce different physical properties at different points in the model. The suture geometry and thickness can be precisely controlled and the “joint” between suture and bone are a seamless run of printed material, absent of physical discontinuities.



(a)



(b)



(c)



(d)

Figure 2.9. Physical 3D models produced by Rapid Prototyping technique. (a) Frontal view. (b) Side view (c) Coronal view (d) the base of the head.

2.2.4 Modelling and material properties of brain and scalp.

To model the brain, a surrogate brain material, gelatin (10% gelatin: 90% water) was injected into a rubber balloon in the brain cavity through the foramen magnum of the 3D printed head model, in accordance with a previous study by Cheng et al. (2010) [102], which conducted a dynamic tensile test and modelled the gelatin as a brain surrogate material. Once the liquid gelatin had set, the foramen was sealed. A surrogate scalp (a pad based on latex rubber, in combination with a polyamide micro fleece), representing the elastic and frictional properties [103] of the scalp, was applied to the outer contact surface of the skull, whilst leaving the skull surface uncovered for the application of the random speckle pattern for subsequent digital image correlation analysis.

2.3 Global validation and regional, local investigation of paediatric physical surrogate

2.3.1 Digital Image Correlation

Digital Image Correlation (DIC) is a full-field displacement and strain measurement technique that is becoming more popular due to the availability of efficient, affordable tools such as cheaper imaging devices and more powerful computational methods. DIC is important because it allows analysis where single measurements, such as strain gauges, do not provide sufficient data. Most importantly, however, it allows contactless analysis, perfect for both hostile environments, such as high temperature or corrosive surfaces [104] or where traditional gauges will directly influence another variable in the test, skewing the results [105]. It is also useful in confirming FE analysis models, where direct measurement comparisons can often be made [106].

Significant advances have been made in the field of DIC in the last few years, mainly due to the improvement in computational algorithms to create higher accuracy deformation measurements [107,108,109]. Initially, DIC was limited to 2D applications, however this is unsuitable for out-of-plane deformation. In these instances, 3D DIC can be performed by utilising a stereo camera setup [110].

2.3.2 Subset correlation and speckle Patterns

DIC works by analysing two images relative to one another. The often compared images are those of video photographic frames, where the resolution or size of the frames is defined by the size of the sensor within the camera and its capabilities. Where grey-scale cameras are used; the images themselves are made up of pixels that store a grey-scale value depending upon the intensity of the light that the sensor 'sees' at a particular point. Regardless of bit depth, the minimum, or zero value, is taken to be black and the maximum value (255 at 8 bits per pixel, 65 535 at 16 bits per pixel) is white, unless otherwise stated. DIC works by comparing the signature of each pixel in a reference image to its related pixel in the deformed image. The signature of a pixel is characterised by the pixels immediately surrounding it, where the pattern of values can be tracked using mathematical methods, which allow the displacement of the original pixel to be determined. This collection of pixels is called a subset or correlation window [111]. The subset size should be determined by the speckle pattern. Specimens that are to undergo DIC analysis need to have a speckle pattern applied. Due to the nature of the testing an isotropic and non-periodic pattern should be applied in a manner that adheres to the surface and will deform with the surface, so there is no loss of correlation throughout testing [112]. To obtain an area with a random, non-repetitive pattern a black-white

speckle pattern, either ink can be directly applied or spray paint, via 'splattering'. In certain cases, if the specimen itself exhibits a natural speckle on its surface, the contrast of the image can be enhanced and adjusted to create an adequate pattern [113]. The DIC analysis software can then determine possible matches of each subset between both the reference image and the deformed image. With these matches the correlation software can determine the displacement of the centre pixel in the subset and as every pixel has its own subset, the software can then calculate the displacement for each pixel in turn. When every subset's displacement has been calculated, a displacement field can be applied over the deformed image, showing the displacement of the marked specimen as a whole. During DIC, it is extremely important that the lighting of the specimen remains constant between the reference image and the subsequent displaced images. Any 'mid capture' shadowing of the speckle pattern, during exposure, may lead to the reading of erroneous pixel values and will directly affect the subset displacement calculations and hence, the overall displacement field calculations.

2.3.3 High Speed Video

High speed video is an essential tool for the investigation and analysis of impact testing [114]. Yet it also has a vital place in other areas of engineering, from motion testing [115], to manufacturing analysis [113]. In the last 15 years or so, the cost/performance ratio of the technology has drastically improved, leading to a much greater uptake in the engineering industry. The DIC software has been proven to function adequately by improving the reliability, quality and repeatability of image collection from the high speed video cameras, most importantly attempting to cover a wide range of possible scenarios for which the cameras can be used. The limiting factors, in being able to produce

sufficient images for DIC analysis, are often parameters such as brightness, resolution and focus, as most other parameters are fixed. The luminosity (lighting) of a specimen will directly affect the signal generated at each pixel on the sensor. It is very important that the specimen is correctly lit, so that detail is not lost in each frame. If the specimen is too dark or too bright, or is reflective the DIC software will be unable to generate good results, as it relies on good contrast between the lights and darks within a speckle pattern. Ideally the specimen will be lit in such a way that both the blacks and the whites in each frame are easily differentiated by the camera. Brightness can be increased by opening up the aperture of the lens, although this comes with drawbacks in terms of focus. The most common method is to use direct lighting, with increasing amounts of light intensity with higher frame rates. The output resolution of each frame from the camera will define how much detail is recorded. This detail will determine how distinct the black/white transition of the speckle pattern is, the better defined, the better the image correlation will work [112]. It is vital that the specimen is in focus throughout the entire test, as any out of focus data will provide unusable results. If the lens is capable, it is advisory to zoom on the specimen with the lens aperture wide open to adjust focus. This will allow greater room for error when the camera is adjusted back for testing, as the depth of field will be increased at the smaller apertures. The DIC analysis software will be unable to process an image that has unacceptable focus. Blurring occurs because the specimen moves during the time frame that the sensor is exposed, this will be dependent upon the shutter speed of the camera. Even at high frame rates such as 1000 fps, where the shutter speed is 1000 microseconds, movement is still likely to occur in certain situations such as fast fracture. Increasing the frame rate and shutter speed will solve these problems, although

this comes with other consequences, such as less light entering the camera each frame, hence the specimen will need to be lit with higher intensity. To reduce this, a sensible frame rate should be chosen for each application, adjusting for the best compromise possible. If possible, test specimens should undergo deformation, to establish that the cameras are capturing correct, clear detail in the speckle pattern.

2.3.4 Experiential setup and procedures

For paediatric populations, there are very few experimental impact tests that can be applied to validate a new physical model of a newborn. To the author's knowledge, only Prange et al. [82] provide sufficient data to validate the global impact behavior of a paediatric head. Prange et al. [82] conducted impact tests with three infant post mortem human surrogate (PMHS) heads (1, 3 and 11 days old) from 0.15 m and 0.30 m, onto five different impact locations (frontal, vertex, right and left parietal and occipital bones) onto a steel force plate. During the PMHS tests [85], the infant head was considered as a rigid body for the purpose of deriving impact acceleration – time curves from the impact force produced at the force plate, by dividing the force by the mass of the infant PMHS head. However, the average peak acceleration of the PMHS head is significantly different for different drop heights but not impact location [82]. An experimental methodology was established to replicate Prange et al.'s [82] force plate experiments, the physical model was raised via a length of cord to two different heights 0.15 m and 0.30 m and dropped by transection of the cord, onto four impact regions resembling the physiological region of the vertex (superior–inferior (SI) direction), forehead (antero-posterior (AP) direction), parietal (left right (LR) direction).and occiput (postero anterioror (PA) direction)

on a metal force plate (Type 4060H, Bertec Corporation, Worthington, OH) as shown in Figures 2.10, 2.11, 2.12 and 2.13.

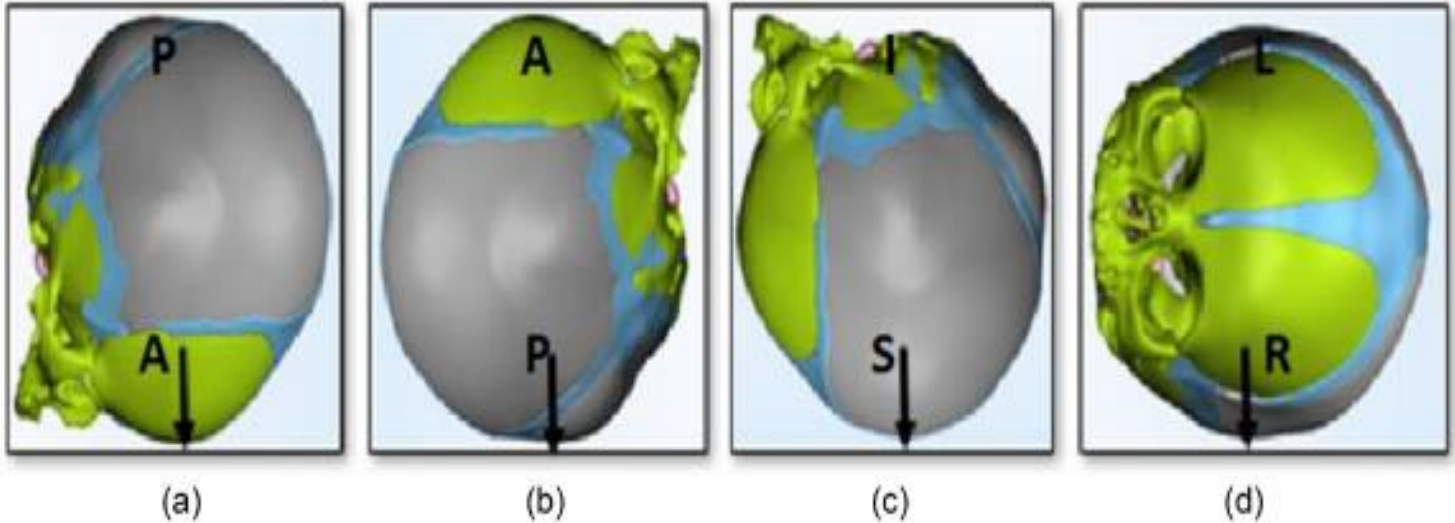
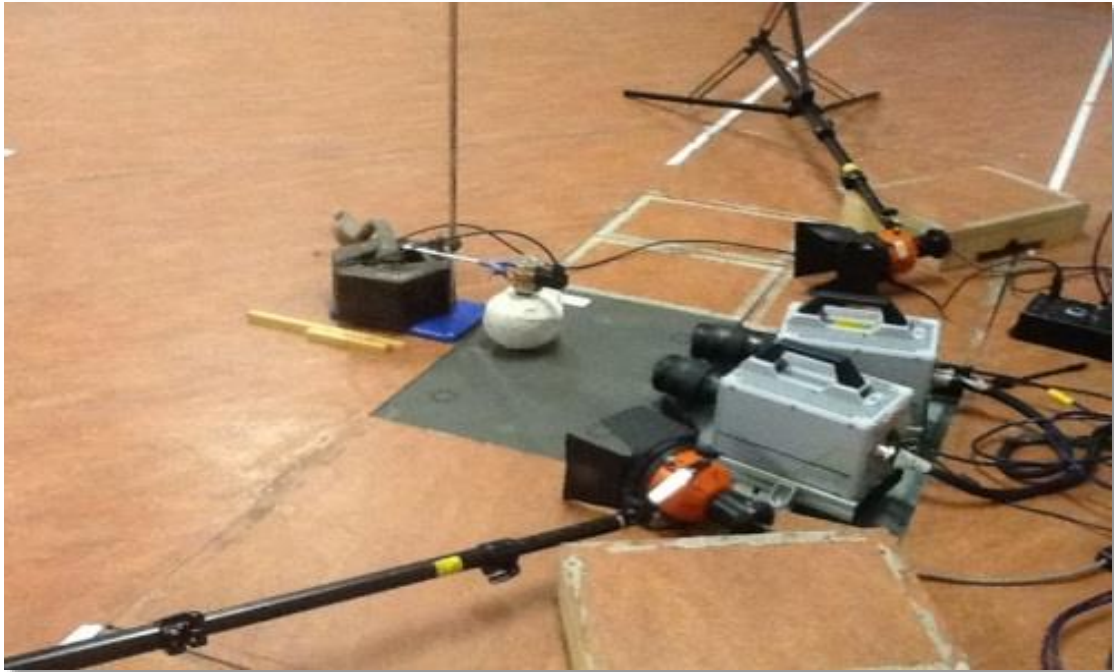


Figure 2.10. Head drop test orientation. (a) frontal bone impact with an arrow illustrating antero-posterior (AP) direction, (b) an occipital impact with an arrow illustrating postero anterior (PA) direction, (c) vertex impact with an arrow illustrating superior–inferior (SI) direction, (d) parietal impact with an arrow illustrating the left right (LR) direction.

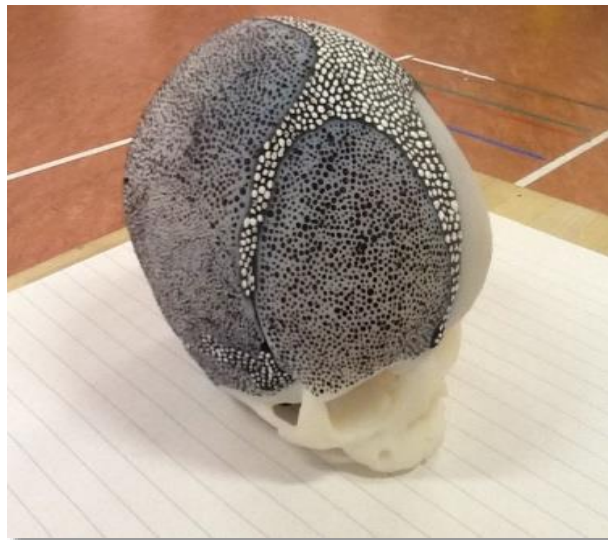
In addition, a High Speed-Digital Image Correlation (HS-DIC) system was applied; high speed video was coupled with an image correlation software to determine how different regions of the skull deformed when subjected to a short fall impact loading. The physical head model was suspended at the required heights and dropped onto the force plate, to permit comparison/validation with Prange's [82] study as illustrated in Figure 2.11a. The HS-DIC system, which uses two high speed cameras capable of taking images up to 100 kHz, was positioned on the floor to video the impact of the drop tests at 10 kHz. Since the HS-DIC system is typically used to analyse strain in structures when subjected to rapid loading and the physical model structure was falling through larger distances than is usual when using this technology, interest was in both macro motion, of the falling head, and the relative micro motion of individual structures.

Hand painted speckle patterns were found to be the most effective method for generating a random speckle pattern, as shown in Figure 2.11b and Figure 2.12, since they allowed the identification of their relative positions and calculation of the different physical parameters during their movement relative to one another. In Figure 2.11b, the manually painted acrylic speckle pattern has been added to half of the 3D printed model. For clear contrast, the black paint was used on the white surface of the bones, whilst white was used on the black surface of the sutures.

A series of known patterns were used to calibrate the camera, such that the software could distinguish the relative movement of each unique speckle to determine the deformation, velocity, strain, strain-rate and relative rotation between speckles. Thus, a more accurate consideration of the paediatric head model and the impact response to short falls as a whole could be achieved. From the initial trials and set up of the HS-DIC system, the greater the contrast between the speckle pattern and the background, the better the DIC measurements, see Figure 2.12. Thus, it appeared that the brighter the model the greater the contrast between the black speckles and the white background.

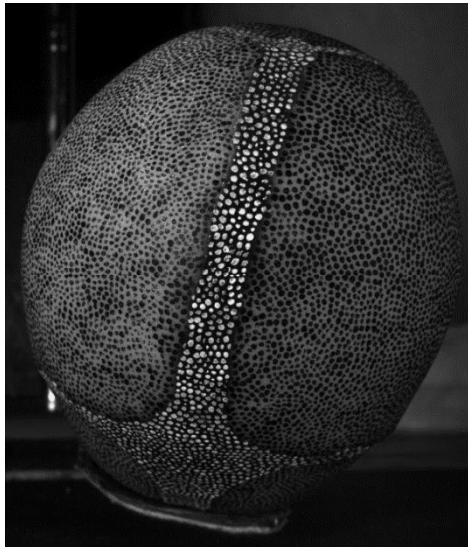


(a)

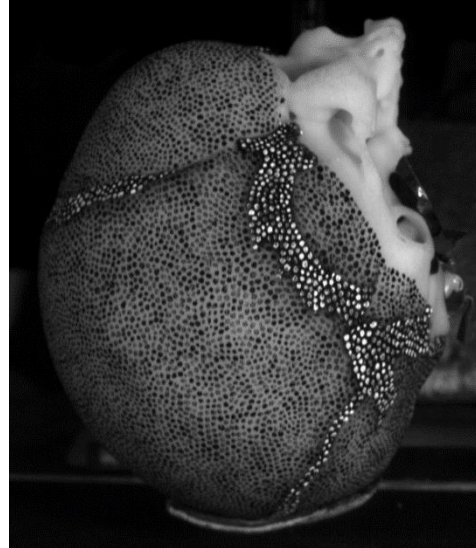


(b)

Figure 2.11. (a) Experimental setup of physical model for perpendicular drop onto force plate, (b) 3D printed physical model with speckle patterns.



(a)



(b)



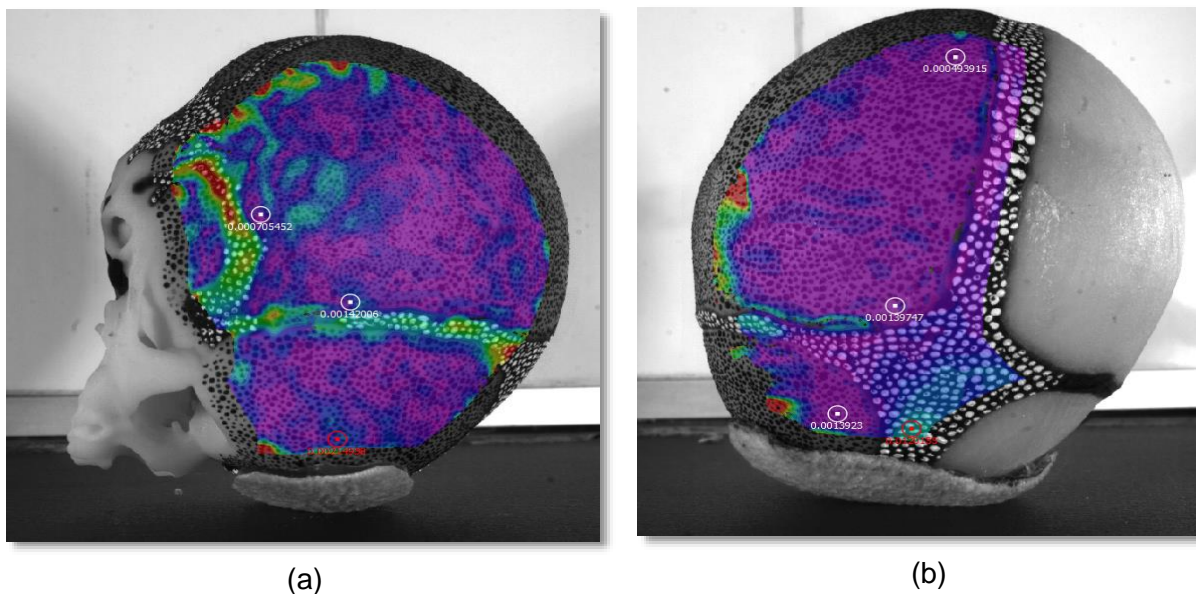
(c)

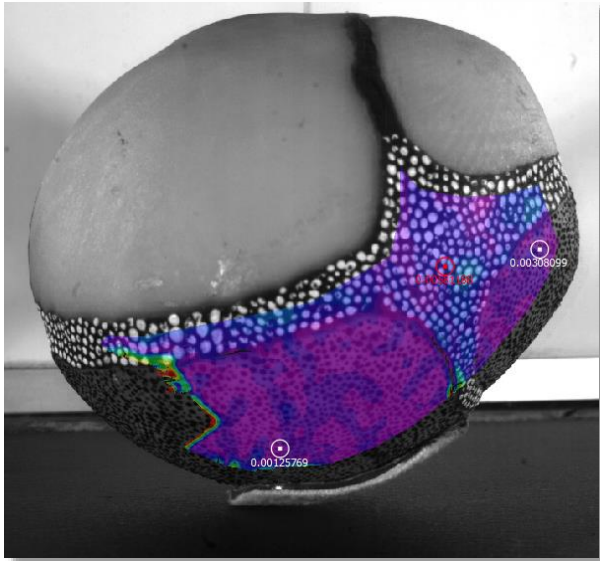


(d)

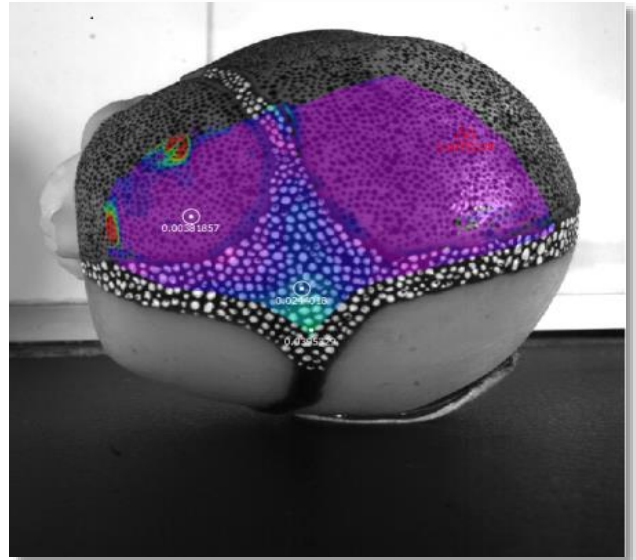
Figure 2.12. Physical head drop test orientation with the contrast of the speckle pattern (a) frontal bone impact, (b) occipital impact, (c) parietal impact and (d) vertex impact.

Out of experimental necessity, the approach taken by Prange et al. [82] was to consider the head as a rigid body, rather than a soft pliant structure, such that to derive impact acceleration values (a correlate for head injury risk), the head impact force at the force plate was divided by the mass of the head. Since the infant skull is not a rigid body, consisting of a number of flexible plates, flexible sutures and fontanelles, the acceleration-time waveform provides only a “form of averaging” of the total response of the head. This approach is incapable of providing localised area specific details with respect to head response. The HS-DIC system allows for collection of a large amount of information; thus, it was important to determine which points to choose during analysis. Given that each physical model impact was different, the selection of the point of analysis had to be made on an individual point-by-point basis, to determine which areas represented the greatest velocity, strain rate and deformation, as shown in Figure 2.13.

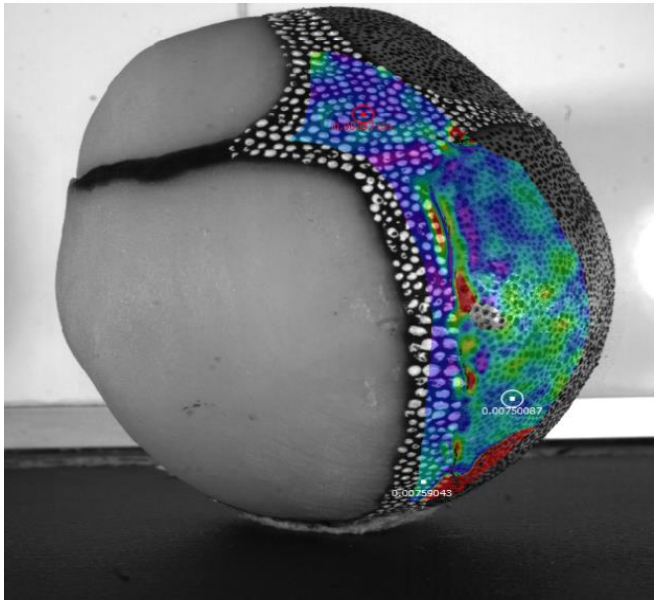




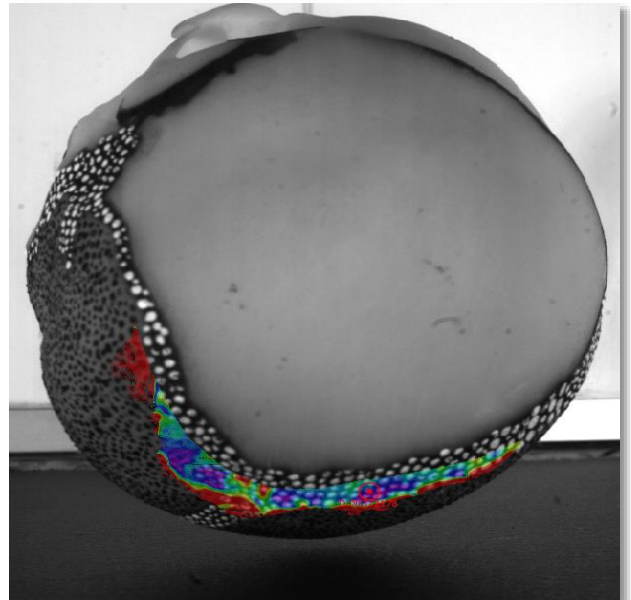
(c)



(d)



(e)



(f)

Figure 2.13. (a,b-forehead, c,d-parietal, e-occipital and f-vertex) Digital Image Correlation of the physical model impact tests.

2.3.5 Output variables and statistical analysis

The global kinematic variables from the force plate approach were peak translational acceleration and duration of impact. These variables are measured from the force plate on impact point at a frequency sampling of 10 KHz. The measured voltage from the force plate was converted to its equivalent force, using a sensitivity value and the impact accelerations derived from the force data, via Newton's 2nd law, using (2.9). Where F is the force from the impact point, M is the mass, a is the translational acceleration.

$$F = M a \quad (2.9)$$

For global validation purpose, two indicators were used to compare head performance of the physical model with the PMHS experiment (a) peak acceleration values (g) and (b) correlation score. The first measure used the peak values at discrete spatial points, whereas the second measures used the 'full-field' spatial information, signified by the two statistical measures RMS error (RMS) and correlation score (CS), between the model and the experiment for model evaluation. The function of the models is evaluated using CS, to assess the agreement between the model prediction and the measured acceleration–time impact curves in terms of phase (N-phase), amplitude (N-amp) and shape (N-shape) [92,116]. The CS values range from 0 to 100, which are classified according to a biofidelity rating [117]. The qualitative index is categorised into five classifications as: Excellent: $86 \leq CS \leq 100$, Good: $65 \leq CS < 86$, Fair: $44 \leq CS < 65$ Marginal: $26 \leq CS < 44$ and Unacceptable: $0 \leq CS < 26$. The error measures (N-phase, N-amp, N-shape), estimated by the NISE method, are used to calculate a CS value. To

compute N-phase, N-amp, N-shape, for two discrete time histories X_i and Y_i , four correlation functions are defined and expressed as in (2.10—2.13):

$$R_{XY}(0) = \frac{1}{N} \sum_{i=1}^N (X_i Y_i) \quad (2.10)$$

$$R_{YY}(0) = \frac{1}{N} \sum_{i=1}^N (Y_i Y_i) \quad (2.11)$$

$$R_{XX}(0) = \frac{1}{N} \sum_{i=1}^N (X_i X_i) \quad (2.12)$$

$$R_{XY}(t)_{\max} = \frac{1}{N-n} \sum_{i=1}^{N-n} (X_i Y_{i+n}) \quad (2.13)$$

Where N is the number of data points in each curve, t is the time delay that maximises function $R_{XY}(t)$, n is the time shift index and is defined as τ divided by the constant time step. The measures of the NISE, according to phase shift (N-Phase), amplitude difference (N-amp) and shape difference (N-shape) are defined as in (2.14 - 2.16):

$$N - \text{Phase} = \frac{2R_{xy}(t)_{\max} - 2R_{xy}(0)}{R_{xx}(0) + R_{yy}(0)} \quad (2.14)$$

$$N - \text{amp} = \frac{R_{xy}(t)\text{max}}{\sqrt{R_{xx}(0) + R_{yy}(0)}} - \frac{2R_{xy}(t)\text{max}}{R_{xx}(0) + R_{yy}(0)} \quad (2.15)$$

$$N - \text{shape} = 1 - \frac{R_{xy}(t)\text{max}}{R_{xx}(0) R_{yy}(0)} \quad (2.16)$$

The CS is then defined as in 2.17 -2.19:

$$CS_{N-\text{Phase}} = 100 - (1 - N - \text{Phase}) \quad (2.17)$$

$$CS_{N-\text{amp}} = 100 - (1 - N - \text{amp}) \quad (2.18)$$

$$CS_{N-\text{Shape}} = 100 - (1 - N - \text{shape}) \quad (2.19)$$

while the local kinematic variables (translational acceleration, duration of impact and rotational acceleration) and head deformations (strain and strain rate) were measured from discrete points of the skull, using the HS-DIC approach. The deformation of the head was measured in four directions, anterior-posterior (AP)/ forehead impact, posterior-anterior (PA)/ occipital impact, Left - Right (LR)/parietal impact and superior- inferior (SI)/vertex impact. The maximum head strain was taken as the maximum of the head strains in each of the four directions (AP, PA, LR and SI). All the analyses performed in this study, assumed that a threshold of 15% difference in a variable's response was a

trigger for consideration and discussion, as has been used by previous authors [71, 77]. However, due to fragility and high cost of the physical model, the reproduction of multiple fall impact test was limited, which in turn, restricted the performance of statistical analyses.

2.4 Computational modelling

2.4.1 Finite element methods

FE analysis is a computational technique used for simulating/reproducing mechanical experiments. FE, initially starts by creating two or three dimensional computational models. Followed by breaking this model down into smaller segments/volumes, generally acknowledged as elements. Each element consists of nodes, representing the geometry surface of the element. These smaller elements jointly represent the whole geometry of the FE model. Afterwards, this model is subjected to loading conditions reproducing those of the mechanical experiments by subjecting some or all of these elements to the external loading criteria. In addition, these elements are used to assign different boundary conditions to the FE model, to set up the same mechanical experimental environment. The FE solver, used to compute the reaction of the model by measuring numerically the response from the elements of the model is based on the given material properties and any assigned constraints.

The overall computed reaction, from the individual elements, define the whole FE models act as a very powerful tool for investigating and understanding how the model performance and response is affected by assigning and applying different material properties, types of load, interactions and restrictions. Further, the accuracy of the FE

model response always needs to be evaluated, since it is dependent on a number of factors, including geometric configuration (simple or complex), mechanical properties, and the size and number of elements (mesh density) of the model.

2.4.2 Mesh generation

Subsequent to the creation of the 3D CAD paediatric head model (cranial bones, brain, sutures and fontanelles) a valid and compatible mesh model was generated. The final segmented 3D representation of the human infant head was meshed with a second order tetrahedral mesh, available in Mimics Remesh (3-matic v.10) see Figure 2.14. This meshing algorithm applies a smoothing function to the surface of different parts of the head by a Laplacian first order method (smoothing factor = 0.7); this process was repeated 100 times for each part. The re-meshing procedure applied different quality parameters and element mesh sizes, to optimise the mesh quality and reduce the number of elements, thus, producing more accurate results and a reduced computational running time. The 'fix wizard' analysis was then used to check the mesh configuration to remove any faults in the mesh, such as, inverted "normals", bad edges, possible noise shells, overlapping triangles and intersecting triangles. Subsequently the 'quality preserving reduce triangles' (QPRT) algorithm was applied to the surfaces of the head model and the volume mesh of the model created. The element mesh quality was inspected, by applying the edge ratio as a shape measure, which is the same as the definition of the aspect ratio in the simulation software (Abaqus/Explicit). This method is also valuable for checking if element distortions are not too great. Subsequent to a range of preliminary tests, to assess the relative suitability of FE modelling packages, the FE model was exported to Abaqus/Explicit (v6.12), since it is suitable for high impact deformation [118]

and it can numerically represent the radially anisotropic properties, reported by Kriewall [66], and adopted by the physical head model. To further replicate the physical head model, an oval shaped pad, to resemble the physical scalp, was designed, meshed and assembled with the FE model. The constitutive properties of the FE model cranial bones, brain, sutures, fontanelles and scalp, all influence the total system response to mechanical loading. The FE model tissue response properties must, therefore, be consistent with those of the corresponding areas of physical model, to be validated against its response.

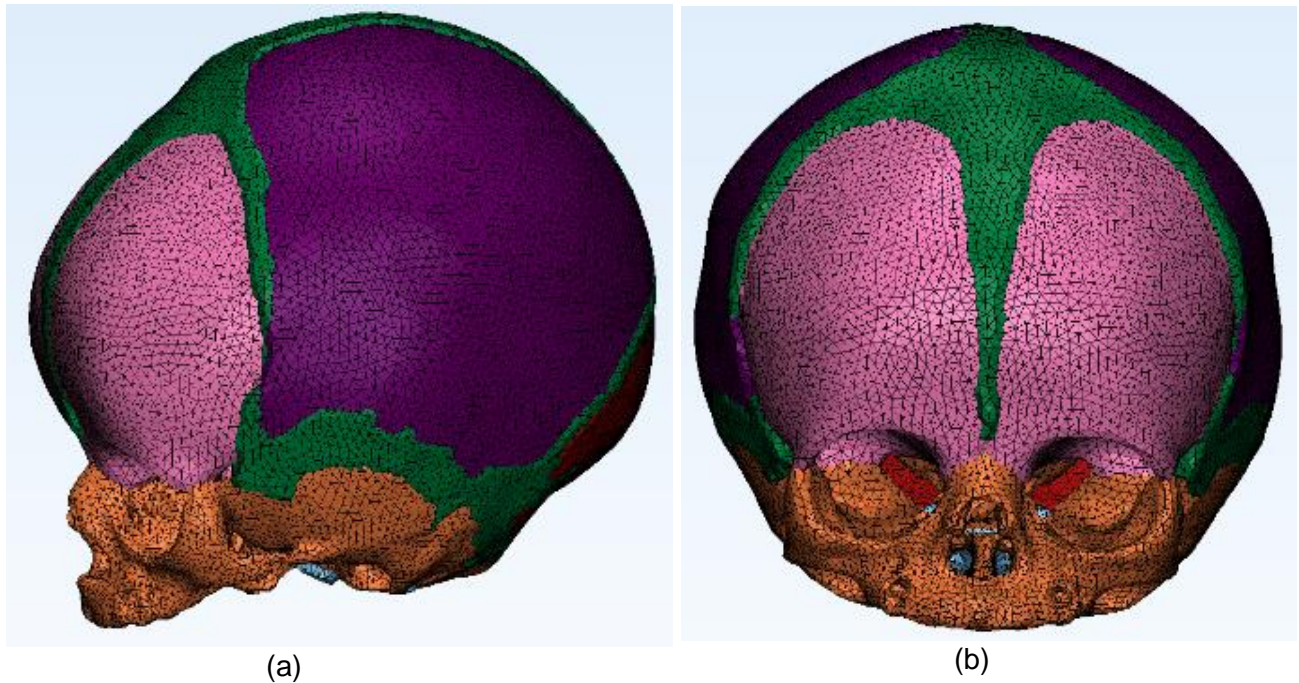


Figure 2.14. Abaqus/Explicit complete head mesh (a) side view (b) frontal view.

2.4.3 Bidirectional and material properties of the FE head model.

Previous attempts at producing validated infant FE head models have represented the material properties of the cranial bone as homogeneous and isotropic [75-77], [89-91]. Paediatric cranial bone is, in actuality, a very thin, heterogeneous and highly curved material with a distinctly orientated fibre pattern [64]. At birth, the cranial bones have a visible fibre orientation, due to the bone trabeculae radiating from a centre of ossification, see Figure 2.15a. McPherson & Kriewall [64], from their infant skull bone material testing describe a dissimilarity in the elastic modulus between tangential and radial fibre orientation. Coats & Margulies [66] report that infant cranial bone specimens are inhomogeneous, with the parietal and occipital bone having different stiffness properties. These differences in the elastic modulus, between the parallel and perpendicular specimens, confirm the significant anisotropic nature of the immature cranial bone. Correspondingly, the cranial bones of this FE model were modeled to be in-plane, orthotropic and with different elastic moduli in the parallel and perpendicular directions, relative to the fibres.

The material constant, used to define orthotropic material, was calculated using a mathematical equation in the Abaqus software [118]. The constitutive equations of the stress in equation (2.20), represented as a vector, σ ; as a function of the strain vector, ϵ (with elasticity matrix E) used in this study.

$$\sigma = E\epsilon \quad (2.20)$$

Based on the work by McPherson and Kriewall [64], the ratio of parietal bone stiffness, between parallel and perpendicular, was 4.2: 1 and frontal bone stiffness was 1.8: 1. No tests were performed on the occipital bones; therefore, a ratio of 4.2:1 was assumed, equivalent to the parietal bones. The infant cranial bones, modeled as an orthotropic solid element material model in Abaqus (Version 6.12, DSS 12), were defined, based on the elastic stiffness matrix [118] outlined in (2.21 – 2.31) below:

$$\begin{Bmatrix} \sigma_{11} \\ \sigma_{22} \\ \sigma_{33} \\ \sigma_{12} \\ \sigma_{23} \\ \sigma_{22} \end{Bmatrix} = \begin{bmatrix} D_{1111} & D_{1122} & D_{1133} & 0 & 0 & 0 \\ 0 & D_{2222} & D_{2233} & 0 & 0 & 0 \\ 0 & 0 & D_{3333} & 0 & 0 & 0 \\ 0 & 0 & 0 & D_{1212} & 0 & 0 \\ 0 & 0 & 0 & 0 & D_{1313} & 0 \\ 0 & 0 & 0 & 0 & 0 & D_{2323} \end{bmatrix} \begin{Bmatrix} \varepsilon_{11} \\ \varepsilon_{22} \\ \varepsilon_{33} \\ \gamma_{12} \\ \gamma_{13} \\ \gamma_{23} \end{Bmatrix} \quad (2.21)$$

$$(2.22)$$

$$D_{1111} = E_1(1 - \nu_{23}\nu_{23})\Gamma$$

$$(2.23)$$

$$D_{2222} = E_2(1 - \nu_{13}\nu_{31})\Gamma$$

$$(2.24)$$

$$D_{2233} = E_2(\nu_{32} - \nu_{12}\nu_{31})\Gamma$$

$$(2.25)$$

$$D_{1122} = E_1(\nu_{21} - \nu_{31}\nu_{23})\Gamma$$

$$(2.26)$$

$$D_{1133} = E_1(\nu_{31} - \nu_{21}\nu_{32})\Gamma$$

$$(2.27)$$

$$D_{2233} = E_2(\nu_{32} - \nu_{21}\nu_{31})\Gamma$$

$$(2.28)$$

$$D_{1212} = G_{12}$$

$$(2.29)$$

$$D_{1313} = G_{13}$$

$$D_{2323} = G_{23} \quad (2.30)$$

$$\Gamma = \frac{1}{(1 - \nu_{12}\nu_{21} - \nu_{23}\nu_{32} - \nu_{13}\nu_{31} - 2\nu_{21}\nu_{32}\nu_{13})} \quad (2.31)$$

The material constants used in the FE model were the elastic moduli (E_1, E_2, E_3), the shear moduli (G_{12}, G_{23}), and Poisson's ratio ($\nu_{12}, \nu_{23}, \nu_{13}$); where the subscript "1" refers to a parallel fibre direction, subscript "2" relates to a perpendicular direction and subscript "3," the direction perpendicular to both the 1 and 2 directions. Only E_2 is known for each cranial bone from high rate material testing [66]. E_1 was, therefore, calculated from the scaling of McPherson and Kriewall [64]. An assumption was made that E_3 be equal E_2 . Poisson's ratio (ν_{23}) was assumed to be the equivalent Poisson's ratio for tangential compression of adult cranial bone, reported in McElhaney et al. [64]. An assumption was made that E_3 was the equivalent of E_2 ; thus, due to symmetry ν_{32}, ν_{31} and ν_{21} were equal to ν_{23} . The shear modulus G was calculated from (2.32):

$$G_{23} = \frac{E_2}{2(1 + \nu_{23})} \quad (2.32)$$

The non-symmetric Poisson's ratio was calculated using (2.33):

$$\frac{\nu_{12}}{E_1} = \frac{\nu_{21}}{E_2} \quad (2.33)$$

For non-symmetric planes, Huber's in plane orthotropic equation (2.34) used to calculate the shear modulus.

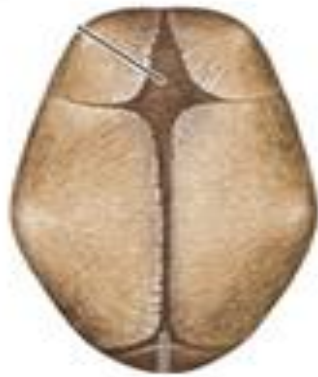
$$G_{12} = \frac{\sqrt{E_1 E_2}}{2(1 + \sqrt{\nu_{12} \nu_{21}})} \quad (2.34)$$

The final material properties are shown in Table 2.4. The material orientation representation of the cranial bones in the FE head model, compared to reality, is shown in Figure 2.15 and further replicated the fibrous appearance of the cranial bones in the physical model, shown in Figure 2.16. The sutures, fontanelles, brain and scalp have the same material properties from the physical model.

Table 2.4. Material constant used to define the FE mechanical property

FE head model structure	Material properties
Cranial bones	$\rho=1896 \text{ Kg.m}^{-3}$
Occipital	$E_1=1412 \text{ MPa}, E_2=336 \text{ MPa}, E_3=336 \text{ MPa}$ $\nu_{12}=0.19, \nu_{13}=0.045, \nu_{23}=0.22, \nu_{21}= 0.045$ $G_{12}=281\text{MPa}, G_{13}=312, \text{ MPa}, G_{23}=137 \text{ MPa}$
Parietal	$E_1=2201 \text{ MPa}, E_2=524 \text{ MPa}, E_3=524 \text{ MPa}$ $\nu_{12}=0.19, \nu_{13}=0.045, \nu_{23}=0.22, \nu_{21}= 0.045$ $G_{12}=439 \text{ MPa}, G_{13}=513.3 \text{ MPa}, G_{23}=214 \text{ MPa}$
Frontal	$E_1=2201 \text{ MPa}, E_2=1222 \text{ MPa}, E_3=1222 \text{ MPa}$ $\nu_{12}=0.19, \nu_{13}=0.11, \nu_{23}= 0.22, \nu_{21}= 0.11$ $G_{12}=627\text{MPa}, G_{13}=750.6 \text{ MPa}, G_{23}=500\text{MPa}$
Sutures and Fontanelles	$\rho=1025 \text{ Kg.m}^{-3}, E= 8.1 \text{ MPa}, \nu=0.49$
Brain	$\rho= 997 \text{ Kg.m}^{-3}, E= 0.0272 \text{ MPa}, \nu=0.499$
Scalp	$\rho= 399 \text{ Kg.m}^{-3}, E= 0.42 \text{ MPa}, \nu=0.42$

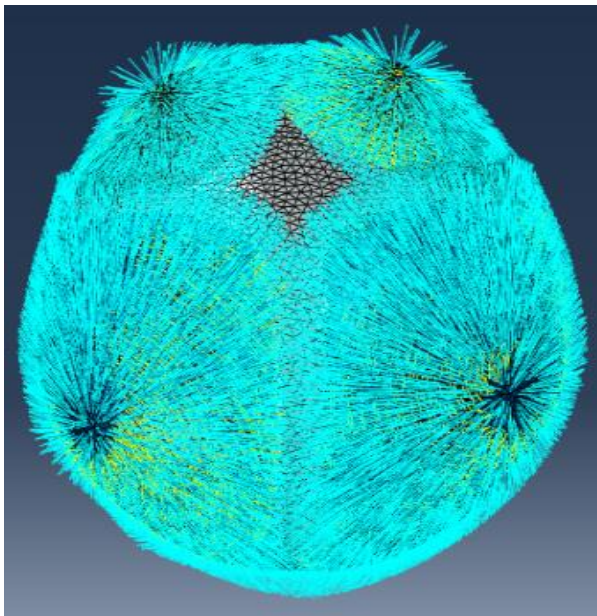
Top View



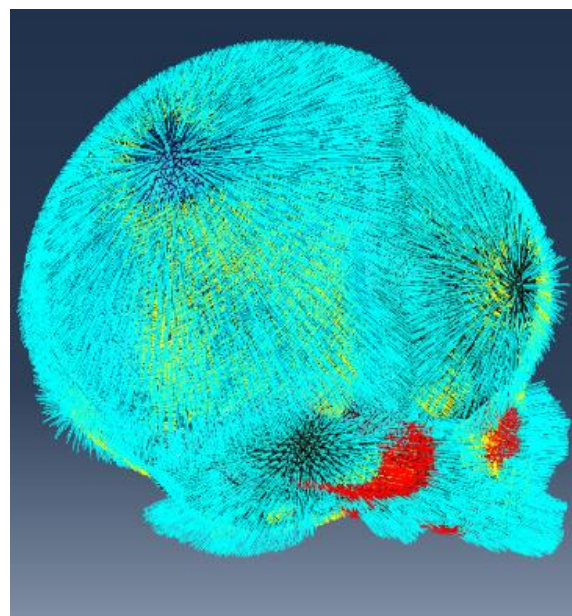
Side View



(a)



(b)



(c)

Figure 2.15. Material orientation of the cranial bones (a) paediatric head [18] (b) top view of FE head model (c) side view of FE head model.

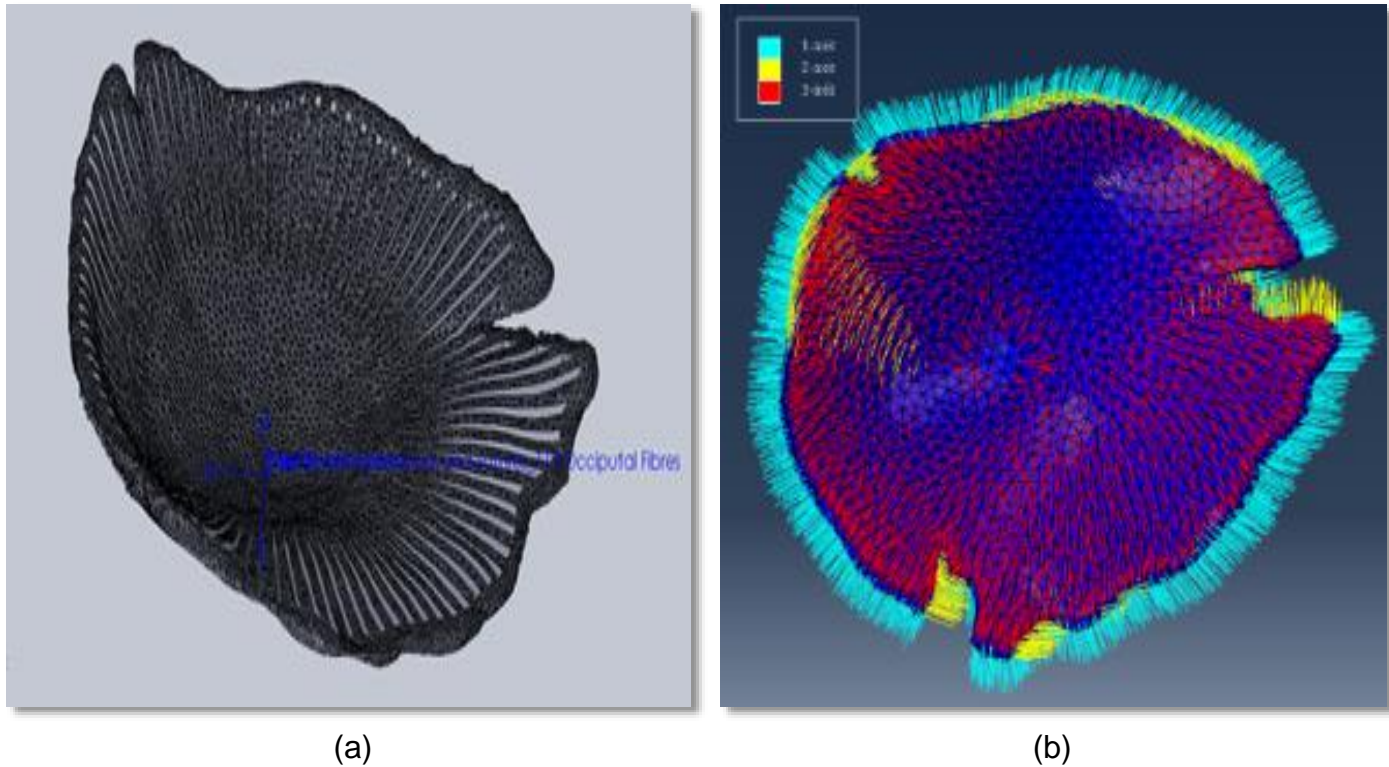


Figure 2.16. Fibrous appearance of the cranial bone in (a) physical model (b) FE model.

2.4.4 Analytical procedure and time integration

For nonlinear dynamic analyses, direct integration must be applied by FE solvers. Explicit time integration methods were used, based on the central difference method for kinematic variables, such as displacement and velocity, where a subsequent time step ($t+\Delta t$) is calculated, based on a current time step [118]. Thus, a stiffness matrix does not need to be created and inverted at each time step, making this method less computationally expensive. Whilst the time steps that can be used by an explicit analysis are limited, since they are based on the size of the smallest element and the time taken for a stress wave to pass through it, this form of analysis is suited to contact problems with a short time duration. Due to this, and in recognition that previous FE head impact models have successfully applied an explicit solver [75-77], [89-91], explicit time integration was

adopted for all the simulations in this study. Abaqus (Version 6.12, DSS 12) was used as an FE solver to study impacts with high deformation. Preliminary numerical simulations were conducted on an Intel Xeon machine with eight core processor with 128 GB of RAM. Simulations requiring longer processing time were run on the Cardiff University High Performance Computing (HPC) Linux cluster. Given the greater complexity (number of elements) of this FE model, a 'scale up study' was conducted to optimise the number of processors required to run the numerical simulations, which was automated using 'python script' on a 'supercomputer'. The computational model, was run initially on a minimum number of processors, which were subsequently increased, such that the simulation time decreased and subsequently plateaued, indicating optimisation, see Figure 2.17. From Figure 2.17, it can be observed that the total analysis time was approximately halved using the scale up study (MPI method). Increasing the number of processors beyond a maximum of three, produced no significant decrease in analysis run time.

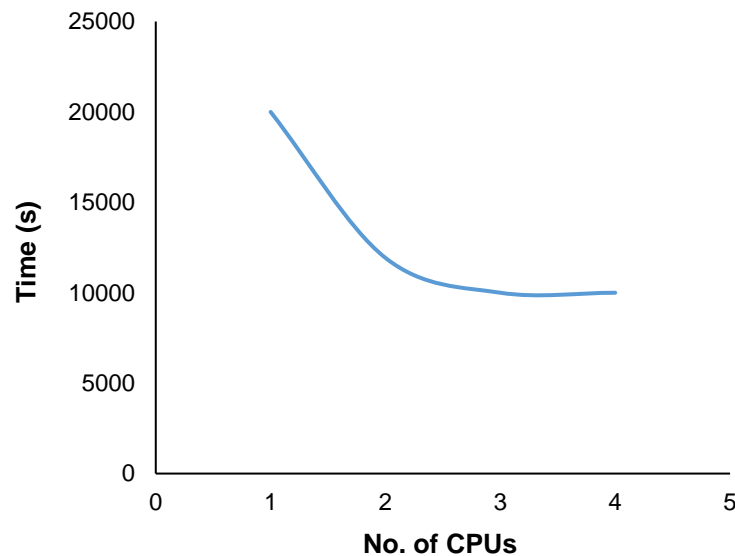


Figure 2.17. Profile of speed of analysis against the number of processors used.

2.4.5 Boundary and loading conditions.

Subsequent to the development of the FE model mesh, the boundary and impact test loading conditions were established, using the FE solver (Abaqus/ Explicit™ 6.12). The computational simulation runs were 0.02s in duration, which was sufficient to simulate both the impact of the head against the plate and the subsequent rebound. Further, there was a need for a parametric analysis to be conducted, where two parametric models were developed and assessed against the baseline model from the validation process.

2.4.5.1 First parametric model

From the base line model, the foramen magnum, the hole in the base of the skull through which the spinal cord passes, was not closed, such that the brain could move freely as outlined by previous author [71] However, the foramen magnum was closed in the infant PMHS heads used by Prange et al.[82]. Thus, in order to test this constraint, a parametric model was developed, where the foramen magnum was closed so the brain nodes were not free to pass through.

2.4.5.2 Second parametric model

Different techniques have been used by previous researchers for modelling the brain-skull interaction, which is relate to the pia / arachnoid complex [71,119,120]. Basically, this interface must be modelled via a fluid-solid interaction; still this area of computational modelling under development and needs extensive resources. However, different approached and techniques recommended to model this interface, either by adding a solid CSF elements has a low shear modulus, or via a tied constraint / sliding contact. With regard to the CSF, to adequately represent the effect of skull–brain interface it has

been suggested that the fluid be modelled as a fluid, rather than a structural element [119, 110]. Fluid structure interaction (FSI) analysis is in its relative infancy and currently considered a limitation with most commercially available FE packages. In response, a contact algorithm approach (sliding interface) was applied to describing the CSF at the skull-brain interface, rather than implement fluid elements. While researcher's conducted that impact response of adult FE head models is affected by this interaction via using the parametric tests, Kleiven and Hardy [119] reported that brain motion is insensitive to the interface condition for low severity impacts. Subsequently, initially Sliding contact was used for the baseline FE model, to model the interaction between the FE head model and the rigid plate, using the frictional coefficient (0.2) reported by Miller et al. [120], an interaction that has been used by previous authors [71, 119, 120], however, a parametric model was developed, where a tie constraint was assessed for the interaction between the brain and skull.

2.4.6 Mesh convergence

Due to the high resolution of the CT images, meshing resulted in an extremely large number of elements and required long processing times. Running simulations on a supercomputer cluster with multiple processors in parallel, helped to decrease the computational times, however, the models still required 1 to 5 days. Since a decrease in mesh resolution would greatly reduce the total number of elements in the model and significantly reduce the total processing time, albeit at the loss of solution accuracy, a mesh sensitivity analysis was performed to see what effect mesh resolution would have on the simulation result convergence. It became a requirement, therefore, that an optimal balance be established, between reducing processing times and maintaining sufficient

model accuracy. A convergence study was performed on the infant FE head model with the goal of determining the coarsest mesh that could be used, whilst still producing accurate results. From anatomical, geometrical, acquisition and mesh generation of the 3D infant head model, the nodes of each anatomical structure in the head model were tied to those of neighbouring structures. Due to the complexity of the infant head geometry, this was best achieved by meshing all the structures together and sharing surface nodes between adjacent structures, to create a good matching nodal interface. However, due to the structures of the head having a similar mesh density, a global mesh refinement was used in the convergence analysis, rather than a regional mesh refinement. Re-meshing software (Mimics 3-matic) was used to change the mesh resolution of the FE model to create five mesh resolutions for consideration (0.5, 1, 1.5, 2 and 3 mm (base)). The convergence study consisted of a simulated vertex impact from 0.30m onto a rigid plate [85]. The FE head model was provided with a 2.43 m.s^{-1} pre impact velocity, calculated from the law of conservation of energy as in equation (2.35).

$$V = \sqrt{2gh} \quad (2.35)$$

The simulation of the vertex impact onto a rigid plate was created for each mesh resolution and the impact response compared, to determine the optimum mesh density for the impact conditions. The output variable was peak impact force, which was normalised relative to the value output from the base mesh (3 mm).

A mesh convergence analysis was conducted to evaluate the accuracy of the present FE model. For each mesh resolution simulation, the impact force response was extracted. It can be seen from Figure 2.18 that a reduction in mesh resolution below 20×10^5 , whilst producing a significant saving in the computational running time, resulted in an increase in error. As a consequence, a model with a mesh resolution of 20×10^5 was chosen for the remainder of the analysis. This resolution was selected as an optimal mesh, because of its relatively minimal residual error and significantly shorter computational time. The final mesh consisted of 2626855 second order modified tetrahedral elements.

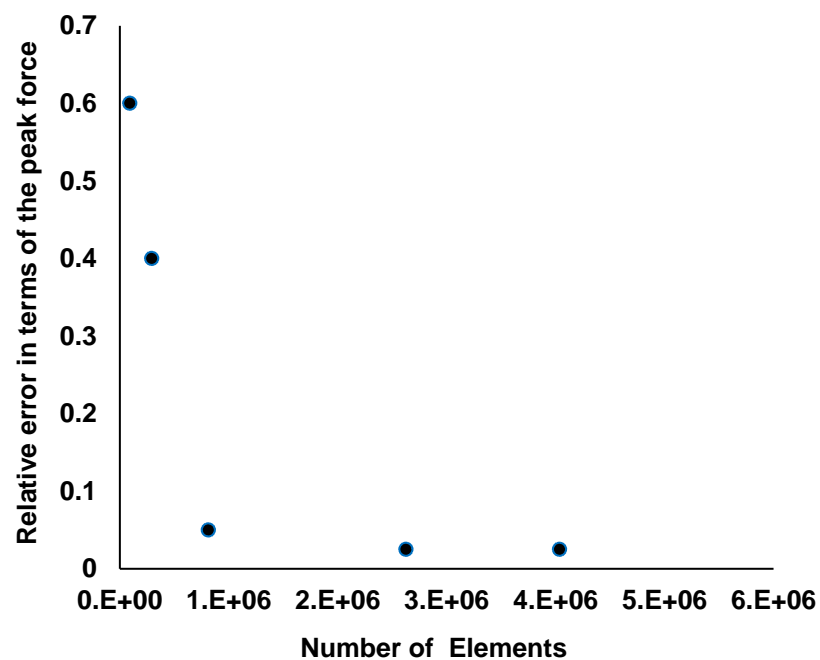
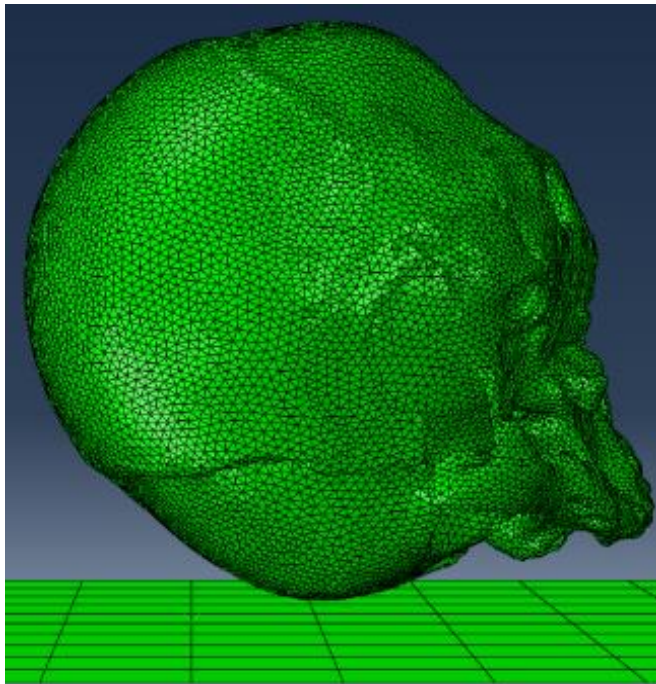


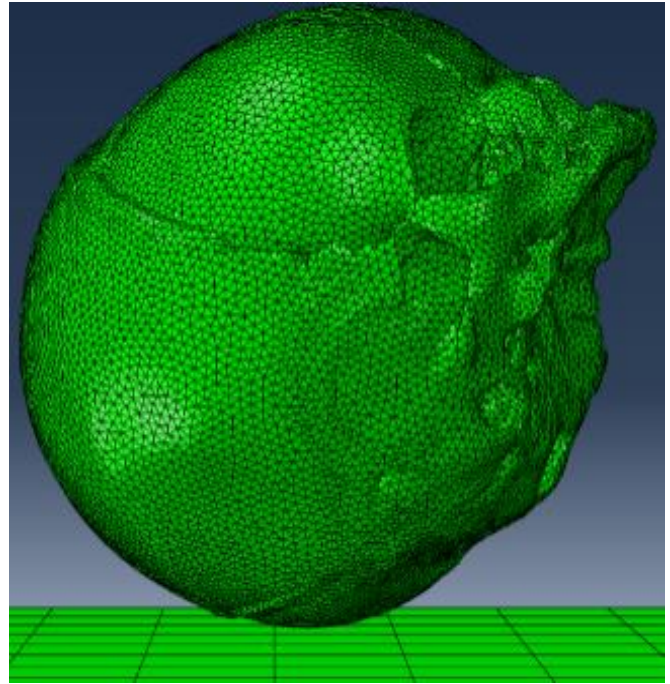
Figure.2.18. The error in the peak force against mesh density (number of elements).

2.5 Global validation of the paediatric FE head model against PMHS data

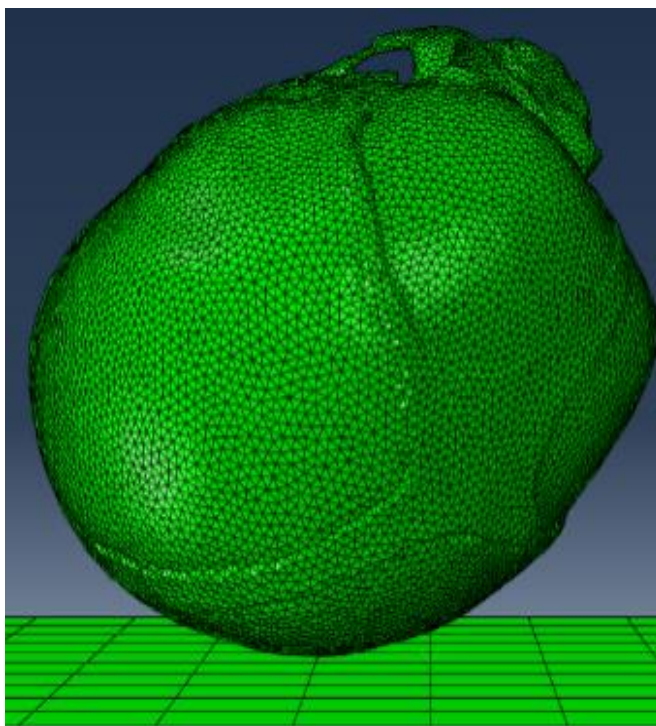
Computational modelling of the adult FE head was validated against experimental impact response values, in terms of intracerebral pressure, brain displacement and intracranial skull fracture [86, 87, 88]. As discussed previously, however, there has been very little work conducted on paediatric head trauma with which to validate models. To the authors' knowledge, only Prange et al. [82] provide sufficient data to validate the global impact behavior of a paediatric head. Prange et al. [82] conducted impact tests with three infant post mortem human surrogate (PMHS) heads (1, 3 and 11 days old) from heights of 0.15m and 0.30m, onto five different impact locations (frontal, vertex, right and left parietal and occipital bones) onto a steel force plate. During the PMHS tests [82], the infant head was considered as a rigid body for the purpose of deriving impact acceleration – time curves from the impact force produced at the force plate, by dividing the force output by the mass of the infant PMHS head. The authors concluded [82], that the average peak acceleration of the PMHS head is significantly different for different drop heights but not impact location. The PMHS tests [82] were used to validate the response of the present infant FE head model by simulation of the experimental tests, see Figure 2.19. Eight different impact scenarios were simulated and compared against the kinematic response data from [82]. During each impact, the FE model was placed in contact with the rigid surface and assigned a predefined impact velocity of 1.716 m.s^{-1} or 2.426 m.s^{-1} , corresponding to the drop height of 0.15m or 0.30m, respectively. The Impact locations of the head used in finite element analysis was in four directions, anterior-posterior (AP)/forehead impact, posterior-anterior (PA)/occipital impact and superior- inferior (SI)/vertex impact, left-right (LR)/parietal impact.



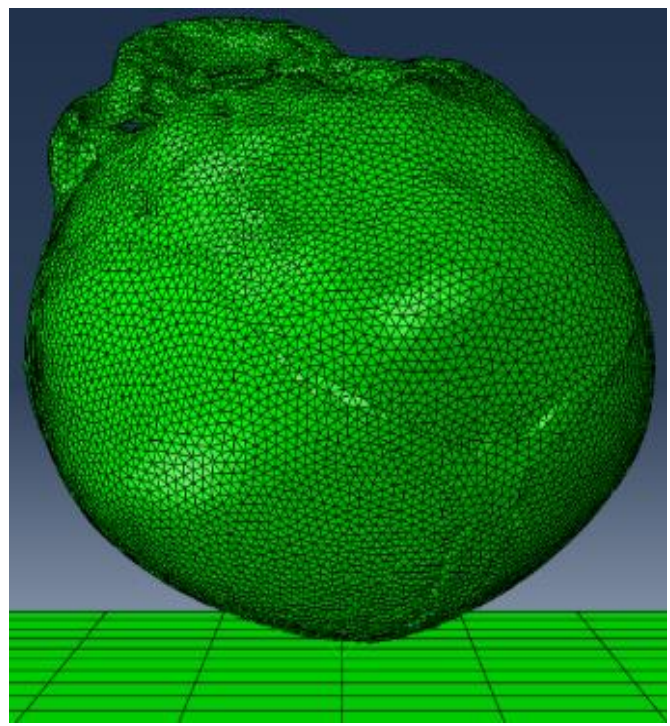
(a)



(b)



(c)



(d)

Figure 2.19. The FE model impacted onto a rigid surface at (a) forehead region (b) occiput region (c) parietal region (d) vertex region.

2.6 Sensitivity analysis

2.6.1 Influence of the Impact location

To increase the reliability of the simulations with the FE model, it was necessary to perform a sensitivity analysis (parametric study), since the limited general description of the impact location in the PMHS study [82] fails to provide sufficient guidance, regarding the exact area of impact, for the purpose of precise simulation. The geometrical/anatomical complexity of the infant head has many potential impact sites, for example an occipital impact could be to the middle or edge of the occipital bone, near the sutures, near the vertex, base or parietal bone. For the purpose of FE model simulations in the model performance evaluation (global validation), the impact was assumed to be at the “centre” of the occipital bone (baseline impact region). An analysis was conducted, using both the ‘global approximation approach’ and the ‘local, regional approximation approach’.

This sensitivity study included cases of impact at the occipital, parietal and forehead bones with different impact regions in each cranial bone at $2.43 \text{ m}\cdot\text{s}^{-1}$, corresponding to the drop height of 0.30 m. For occipital impact tests, the selected impact regions will be (1) close to the base of skull, (2) close to the vertex, (3) close to the left parietal and (4) close to the right parietal, see Figure 2.20a. For parietal impact tests, the selected impact regions will be (1) close to the base of the skull, (2) close to the vertex, (3) close to the occiput and (4) close to the forehead, see Figure 2.20b. For forehead impact tests, in addition to the upper region of the forehead (baseline impact region), which is close to the soft cranial bone and membranous fontanelle, other impact regions in the lower region of the forehead will be tested, see Figure 2.20c.

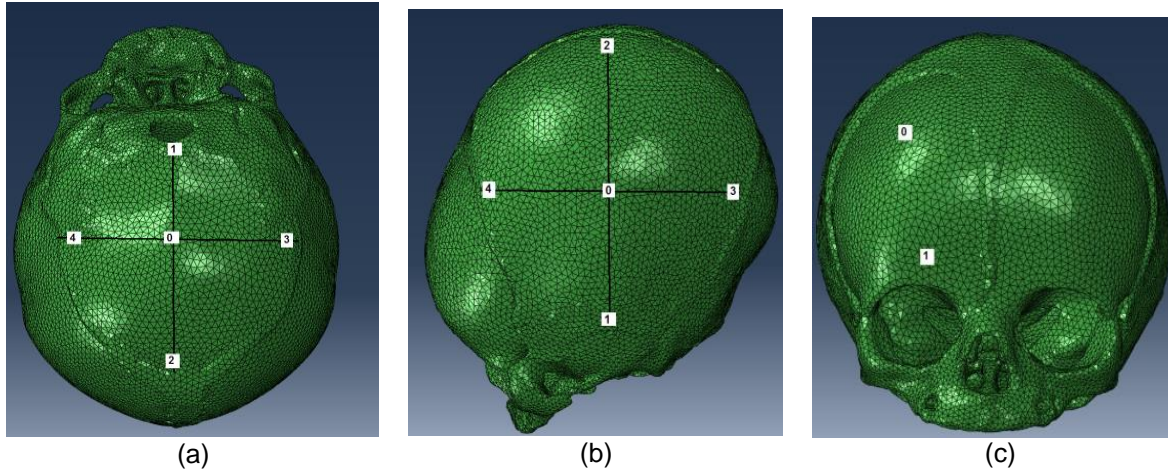


Figure 2.20. The FE head model with different impact regions at the (a) Occiput (b) Parietal (c) Forehead cranial bones.

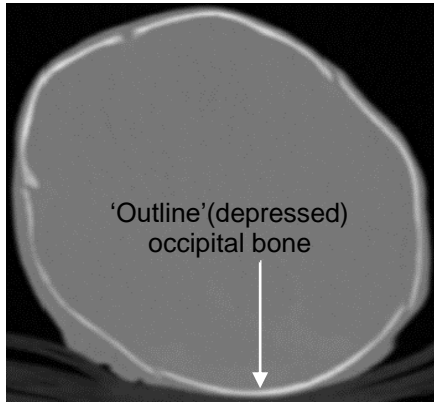
2.6.2 Influence of the position of the occipital bone in relation to the parietal bones

As outlined previously, the validation of an FE head model, from the paediatric population is limited, due to the lack of PMHS impact response data. Prange's PMHS [82] study, often considered as the "gold standard" for validation, does not report whether the newborn PMHS heads (1, 3 and 11days-old) had an inline or out of line (depressed) occipital–parietal bone configuration [82].

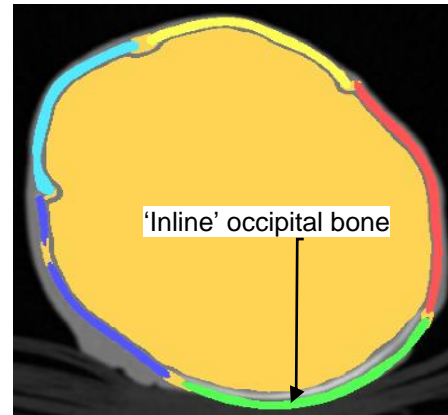
Figure 2.1 shows the infant CT scan image has a significantly depressed occipital bone. To represent a wider infant population, the occipital bone was repositioned outwards, to align with the edges of the parietal bones on each side and produce an FE head model, see Figure 2.21 e, f, g, h. A sensitivity analysis was considered: (1) to evaluate the performance of this inline FE head model to investigate anomalies that occurred during the validation process, (2) to investigate the assumption that Prange's PMHS head, used in this study, either had and out of line, depressed or inline occipital–parietal bone

configuration and (3) to investigate the influence of the occipital bone in relation to the parietal bones on head impact response.

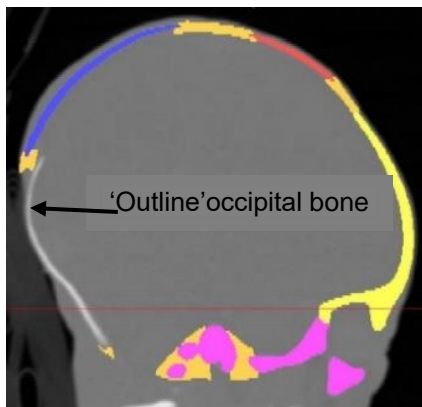
Therefore, a second newborn FE head model was produced, with an out of line, depressed, occipital bone-parietal bone configuration, to mimic that observed instantly after birth, see Figure 2.21 a, b, c, d. The sensitivity analysis was performed by simulating the impact experimental tests, shown in Figure 2.19. Eight different impact scenarios were simulated and during each impact, the FE model was placed in contact with the rigid surface and assigned a predefined pre impact velocity of 1.72 m.s^{-1} or 2.43 m.s^{-1} , corresponding to the drop height of 0.15m or 0.30m, respectively. The analysis was performed by comparing the impact response from the out of line FE model, shown in Figure 2.21 a, b, c, d, with the inline FE model, shown in Figure 2.21 e, f, g, h and Prange's PMHS data [82]. The impact acceleration response from all the tested models was also obtained by dividing the impact force by the head mass, in accordance with the measurement method in Prange's study [82]. As this research has less confidence in the global approximation approach, a second part of this sensitivity analysis used the local, regional approach from the impact acceleration to explore the bone accelerations to see if there is any difference between the FE models related to the occipital-parietal bone configuration. A comparative study was performed using the impact acceleration response of a newborn FE head model that had an out of line occipital bone, relative to the parietal bone configuration with an inline occipital-parietal bone configuration. The response was calculated by local, regional approach at impact velocities of 1.72 m.s^{-1} and 2.43 m.s^{-1} .



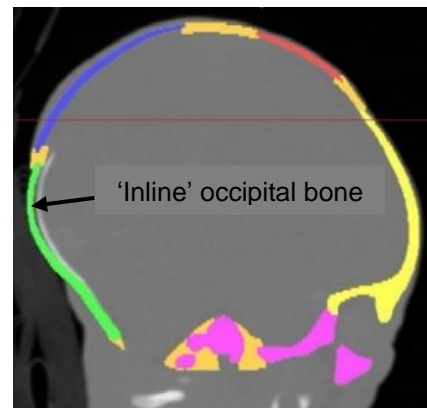
(a)



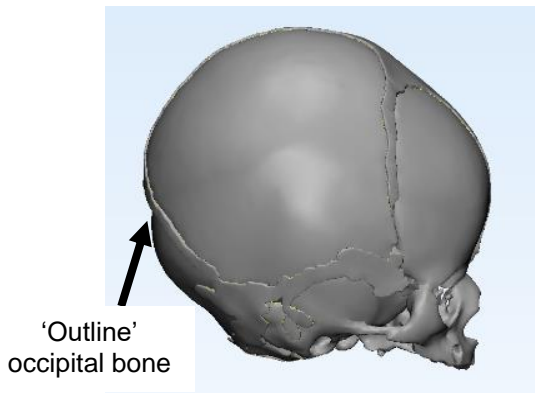
(e)



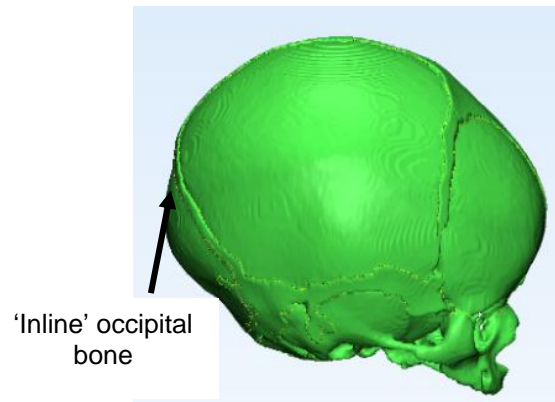
(b)



(f)



(c)



(g)

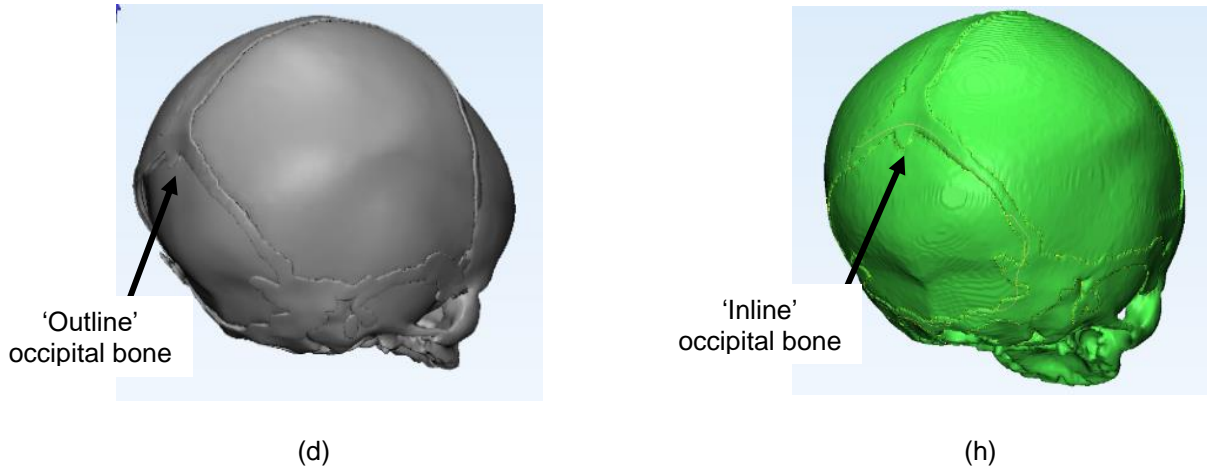
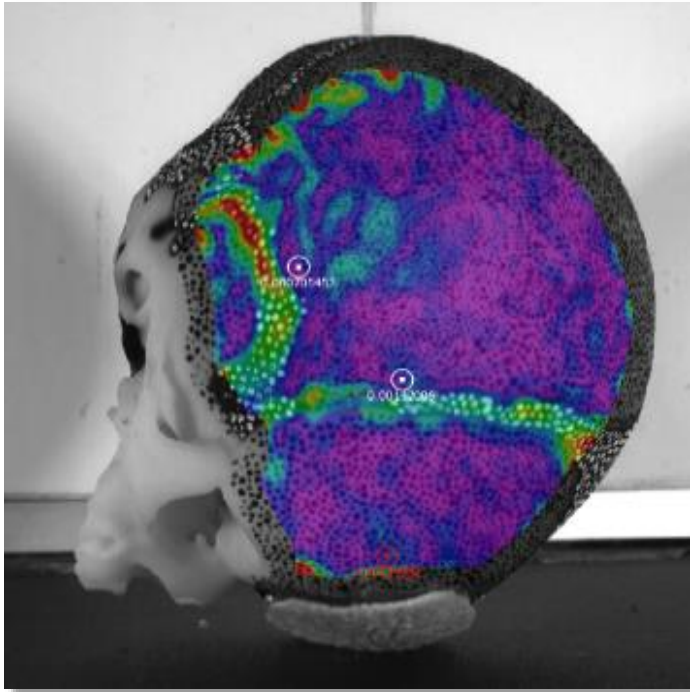


Figure 2.21. Comparison of the 3D CAD model with depressed occipital – parietal bone configuration (a-d) and with FE model have inline occipital – parietal bone configuration (e-h).

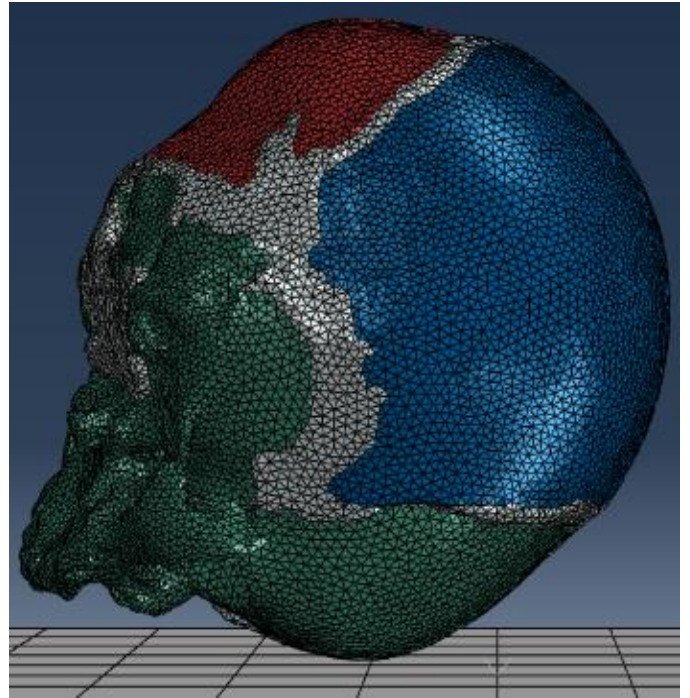
2.7 Global, regional and local validation of the paediatric FE head model against physical model impact response.

The physical model was subjected to “global” validation by simulated impacts against the PMHS study of Prange et al. [82]. The computational FE head model was subjected to the same “global” PMHS validation. During “global” validation the physical model was subjected to additional measurement by HS-DIC, which generated regional and local measurement data. Thus, the FE model could be subjected to additional validation against the physical model regional and local data. Provision of regional and local validation of the FE model for the first time provided the opportunity to challenge, the “rigid body approximation”, used in Prange’s [82] and other’s studies [84,85,89-93] by measuring the acceleration and deformation at different regions of the head and comparing it with the response of the physical model. Whilst also, overcoming the practical limitations of the physical model and sustaining the effective future investigation of complex internal structures. “Global” validation of the FE head model was achieved by

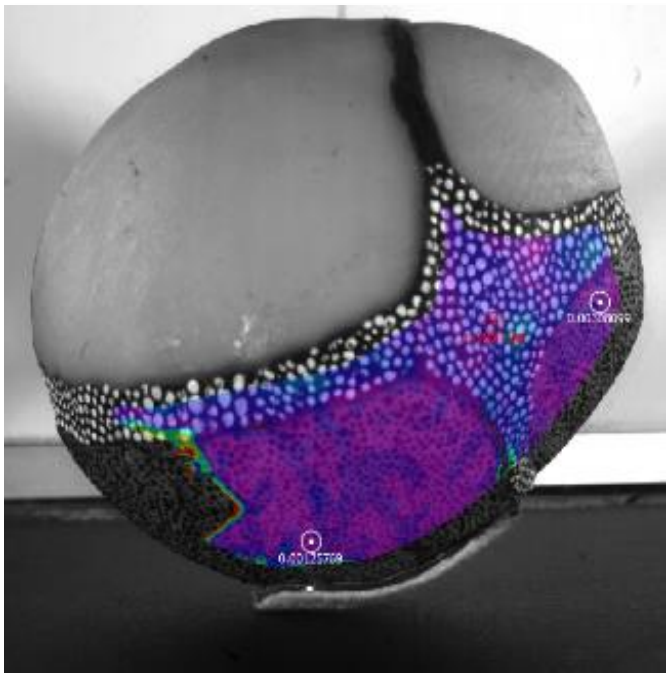
a series of impact simulations, conducted in accordance with the physical head model impact experiments. Impacts were simulated onto different regions of the head (forehead, parietal, occipital and vertex), at pre impact velocities of 1.72 m.s^{-1} and 2.43 m.s^{-1} onto a 'rigid surface', see Figure 2.22 (e-h). A total of eight drop impact conditions were included in the simulations. The mass of the present computational FE model and the corresponding physical model was that of the 10-day-old infant head scan, which matched that of the 3-day-old infant PMHS head in Prange et al. [82]. Regional and local validation, was possible from the experimental data of the physical model, since the HS-DIC system provided the translational impact response, including the distribution of the strain throughout the different structures of the head. From the translational acceleration response of the physical model a series of computational FE simulations were conducted, replicating the different orientations of the head. A correlation was established between the regional and local impact response, see Figure 2.22, to obtain the important features of the physical model head impact tests and the numerical analyses. So when looking at a regional or localised area of the physical model, being able to manipulate "on screen" the numerical simulation, to focus on regions of interest.



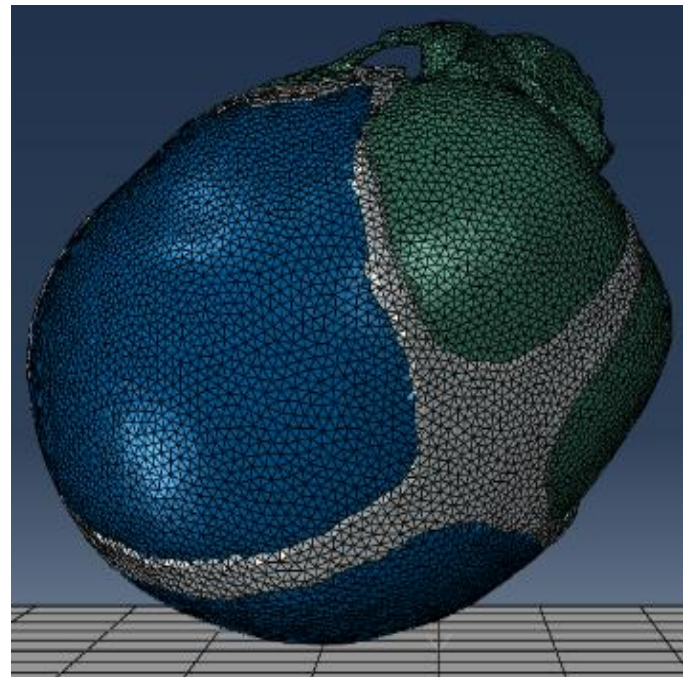
(a)



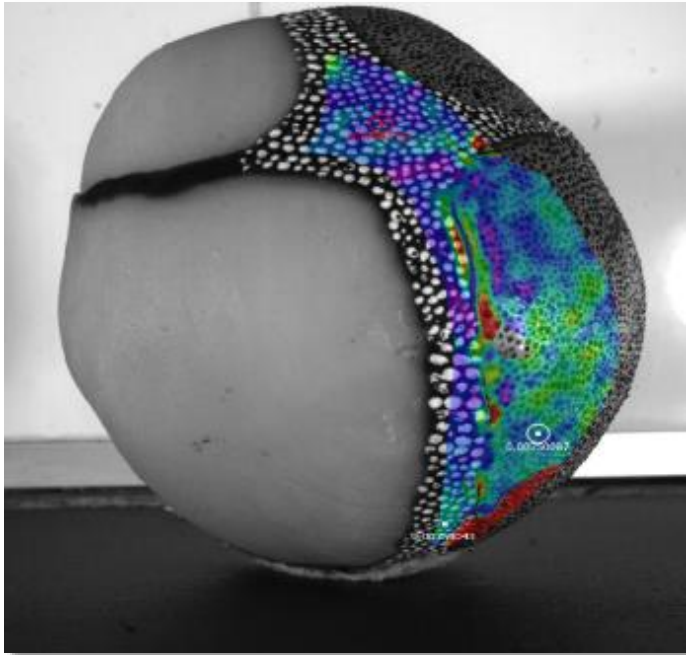
(e)



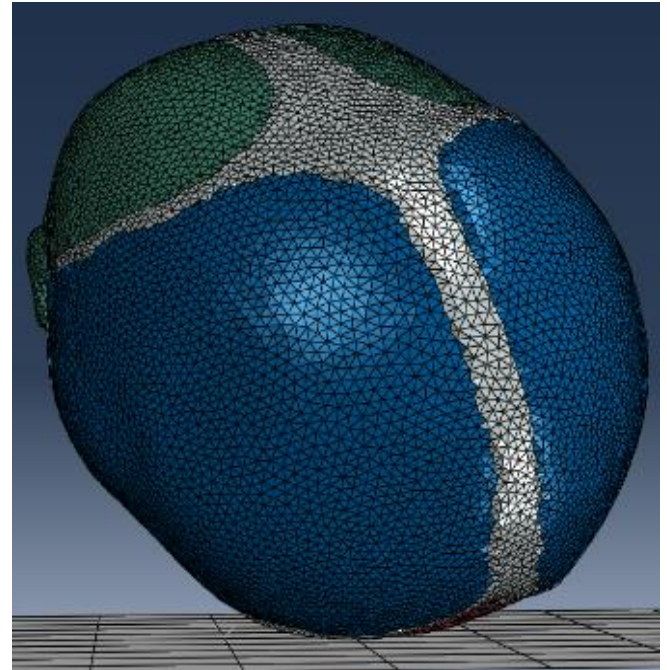
(b)



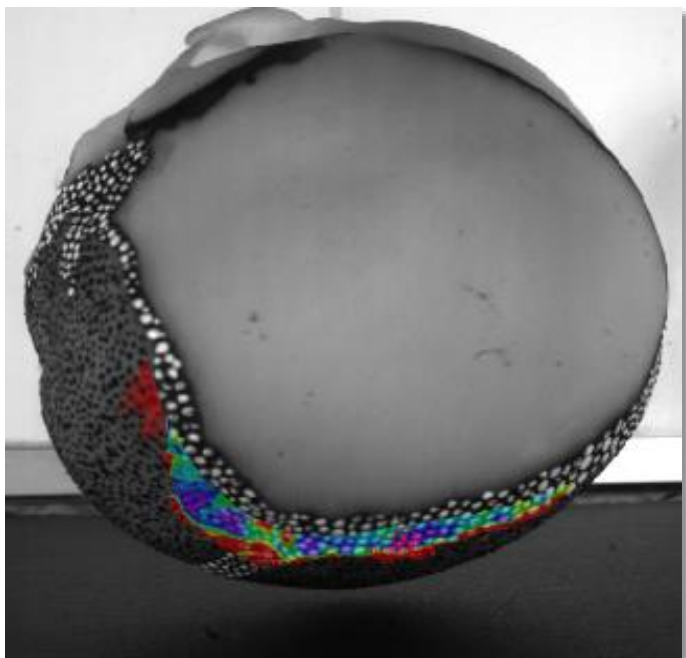
(f)



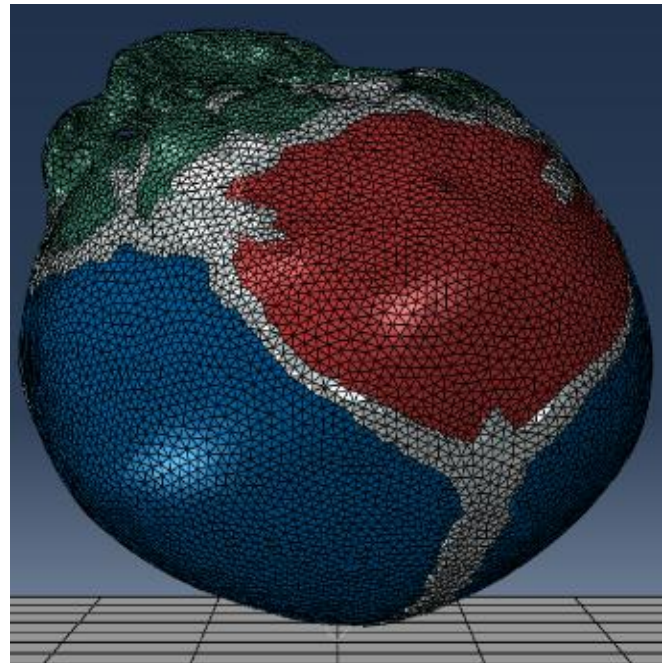
(c)



(g)



(d)



(h)

Figure 2.22. Comparison of the physical model head's impact Digital Image Correlation tests (a - forehead, b-parietal, c-occipital and d-vertex) with FE numerical simulations of the FE mode (e-forehead, f-parietal, g-occipital and h-vertex).

2.8 Investigating skull fracture from the literature.

Subsequent to the computational global and local validation of the paediatric FE head model, the FE head surrogate was applied to predicting the head fall response of skull fracture at different paediatric fall heights. In the literature, the kinematic and material response variables from paediatric PMHS test data linked with head injuries is very limited.

In a series of studies in 1984 and 85, Weber [80, 81] conducted experimental fall tests using 50 paediatric PMHS specimens, aged between 0 and 9 months old. The PMHS subjects were dropped from a height of 0.82 m onto the parietal–occipital region of the skull onto five different stiffness impact surfaces. This study reported the production of linear skull fractures in 20 samples, among all 50 PMHS subjects, see Figure 1.8. To the author’s knowledge, Weber’s study [80, 81] has the greatest number of paediatric PMHS subjects in the literature and provides valuable data for appraising the risk for paediatric skull fracture without the necessity to scale from adult data. However, there was no quantitative magnitudes from this PMHS study, for instance head impact acceleration and contact force response and the study provides only simply sketches of the skull fracture patterns. Prange et al. [82] conducted three neonate PMHS impact tests, by dropping the PMHS heads onto a concrete surface at a fall height of 0.15 and 0.30 m, onto four different impact locations (vertex, forehead, parietal, occipital). In contrast to Weber’s [80, 81] studies, Prange reported the peak head acceleration of 80 g at 0.30 m fall height, whilst he did not observe any skull fractures in all of the study impact test. Recently, Hughes [12] conducted an epidemiological study and proposed 0.6m as a minimum

threshold for serious head injuries based on the fact that no cases of skull fracture and no serious head injuries occurred below a height of 0.6 m.

Given all of these reported data from the literature, initially the biofidelic FE head was applied to predicting the skull fracture risk by reconstructing Weber study [80, 81]. A single impact test of a 0.82 m fall onto the parieto-occipital region onto stone was considered and replicated computationally via this validated FE tool, see Figure 2.23, so comparisons could be made with paediatric skull fracture patterns reported by Weber, see Figure 1.8

In conjunction, the FE model used to conduct a parametric study with four different fall heights 0.15, 0.30, 0.6 and 0.82 m, by drooping the head using the same experimental method as Weber's PMHS test onto the parieto-occipital region onto rigid surface. The parametric study will assist in discriminating between the PMHS impact test conducted by Prange et al. [82] and that conducted by Weber [80, 81] and evaluating its performance against the 0.6 m threshold, reported by Hughes [12], that clinically there is no risk of skull fracture at heights <0.6 m.

This parametric study used the fracture pattern strategy, based on the maximum stress, to predict the skull fracture risk from each fall height. The fracture was said to occur, if the maximum principal stress was greater than the ultimate stress of cranial bone from the presented mechanical characterisation of the polymeric materials that matched the tissue response values reported by Coats and Margulies [66] at any time during the simulations. The probability of fracture of the FE head model was estimated, based on

the fracture probability graph of the parietal and occipital bones created by Coats study [71], see Figure 1.10.

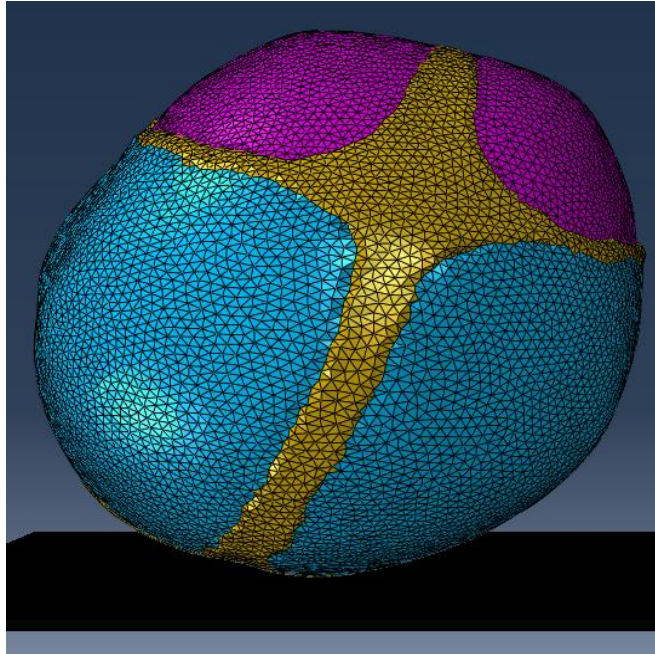


Figure 2.23. Parietal-occipital impact simulating published paediatric PMHS from 0.82 m onto stone.

2.9 Output variables and Statistical analysis.

The general contact force of the impact point between the FE model and the rigid plate and the duration of impact were exported from Abaqus (Version 6.10, DSS 12) into Excel. The translational acceleration was calculated in units of g, using equation (2.9). For global validation of the FE model with the PMHS and physical model experiments, the same two indicators were used to evaluate the performance of the FE model. The peak acceleration (g) values and correlation score, using the same equations (2.10-2.19) presented in section 2.3.5. Like the physical model HS-DIC approach, the local kinematic variables (translational acceleration, duration of impact and rotational acceleration) and head deformation (strain) were measured from discrete points on the skull. The deformation of the head was measured in four directions, anterior-posterior (AP)/ forehead impact, posterior-anterior (PA)/ occipital impact, Left - Right (LR)/ parietal impact and superior-inferior (SI)/vertex impact. The maximum head strain was taken as the maximum of the head strains in each of the four directions (AP, PA, LR and SI). Also, the maximum stress was used to predict material failure of the FE model. All the analyses performed in this study, assumed that a threshold of 15% difference in a variable's response was a trigger for consideration, as has been used by previous authors [71, 77].

3. RESULTS

3.1 Mechanical characterisation of the Poly jet printed materials.

Three printed polymeric materials (White, Grey and Black) were subjected to tensile testing in batches of six samples. Paediatric tissue material properties were derived from the literature, including the Young's modulus for tensile and bending from different strain rates tests [64, 65, 37, 66, 67]. However, to provide an insight into the material behaviour and to justify the suitability of these materials for the construction of a physical head model the ultimate tensile strength (σ_{uts}) and strain at failure (ϵ_{max}), were calculated for each sample material. Each of these material properties are highlighted in Figure 2.6, which illustrates how each property was calculated. Young's modulus (E), was calculated along the linear portion of the stress - strain curve to 0.1% strain of the White, Grey and Black materials. Further, the Young's modulus of the rubberlike materials (the Black) was calculated for 1%, 10%, 20% strain and break point strain. The ultimate strength (σ_{uts}) at the maximum stress value was acquired. Strain at failure was calculated from the final value available before sample failure. All of the mechanical properties were evaluated for each material and the results presented in Table 3.1. The mechanical properties (stiffness (E), ultimate tensile strength (σ_{uts}) and maximum strain (ϵ_{max})) of the rigid and rubber additively manufactured acrylate polymers (White, Grey, and Black) from uniaxial tensile testing at low strain rate ($1 \text{ mm}\cdot\text{min}^{-1}$) are shown in Table 3.1. In addition to the results being detailed in Table 3.1, each tensile test was analysed and plotted as a stress-strain curve to illustrate the data graphically. All six tests, from each polymeric material, were then averaged together to provide a representation of the "typical stress-strain behaviour" for the specific material, see Figures 3.1, 3.2, 3.3. The average specimen

stress-strain curves illustrate the relatively uniform behaviour of the White and Grey material specimens through ultimate strength, where material specimens do have a variation in strain at failure. Further the average response of the White and Grey specimens show an ultimate strength peak, followed by a long period of plastic deformation. The Black material specimens have an elastic and plastic region, quickly followed by failure, their average is shown in Figure 3.3. The mechanical properties of these materials were mostly consistent, with the material properties provided by the supplier data sheet, as shown in Tables 3.2 and Figure 3.4. Comparing the difference between the mechanical output values from the tensile experiments with those reported material properties of infant tissue samples as in Table 3.3, it was more appropriate and more biofidelic to use these materials in the construction of the physical model by printing the sutures in Black, the occipital bone in Grey and the frontal and parietal bones in White.

Table 3.1. Mechanical properties (Mean \pm SD) of the White, Grey and Black materials at 1mm min⁻¹ strain rate.

Materials	$(\sigma_{uts})/MPa$	$(\epsilon_{max})/\%$	(E) to 0.1 % strain (MPa)	(E) to 1% strain (MPa)	(E) to 10% strain (MPa)	(E) to 20% strain (MPa)	(E) to failure (MPa)
White (Vero White Plus)	24.82 \pm 0.85	26.10 \pm 7.48	1836 \pm 365	-----	-----	-----	-----
Grey (Rigid Light Grey)	23.66 \pm 0.8	27.34 \pm 2.98	1687 \pm 275	-----	-----	-----	-----
Black (Tango Black Plus)	0.833 \pm 0.05	58.7 \pm 1.4	7 \pm 2	6.53 \pm 2.15	2.2 \pm 0.09	1.8 \pm 0.09	1.41 \pm 0.06

Table 3.2. Comparison of the mechanical properties (mean \pm SD) tensile test specimens with supplier data sheet.

	White (Vero White Plus)	Supplier data sheet
$(E)/\text{MPa}$	1836.00 \pm 365.00	2000-3000
$(\sigma_{uts})/\text{MPa}$	24.82 \pm 0.85	50-65
$(\epsilon_{max})/\%$	26.10 \pm 7.48	10-25
	Grey (Rigid Light Grey)	Supplier data sheet
$(E)/\text{MPa}$	1687.00 \pm 275.00	1700-2300
$(\sigma_{uts})/\text{MPa}$	23.66 \pm 0.80	40-60
$(\epsilon_{max})/\%$	27.34 \pm 2.98	15-25
	Black (Tango Black Plus)	Supplier data sheet
$(E)/\text{MPa}$	6.5 \pm 2.15	none given
$(\sigma_{uts})/\text{MPa}$	0.833 \pm 0.05	3.5-5.0
$(\epsilon_{max})/\%$	58.7 \pm 1.41	65-80

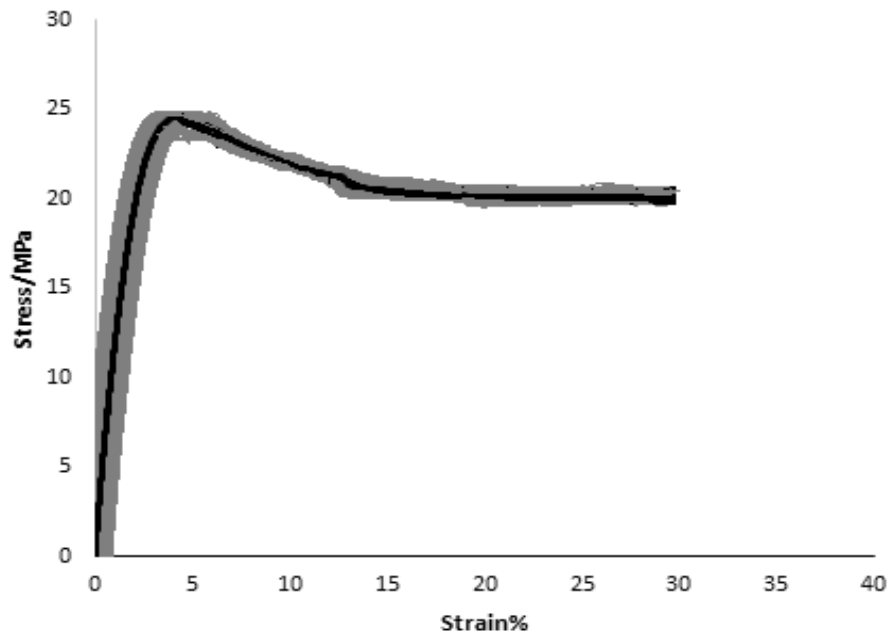


Figure 3.1. Stress-strain curves for the average of the six tension specimens of White material.

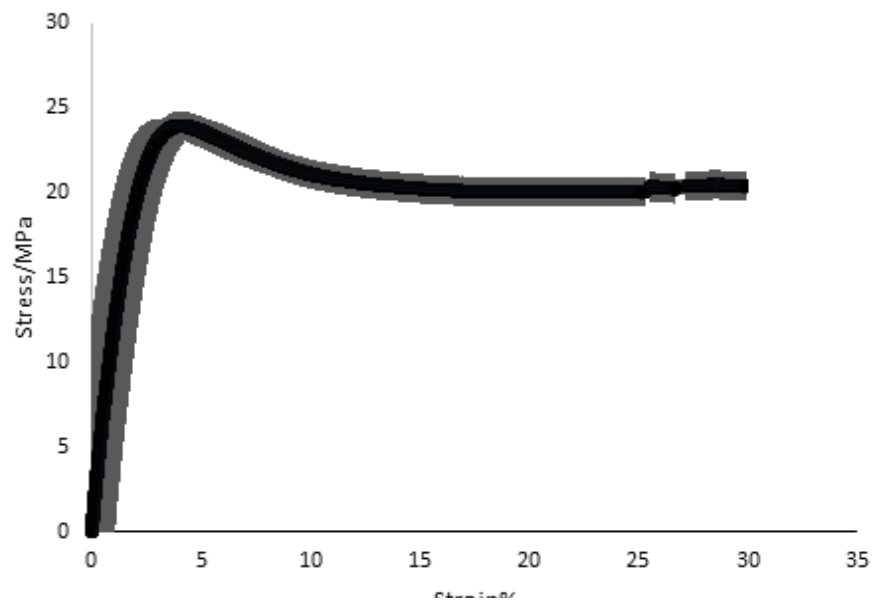


Figure 3.3. Stress-strain curves for the average of the six tension specimens of Gray material.

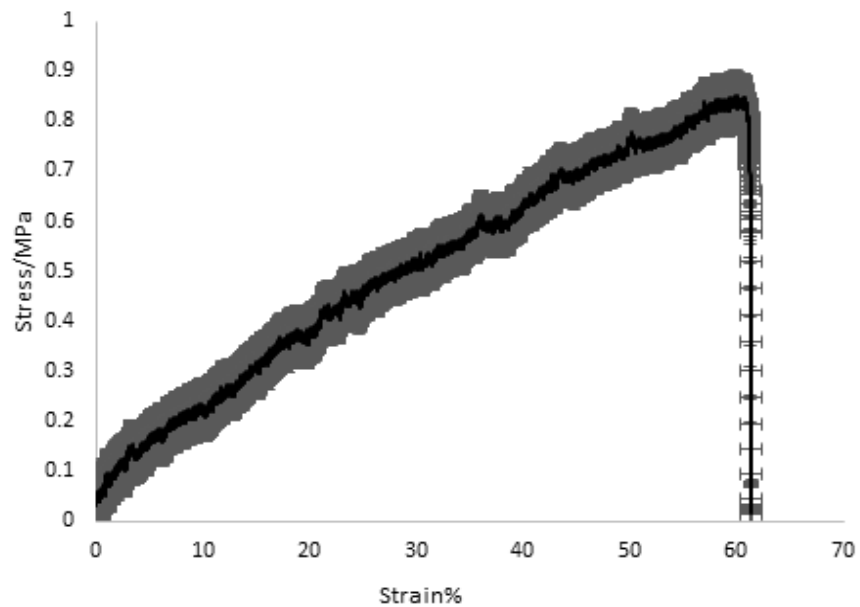


Figure 3.2. Stress-strain curves for the average of the six tension specimens of Black material.

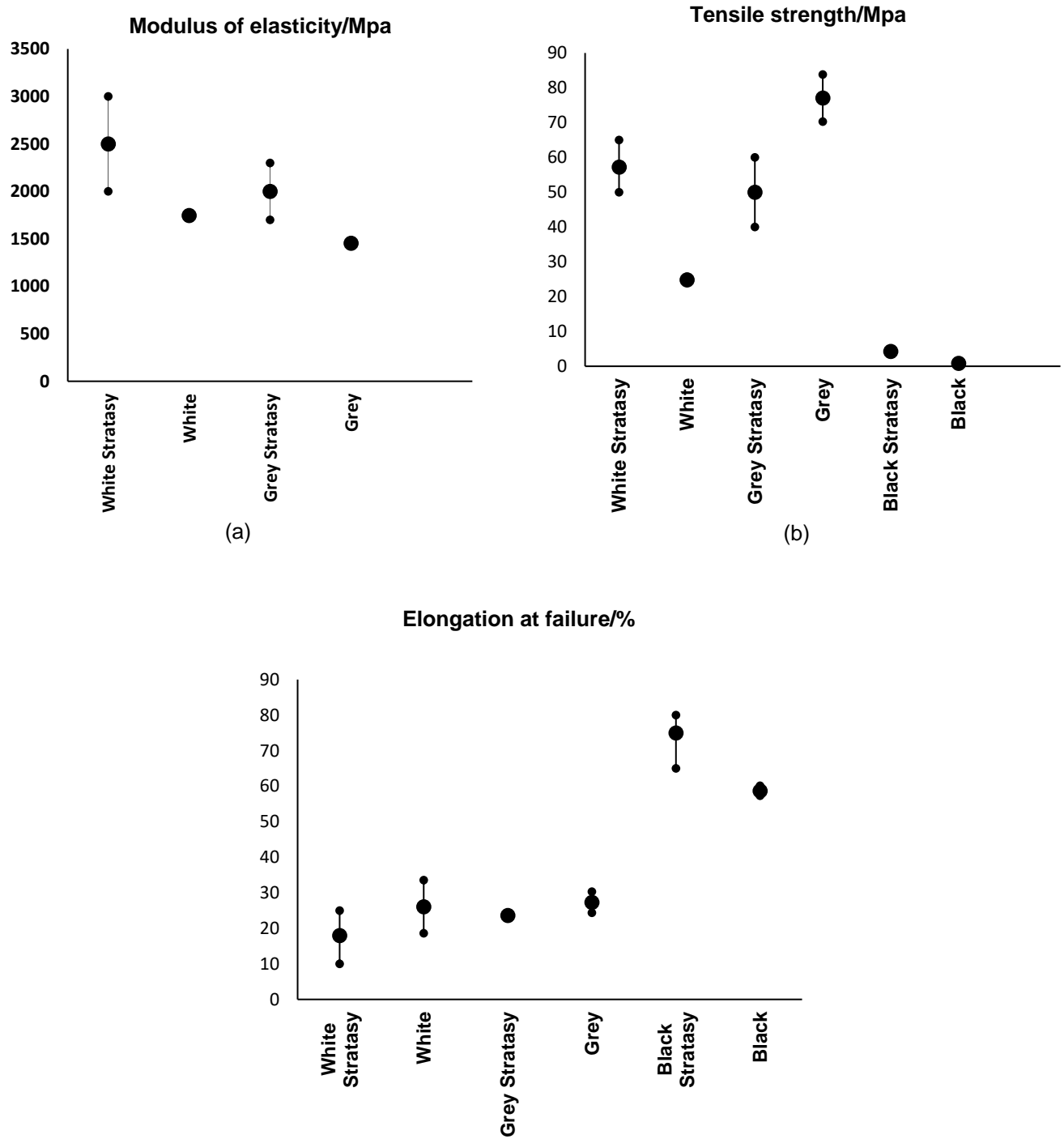


Figure 3.4. Comparison of (a) Young's modulus (MPa) (b) Tensile strength (MPa) and (c) Elongation at failure from test specimens White, Grey and Black with data sheet.

Table 3.3. Comparison of mechanical properties from tensile test specimens with reported values.

	White (Vero White Plus)	Parietal and Frontal Bones
$(E)/\text{MPa}$	1836.00±365.00	Parietal bone – 2660 - 5290 [64], 1873 - 5158 [65] Frontal bone – 1870 - 4000 [64], 2579 - 3999 [65] (term-3 months)
$(\sigma_{uts})/\text{MPa}$	24.82±0.85	Parietal bone - 8.4 - 53.7 [66]
$(\varepsilon_{max})/\%$	26.10±7.48	-----
	Grey (Rigid Light Grey)	Occipital bone
$(E)/\text{MPa}$	1687.00±275.00	29 - 551MPa (term-3 months) [66], 318 - 1318MPa (3-6 months) [66]
$(\sigma_{uts})/\text{MPa}$	23.66 ± 0.80	3.3 - 31.4 (25 < term), 3.1 - 18.5 (term-3 month) [66], 16.4 - 43.4 (3-6 month) [66]
$(\varepsilon_{max})/\%$	27.34 ± 2.98	-----
	Black (Tango Black Plus)	Sutures and Fontanelles
$(E)/\text{MPa}$	6.50±2.15	4.3 - 14.2 (25<term) [66], 3.8 - 6.4(term-3 months) [66]
$(\sigma_{uts})/\text{MPa}$	0.833±0.05	4.2 - 6.7 (25 < term) [66], 2.2 - 7.2 (term-3 months) [66]
$(\varepsilon_{max})/\%$	58.70±1.41	-----

3.2 Global validation of the paediatric physical model against PMHS data

3.2.1 Impact translational acceleration.

The physical head model validation was accomplished by a series of impact simulations, shown in accordance with the PMHS infant head impact experiments [82]. Impacts were simulated onto different regions of the head (frontal bones, parietal bones, occipital bones and vertex), from 0.15 m and 0.30 m onto a 'rigid surface'. From the experimental work, the drop heights of 0.15m and 0.30m corresponded to - impact velocities of 1.72 m.s⁻¹ and 2.43 m.s⁻¹, respectively. The translational acceleration values, see Table 3.4, were

calculated by dividing the impact force, from the force plate, by the head mass, following the PMHS experiments [82]. A total of eight impact conditions were included in the simulations. Validation of the physical model was achieved by comparing peak impact accelerations against Prange's PMHS data [82], the mass of the physical head model of the 10-day-old infant (0.46 kg) was closest to the mass of the 3-day-old infant PMHS head (0.49 kg), since, the scalp of the physical model was present only at the impact site, due to the painted random speckle pattern on the bones needing to be visible to the HS-DIC cameras. From Figure 3.5 and Table 3.4, it can be seen that the physical model and PMHS peak resultant accelerations, for all the eight drop tests, show a close correlation for all conditions. However, slight variations could be observed at the occipital and parietal bones. The physical model acceleration–time impact curves were observed to generally correlate well with the PMHS impact data, see Figure 3.7. Acceleration-time contact curve characteristics, at four different impact locations from a 0.30m height drop (2.43 m.s^{-1}), produce a correlation score equal to or greater than 86, (see equations 2.17, 2.18 and 2.19) , shown in Table 3.5.

Table 3.4. Output variables (global translational acceleration, duration of impact) from the physical model at two impact velocities.

Impact location	Impact velocity (m.s⁻¹)	Peak acceleration (g)	Durations of impact (s)
Vertex	1.72	60 ± 2	0.006±0.0016
Occipital	1.72	82 ± 9	0.005±0.0010
Forehead	1.72	58 ± 6	0.002±0.0010
Parietal	1.72	69 ± 11	0.003±0.0010
Vertex	2.43	86 ± 3	0.007±0.0010
Occipital	2.43	117 ± 6	0.005±0.0010
Forehead	2.43	118 ± 42	0.002±0.0010
Parietal	2.43	84 ± 10	0.008±0.0010

Table 3.5. Comparison of model performance between the PMHS and physical model experiments using the correlation score (CS) measured from CS_{N-phase}, CS_{N-amp} and CS_{N-shape} from a 0.30m height drop (2.43 m.s⁻¹).

Impact location	Impact velocity (m.s⁻¹)	CS_{N-phase}	CS_{N-amp}	CS_{N-shape}	CS average
Vertex	2.43	98.89	99.19	99.44	99.20
Occipital	2.43	99.42	97.32	91.17	95.97
Forehead	2.43	98.98	99.19	99.44	99.20
Parietal	2.43	99.40	90.14	96.71	95.41

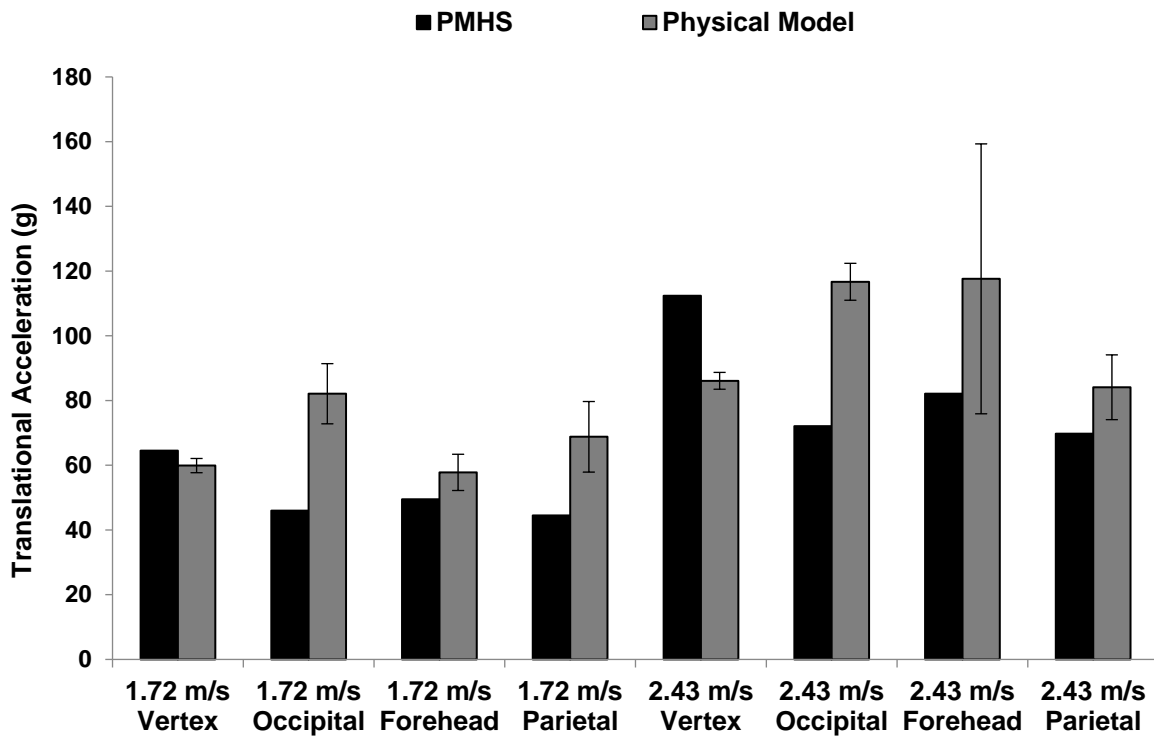


Figure 3.5. Peak acceleration and drop height for infant PMHS and physical model impact tests

3.2.2 Duration of Impact

During the validation process the impact time durations of the PMHS tests were compared against the physical model, see Table 3.4. The average time durations for the physical model, during both $1.72 \text{ m}\cdot\text{s}^{-1}$ and $2.43 \text{ m}\cdot\text{s}^{-1}$ impacts, were observed to be slightly shorter than those in PMHS tests [82], see Figure 3.6. It is of particular interest that during different drop tests, the peak accelerations appeared to be close to those of the PMHSs [82], see Figures 3.5 and 3.7, whilst the impact time durations were not, see Figures 3.6 and 3.7. Evidenced by the acceleration - time contact curve for the forehead, occiput, parietal and vertex regions, at a velocity of $2.43 \text{ m}\cdot\text{s}^{-1}$, shown in Figure 3.7. The peak impact accelerations, from the physical head model, are closer to the peak impact

acceleration measured by PMHS [82], while the impact time durations of the physical model are shorter, compared to the PMHS.

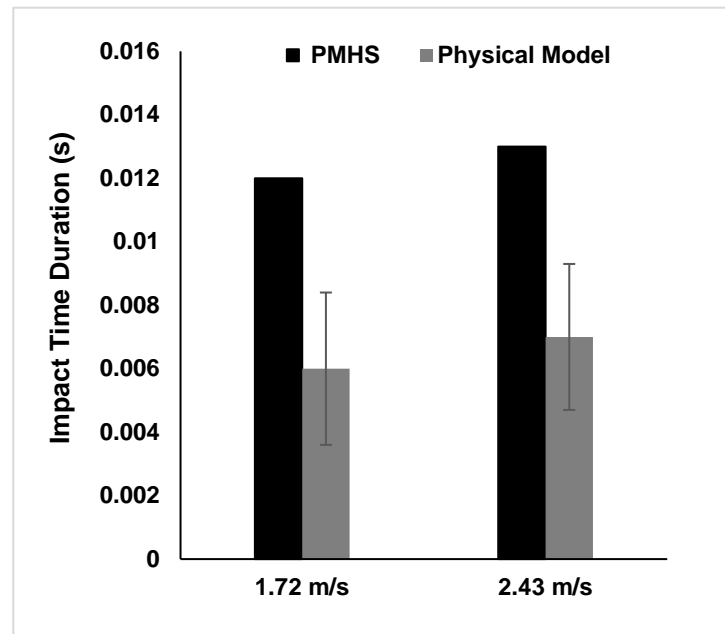


Figure 3.6 Comparison of impact time duration between PMHS test and physical model from two different drop heights.

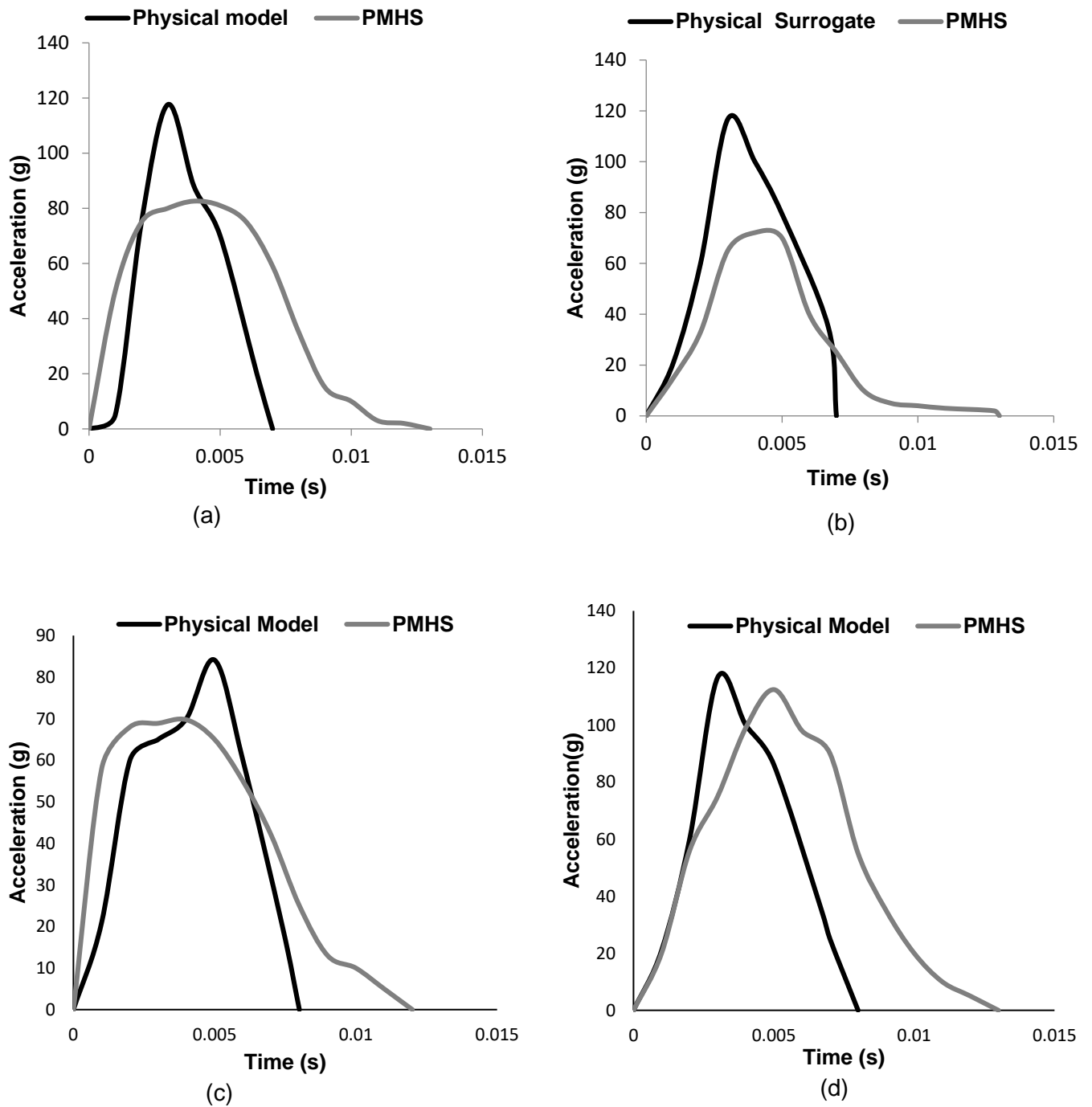


Figure 3.7. Acceleration-time contact curve for the PMHS and physical model from a 0.30m height drop ($2.43 \text{ m}\cdot\text{s}^{-1}$) at the (a) forehead, (b) occiput, (c) parietal and (d) vertex regions.

3.3 Regional and local investigation of the paediatric physical model.

3.3.1 Impact translational and rotational accelerations.

The physical head model was validated for acceleration vs time, against published PMHS data by applying the same PMHS drop test method and the rigid body assumption. To assess this assumption, the HS-DIC system was used to measure the linear and angular acceleration response at different impact locations at the two impact velocities of 1.72 m.s⁻¹ and 2.43 m.s⁻¹, see Table 3.6. The head response was then compared with the impact response of the physical model from the force plate tests, see Figure 3.8, which shows that the local translational accelerations, from the DIC, are significantly higher than the global acceleration response from the force plate. Interestingly, the greatest difference between the rigid body assumption and the DIC output, was 112% for the 1.72 m.s⁻¹ impact velocity onto the frontal bones. Whilst, the smallest difference was 32% for the 1.72 m.s⁻¹ impact velocity onto the parietal bones.

The difference in angular acceleration response, demonstrated by the physical model, impacted from two different fall heights is shown in Figure 3.9. The physical model's peak angular acceleration was measured for each drop test, see Table 3.7. The maximum angular acceleration at the vertex, occiput and forehead impact at 1.72 m.s⁻¹ is as high as 2.43 m.s⁻¹.

Table 3.6. Physical model local translational impact acceleration and duration at two impact velocities.

Impact location	Impact velocity (m.s⁻¹)	Peak acceleration (g)	Duration (s)
Vertex	1.72	90 ± 9	0.006±0.0016
Occipital	1.72	188 ± 23	0.005±0.0010
Forehead	1.72	206 ± 64	0.002±0.0010
Parietal	1.72	219 ± 13	0.003±0.0010
Vertex	2.43	137 ± 30	0.007±0.0010
Occipital	2.43	173 ± 73	0.005±0.0010
Forehead	2.43	256 ± 35	0.002±0.0010
Parietal	2.43	116 ± 25	0.008±0.0010

Table 3.7. Physical model maximum rotational acceleration at different impact locations at two impact velocities.

Impact location	Impact velocity (m.s⁻¹)	Maximum angular acceleration (rad sec⁻²)
Vertex	1.72	4121 ± 2328
Occipital	1.72	9371 ± 4858
Forehead	1.72	12983 ± 1936
Vertex	2.43	9530 ± 1882
Occipital	2.43	23459 ± 3728
Forehead	2.43	32110 ± 5888

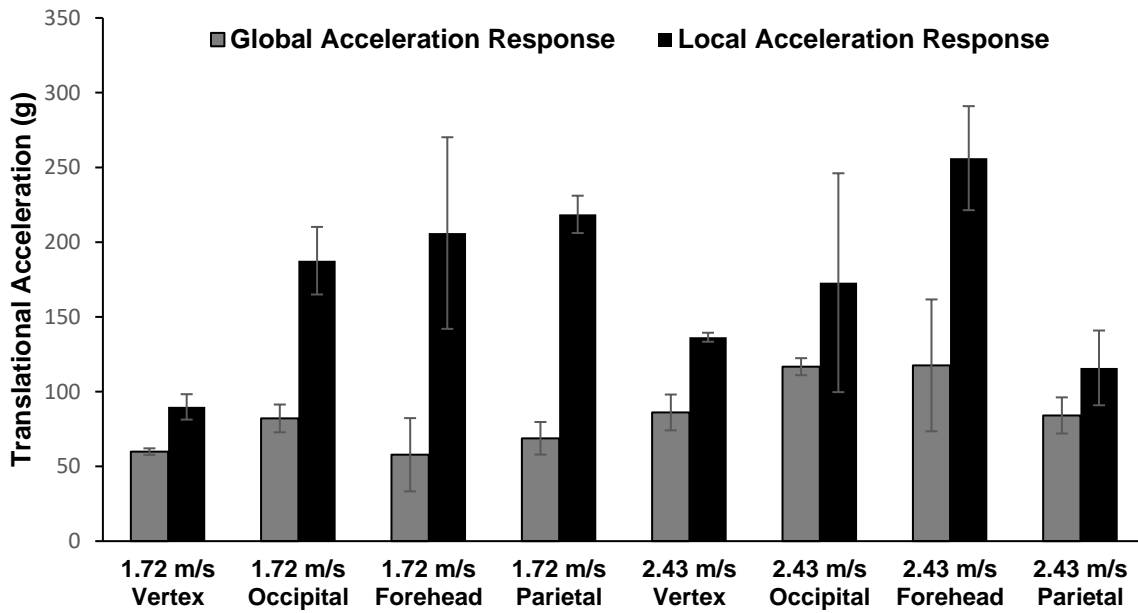


Figure 3.8. Comparison between the physical model’s global and local translational acceleration from the force plate and DIC system, respectively.

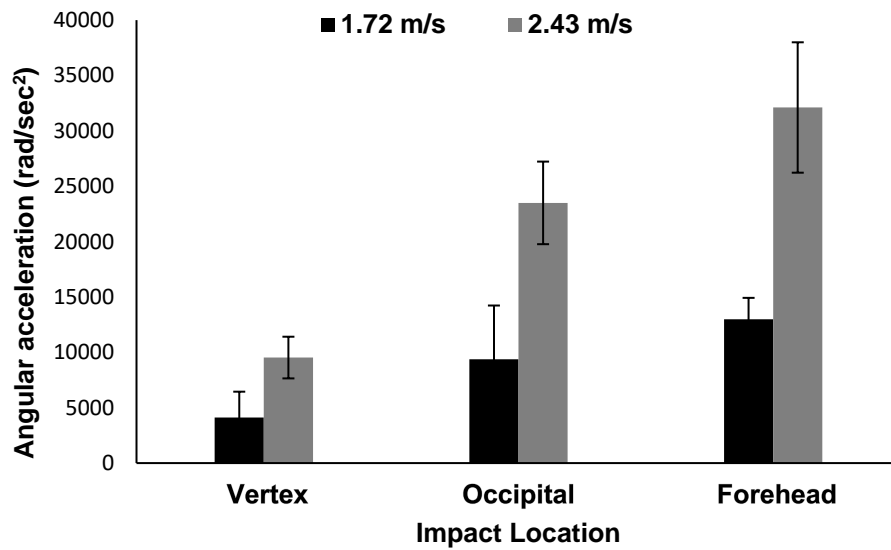


Figure 3.9. Physical model maximum angular acceleration at different impact locations at two impact velocities.

3.3.2 Head deformation

The potential level of head impact deformation that the paediatric head sustained on impact was demonstrated by the physical head model, see Figure 3.10. During impact, the physical head was observed to deform, thereby decelerating, followed by a rapid acceleration as the accumulated elastic energy from the head deformation was converted to kinetic energy. Figure 3.10. shows the deformation of the physical model on impact from an impact velocity 2.43 m.s^{-1} onto a metal plate, prior to impact, and 2ms, 3 ms and 5 ms, post impact.

The HS-DIC system was applied to determining which areas of the physical model produce the greatest deformation, strain and strain rate using the HS-DIC approach, from different impact locations at the two impact velocities (1.72 m.s^{-1} and 2.43 m.s^{-1}) shown in Tables 3.8 and 3.9. It was observed that the majority of the strain and strain rate was dissipated by the sutures and fontanelles see Figures 3.11, 3.12 and 3.13.

The sutures and fontanelles produce strain values as high as areas of the cranial bones from the same impact tests at two impact velocities (1.72 m.s^{-1} and 2.43 m.s^{-1}), see Figure 3.11. The maximum percentage strain values in the suture and fontanelle areas, when impacted onto the vertex, frontal and occipital bones were increased by 186%, 155% and 109%, respectively at 1.72 m.s^{-1} and by 169%, 166% and 188% at 2.43 m.s^{-1} , compared to those measured at the cranial bones.

The values of maximum strain from the suture and fontanelle areas at 2.43 m.s^{-1} is significantly higher; 32 % from the vertex impact test; 31% from forehead impact test and 29 % from occipital impact test, compared to the strain values from the same areas at

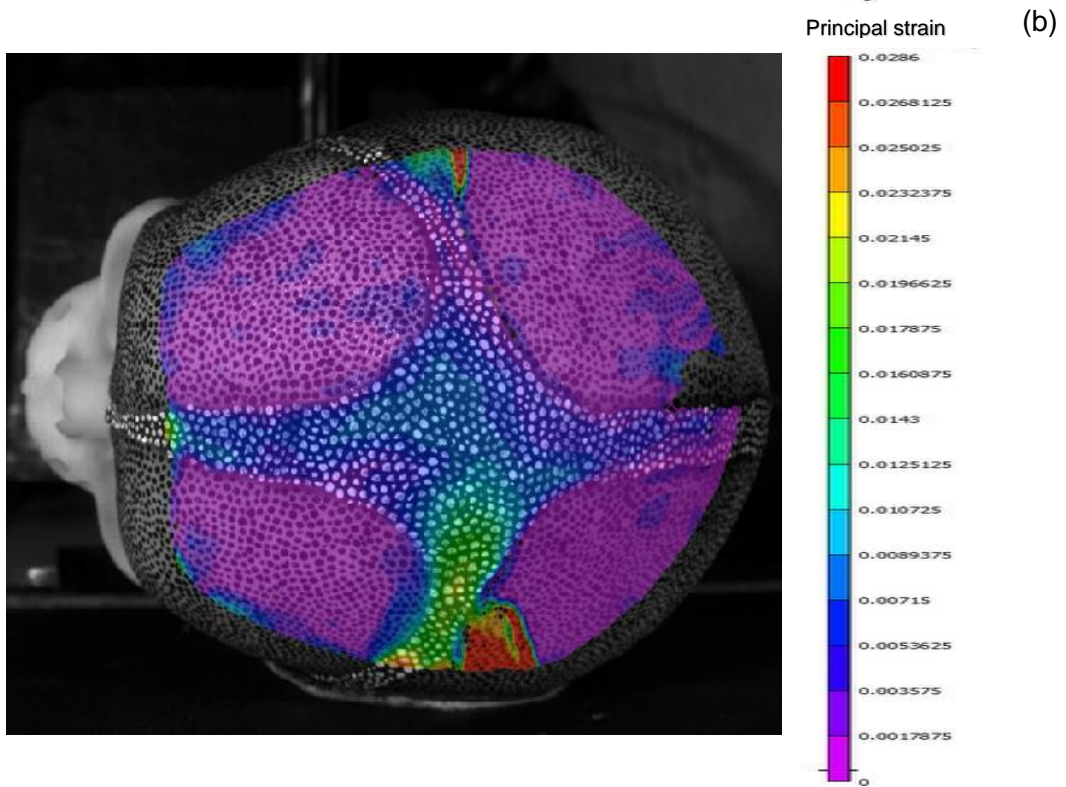
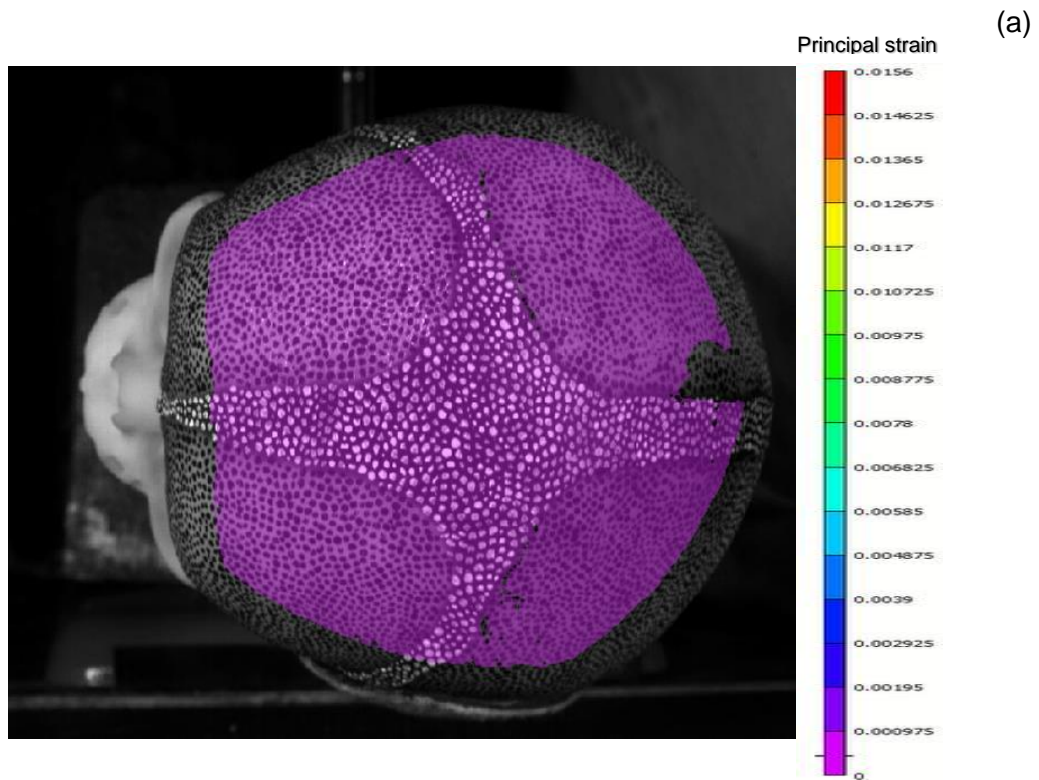
1.72 m.s⁻¹, see Figure 3.12. Further, the strain rate values in the sutures and fontanelles ranged between 1000% s⁻¹ and 2000% s⁻¹, see Figure 3.13.

Table 3.8 . Maximum strain produced by the physical model at different impact locations at two impact velocities.

Impact location	Impact velocity (m.s⁻¹)	Max strain in sutures and fontanelles (%)	Max strain in cranial bones (%)
Vertex	1.72	3 ± 0.5	0.9
Forehead	1.72	3 ± 0.9	0.9±0.1
Occipital	1.72	3 ± 0.6	0.6±0.1
Vertex	2.43	3 ± 0.3	0.2±0.2
Forehead	2.43	3 ± 0.3	0.2±0.3
Occipital	2.43	3± 0.2	0.2±0

Table 3.9. Maximum strain rate produced by the physical model at different impact locations at two impact velocities.

Impact location	Impact velocity (m.s⁻¹)	Max Strain rate (%)
Vertex	1.72	637 ± 83
Forehead	1.72	1911 ± 1084
Occipital	1.72	2131 ± 796
Vertex	2.43	1516 ± 305
Forehead	2.43	2275 ± 684
Occipital	2.43	2720 ± 400



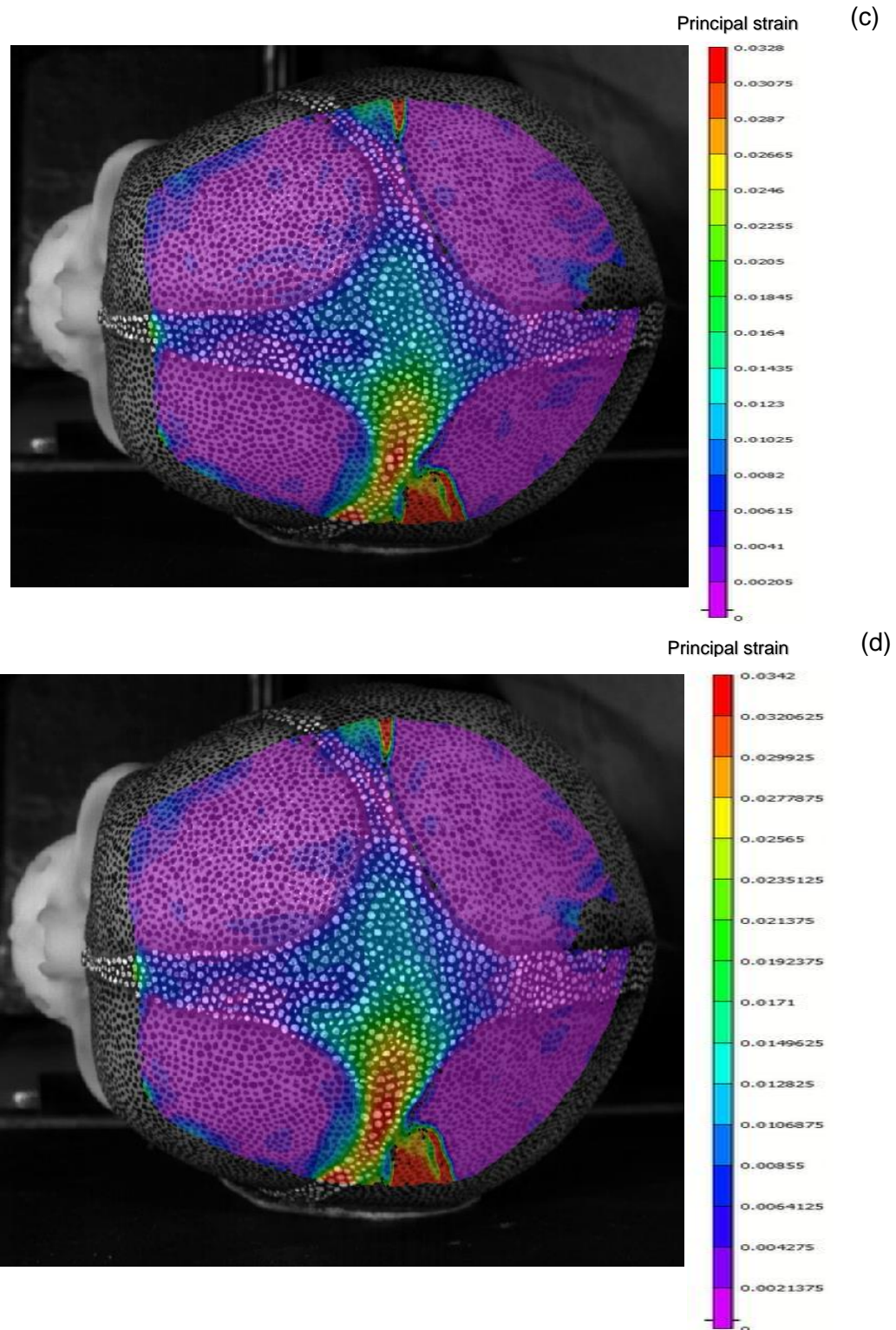


Figure 3.10. Coronal view of physical head model deformation for a $2.43\text{m}\cdot\text{s}^{-1}$ impact onto a metal plate using HS-DIC (a) prior to impact - no head deformation, (b) 2ms post impact - 0.028mm deformation, (c) 3ms post impact - 0.032mm deformation, (d) 5ms post impact - 0.034mm deformation.

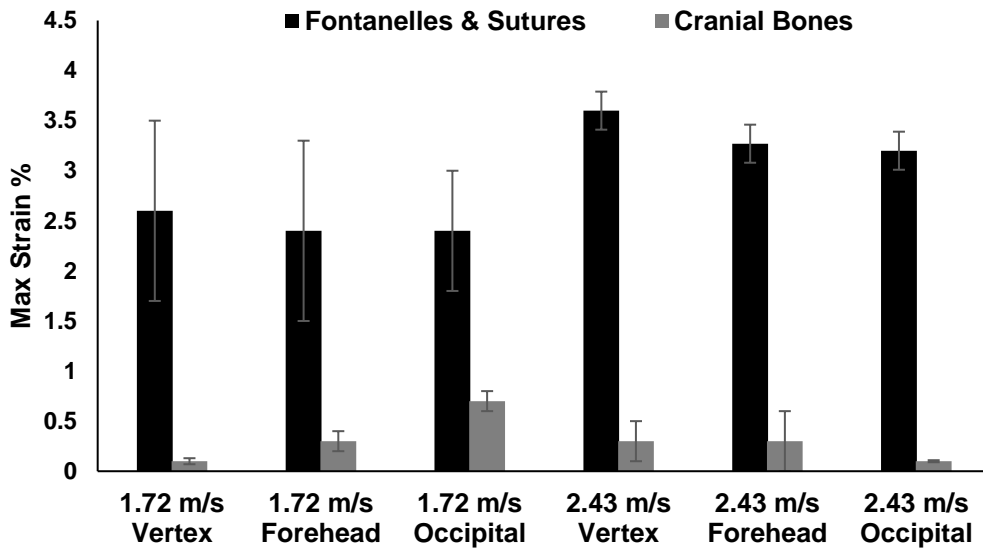


Figure 3.11. Physical model comparison of max strain from different impact locations at two impact velocities.

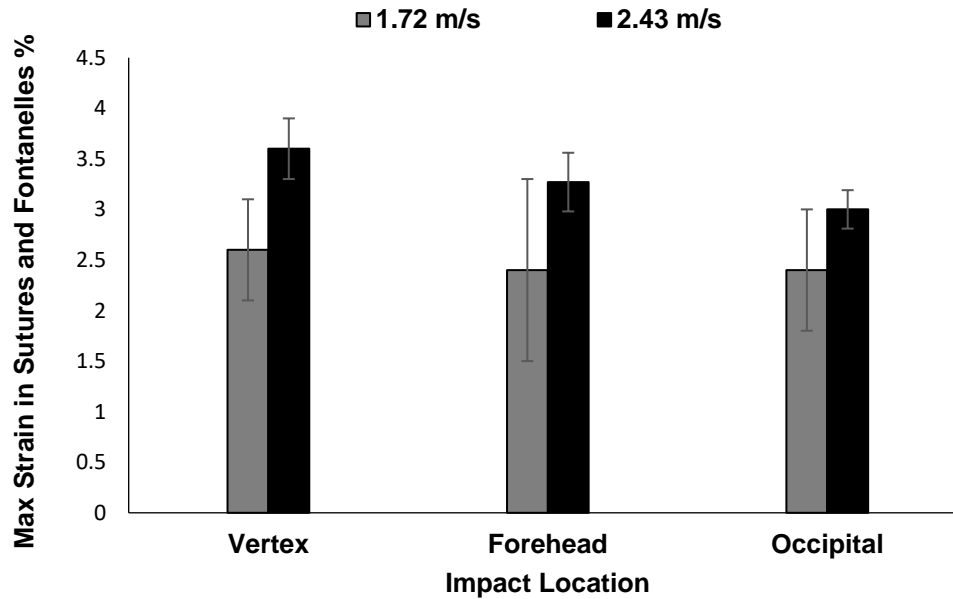


Figure 3.12. Maximum strain and drop height from different impact locations of physical model at two impact velocities.

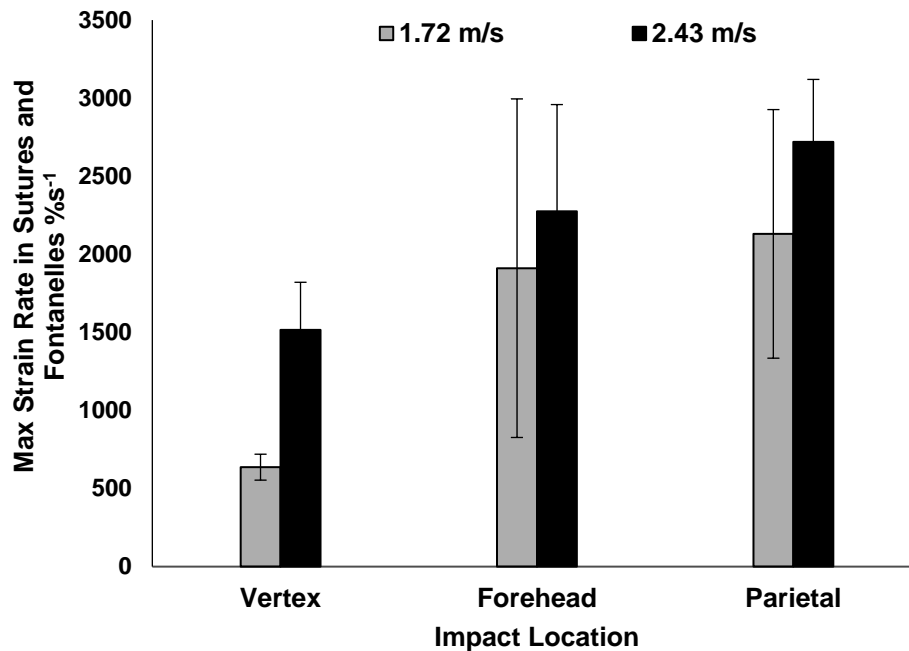


Figure 3.13. Maximum strain rate at different impact locations of physical model at two impact velocities.

3.4 Global validation of the paediatric FE head model against PMHS data.

Validation of the FE head model was achieved by a series of impact simulations, conducted in accordance with the PMHS infant head impact experiments [82]. Impacts were simulated onto different regions of the head (forehead, parietal, occipital and vertex), at 1.72 m.s^{-1} and 2.43 m.s^{-1} onto a 'rigid surface'. A total of eight impact conditions were included in the simulations. The numerical acceleration was also obtained by dividing the impact force by the head mass, as applied during the PMHS experiments [82]. The mass of the computational head model of the 10-day-old infant was closest to the mass of the 3-day-old infant PMHS head in [82]. The kinematic variables measured with the FE study are absolute values and do not include a measure of variation. Thus, statistical significance cannot be calculated for these parameters. An upper bound of variation was applied such that only values equal to or greater than 15% between the FE model and

the PMHS tests [82], are discussed further, an approach, which is in accordance with previous studies [71, 77].

3.4.1 Impact translational acceleration.

A validation was conducted based on a comparison between the numerical simulation of the FE head model and the experimental results from the series of PMHS tests [85]. The results are presented as a profile of the acceleration – time impact response from a free fall through 0.30 m (corresponding to 2.43 m.s^{-1}) onto the four different head impact locations, shown in Figures 3.14 a - d. The FE model acceleration–time impact curves were observed to generally correlate well with the PMHS impact data, see Figure 3.14. Acceleration-time contact curve characteristics, at four different impact locations from a 0.30 m height drop (2.43 m.s^{-1}), produce a correlation score equal to or greater than 86, (see equations 2.17, 2.18 and 2.19), shown in Table 3.10.

Table 3.10. Comparison of model performance between the PMHS and FE model experiments using the correlation score (CS) measured from $CS_{N\text{-phase}}$, $CS_{N\text{-amp}}$ and $CS_{N\text{-shape}}$ at 2.43 m.s^{-1} .

Impact location	Impact velocity (m.s^{-1})	$CS_{N\text{-phase}}$	$CS_{N\text{-amp}}$	$CS_{N\text{-shape}}$	CS average
Vertex	2.43	98	99	99	99
Occipital	2.43	99	97	91	96
Forehead	2.43	98	90	99	96
Parietal	2.43	99	99	96	98

From Figures 3.14 a - d and 3.15, it appears that the values for peak resultant acceleration, for all eight drop tests, show a good correlation for all the conditions, although a variation of greater than 15% can be observed at the occipital, frontal and

parietal regions and less than 15% at the vertex, at both 1.27 m.s⁻¹ and 2.43 m.s⁻¹. A comparison of the output variables between the FE head model and PMHS can be seen in Figure 3.15. The kinematic variable of global translational acceleration from the FE model at the two impact velocities is presented in Table 3.11.

Table 3.11. Global translational acceleration and duration of impact from the FE model at 1.72 m.s⁻¹ and 2.43 m.s⁻¹.

Impact location	Impact velocity (m.s⁻¹)	Peak acceleration (g)	Durations of impact (s)
Vertex	1.72	61	0.005 ±0.0010
Occipital	1.72	63	0.004±0.0010
Forehead	1.72	78	0.002 ±0.0010
Parietal	1.72	67	0.003 ±0.0010
Vertex	2.43	91	0.006 ±0.0010
Occipital	2.43	101	0.004 ±0.0010
Forehead	2.43	121	0.002 ±0.0010
Parietal	2.43	92	0.007 ±0.0010

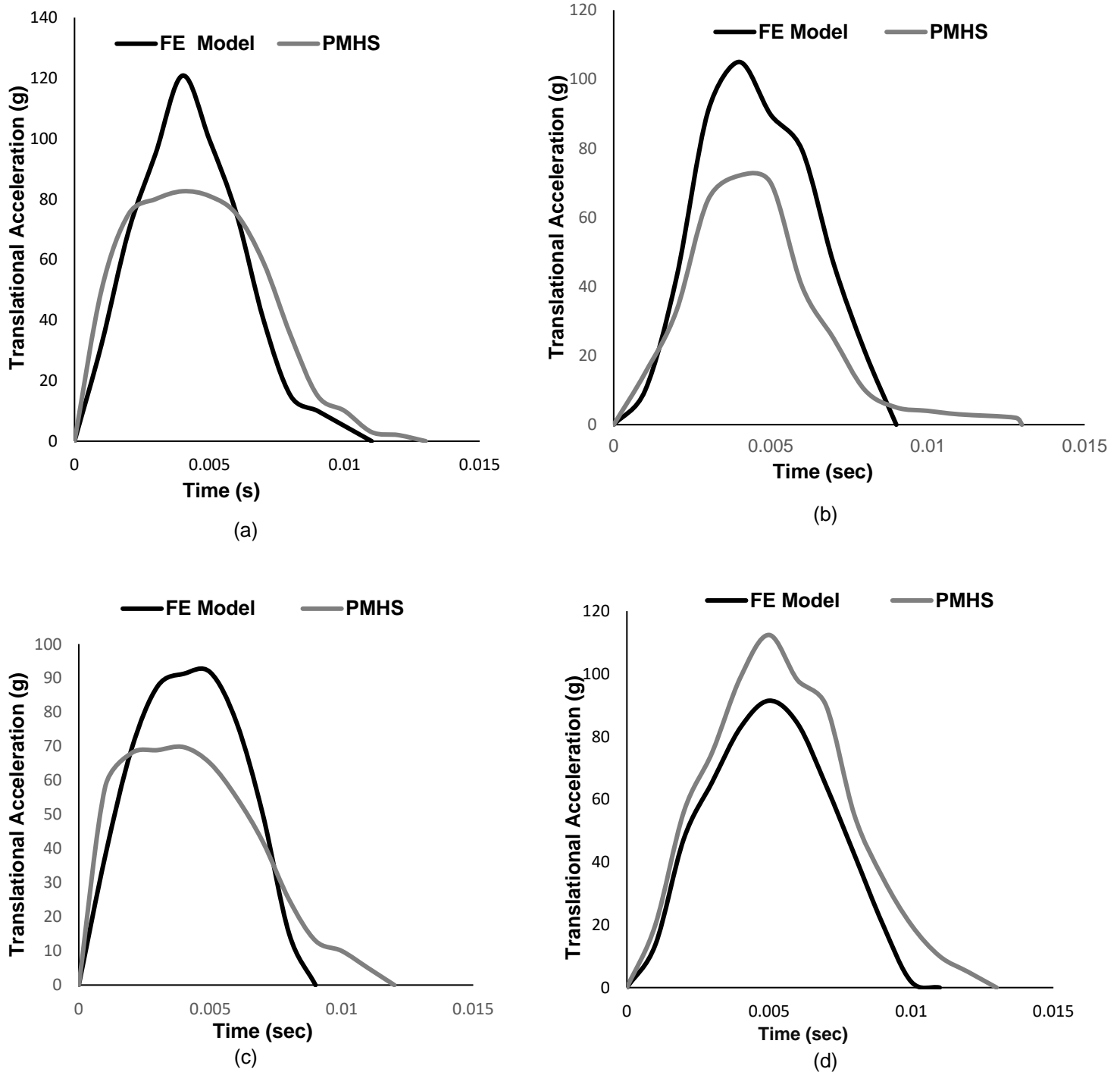


Figure 3.14. The FE head model was impacted onto a rigid surface at the (a) forehead (b) occiput (c) parietal and (d) vertex regions at $2.43 \text{ m}\cdot\text{s}^{-1}$.

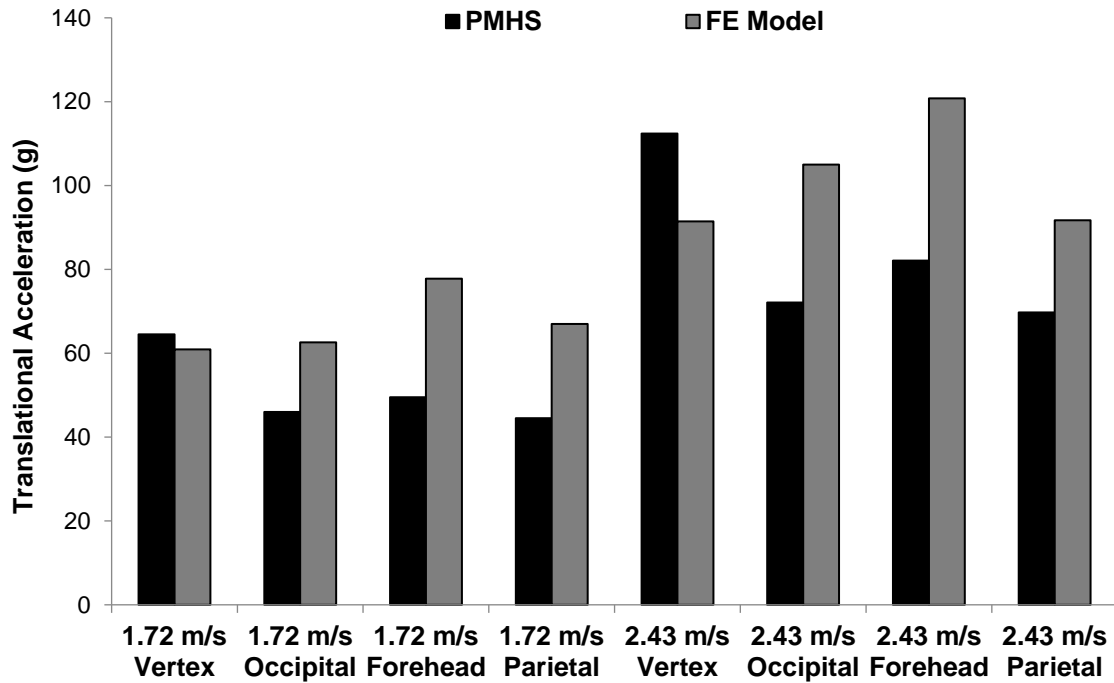


Figure 3.15. Peak acceleration and impact velocity for infant PMHSs and FE head model impact simulations.

3.4.2 Duration of Impact

Typical impact time durations between the PMHS and FE model throughout the validation process are shown in Figure 3.16. The average impact time durations for the FE model were observed to be 10ms at the impact velocity of 1.27 m.s⁻¹ and 11ms at 2.43 m.s⁻¹, compared to the PMHS values, which were 12ms at 1.27 m.s⁻¹ and 13ms at 2.43 m.s⁻¹, representing a shorter impact duration by 18 %, and 17% respectively. There is a significant variation in impact time duration, which is greater than 15% between the FE model and PMHS tests at both impact velocities.

Figure 3.15, demonstrates that the peak accelerations for the FE model appeared to be close to the PMHS's impact response. However, the impact - time durations from the

simulation were shorter than those in the PMHS tests. Figure 3.14a - d shows the acceleration - time contact curve for different impact regions at an impact velocity of 2.43 m.s⁻¹, which evidences the existence of a variation in the impact duration. From the above comparisons, it is apparent that the paediatric FE head model responses are generally in favorable agreement with the PMHS results [82]. Even when a slight variation in resultant peak acceleration values were observed, with respect to different velocities, they did not vary significantly with respect to different impact locations.

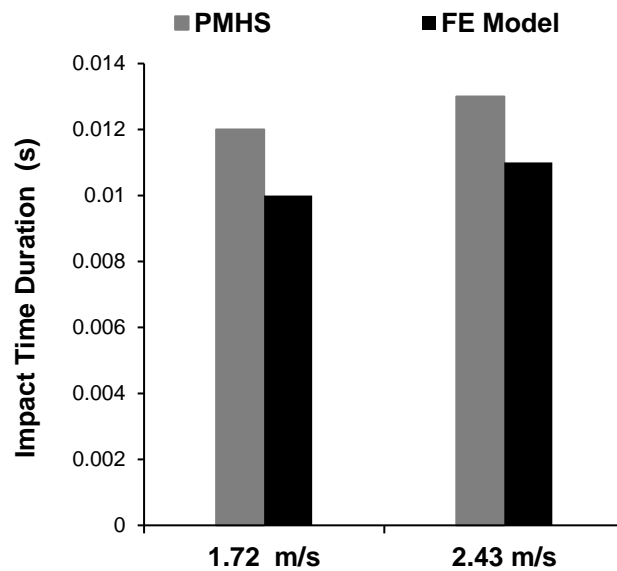


Figure 3.16. Comparison of impact - time durations, between the FE head model with the closest mass to PMHS.

3.5 Parametric study of the paediatric FE model

Each of the parametric models was assessed against the baseline model from the validation process. Again, a greater than a 15% difference in the output variable for each parametric model is discussed below, see Tables 3.12. and 3.13.

3.5.1 First parametric model

From this parametric analysis, it appears that the output variables of peak translational acceleration from the parametric FE model (with closed foramen magnum), did not change by greater than 15%, compared to the baseline FE model (with open foramen magnum), see Table 3.12.

Table 3.12. Comparison of global translational acceleration from the baseline and the parametric FE model at two impact velocities.

Impact location	Impact velocity (m.s ⁻¹)	Baseline FE model peak acceleration (g)	Parametric FE model peak acceleration (g)
Vertex	1.72	61	61
Occipital	1.72	63	63
Forehead	1.72	78	78
Parietal	1.72	67	67
Vertex	2.43	91	91
Occipital	2.43	101	101
Forehead	2.43	121	121
Parietal	2.43	92	92

3.5.2 Second parametric model

From this parametric analysis, the output variables of peak translational acceleration from this parametric FE model (modelled using tied constraints) have no effect, compared with the baseline FE model (modelled using sliding interface), see Table 3.13.

Table 3.13. Comparison of global translational acceleration from the baseline and the parametric FE model at two impact velocities.

Impact location	Impact velocity (m.s ⁻¹)	Baseline FE model peak acceleration (g)	Parametric FE model peak acceleration (g)
Vertex	1.72	61	61
Occipital	1.72	63	63
Forehead	1.72	78	78
Parietal	1.72	67	67
Vertex	2.43	91	91
Occipital	2.43	101	101
Forehead	2.43	121	121
Parietal	2.43	92	92

3.6 Sensitivity analysis

3.6.1 Influence of the Impact location

The peak accelerations for the occipital, parietal and frontal bones from the impact simulations at 2.43 m.s⁻¹ onto different impact regions are shown in Figure 3.17 and Table 3.14. For an occipital impact simulation, see Figure 3.17a, the peak acceleration response from regions ‘close to the base’, the vertex and the right and left parietal bones are 92g, 93g, 97g and 96 g, respectively, which are less than 15%, compared to the peak acceleration response (101g) from the baseline impact region (center of the occiput) at

2.43 m.s⁻¹. For a parietal impact simulation, as shown in Figure 3.17b, the peak acceleration response from regions 'close to the base', the vertex, the occiput and forehead are 89g, 85g, 98g and 93 g, respectively, which are less than the threshold 15%, compared to the peak acceleration response (92 g) at the baseline impact region (center of the parietal bone) at the impact velocity of 2.43 m.s⁻¹.

The 2.43 m.s⁻¹ forehead impact simulation peak acceleration response at the baseline impact region, the lower region of the forehead, shown in Figure 3.17c, is 121g, and greater than the 82g at the region close to upper forehead, near the soft cranial bone and membranous fontanelle, exceeding the threshold 15% difference. So the impact location at the simulated experimental fall height has a limited effect on the "global" impact response of the parietal and occipital bones, though a significant effect on the frontal bones.

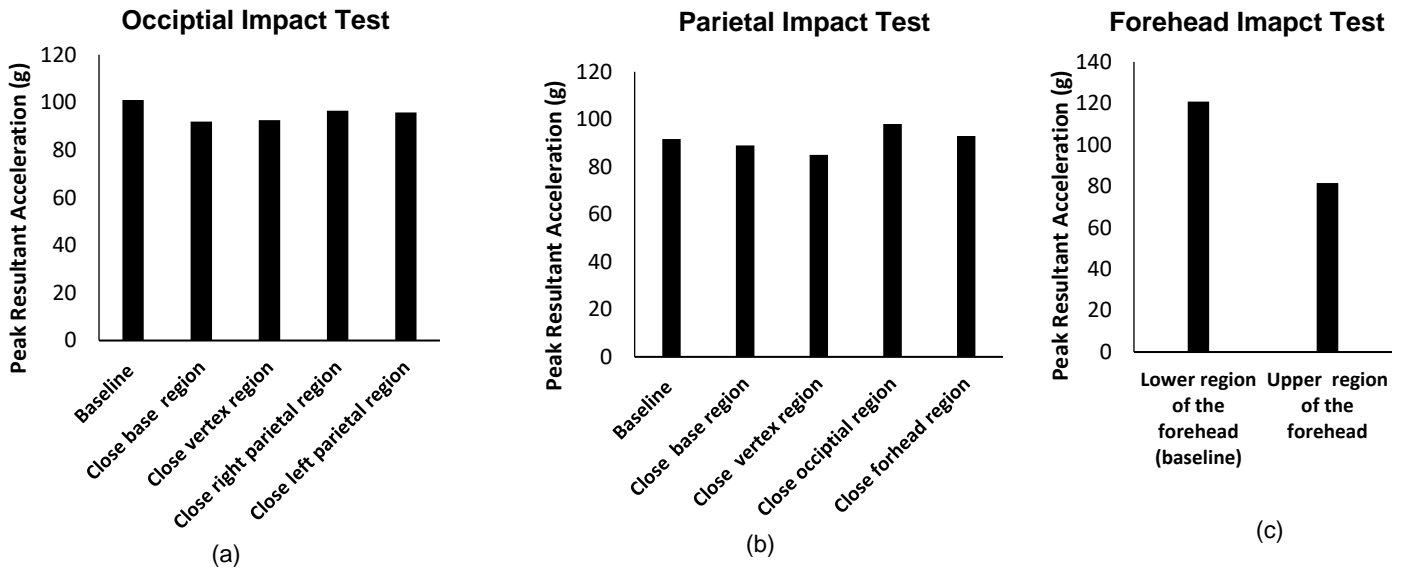


Figure 3.17. Comparison of the peak acceleration response at the baseline and parametric FE head model at different impact regions at the impact velocity of 2.43 m.s⁻¹.

Table 3.14. Peak acceleration response of the baseline FE head model and parametric FE model at different impact regions at the impact velocity of 2.43 m.s⁻¹.

Impact simulation	Impact location	Peak acceleration (g)
Occipital impact	Baseline (“centre” of the occipital bone)	101
	Close base region	92
	Close vertex region	93
	Close right parietal region	97
	Close left parietal region	96
Parietal impact	Baseline (center of the partial bone)	92
	Close base region	89
	Close vertex region	85
	Close occipital region	98
	Close forehead region	93
Forehead impact	Baseline (lower region of the forehead)	121
	Upper region of the fore head	82

3.6.2 Influence of the position of the occipital bone, in relation to the parietal bones.

The comparison of the impact acceleration response between the inline FE occipital – parietal bone configuration, FE depressed occipital – parietal bone configuration and PMHS study [82] are shown in Figure 3.18 and Table 3.15. The same peak acceleration responses of both FE head model were observed at the vertex and forehead impact simulation resented by 61g, 78g respectively at 1.72 m.s⁻¹ and 92 g, 121 g at 2.43 m.s⁻¹, respectively. On the other hand, the peak acceleration responses of the occipital and parietal impact simulations of the FE model have the inline occipital – parietal bone configuration, represented by 63 g (occipital), 67g (parietal) at 1.72 m.s⁻¹ and 101g (occipital), 92 g (parietal) at 2.43 m.s⁻¹ are greater than 15%, compared to the peak accelerations response of the occipital and parietal impact simulations of the FE model have the depressed occipital – parietal bone configuration, represented by 63g (occipital), 67g (parietal) at 1.72 m.s⁻¹ and 101g (occipital), 92g (parietal) at 2.43 m.s⁻¹ respectively. It seems that the position of the occipital bone, in relation to the parietal bones, have a significant effect on the impact acceleration response of the occipital and parietal impact simulations. Also, there was no significant variation (less than 15%) in the impact acceleration response from the FE depressed occipital – parietal bone configuration and the PMHS study [82] at both the occipital and parietal impact simulations.

Table 3.15 Comparison of peak translational acceleration from the FE 'inline' and FE 'out of line' head model with infant PMHS impact tests at two impact velocities.

Impact location	Impact velocity (m.s ⁻¹)	FE 'inline' model Peak acceleration (g)	FE 'out of line' (depressed) model. Peak acceleration (g)	PMHS Peak acceleration [82] (g)
Vertex	1.72	61	61	65
Occipital	1.72	63	44	46
Forehead	1.72	78	78	50
Parietal	1.72	67	50	45
Vertex	2.43	91	91	112
Occipital	2.43	101	70	72
Forehead	2.43	121	121	82
Parietal	2.43	92	72	70

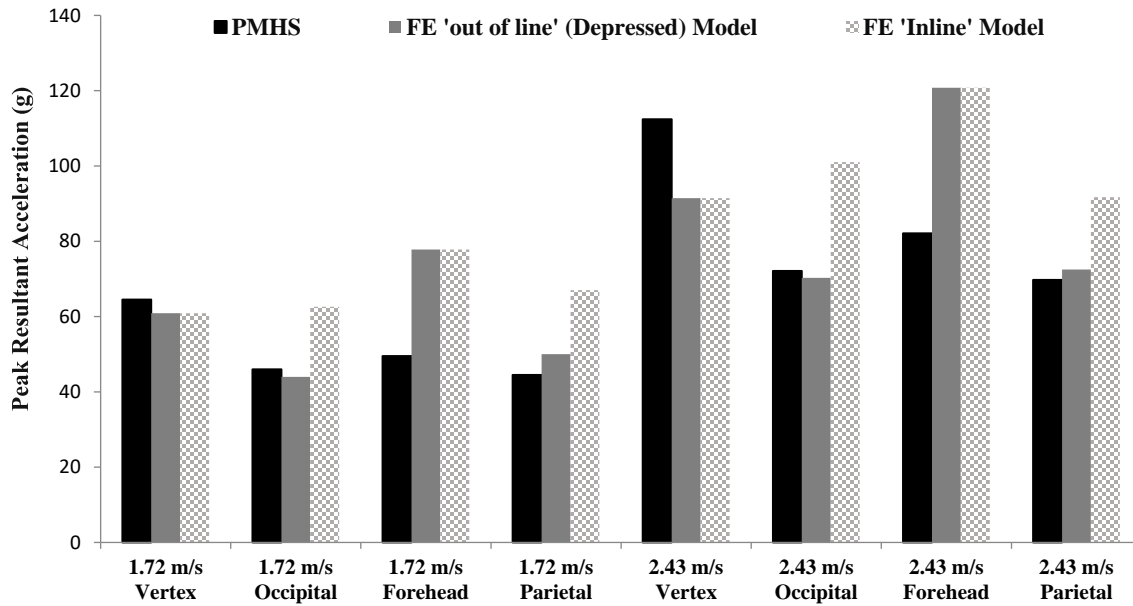


Figure 3.18. Peak acceleration and drop height for infant FE 'inline' and FE 'out of line' (depressed) head model with infant PMHS impact tests.

3.7 Global validation of the paediatric FE model against physical model data.

Post validation of the FE head model with PMHS study reported by Prange et al.[85]. Another, computational simulation was running and a numerical acceleration was also calculated, in accordance with physical model, by dividing the impact force by the head mass, as applied during the PMHS experiments [82]. The developed FE head model was subjected to eight different fall impact scenarios and all the kinematic variables were assessed against the output variables from the physical model.

3.7.1 Impact acceleration

The results of the impact acceleration response are shown in Figure 3.19 a - d as a profile of the acceleration – time impact response, from an impact velocity of 2.43 m.s^{-1} , onto the four different head impact locations. From Figure 3.19, it appears that the values for peak acceleration, for all eight drop simulations, show a good correlation for all the conditions. The FE model acceleration–time impact curves were observed to generally correlate well with the physical model impact data, see Figure 3.19. Acceleration-time contact curve characteristics, at four different impact locations from a 0.30m height drop (2.43 m.s^{-1}), produce a correlation score equal to or greater than 86, (see equations 2.17, 2.18 and 2.19), shown in Table 3.16. The variation in impact acceleration responses from the FE simulation and the corresponding physical model was less than 15% for the same impact tests at the vertex, occipital, forehead and parietal bones, at both impact velocities. The impact acceleration response from the FE simulations, see Table 3.11, was subsequently compared with the “Global” physical model response, for each impact, see Table 3.4, calculated using the “rigid body approximation”, shown in Figure 3.20.

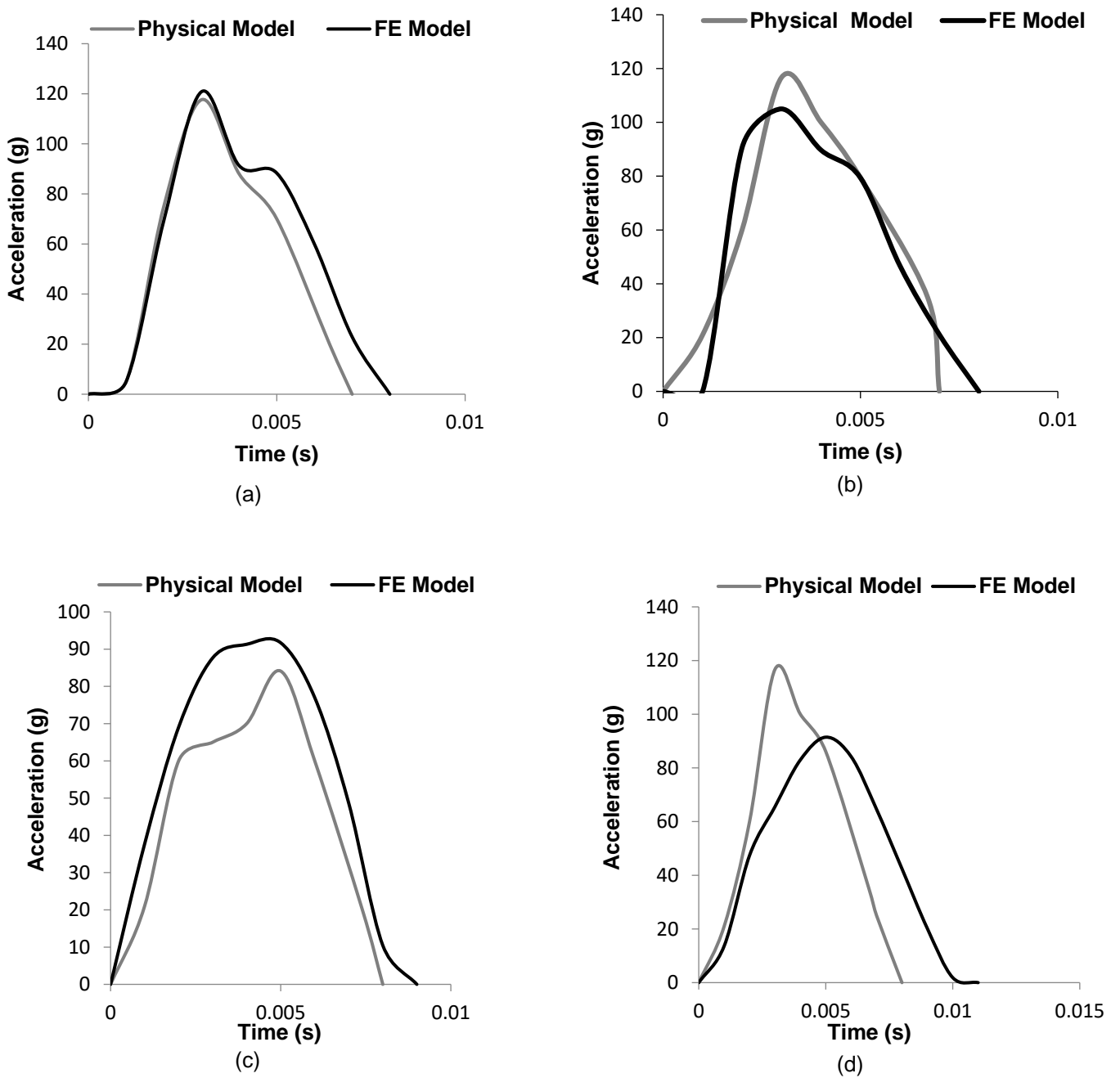


Figure 3.19. Infant head acceleration - time contact response from different impact locations from the physical model experiments and FE simulations (a) forehead, (b) occipital, (c) parietal and (d) vertex, at 2.43 m.s⁻¹ impact velocity.

Table 3.16. Comparison of model performance between the physical model and FE model experiments using the correlation score (CS) measured from CS_{N-phase}, CS_{N-amp} and CS_{N-shape} at 1.72 m.s⁻¹ and 2.43 m.s⁻¹.

Impact location	Impact velocity (m.s ⁻¹)	CS _{N-phase}	CS _{N-amp}	CS _{N-shape}	CS average
Vertex	1.72	98	99	99	99
Occipital	1.72	99	97	91	96
Forehead	1.72	98	99	99	99
Parietal	1.72	99	90	96	95
Vertex	2.43	98	99	99	99
Occipital	2.43	99	97	91	96
Forehead	2.43	98	90	99	96
Parietal	2.43	99	99	96	98

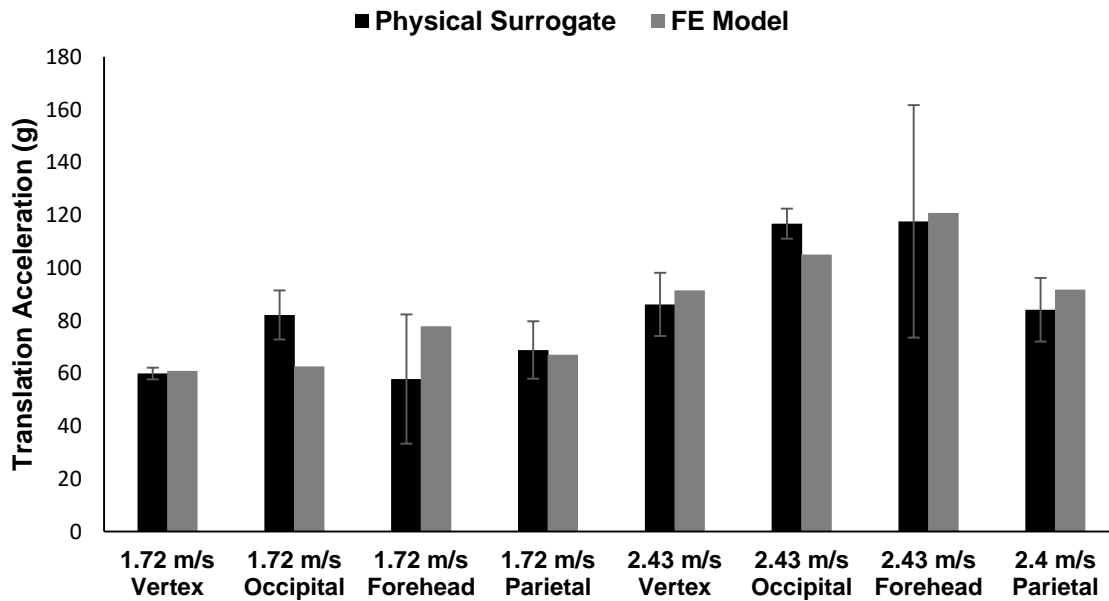


Figure 3.20. Peak acceleration (global response) of the paediatric head in physical and computational simulations at two impact velocities.

3.7.2 Duration of Impact

The impact time durations, between the FE model and the physical model, during the global validation process is shown in Figure. 3.21. The average impact time durations of the FE model were observed to be slightly shorter by 13% and 10%, at impact velocities of 1.27 m.s⁻¹ (5ms) and at 2.43 m.s⁻¹ (6ms), respectively; compared to the physical model tests [82] at impact velocities of 1.27 m.s⁻¹ (6ms) and 2.43 m.s⁻¹ (7ms). There is no significant difference in impact time duration of greater than 15% between the FE model simulations and the physical model tests at both impact velocities of 1.27 m.s⁻¹ and 2.43 m.s⁻¹.

From the above comparisons, it is apparent that the paediatric FE head model response shows a good agreement with the global response of the physical model. Even when some resultant peak acceleration values varied, with respect to differences in impact velocity (drop heights), they did not vary significantly with respect to different impact locations.

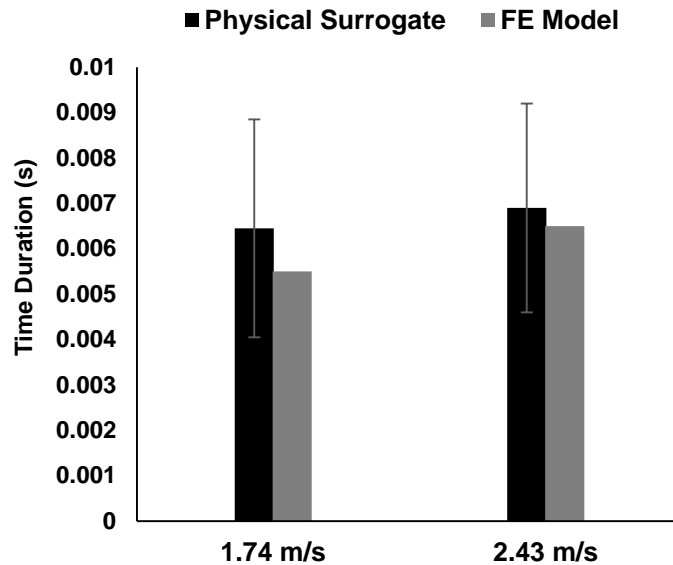


Figure 3.21. Comparison of impact time duration with different impact velocity (drop height) between physical and numerical simulation experiments of paediatric head model.

3.8 Physical model regional and local validation of the FE head model.

3.8.1 Impact acceleration

Subsequent to the FE model being “globally” validated against the physical model data, applying the same “rigid body approximation” as reported in the previous section, the validity of the assumption was tested by comparing/measuring the translational acceleration response at different impact locations in the skull. Firstly, the relative translational accelerations, from different regions of the FE model, are significantly higher by greater than 15% than those calculated using the “global” “rigid body approximation”, see Figure 3.22. The local acceleration response from the vertex, occipital, forehead and parietal regions at both impact velocity $1.72 \text{ m}\cdot\text{s}^{-1}$ and $2.43 \text{ m}\cdot\text{s}^{-1}$ were reported, see Table 3.17 and compared to the global acceleration response, see Table 3.11. Interestingly, the impact of the FE model showing the greatest difference is the occipital bone impact, where at an impact velocity of $1.72 \text{ m}\cdot\text{s}^{-1}$, the difference between the mean recorded bone

acceleration at the skull structure and the measured force at the force plate is 59%. However, the smallest variation, from the “rigid body approximation” is at the vertex, where the difference is 7%.

Table 3.17. FE model local translational impact acceleration and duration at two impact velocities.

Impact location	Impact velocity (m.s ⁻¹)	Peak acceleration (g)	Durations (s)
Vertex	1.72	81 ± 4	0.006 ±0.0010
Occipital	1.72	195 ± 4	0.004±0.0010
Forehead	1.72	220 ± 7	0.002 ±0.0010
Parietal	1.72	192 ± 8	0.003 ±0.0010
Vertex	2.43	120 ±3	0.006 ±0.0010
Occipital	2.43	167± 20	0.004 ±0.0010
Forehead	2.43	270 ± 6	0.002 ±0.0010
Parietal	2.43	130 ±10	0.007 ±0.0010

Further, the local acceleration response of the FE model is shown in Table 3.17, comparing the corresponding local acceleration response of the physical model from the same areas (vertex, occiput, forehead and parietal), see Table 3.6 at the impact velocities of 1.72 m.s⁻¹ and 2.43 m.s⁻¹. Figure 3.23 illustrates the FE model’s local/regional acceleration response, which shows a good correlation with the regional response from the physical model. There is no variation in local impact acceleration response greater than 15%. Thus, the FE head model acceleration response is in a good agreement with the physical model.

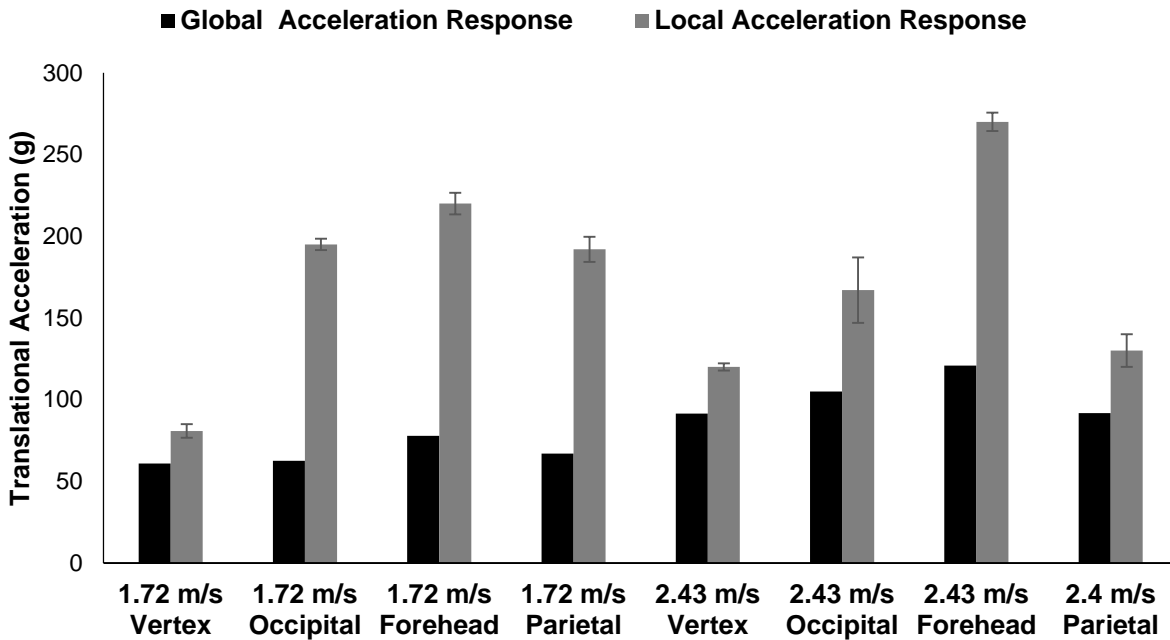


Figure 3.22. Comparison of global acceleration and local acceleration response of the FE model.

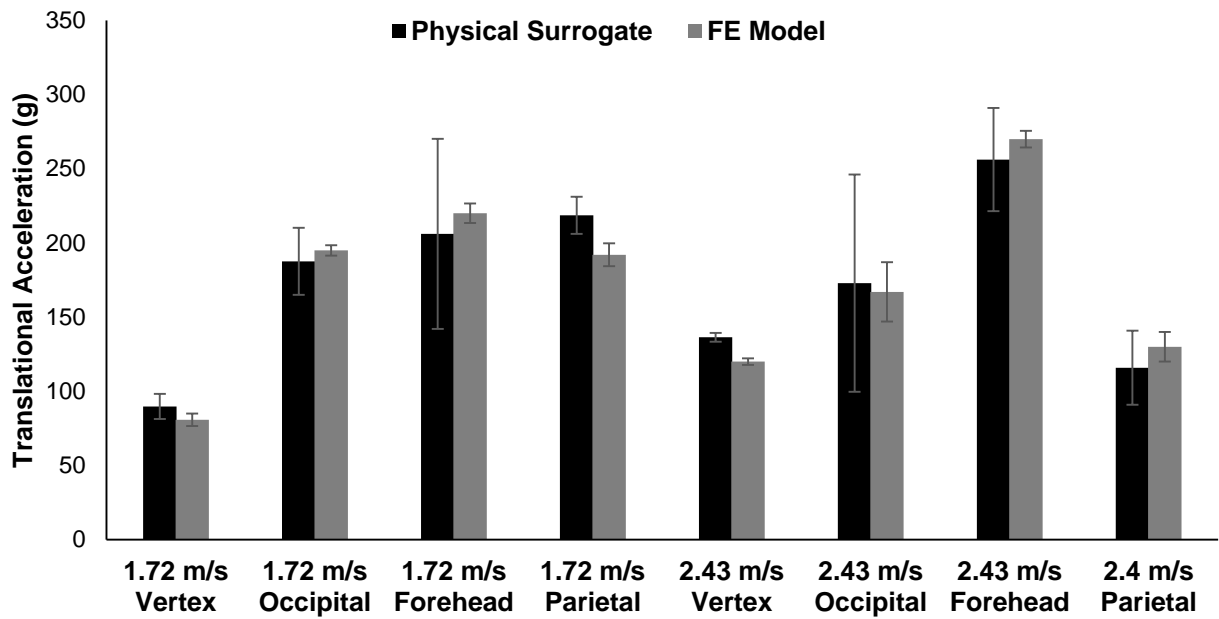


Figure 3.23. Local response from the present FE simulation compared against the local response from physical model.

3.8.2 Sensitivity analysis

3.8.2.1 Influence of the Impact location

The peak accelerations of the occipital, parietal, and forehead bones from the fall impact test at 0.30 m of the present FE model at different impact regions can be seen in Figure 3.24 and Table 3.18.

For an occipital impact simulation, see Figure 3.24a, the peak acceleration response from the region close to the base, vertex region, right and left parietal regions are 200 ± 15 g, 142 ± 26 g, 202 ± 18 g, 215 ± 23 g, respectively, which are higher than 15%, compared to the peak acceleration response (167 ± 20 g) from the baseline impact region (center of the occiput) at 2.43 m.s^{-1} impact velocity.

For a parietal impact simulation, as shown in Figure 3.24b, the peak acceleration response from close to the base region, vertex region, occiput regions and forehead region are 155 ± 15 g, 158 ± 14 g, 161 ± 19 g, 169 ± 13 g, respectively, which are less than 15%, compared to the peak acceleration response (130 ± 10 g) of the baseline impact region (center of the parietal) at 2.43 m.s^{-1} impact velocity.

For a forehead impact simulation, the peak acceleration response (270 ± 60 g) of the baseline impact region (lower region of the forehead), from Figure 3.24c, is higher than 15% compared to the peak acceleration (198 ± 13 g) close to upper region of the forehead, (close to the soft cranial bone and membranous fontanelle) at 2.43 m.s^{-1} impact velocity.

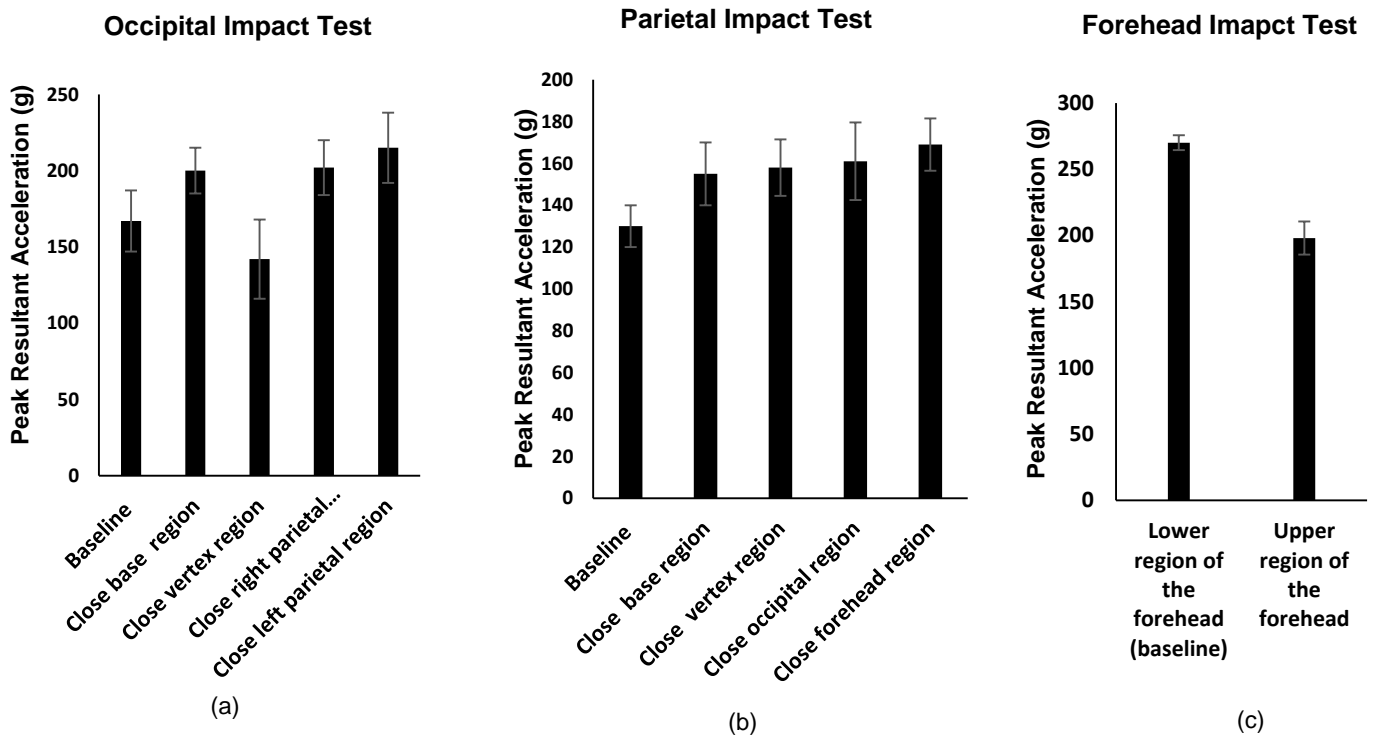


Figure 3.24. Comparison of local peak acceleration response of the baseline and parametric FE head model with different impact regions at 2.43 m.s⁻¹ impact velocity.

Table 3.18 Peak acceleration response of the baseline FE head model and parametric FE model with different impact regions at a 2.43 m.s⁻¹ impact velocity.

Impact simulation	Impact location	Peak acceleration (g)
Occipital impact	Baseline (“centre” of the occipital bone)	167±20
	Close base region	200±15
	Close vertex region	142±26
	Close right parietal region	202±18
	Close left parietal region	215±23
Parietal impact	Baseline (centre of the partial bone)	130±10
	Close base region	155±15
	Close vertex region	158±14
	Close occipital region	161±19

	Close forehead region	169±13
Forehead impact	Baseline (lower region of the forehead)	270±60
	upper region of the forehead	198±13

3.8.2.2 Influence of the position of the occipital bone in relation to the parietal bones

The comparison of the impact local acceleration response between the inline FE occipital – parietal bone configuration, FE depressed occipital – parietal bone configuration is presented in Figure 3.25 and Table 3.19.

The same peak accelerations response of both FE head models were observed at the vertex and forehead impact simulations represented by 81 ± 5 g, 220 ± 7.0 g, respectively at 1.72 m.s^{-1} and 120 ± 2.2 g, 270 ± 70 g at 2.43 m.s^{-1} , respectively. On the other hand, the peak accelerations response of the occipital and parietal impact simulations for the FE model have the 'inline' occipital – parietal bone configuration represented by 195 ± 4 g (occipital), 192 ± 8 g (parietal) at 1.72 m.s^{-1} and 167 ± 20 g (occipital), 130 ± 10 g (parietal) at 2.43 m.s^{-1} are greater than 15%, compared to the peak accelerations response of the occipital and parietal impact simulations of the FE model which has the depressed occipital – parietal bone configuration represented by 164 ± 30 g (occipital), 135 ± 70 g (parietal) at 1.72 m.s^{-1} and 126 ± 16 g (occipital), 95 ± 90 g (parietal) at 2.43 m.s^{-1} , respectively. It seems that the position of the occipital bone in relation to the parietal bones has a significant effect, greater than 15%, on the local impact acceleration response of the occipital and parietal impact simulations.

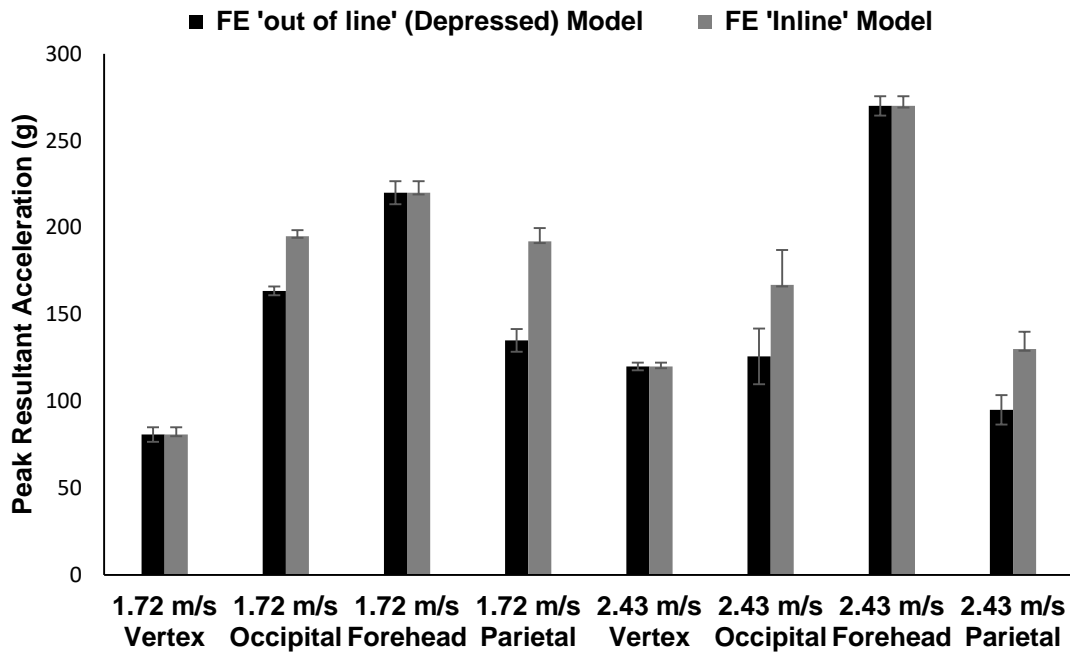


Figure 3.25. Comparison of local acceleration response and drop height for infant FE ‘inline’ and FE ‘out of line’ (depressed) head model.

Table 3.19. Output variables (local translational acceleration, duration of impact) from the FE model at two impact velocities.

Impact location	Impact velocity (m.s ⁻¹)	FE ‘inline’ model Peak acceleration (g)	FE ‘out of line’ (depressed) model Peak acceleration (g)
Vertex	1.72	81 ± 4	81 ± 4
Occipital	1.72	195 ± 4	164±3
Forehead	1.72	220 ± 7	220 ± 7
Parietal	1.72	179 ± 8	135±7
Vertex	2.43	102 ± 2	102 ± 2
Occipital	2.43	167±2	126±2
Forehead	2.43	270±6	270±6
Parietal	2.43	130±1	95±9

3.8.3 Duration of Impact

The total time duration of FE model was compared to the impact time duration of the physical model at impact velocities of $1.72 \text{ m}\cdot\text{s}^{-1}$ and $2.43 \text{ m}\cdot\text{s}^{-1}$. During the regional and local response validation both the FE and physical model, shows little variation, by less than 15%, in impact time duration at both drop heights, see Figure 3.26.

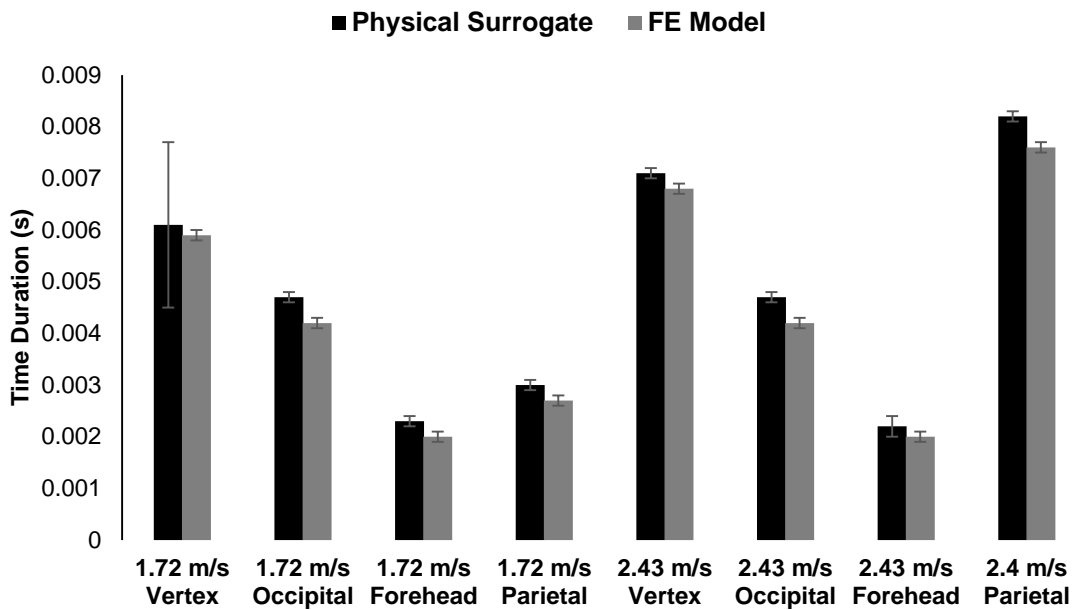


Figure 3.26. Comparison of impact time duration between the physical model experiments and FE simulation.

3.8.4 Head Deformation

The FE simulation was used to determine which region produces deformation for subsequent comparison with the physical model. Figures 3.27 and 3.28 demonstrate that the majority of the strain in the FE model is produced within the relatively elastic sutures and fontanelles regions. The Maximum strain of the FE model from different impact locations at two impact velocities is presented in Table 3.20.

Figure 3.29 shows a comparison between the maximum strain values in the suture and fontanelle regions, of the FE and physical model, where the head was dropped from the two impact velocities 1.72 m.s^{-1} and 2.43 m.s^{-1} onto different head impact locations. The change in maximum strain percentage response of the FE model and the physical model was less than 15% from same impact regions (vertex, forehead and occiput) and at the same impact velocities.

Table 3.20. Maximum strain of FE model from different impact locations at two impact velocities.

Impact location	Impact velocity (m.s^{-1})	Max strain in sutures and fontanelles (%)
Vertex	1.72	3.0
Forehead	1.72	2.9
Occipital	1.72	2.7
Vertex	2.43	4.2
Forehead	2.43	3.8
Occipital	2.43	3.3

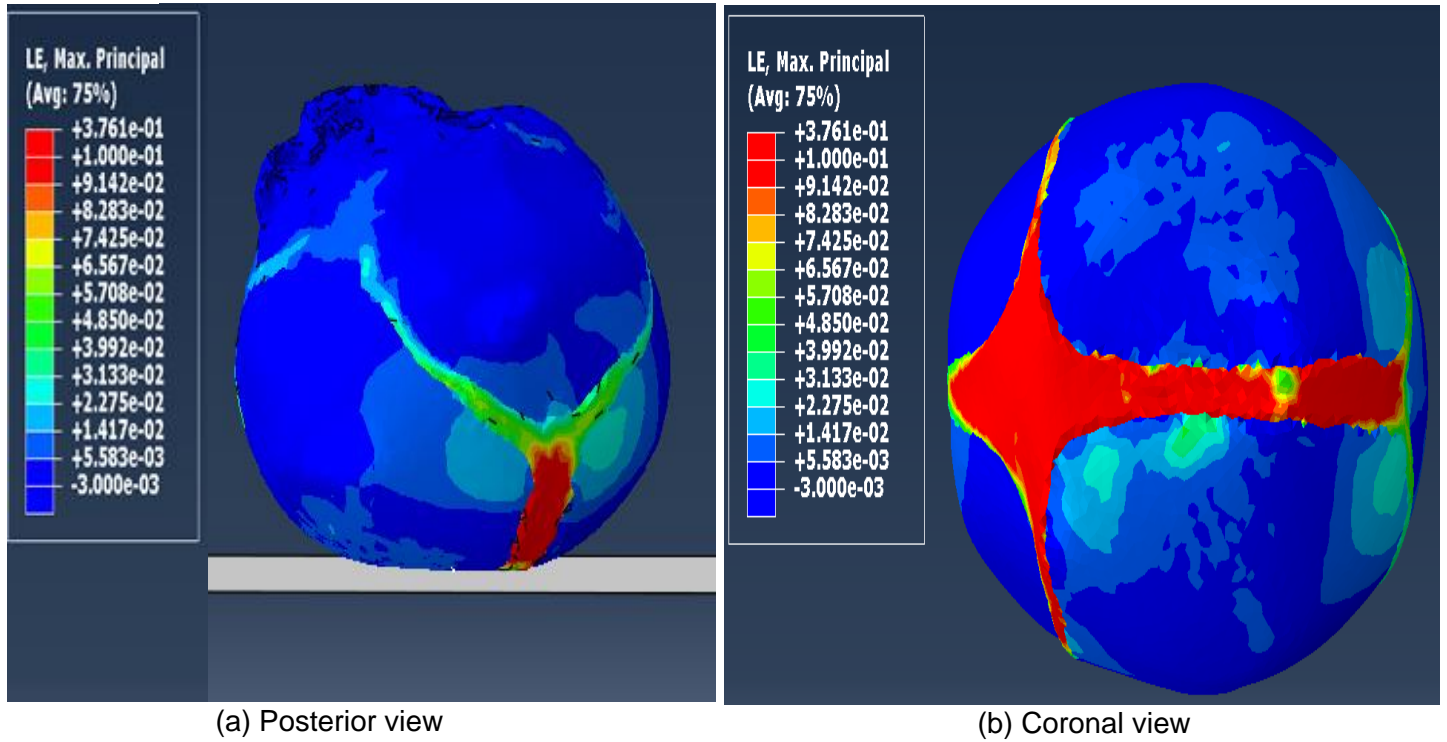


Figure 3.27. Vertex impact illustrating strain zone in coronal sutures and fontanelles

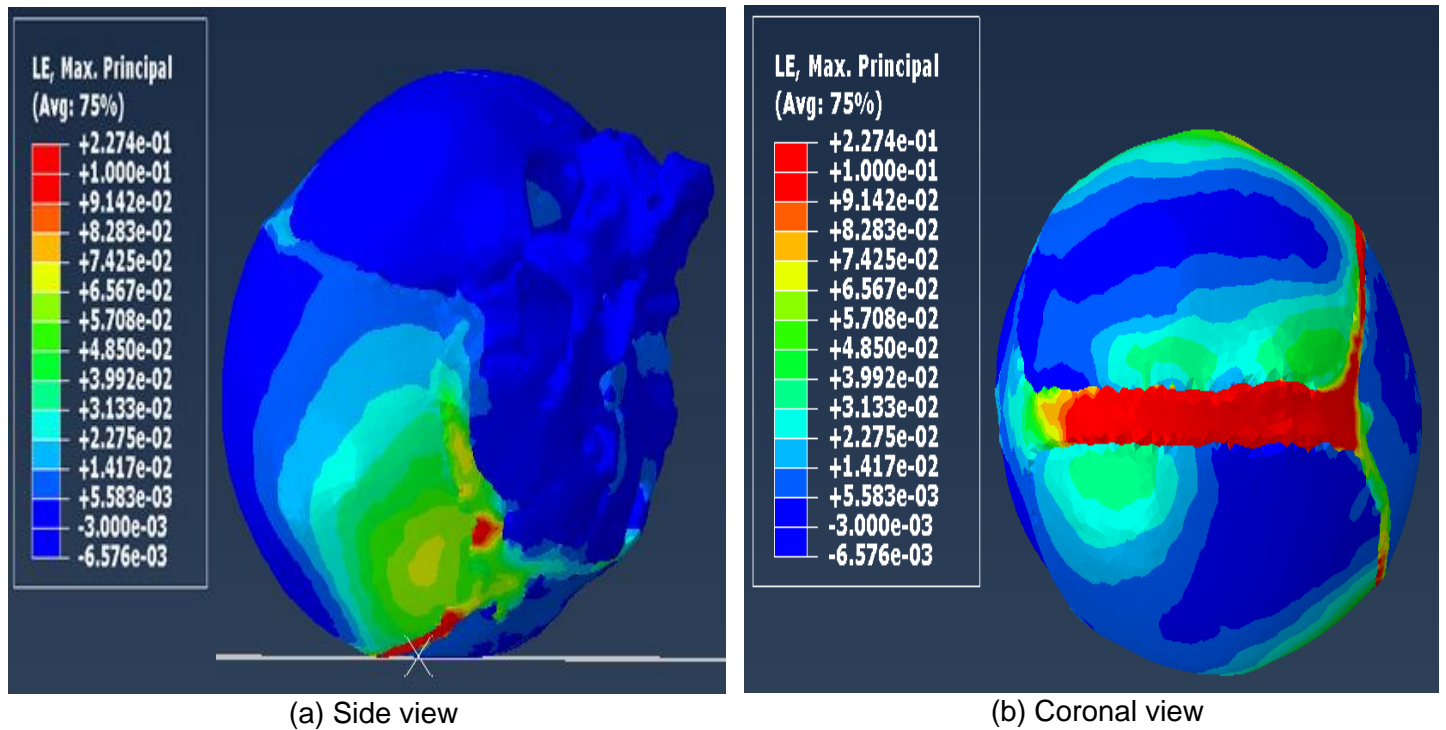


Figure 3.28. Occipital impact illustrating strain zone in coronal sutures and fontanelles.

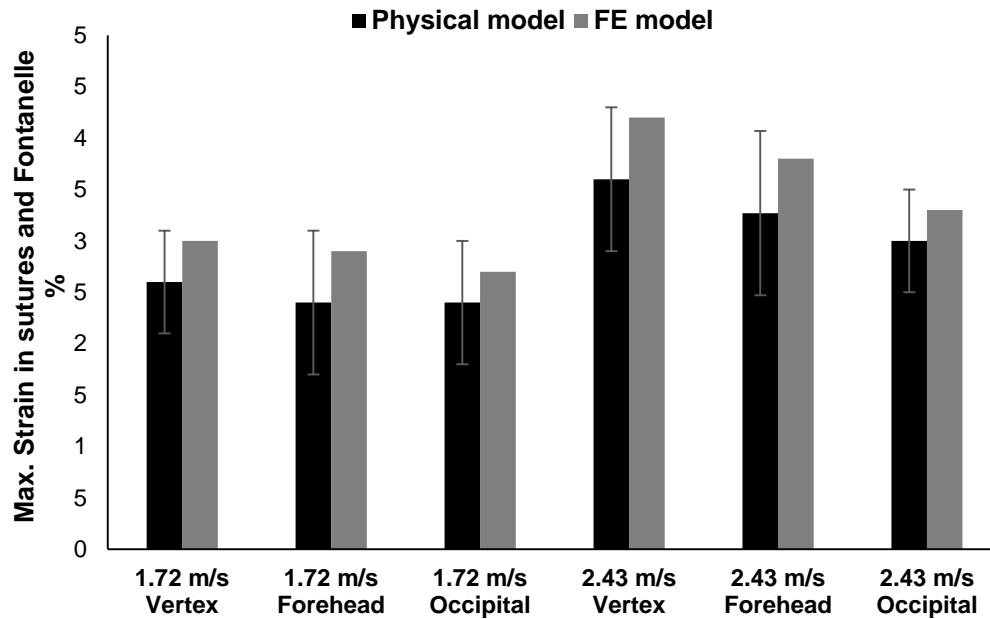


Figure 3.29. Maximum strain of the physical and FE models at different impact locations and two impact velocities.

3.9 Investigating skull fracture from the literature

To validate the models ability as a tool to predict skull fracture, a single 0.82m fall onto the parieto-occipital region was investigated so that assessments could be made with PMHS infant skull fracture patterns reported by Weber studies [80, 81]. From the FE simulation of the 0.82m parieto-occipital impacts, red "hot zone" (high stress zone) can be observed to dissipate within the left lambdoid suture, with the Weber's [80, 81] drawings of the skull fracture location and orientation within the right parietal bone. Figure 3.30, illustrates (a) a sketch of a newborn skull from Weber's PMHS study [80, 81], in accordance with (b) posterior view, (c) side view and (d) coronal view of parietal fracture pattern from FE impact simulation to the parietal-occipital region at drop height of 0.82 m onto an impact surface - stone tile.

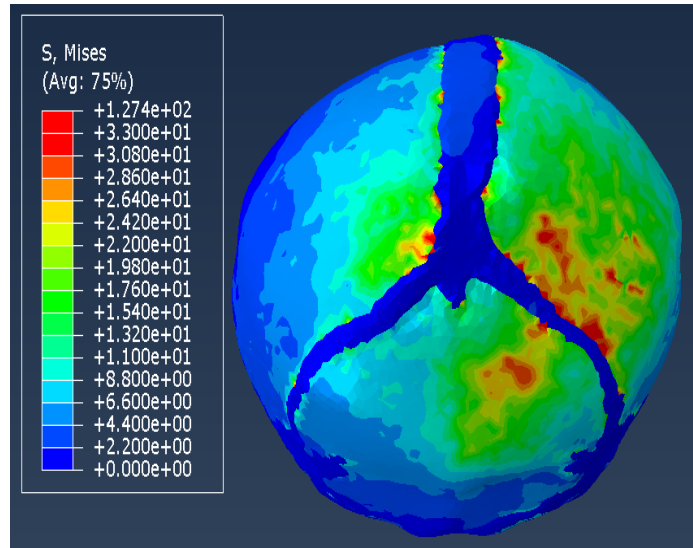
From Figure 3.30b, the posterior view and Figure 3.30c the side view, can be observed, showing an area of parietal bone peak loading and the potential site of fracture

propagation compared to the fracture line sketch from Weber study, at the same drop height- 0.82 m, and impact surface - stone tile. From Figure 3.30, the comparisons of high stress pattern, intimating skull fracture risk, is demonstrated by the FE model and the result from the impact experiments of PMHS head, which show a good qualitative match. The biofidelic FE model of the newborn infant showed a good correlation with the fracture pattern of the 3-month-old PMHS infant in the Weber studies [80, 81]. The fracture pattern is linear and associated with the suture.

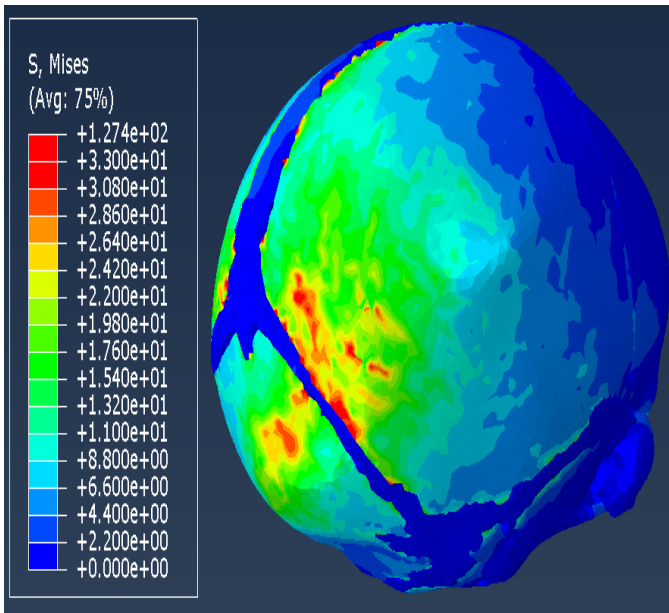
From the parametric study, shown in Table 3.21, the FE head model parietal – occipital region was impacted onto a simulated stone tile from four simulated fall heights, 0.15m, 0.3m, 0.6m and 0.82m, respectively. The response was evaluated by comparing the distribution of the maximum stresses against the fracture pattern described by Weber [80, 81]. The maximum principle stresses, see Figure 3.31, were 22 MPa, 26 MPa, 49 MPa and 68 MPa in the right parietal bone at fall heights of 0.15m, 0.3m, 0.6m and 0.82m, respectively. This maximum principle stress is not raised by greater than 15% through from drops from 0.15 m, 0.3 m, 0.6 m and 0.82 m, respectively. The associated parietal bone fracture risks were 29%, 49%, 79% and 92%, respectively, using the probability of ‘parietal and occipital fracture graph’ from Coats study [71]. At this impact location, there are also stresses in the occipital bone, for fall heights 0.15 m, 0.3 m, 0.6 m and 0.82 m of 2 MPa, 3 MPa, 6 MPa and 5 MPa, respectively, see Figure 3.31. The associated occipital bone fracture risks were 5%, 7%, 9% and 11%, respectively.



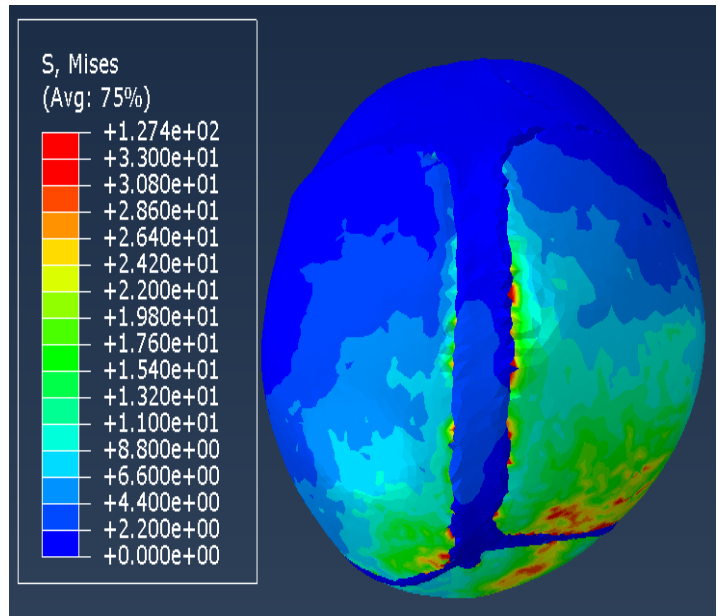
(a)



(b) Posterior view



(c) Side view



(d) Coronal view

Figure 3.30. Comparison of stress zone from the FE simulation (b, c and d) and the fracture pattern observed in the PMHS infant skull [80, 81] (a) at 0.82m drop height onto stone tile.

Table 3.21. Maximum principle stress of FE model from the parametric study with different fall heights.

Fall height (m)	Max stress of parietal bone (MPa)	Max stress of Occipital bone (MPa)
0.15m	22	2
0.30m	26	3
0.60m	49	5
0.82m	68	5

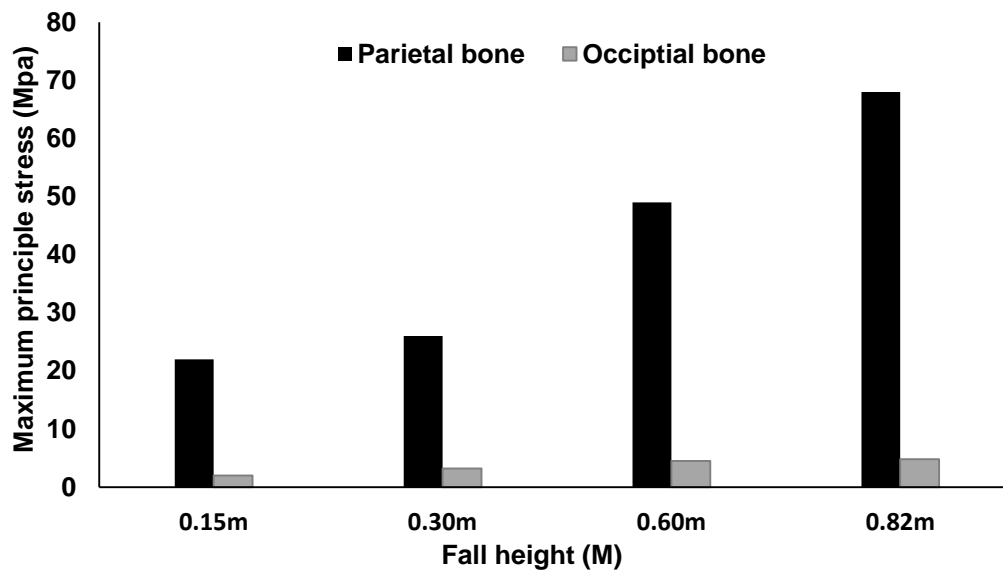


Figure 3.31. Maximum principle stress from the FE model from the parametric study at different fall heights - 0.15, 0.3, 0.6 and 0.82m.

4. DISCUSSION

4.1 Introduction.

The infant head is significantly different from that of the adult. Burdi et al.[27] commented that a 'child's body dimensions, proportions and biomechanical properties are so markedly different from that of an adult that a child cannot, for design purposes, be considered simply as a scaled-down adult'. The structure of infant cranial bones is that of a single layer, unlike the composite structure in adults. This, along with their thickness, 1 - 2mm, makes them very flexible. The bones are jointed together by even more flexible structures called sutures and fontanelles making the infant skull very unlike the inflexible shell structure of an adult.

The majority of head impact research to date has been focused on improving safety environments and equipment for adults. Initial anthropometric sizing investigations were driven by medical investigation but more recent progress, particularly that of dynamic responses has been motivated by the automotive industry. Relatively recently, this work has been expanded further, to incorporate infants and children, leading to the development of anthropometric test devices (ATDs). For the most part, these are based on scaled adult data, which limits their validity due to the physical and material property differences mentioned above. ATDs are generic and include wide anthropomorphic population ranges, to be economically justifiable, this unfortunately naturally leads to a scarcity of appropriate physical head models for very young infants. No existing commercial device considers the specific anatomy of the separate bone structures and flexible nature of the infant skull. There is, therefore, no appropriate test device to properly investigate young infant head impact response and thus, inform safety device

design. Given the above issues, researchers have published biomechanical and medical efforts to develop physical models and investigate their response to dynamic scenarios. Prange [84] developed a physical infant head model by improving the biofidelity of a child doll, whilst Coats [85] went a step further, manufacturing individual skull plates jointed with silicone rubber fitted to the facial portion of a child doll. These researches led to thought-provoking and useful findings, though are somewhat limited by their unknown level of biofidelity. Further limitations include their ability to measure the response of the head by using accelerometers, which by their presence can both affect the response and only provide measurements specific to their location in the structure. The shortcomings associated with physical models have resulted in other researchers of young infant head impact response approaching the problem by computational modelling. A significant limitation of the computational modelling is its need for validation against the physical “real” world interactions.

Thus, this present study describes the development of a coupled physical and computational modelling methodology; one that advances biofidelic physical models, globally validated against real world PMHS impact tests, to establish real world regional and local response values from a range of impact scenarios. The physical model impact response is applied to informing both the development of validated computational models and an understanding of the impact response of a range of physical impact tests, conducted at different heights and angles, against different impact surfaces. The FE model was globally validated by comparing its simulated impact response against the response of the real world PMHS impact tests. Further global and local validation was performed against the response of the physical model, which was considered a “real

world” reference, due to the geometrical and material response similarities between the physical and proposed FE models. The FE model was subsequently applied to investigating the fracture occurrence by replicating the PMHS experimental study and used to investigate the effects of different fall heights on head impact response, to address the ability of the model to predict the region of maximum stress response and fracture risk probability. Thus, establishing cause and effect relationships that can be used to predict the causal mechanisms of presented injuries in the paediatric infant population.

4.2 Mechanical characterisation of the Poly Jet printed materials.

Poly Jet 3D printing technology presents a significant opportunity to advance the production of complex geometric models with more than one material property. Currently two different materials, with different physical properties, can be combined in different proportions in a print-head to produce different materials, with different physical properties, at different areas in the model. This technology has the advantages over the previous methods of manufacture of infant skull models. The geometry of the skull can be as precise as the available 3D data. Suture geometry and thickness can be very precisely controlled. The joints between suture and bone are as strong as any other part of the model. Bone and suture properties can be matched to the few available infant values in the literature, including variation for different bones in the head. However, the anisotropic nature reported in the literature [64, 65], cannot be directly replicated, necessitating a solution to be implemented by manipulating the 3D CAD data. A physical model of a newborn infant was produced, with a high resolution structural fidelity and

tissue response matched materials, which was applied to recreating the infant PMHS experiments [82].

This infant physical skull model consists of the cranial bones and sutures. The cranial cavity was printed using polypropylene polymers from Stratasys and the materials selected as the RGD835 Vero White Plus (White) for the frontal and parietal bones, RGD8510 DM Rigid Light Grey 25 (Grey) for the occipital bone and FLX9870 DM7 (Black) for the sutures and fontanelles. However, these polymeric materials were provided by the manufacturer as a range of mechanical properties, rather than specific numerical data. To evaluate the suitability of these PJP materials, the mechanical properties of those different commercially available digital materials, White, Grey and Black, were measured at low rates ($1 \text{ mm}\cdot\text{min}^{-1}$) using a uniaxial tensile test machine. The uniaxial tensile tests were carried out using type 1BA dog bone specimens of BS EN ISO 527-2:2012. Subsequently, the engineering stress (σ_{uts}), engineering strain (ϵ_{max}) and young's modulus (E) were calculated. A comparison of these three polymeric materials was made with both the supplier data sheet range values, shown in Table 2.2 [97, 98] and the reported mechanical properties from infant tissue samples, shown in Tables 1.1 and 1.2, including the variation for different cranial bones [64, 37, 66, 67].

Regarding the tests performed on the White material, see Table 3.2 and Figure 3.4, young's modulus (E) has a mean value of 1836.00 ± 365.00 MPa, which falls within the 2000 - 3000 MPa range, provided by the Poly Jet datasheet. Furthermore, the stiffness (E) of the Grey material was 1687.00 ± 275.00 MPa, which falls within the 1700 - 2300 MPa range, see Table 3.2 and Figure 3.4. However, the tensile strength (σ_{uts}) of

the White material was 24.82 ± 0.85 MPa and the Grey was 23.66 ± 0.80 MPa, which were low compared to the tensile strength values reported in the data sheet for White (50-65) and Grey (40-60), respectively, see Table 3.2 and Figure 3.4. The same was true for the elongation at failure (ϵ_{max}) of the White (26.10 ± 7.48) and Grey (27.34 ± 2.98), which were high, compared to White (10-25) and Grey (15-25) from the manufacture's data sheet.

In terms of comparison between the mechanical properties of the three tested polymeric materials and the material properties of the infant cranial bones and sutures reported in the literature, the stiffness (E) at ambient temperature of White (1836.00 ± 365.00 MPa), shown in Table 3.3, is of an appropriate order of magnitude, up to 0.1% strain, to mimic parietal and frontal bone response from birth to 3 months, as shown in Table 3.3. This compares favourably with McPherson & Kriewall [64] (parietal, 2660 - 5290 MPa, frontal, 1870- 4000 MPa) and Kriewall et.al. [65] (parietal, 1873 - 5158 MPa, frontal, 2579 - 3999 MPa) when fibre orientation is taken into account. The same is true for tensile strength (σ_{uts}) (24.82 ± 0.85 MPa) when compared with Coats & Margulies [66] (8.4 – 53.7 MPa) from birth (0 months) to 3 months, as shown in Table 3.3.

The Young's modulus (E) of the Grey material was 1687.00 ± 275.00 MPa at 1mm min^{-1} , which was stiff, compared to the occipital bone of the young infant skull from birth to 3 months (29 - 551 MPa) and 3 - 6 months (318 - 1318 MPa) [66]. However, the reported data was from tissue with fibres oriented perpendicular to the test direction and the influence of fibre direction has not been quantified in occipital bone. It is, however, noteworthy that McPherson and Kriewall's studies [64, 65], found that the age (pre-term vs term) and fibre orientation (parallel vs perpendicular) had a significant effect on the

elastic modulus of the parietal and frontal bones. The modulus of elasticity was observed to increase with age and across all ages and the parietal bone stiffness was nearly three or four times greater when grain fibres were oriented parallel to the long axis of the specimen.

It is certainly a possibility that the reported data from birth to 3 months (29 - 551 MPa) and 3 - 6 months (318 - 1318 MPa) by Coats & Margulies [66] is an underestimate and the Grey material could be of an appropriate stiffness (1687.00 ± 275.00 MPa) to mimic infant occipital bone. Further, the strain rate in this study (1 mm min^{-1}) is below the rate of testing reported by Coats & Margulies [66] at more representative physiological rates, such that the Grey material may be suitable to mimic occipital bones in younger infant skulls. Furthermore, the tensile strength (σ_{uts}) ($23.66 \pm 0.8.00$) of the Grey material falls within the range reported by Coats & Margulies [66] from pre-term up to 12 months 3.3 - 31.4 (25 < term weeks), 3.1 - 18.5 (term - 3 months), 16.4 - 43.4 (3 - 6 months), 6.2 - 37.6 (11 - 12 months), shown in Table 1.2 and 3.3.

The Black rubbery material appears to demonstrate an appropriate stiffness (6.50 ± 2.00 MPa) when tested at 1 mm min^{-1} , to mimic the sutures of infants reported by Coats & Margulies [66] 4.3 – 14.2 MPa (25 < term weeks), 3.8 - 6.4 MPa from birth up to 3 months.

The different materials testing methodologies reported in the literature makes comparison of material response data difficult, as illustrated in Tables 1.1 and 1.2. Factors, such as different loading modes (tension, compression, bending and shear) and speeds (quasi-static and dynamic), contribute to large variations in data for any one parameter. In the absence of a unified method of testing and for the purpose of modelling, all the materials

response values were considered to be “roughly appropriate” for modelling the infant cranium under the experimental impact test condition, though it is acknowledged that a further unified research protocol is required at representative strain rates. In general terms, the White material best matched the parietal and frontal bones, the Grey the occipital bones and the Black the sutures and fontanelles.

4.3 Global validation of the paediatric physical model against PMHS data

Global validation of the physical model was achieved in accordance with the PMHS infant head impact study of Prange et al. [82], in which a PMHS head was dropped into free fall from 0.15 m and 0.30 m, corresponding to impact velocities of $1.72 \text{ m}\cdot\text{s}^{-1}$ and $2.43 \text{ m}\cdot\text{s}^{-1}$, onto a ‘rigid surface’. The study is currently considered as a reference, since no better infant PMHS data is available. For global validation purpose, two indicators were used to compare head performance of the FE model with the PMHS experiment (a) peak values, and (b) correlation score. All the analyses performed in this study, assumed that a threshold of 15% difference in a variable’s response was a trigger for consideration as has been used by previous authors [71, 77].

4.3.1 Impact translational acceleration.

The head model global validation data is shown in Figure 3.5. Peak resultant translational acceleration, for all the impact tests, demonstrate a close relationship to the PHM.S impact tests [82]. For the global validation, the correlation score was implemented. The acceleration–time impact curves generally correlate well see Figure 3.7, showing the predicted curve characteristics at different impact locations corresponding to a correlation score greater than the threshold of 86, see Table 3.5.

Some relatively minor variations were observed in the peak accelerations at the occipital and parietal impacts. For vertex impacts, see Figure 2.10c, the peak accelerations from the force plate, were very close to the PMHS [82] at 1.72 m.s^{-1} , with only an 8% difference, compared to the 2.43 m.s^{-1} that produced a 26% difference. However, for the occipital bone impacts, see Figure 2.10b, the difference between PMHS and physical model impact response was 56% at 1.72 m.s^{-1} and 47% at 2.43 m.s^{-1} . Perhaps a significant consideration, was the position of the occipital bone in relation to the parietal bones. The original scan images show the occipital bone positioned 'out of line' (depressed) relative to the parietal bones. In utero, the occipital and parietal bones are positioned 'in line' prior to birth. However, during passage through the birth canal, quasi static forces act on the head to produce head moulding, shape changes, which facilitate the head passing through the birth canal. It is believed that displacement of the occipital bone is a result of quasi – static forces, the effects of which result in the occipital bone remaining depressed for some days-weeks postpartum. In an attempt to create a model which was relevant, not just to the first days – weeks after birth but to the first three months, a decision was made to model the occipital bone of the physical model 'in line' with the edges of the parietal bones.

It is noteworthy, that whilst the occipital bone moves out of line, relative to the parietal bones during birth, the displacement can persist throughout the first few weeks of life, especially if an infant is placed on its back, to sleep. From a head modelling perspective, it is quite possible that the PMHS heads used by Prange [82], given their young age, presented with their occipital bones depressed, since natural birth rates are predominant in occurrence (67%) in the US. If this was the case, a question arises as to whether this

could have had an effect on the head impact response, since a head with bones in line is likely to behave more like a shell structure than one whose bones are out of line. It is a possibility that displacement of the occipital bone could result in less impact loading being transmitted to the surrounding parietal bones, such that the bone's response relies more on the support of the brain and pressure inside the head. It was speculated that this could result in a less stiff response and hence, a lower impact acceleration and may explain why the physical model response was greater than the PMHS study, as shown in Figure 3.5.

For parietal impacts (Figure 2.10d), the results in Figure 3.5 illustrate that the difference between the PMHS and physical model impact response was 43% and 19% at $1.72 \text{ m}\cdot\text{s}^{-1}$ and $2.43 \text{ m}\cdot\text{s}^{-1}$, respectively. The impact response also appears to be affected by minor perturbations in impact location, combined with the position of the occipital bone. With the occipital bone in line with the parietal bone, the head's structure, from a parietal loading perspective, is likely to be stiffer at the posterior side. This is most likely if the impact is slightly towards the posterior of the parietal bone, rather than the anterior, and could explain the higher accelerations, shown in Figure 3.5, since the model's occipital bone was in line, compared to the PMHS bones, which may have been depressed. It is not clear what specific orientations were tested by Prange et al. [82], but it is noteworthy that the PMHS results are closer to the physical response at $2.43 \text{ m}\cdot\text{s}^{-1}$ than at $1.72 \text{ m}\cdot\text{s}^{-1}$.

With regard to the forehead (frontal bone) drop test, see Figure 2.10a, the difference between PMHS and physical model impact response was 15%, at $1.72 \text{ m}\cdot\text{s}^{-1}$ and 36% at $2.43 \text{ m}\cdot\text{s}^{-1}$, respectively, see Figure 3.5. Exceeding the 15% threshold triggers the need

for further consideration and discussion. Analysing the HS-DIC images, see Figure 2.13b, during impact, variations in deformational response were observed. These variations could be explained by slight alterations in the drop test orientation. All drops that were observed to strike the facial bones before the forehead were excluded, since the facial area is relatively stiff and buttressed by a complex bone structure. The impacts onto the lower part of the forehead produced significantly higher accelerations than the upper part of the forehead (no facial bones). However, when the impact occurred at the upper part of the forehead, lower acceleration profiles were observed, since the loads were being transferred to the more flexible parietal bones and anterior fontanelle. Direct comparison of these observations with the PMHS study, is however, problematic, since the exact area of contact or orientation of the forehead was not provided, only a generalised description of the forehead drop test. Given, that the impact acceleration response from the physical model is 19% greater at 2.43 m.s^{-1} and 43% greater at 1.72 m.s^{-1} than the PMHS, the physical model response was still stiffer, even when the region of the impact was at the upper part of the forehead, this is a region that requires further attention to address this phenomenon.

For the majority of the physical tests, most impact locations produce peak acceleration values in excess of those produced during the PMHS tests of Prange et al. [82], however, the values still fell within the published impact response corridors. Thus, indicating that the stiffness of the physical head model is greater than the PMHS head. It appears from Figure 3.5, that average peak accelerations for the physical head model, are significantly different for different drop heights but do not vary between impact locations, which is in good agreement with the conclusion of Prange [82]. Comparing the results, and taking

into consideration the inherent variation that exists between different specimens, it can be considered that the responses from the physical paediatric head model and PMHS head are in favourable agreement under the experimental drop conditions [82].

4.3.2 Duration of Impact.

The peak impact acceleration measured by the physical model shows close agreement with the PMHS response. Also, the physical model's head impact curve has a bell shape, closely resembling the shape of the PMHS curve for the same impact velocity of 2.43 m.s^{-1} and same impact location, see Figure 3.7. There is, however, a 67% difference in impact time duration between the PMHS test (12 ms) and the physical model (6 ms) for the same impact height 0.3m (2.43 m.s^{-1}) and location, see Figure 3.7. The variations in impact-time duration were significant, deviating by 67% and 60% at drop heights 0.15 m (at 1.72 m.s^{-1}) and 0.3 m (2.43 m.s^{-1}), respectively, shown in Figure 3.6., which again could be a result of differences in stiffness between PMHS and the physical model. Furthermore, Coats and Margulies [71], found that the impact response of the paediatric skull appeared to be sensitive to the Poisson's ratio that represented brain compressibility. The brain in the physical model was modelled as homogenous, with no distinction between the grey and white matter and no inclusion of the ventricles, falx cerebri /tentorium. The physical model's surrogate gelatin brain has a lower Poissons' ratio (0.499) making the brain softer and therefore, potentially more prone to impact deformation. Consequently, a softer, more deformable brain is likely to provide less resistance to the cranial plates during impact at physiological loading rates, thus, allowing greater cranial bone deformation until it made contact with an adjacent cranial bone. The cranial bone contacts significantly shorten the impact time durations, see Figure 3.7.

4.4 Regional and local investigation of the paediatric physical model.

Following the validation of the physical head model for acceleration-time against published PMHS data using the PMHS experimental methodology of a force plate and rigid body “assumption”, a HS-DIC system was applied to measure the linear and angular accelerations and strains to assess the suitability of the “assumption”, by comparing global, regional and local accelerations. The output variables from the DIC approach were the impact translational and rotational accelerations and deformation, which will be discussed below. All the analyses performed in this study, assumed that a threshold of 15% difference in a variable’s response was a trigger for consideration as has been used by previous authors [71, 77].

4.4.1 Impact translational and rotational accelerations.

The translational accelerations measured at the skull vertex, occiput, frontal and parietal regions are shown in Figure 3.8, and appear to be significantly greater (by 40%, 78%, 112% and 104% at 1.72 m.s⁻¹, and by 45%, 39%, 74% and 32% at 2.43 m.s⁻¹) than those measured at the force plate. This is likely a result of the mass of the skull bones constituting a comparatively small measure of the overall mass of the head [27]. Thus, the skull bones are likely to come to rest more quickly than the more massive brain structures, it is noteworthy that quantification of the relative accelerations will prove invaluable in any subsequent modelling of the cause of meningeal haemorrhaging.

The DIC system was used to measure local area deformation at the outside of the skull rather than considering the head as a lump mass viewed from the perspective of acceleration against time, as shown in Figure 2.11. The DIC system provided the kinematic data associated with the impact velocities of 1.72 m.s⁻¹ and 2.43 m.s⁻¹. Angular

acceleration, shown in Figure 3.9, illustrates that the maximum angular acceleration of the vertex, occipital and frontal impact tests, at an impact velocity of 2.43 m.s⁻¹, were as high as the impact velocity of 1.72 m.s⁻¹, from the same impact views. The difference between the angular acceleration response of the physical model, at two different impact heights, 1.72 m.s⁻¹ and 2.43 m.s⁻¹ was 79% at the vertex, 86% at the occiput and 85% at the frontal regions, respectively. Thus, confirming that the infant head significantly deforms during impact, whilst concomitantly producing different angular accelerations in different structures of the head at different times during the impact. The maximum angular accelerations of the physical model at the vertex, occiput and frontal regions at an impact velocity of 1.72 m.s⁻¹ were 4121 ± 2328 rad sec⁻², 9371 ± 4858 rad sec⁻² and 12983 ± 1936 rad sec⁻² and at 2.43 m.s⁻¹ were 9530 ± 1882 rad.sec⁻², 23459 ± 3728 rad.sec⁻² and 32110 ± 5888 rad sec⁻², for the same impact views. This data is extremely valuable for quantifying local and regional deformational accelerations of the head and for determining both the nature and risks associated with head impacts. The DIC software concomitantly allowed calculation of the angular accelerations at points across the head and comparison between regions; such that the greatest peak angular acceleration for each impact could be quantified. For example, the peak angular accelerations for side (parietal) views of vertex impacts were as great as 4121 rad.s⁻², compared to the frontal and rear (occipital) views, which were 1779 and 1107 rad.s⁻², respectively.

4.4.2 Head deformation.

During impact, the majority of the strain was dissipated by the sutures and fontanelle areas of the head, see Figures 3.10, 3.11 and 3.12. Given that the infant head naturally deforms in these areas during the quasi-static loading of child birth [16, 17], this response might be expected. During impacts, however, the head is loaded at a much higher rate, such that the skull is observed to deform, and as a consequence the brain and other structures inside the cranium deform. The experimental DIC results, for the strains within the bones, were very much more “noisy” than the sutures and fontanelles by factor of 1.6, but the response from the cranial bones do suggest an engineering strain order of magnitude of approximately 0.3%, for both 1.72 m.s⁻¹ and 2.43 m.s⁻¹ impacts. In contrast, due to their much larger strain and strain rate values, the response of the suture and fontanelle areas are “cleaner”, by approximately 2.5 % for 1.72 m.s⁻¹ and 3.3% for 2.43 m.s⁻¹ impacts with magnitudes of strain in the sutures and fontanelles ten times greater than cranial bones, and strain rate values in the sutures and fontanelles between 1000% s⁻¹ and 2000% s⁻¹. There is a significant, 30%, difference in the strain magnitude of the sutures and fontanelles at impact velocities of 1.72 m.s⁻¹ and 2.43 m.s⁻¹, see Figure 3.12.

Whist it must be acknowledged that the model represents only one age matched infant head, which has been assumed to be representative of Prange’s [82] PMHS and further, of infants in general, there will certainly be variation between individuals. With respect to skull size, composition and geometry, it is, however, anticipated that since the head appears unremarkable, the principles of the observations will hold true. With respect to the mechanical testing of PMHSs [37,64,65], experimentation has shown that the mechanical response of the head is relatively constant parietal and frontal bone have

stiffness values (E) of 1836 ± 365 MPa and tensile strength (σ_{uts}) 24.82 ± 0.85 MPa. Occipital bone stiffness (E) was 1687 ± 275 MPa and tensile strength (σ_{uts}) 23.66 ± 0.8 within the early post-mortem period (first 4 days), subject to appropriate storage and handling, however, an increasing post mortem period results in decomposition of the brain which has an increasing effect on brain - skull decoupling [121]. Whilst an absence of living physiological pressurisation has been suggested to have an effect on brain–skull coupling in adults, the combined limitations of technical instrumentation and infant PMHS availability will continue to prove a study limitation [121].

4.5 Implications and limitations of the physical model.

The physical model demonstrates the considerable potential of producing 3D models with complex geometries and tissue matched materials for head kinematic analyses. Different areas of the head produce significantly greater accelerations than others. Thus, the measured response at one selected region of the head is different to the response of the whole head which provides a “global response” measurement [82]. The physical modelling approach allows the optical observation and measurement of the response of each individual bone, suture and fontanelle, which is experimentally elegant. Indeed, the physical model proved of significant value in providing regional and localised data, evidenced by the provision of impact response data with which the limited “global response” approximation, associated with infant head impact analyses, can be challenged. The physical model produced different regional acceleration patterns, with which comparisons can be made with epidemiological findings. Cases of accident and abuse can be investigated by simulating impact scenarios from similar heights onto different skull locations producing very varied responses, which may, in part, explain the

very varied clinical outcomes. It was, however, the elucidation of regional and localised impact response values, for the development and subsequent validation of computer models, that was the physical model's intended primary purpose. Since, for the purpose of detailed kinematic analyses, the physical model had a number of limiting shortcomings, including: significant monetary and time costs associated with printing and model preparation (painting of speckle pattern, production of gel brain and scalp simulant), respectively; the fragility of the model meant that destructive tests proved prohibitively expensive and physical head impact simulations were difficult to conduct with reproducible precision, thus, making the parametric analysis of introduced minor perturbations infeasible. Finally, the physical model was incapable of sustaining effective future development of complex internal structures, or techniques, such as reverse engineering, parametric analysis and parameter optimisation.

4.6 Global validation of the paediatric FE head model against PMHS data.

In recognition of both the potential and limitations of the physical model, a geometrically accurate computational FE head model was produced, utilising the same scan data as used during the development of the physical model and comprising material structures, whose responses were matched to published infant human tissue data [37, 64, 65] to more fully represent the physical model. The infant FE head model, computationally replicated the fibre orientation of immature cranial bone and therefore, provided an orthotropic response for each cranial bone. To ensure that this FE model biofidelity corresponded "globally" with that of Prange et al.'s PMHS impact experiments [82], the model was subjected to a series of validity simulations. Head model validation was achieved again by reference to the only published quantitative PMHS experimental work

available, by Prange et al. [82], which provided data on the global behaviour of the head, in terms of the acceleration-time response of the head under impact loading conditions. Whilst only three infant (PMHS) heads (1, 3 and 11 days old) were impacted, from only two drop heights (0.15m and 0.30m) corresponding to impact velocities of 1.72 and 2.43 m.s⁻¹, at only one angle (perpendicular) onto a single surface, these PMHS tests [82] provided invaluable biomechanical data for validating the FE infant head model. The impact acceleration response was also obtained by dividing the impact force by the head mass, as applied during the PMHS experiments [82]. The mass of the computational head model of the 10-day-old infant was that of the physical model, which the mass was closest to that of the 3-day-old infant PMHS head in [82]. The ‘mass to age variation’ can be explained by the natural population variation as a result of genetic variation, the developmental progress of pregnancy and the gestational age at the time of birth. A validation of the computational model was conducted based on a comparison between the simulation results of the FE head model and the experimental results from the series of PMHS tests [82]. The output variables from the global validation approach are the impact translational accelerations and time durations.

A parametric study was conducted to assess two FE head model boundary conditions, the foramen magnum and skull – brain interface. Previous research has suggested that the foramen magnum of the FE head model should be developed as a “force free” opening [71]. In response, the present FE model had no restraints. During Prange’s PMHS experiments [82], however, the foramen magnum was closed. Consequently, a parametric FE study was developed with constraints, to prevent nodes from passing through the foramen magnum, to assess the effect. From this parametric analysis, it

appeared that this change in the constraint did not affect the output variables peak translational acceleration, which remained unchanged (61g, 91g at vertex, 63g, 101g at occipital, 78g, 121g at forehead, and 67g, 92g at parietal, at impact velocities of 1.72 and 2.43 m.s⁻¹ respectively) and by implication, below the 15% baseline, for the FE model (open foramen magnum).

A second parametric analysis was conducted, for developing the brain - skull interface. Justification for the use of the constraints is provided by the parametric study of an adult FE head response compared with PMHS experiments [119], which investigated the effects of the skull – brain interface and chosen brain material properties on local brain motion and pressure response. Local brain motion for “low severity” impacts was demonstrated to be insensitive to the type of contact algorithm used for modelling the skull - brain interface, while it was sensitive to the constitutive parameters chosen for the brain tissue. The pressure response, however, appears to be more dependent on the type of contact interface than on the constitutive parameters used for the brain tissue. However, there is no PMHS data available to validate the brain - skull interaction in the paediatric head, thus, a second parametric analysis was conducted, applying two different contact algorithms the ‘sliding interface’ and the ‘tie constraint’. In the present FE model, the sliding interface condition was established as a baseline, with a frictional coefficient (μ) of 0.2 [120]. The further parametric FE study was conducted with a tie constraint for comparison with the sliding interface. During impact simulations, the peak translational acceleration of the parametric model with the tie constraint was shown to have no effect on the peak translational acceleration and impact duration, which remained unchanged (61g, 91g at vertex, 63g, 101g at occipital, 78g, 121g at forehead, and 67g, 92g at parietal,

at impact velocities of 1.72 and 2.43 m.s⁻¹ respectively) and again by implication, below the 15% when compared with the baseline FE model (sliding interface). With regard to the CSF, to adequately represent the effect of skull – brain interface it has been suggested that the fluid be modelled as a fluid, rather than a structural element [119, 120]. Fluid structure interaction analysis is in its relative infancy and is currently considered a limitation with most commercially available FE packages. In response, a contact algorithm approach (sliding interface) was applied to describing the CSF at the skull - brain interface, rather than implement fluid elements.

4.6.1 Impact acceleration.

During the FE simulated impact, the acceleration – time waveform can be observed to rise and fall, as illustrated in Figures 3.14 a - d. The acceleration acting on the FE head model changes from zero to a peak acceleration and then again to zero during the total duration of impact as the head is brought to rest. During the initial portion of the impact waveform, ‘the rise’, the FE head model will be subjected to compressive deformation, whilst the head decelerates. In the course of the subsequent portion of the waveform it is observed to peak and almost plateau, due to the rate of change of head velocity between decelerating and accelerating. For the period of the final portion of the waveform, the profile reflects the reformation of the impacting (FE head model (cranial bones, sutures and fontanelles)) and impacted (rigid plate) surfaces “springing back” to their pre-impact shape, evidenced by the FE model being seen to rebound, accelerate, off the surface. In a paediatric head, the pliancy of the cranial bone, with unfused sutures and soft membranous fontanelles, allows greater movement of the brain [27].

From Figure 3.14, when the PMHS head contacts the surface, the skull will “adhere” to the surface and began to decelerate rapidly, due to its material stiffness and low mass, compared to the paediatric brain, which has a greater mass than the skull, and has a soft pliable nature and is cushioned by cerebro spinal fluid (CSF), such that it decelerates at a lower rate. Also, a separation exists between the skull and brain, as a result of the subdural space, which contains the CSF. Any disparity between the initial rates of acceleration, experienced by the skull and the brain, may be referred to as a ‘deceleration lag’, which may produce different impact acceleration responses. An absence of the CSF and subdural space in the present FE head model, resulted in the skull and brain having to be constrained using Abaqus constraints. Thus, any modelled deceleration lag may have been relatively small, compared to that of the PMHS and may have resulted in a variation existing in the acceleration – time response between them.

In the framework of model validation, the present infant FE head model was validated against the PMHS data [82]. The acceleration–time impact curves generally correlate well, see Figure 3.14, showing the predicted curve characteristics at different impact locations corresponding to a correlation score greater than the threshold of 86.

The global kinematic response of the infant FE head model was studied and its biofidelity assessed. Figure 3.15 shows that the response of the present paediatric FE head model is in favourable agreement with the PMHS results [82], with respect to resultant peak acceleration and it does not show any significant difference between different impact locations or any variation between the 1.72 m.s^{-1} and 2.43 m.s^{-1} , impact velocity. Some relatively minor variations were observed in the peak accelerations of the occipital and parietal impact test, which could be the result of one or more of several factors.

For occipital impact tests, the differences in impact response between the PMHS and the FE model were 30% at 1.72 m.s⁻¹ and 37% at 2.43 m.s⁻¹. One consideration is the position of the occipital bone in relation to the parietal bones. As discussed previously, during natural child birth, quasi-static forces act on the head to produce head deformation (moulding), which allow it to pass through the birth canal. The occipital bone, at the posterior cranium, is pushed inwards and downward relative to the parietal bones, which in combination with the sutures form the “roof” of the head. The CT scan, see Figure 2.1a, shows that the occipital bone is significantly depressed, a likely consequence of natural birth and that the sutures are slightly folded to allow this to happen. Typically, during the first weeks of life the head deformation remoulds and returns to relatively normal. To produce an FE skull model that represents a wider age range than the infant shortly after birth, shown in the CT scan, the depressed occipital bone was moved outwards and upwards to line up with the edges of the parietal bones on each side, producing a more rounded skull profile than the oblong profile, see Figure 2.1a.

It must be acknowledged, however, that in contrast to the aligned occipital and parietal bones in the present FE study, that since the Prange et al. PMHS experiments [82] were conducted on three newborn specimens (ages 1, 3 and 11 days old), it is perfectly possible that if the infants had been subjected to natural births, that depressed occipital bones would have been present. As discussed earlier, this was a concern during the physical model development, since a decision had been made to develop the model with an inline occipital – parietal bone configuration, thus, a series of FE head impact simulations were performed with different head configurations, see Figure 2.19. It can be seen in Figures 3.14b and 3.15, that there are higher accelerations produced during the

FE simulation than the PMHS experiments [82] when the occipital and parietal bones are aligned. It is speculated that this is as a result of the aforementioned inline positioning of the occipital bone relative to the parietal bones, which was likely not the case in the PMHS specimens, that is, where there was less loading transmitted to the right and left parietal bones. Thus, most of the PMHS occipital impact response depends on the supporting structures, rather than being transmitted through the evolving 'shell structure' of the cranium.

A further consideration is that Prange et al. [82], provided only a limited general description of the impact location in the PMHS study, rather than a defined area of impact for the purpose of precise simulation. The geometrical/anatomical complexity of the infant head has many potential impact sites, for example an occipital impact could be to the middle or edge, near the sutures of the vertex, base or parietal bone. Consequently, during simulated FE impacts to the parietal region of the head, shown in Figure 2.19c, both the relative position of the occipital bone and the location of the impact appear to affect the impact response of the parietal bone. As speculated above, an inline occipital bone, with respect to the parietal bone, is thought likely to produce greater acceleration values, potentially as a result of a more "shell like" structure. Parietal impact loading appears to produce higher acceleration values towards the posterior region. Furthermore, whilst the intention was to impact the parietal bone at its centre, as a result of its irregular shape, the location of the impact was observed to be slightly towards the posterior region of the parietal bone. Hence, this, and the fact that the occipital bone was in line, may explain why a higher impact acceleration was produced, see Figures 3.14c and 3.15.

For parietal impact tests, the differences in impact response between the PMHS and the FE model were 40% at 1.72 m.s⁻¹ and 27% at 2.43 m.s⁻¹, thus, a sensitivity analysis was conducted to investigate. For vertex impacts, shown in Figure 2.19d, the FE model response was very close (less than 15%) to the PMHS study [82] represented by 6% and 11% at impact velocities 1.72 m.s⁻¹ and 2.43 m.s⁻¹, see Figures 3.14d and 3.15.

With respect to the forehead impact test, shown in Figure 2.19a, there is variation in the acceleration response between the FE model and PMHS test, see Figures 3.14a and 3-15. The differences in impact response between the PMHS and the FE model were 44% at 1.72 m.s⁻¹ and 38% at 2.43 m.s⁻¹. Variations could be a result of differences between the impact locations, between the FE model and the PMHS tests. For example, the lower region of the forehead is an anatomical region which is comprised of many complex bone structures. This area is relatively stiff and thus, as observed in the FE simulations, an impact to this region produces relatively high accelerations. If, during the PMHS tests the impact had occurred at the upper region of the forehead, close to the soft cranial bone and membranous fontanelle, a lower acceleration response might be expected. Whilst acknowledging that the FE model is “stiff”, compared to the PMHS response, it can still be considered to be validated for the purpose of developing an understanding of infant head impact biomechanics.

4.6.2 Sensitivity analysis.

4.6.2.1 Influence of the Impact location.

The limited general description of the impact location in the PMHS study [82], did not provide sufficient guidance, regarding the exact area of impact, for the purpose of precise simulation. The influence of the impact location on the impact acceleration response, obtained through the global validation of the FE model with PMHS study [82], was investigated by dropping the present FE head model with different orientations and impact regions, see Figure 2.20.

During impact tests to the occipital bone, impacts were produced (1) close to the base of skull, (2) close to the vertex, (3) close to the left parietal bone and (4) close to the right parietal bone, compared to the baseline region (0) “centre” of the occipital bone. For the parietal bone, impacts were produced (1) close to the base of the skull, (2) close to the vertex (3), close to occipital bone and (4) close to the frontal bones, compared to the (0) baseline impact region “centre” of the parietal bone. For the frontal bone, impacts were produced (1) to the upper region of the frontal bones, (close to the soft cranial bone and membranous fontanelle) compared to the baseline region (the lower region of the forehead) at an impact velocity of $2.43\text{m}\cdot\text{s}^{-1}$, corresponding to the drop height of 0.30m.

For an occipital bone impact test, the relative impact acceleration response between different regions was 92g close to the base region, 93g at the vertex region, 97g at the right and 96g at the left parietal regions, respectively. Representing differences between impact responses of less than 15%, compared to the baseline impact acceleration response of 101g at the centre of the occiput, see Figure 3.17a.

For a parietal bone impact test, the difference in impact acceleration response from different regions of the bone was 89 g close to the base region, 85g at the vertex region, 98 g at the occipital region and 93 g at the frontal bone region. Again, representing differences less than 15%, compared to 92 g impact acceleration response at the baseline impact region (centre of the parietal bone) from the same height, see Figure 3.17b.

For frontal bone (forehead) impact tests, the difference in impact acceleration response from the upper region of the forehead, close to the soft cranial bone and membranous fontanelle of 82 g was 38% lower, compared to the impact acceleration response of 121 g recorded at the baseline impact region (lower region of the forehead), for the same impact velocity, see Figure 3.17c.

For occipital bone and parietal bone impact tests, the simulation result show that there were no significant variations in the impact acceleration responses between different impact locations, compared to the baseline impact location of each cranial bone; producing only minor differences, of less than 15%, compared to the acceleration values calculated using the “global approximation” approach adopted by Prange et al. Whilst, for frontal bone impact tests, a variation of 38% was produced, as a result of the anatomical variation between the lower region, which has a stiffer structure than the upper region of the forehead, which has an impact response more closely resembling that of membrane than “stiffer” bone.

Thus, impact location at the simulated experimental fall heights has a limited effect on the “global” impact response of the parietal and occipital bones, though a significant effect on the frontal bones. However, further investigations were proposed using the local and

regional approach, since neither the global approximation approach or changing impact appeared capable of providing the necessary sensitivity to determine if orientation changes the impact response.

4.6.2.2 Influence on impact response of the relative positions of the occipital and parietal bones.

To investigate the influence on the impact response of the relative positioning of the occipital and parietal bones, a FE sensitivity analysis was conducted. A comparative study was performed using the impact acceleration response of a newborn FE head model that had a depressed 'out of line' occipital bone, relative to the parietal bone configuration with an inline occipital - parietal bone configuration. The response was calculated by global measurement which was compared with published PMHS study [82].

During an occipital impact, the peak acceleration response of the FE head model, inline occipital - parietal bone configuration, was greater by 35 % at 1.72 m.s⁻¹ and 36% at 2.43 m.s⁻¹, compared to the FE model depressed occipital - parietal bone configuration, see Figure 3.18. As discussed previously, this could be due to the fact that the depressed occipital bone transmitted less impact force to the adjacent parietal bones, such that the bone response represents a significant contribution from the supporting intracerebral pressure that is CSF and brain. It would seem feasible that this could result in a less stiff impact response and hence, a lower impact acceleration, were this to be the case and may well explain the higher accelerations observed in the Inline FE model, as shown in Figure 3.18.

During parietal bone impacts, the peak acceleration response for the inline configuration was 29 % greater at 1.72 m.s⁻¹ and 23.3% at 2.43 m.s⁻¹, compared to the depressed configuration, see Figure 3.18. The simulation results appeared to be affected by the position of the occipital bone. From a parietal impact loading perspective, the inline configuration is likely to be stiffer at the posterior side. This is more likely if the impact is slightly towards the posterior of the parietal bone, rather than the anterior and could explain the higher accelerations shown in Figure 3.18, since the occipital bone was in line with the parietal bone, compared to the second model that had a depressed occipital bone.

For the vertex and frontal bone impacts, all peak acceleration values for the inline configuration were less than 15% at both an impact velocity of 1.72 m.s⁻¹ and 2.43 m.s⁻¹, compared to the depressed configuration.

Hence, the inline configuration seems to be responsible for the previously discussed slight difference between the impact acceleration response between the FE head model (inline occipital - parietal bone configuration) and the PMHS response, during the global validation process.

Further, the FE model depressed occipital bone impact acceleration response was 44 g at 1.72 m.s⁻¹ and 70 g at 2.43 m.s⁻¹ and at the parietal bone 50 g at 1.72 m.s⁻¹ and 73 g at 2.43 m.s⁻¹, a difference of less than 15%, compared to the PMHS occipital response of 46 g at 1.72 m.s⁻¹ and 72 g at 2.43 m.s⁻¹ and parietal bone response of 45 g at 1.72 m.s⁻¹ and 70 g at 2.43 m.s⁻¹, see Figure 3.18. Hence, there is no significant difference between the occipital and parietal impact acceleration response. It is entirely possible,

therefore, that Prange's PMHS specimen (3 day – old child) had a depressed occipital - parietal bone configuration as a result of a natural birth.

4.6.3 Impact time.

The FE model's head impact curve has a bell shape, which closely resembles the shape of the PMHS curve for the same impact velocity of 2.43 m.s^{-1} and same impact location see Figure 3.14. However, the impact time duration of the PMHS test was 18% greater (12 ms) than the FE model impact time duration (10 ms) for the same impact velocity 2.43 m.s^{-1} and location, see Figure 3.14. The greater variations in impact - time durations are significantly represented by 18 % and 17 % at 1.72 m.s^{-1} and 2.43 m.s^{-1} , respectively, see Figure 3.16. This could again be related to the difference in stiffness between the PMHS and the FE model or due to dissimilarities between the compressibility of the brain. The brain model in the present FE model was modelled as a homogenous gel, with a lower Poissons' ratio (0.499), thus making the brain more deformable at the point of impact with the rigid plate. This opinion is in agreement with the study of Coats and Margulies [71], who reported that the response of the impacted paediatric skull appeared to be affected by the Poissons ratio that represented brain compressibility.

4.7 Global validation of the paediatric FE model against the physical model.

Global validation of the FE model was achieved by comparing its simulated impact response against the response of the physical model, which can be considered as a “real world” reference, due to the geometrical and material response similarities between the physical and proposed FE models. For global validation purpose, two indicators were used to compare head performance of the FE model with the physical model experiment (a) peak values and (b) correlation score. All the analyses performed in this study,

assumed the threshold of 15% difference in a variable's response as a trigger for consideration [71, 77].

4.7.1 FE model impact acceleration.

The FE model impact acceleration - time response was compared with the physical model response at the same impact locations (vertex and occipital, frontal and parietal bones) at an impact velocity of 2.43 m.s^{-1} , see Figure 3.19. The acceleration–time impact curves generally correlate well with the measurements see Figure 3.19 showing the predicted curve characteristics at different impact locations since the correlation score all above 86.

There were no significant differences between the FE simulation and the physical model impact acceleration response at different impact locations or impact velocities, suggesting that the mechanical characteristic of the physical and FE models were very similar, see Figure 3.20. Differences, expressed as a percentage of peak were 2% at the vertex, 27% at the occipital bones, 29% at the frontal bones and 3% at the parietal bones at an impact velocity of 1.27 m.s^{-1} ; compared to the variation in acceleration response at 2.43 m.s^{-1} represented by 6% (vertex), 11% (occipital), 3% (frontal) and 9% (parietal). Whilst the variation at 1.27 m.s^{-1} at both the vertex and the occipital bone was greater than 15% threshold, difficulties reproducing the exact impact location between the head and the impact surface in the simulation and the physical test provides a potential source of error. The present numerical model demonstrates considerable potential, even if some quantitative differences between the experimental and simulation response values exist. Due to the fact that the brain and skull are considered as a continuum, it could be that higher accelerations, away from the point of impact could be a result of the mass of the

brain acting directly in compression on bones close to the impact point; such that the “effective mass” of that area of the skull is higher, and therefore, accelerating less for the same force than an area where the brain is being moved away from the bone by the impact. A further limitation is that physiologically, CSF facilitates a very low friction coupling between the brain and skull. The “brain” in the physical model consisted of gel contained in a rubber balloon. Though the gel would be relatively unconstrained, a gel boundary layer would still exist at the inner surface of the balloon, how similar this would be to CSF is at present, unknown. The FE model, may demonstrate a similar limitation, albeit for a different reason, due to the use of tie constraints anchoring the surface of the brain and skull, potentially producing a stiffer response.

4.7.2 FE model impact time duration.

The total impact time durations of the FE model were 5 ms at the impact velocity of 1.72 m.s⁻¹ and 6 ms at 2.43 m.s⁻¹ and are very close to the physical model, which was 6 ms at 1.72 m.s⁻¹ and 7 ms at 2.43 m.s⁻¹, a difference of less than 15%, see Figure 3.21. There is no significant difference in impact time duration of greater than 15% between the FE model simulations and the physical model tests at both impact velocities of 1.27 m.s⁻¹ and 2.43 m.s⁻¹.

4.8 FE head model regional and local validation against the physical model.

Throughout the literature, acceleration is considered the most practically achievable measure to establish a correlation between head impact loading and injury. Measurement can be achieved either by impacting the head with a force plate or instrumenting the head with transducers. To practically consider that an acceleration - time response from an impact force plate represents a head impact response, a “solid body assumption” is essential. However, this assumption can only be considered to hold true whilst the skull and brain can be considered to behave as a single structure. With respect to the infant head, the loosely associated shell structure of the skull bones, sutures and fontanelles, is of relatively low mass, compared to the massive brain [27]. Thus, the reliance on head acceleration cannot be justified when considering the movement of the paediatric skull relative to the brain. Clearly in the case of the flexible paediatric head, there must be an assumption that different areas of the head will accelerate at different rates. Given that the rigid body assumption represents a form of acceleration “summation” at the point of impact, it is perhaps more likely to disproportionately represent the acceleration of the most massive part of the structure, that is, the brain. The HS-DIC methodology was applied to the physical model for measuring displacements at the skull surface and henceforth, velocity and acceleration directly from different parts of the head model during impact, without having to apply the rigid body assumption. Subsequent to global validation of the FE head with the physical model impact response data, FE simulation was further applied to investigating the observations reported by the physical model and to challenge the rigid body assumption. Unique to this present study, the FE head model was applied to providing specific regional

and localised response data at different locations on the surface of the skull. The FE head model was subjected to translational head impact, from which local acceleration responses, from different regions of the head, were compared with firstly the global acceleration response (force/mass) from the biofidelic FE head model, obtained using a rigid body assumption, see Figure 3.22. Secondly, the FE model was compared and validated against the local response from the physical model response data from the HS-DIC system, see Figure 3.23.

4.8.1 Impact acceleration.

From the comparison of the global acceleration and local acceleration response of the FE model, the relative translational accelerations, from different regions of the FE model, have a significant variation by greater than 15% than those calculated using the “global” “rigid body approximation”, see Figure 3.22. It appears that during perpendicular impacts, regional and local accelerations in the skull plates, sutures and fontanelles were significantly greater by 18% at the vertex, 59% at the occipital, 55% at the frontal and 53% at the parietal regions, at the impact velocity of 1.72 m.s^{-1} and 7% (vertex), 28% (occipital), 45% (frontal) and 22% (parietal) at the impact velocity 2.43 m.s^{-1} , than the calculated average peak global acceleration response of the FE head model applying the limited global approximation approach, see Figure 3.22. There is, therefore, a major observable difference between the FE model response (skull structures) and the acceleration detected by the force plate. The peak acceleration in the FE frontal, occipital, and parietal bones, at 1.27 m.s^{-1} , is nearly three times greater than the “global” response of frontal, occipital and parietal bones reported by the FE model. Interestingly, from Figure 3.22, the greatest percentage differences are during occipital impacts, where at

1.72 m.s⁻¹ the difference in the recorded bone acceleration was 59% greater than the value for the force plate. The smallest increase, compared with the rigid body assumption, was observed at 2.43 m.s⁻¹ during the impact onto the vertex the difference was 7%. This is probably a result of the acceleration occurring over a significantly shorter time, which produces a greater peak acceleration than reported by the FE model using a limited global approximation approach. In contrast, the computational model calculates accelerations across the entire skull surface; further confirming that the rigid body assumption used by Prange et al. [82] may not be logical, since the cranial bones, sutures and fontanelles move relative to each other. Thus, the FE model shows agreement with the physical model study, which reported that acceleration patterns are very sensitive to impact location. It is evident from Figure 3.23, that the local acceleration values from different regions of the FE head model show a good correlation to those of the physical model – HS-DIC study. There was no variation in local impact acceleration response greater than 15%. It is represented by 11% at the vertex, 4% at the occiput, 6% at the frontal and 13% at the parietal regions at the impact velocity of 1.72 m.s⁻¹ and by 12% (vertex), 3% (occiput), 5% frontal and 11% at the parietal region, at the impact velocity of 2.43 m.s⁻¹. As discussed previously, this is unsurprising, since the mass of the infant skull bones is small relative to the overall mass of the head [27]. The bones are, therefore, likely to come to rest more quickly than the more massive structure of the brain.

4.8.2 Sensitivity Analysis

4.8.2.1 Influence of the Impact location

Prange's PMHS study provided only limited information about effects of head orientation on head response during impact. A sensitivity analysis study was conducted applying the global approximation approach to match the orientation of the FE head model. The impact acceleration response of the FE head model showed no variation at different impact locations. As discussed above, whether the absence of any variation was a result of a lack of sensitivity provided by the global approximation or that no variation exists, required further analysis. A sensitivity analysis, simulating Prange's global approximation assessed the strengths and weaknesses of the approach. With respect to whether orientation had an effect on the impact acceleration response, the previous results using the global approximation sensitivity analysis suggest that it does not. The impact location, at the simulated experimental fall height, has a limited effect on the "global" impact response of the parietal and occipital bones (less than 15%) and a significant effect on the frontal bones, believed to be a result of the anatomical variation between the lower and upper region of the frontal bones.

Since the research highlights that the global approach is relatively insensitive, it is a possibility that changing the orientation of the head makes a difference to the impact response. A second sensitivity analysis was conducted, using the local and regional simulation approach, to investigate whether the head impact response shows any variation with orientation, or that the global validation is insensitive.

The influence of the impact location/rotation on the impact acceleration response, obtained by using the local – regional approach was investigated by impacting the FE head model in different orientations onto different impact regions, see Figure 2.20. During impact tests to the occipital bone, impacts were produced (1) close to the base of skull, (2) close to the vertex, (3) close to the left parietal bone and (4) close to the right parietal bone, compared to the baseline region (0) “centre” of the occipital bone. For the parietal bone, impacts were produced (1) close to the base of the skull, (2) close to the vertex, (3) close to occipital bone and (4) close to the frontal bones, compared to the (0) baseline impact region “centre” of the parietal bone. For the frontal bone, impacts were produced (1) to the upper region of the frontal bones, (close to the soft cranial bone and membranous fontanelle) compared to the baseline region (the lower region of the forehead) at an impact velocity of $2.43\text{m}\cdot\text{s}^{-1}$, corresponding to the drop height of 0.30m.

For an occipital bone impact test, the local-regional impact acceleration response from the FE head model, at different regions, was $200\pm 15\text{g}$ close to the base region, $142\pm 26\text{g}$ at the vertex region, $202\pm 18\text{g}$ at the right and $215\pm 23\text{g}$ at the left parietal regions, respectively. Thus, representing differences between impact responses of greater than 15% (16% close to the base region, 19% close to the vertex region, 25% close to the right parietal region, 25% close to the left parietal region), compared to the baseline impact acceleration response of $167\pm 20\text{g}$ at the centre of the occiput, see Figure 3.24a.

For a parietal bone impact test, the difference in impact acceleration response from different regions of the bone was $155\pm 15\text{g}$ close to the base region, $158\pm 14\text{g}$ at the vertex region, $161\pm 19\text{g}$ at the occipital region and $169\pm 13\text{g}$ at the frontal bone region. Again, representing differences (17% close to the base region, 19% close to the vertex region,

21% close to the occipital region and 26% close to the forehead region) greater than 15%, compared to the 130 ± 10 g impact acceleration response at the baseline impact region (centre of the parietal bone) from the same height, see Figure 3.24b.

For frontal bone (forehead) impact tests, the difference in impact acceleration response from the upper region of the forehead, close to the soft cranial bone and membranous fontanelle of 198 ± 13 g was 30% lower, compared to the impact acceleration response of 270 ± 6 g recorded at the baseline impact region (lower region of the forehead), for the same impact velocity, see Figure 3.24c.

For different impact regions, the simulation results show that there were significant variations in the impact acceleration responses between different impact locations, compared to the baseline impact location of each cranial bone. The parametric study results, using the local - regional approach, show that the impact acceleration response actually is sensitive to orientation and that the previous sensitivity analysis established that orientation is insensitive, as a result of the global approximation, providing further evidence of its unsuitability for the purpose of establishing infant head impact response.

4.8.2.2 Influence of the position of the occipital bone in relation to the parietal bones.

Thus, the global approach has been demonstrated to be unsuitable for the purpose of discriminating orientation sensitivity, evidenced by impact response variation at the force plate of both 'inline' occiput and 'out of line' occiput FE models of greater than 15 %. An 'inline' occipital - parietal bone configuration is stiffer, compared to the 'out of line', depressed occipital bone, and relative to the parietal bone configuration. When using the

global approximation, the 'inline' and 'out of line' FE model produced different accelerations. Whilst this observation was of interest, since the global approximation has been proved to be unreliable, a local - regional FE sensitivity analysis was conducted.

To investigate the influence on the impact response of the relative positioning of the occipital and parietal bones, a comparative study was performed using the impact acceleration response of a newborn that had a depressed, 'out of line' occipital bone, relative to the parietal bone configuration with an 'inline' occipital - parietal bone configuration. The response was calculated by the local - regional approach at impact velocities of 1.72 m.s^{-1} and 2.43 m.s^{-1} .

For the vertex and forehead bone impacts, all peak acceleration values for the 'inline' and 'out of line' configurations were in the region of $81 \pm 4\text{g}$ and $220 \pm 7\text{g}$, respectively, at an impact velocity of 1.72 m.s^{-1} and $102 \pm 2\text{g}$ and $270 \pm 6\text{g}$ at 2.43 m.s^{-1} , see Figure 3.25. Since the local - regional approach measured the impact response at selected nodes or points on the skull plate, for comparison, the same points and nodes were investigated for both FE models.

During an FE occipital impact, the peak acceleration response of the 'inline' occipital - parietal bone configuration was greater by 17% at 1.72 m.s^{-1} and 28% at 2.43 m.s^{-1} , compared to the depressed 'out of line' occipital - parietal bone configuration, see Figure 3.25. During parietal bone impacts, the peak acceleration response for the 'inline' configuration was 28 % greater at 1.72 m.s^{-1} and 31% at 2.43 m.s^{-1} , compared to the depressed configuration, see Figure 3.25.

The 'inline' configuration seems to be responsible for the different impact acceleration response between the occipital - parietal bone configuration and the 'out of line' depressed occipital - parietal bone configuration using the local - regional approach. Hence, there is a difference in the impact accelerations response at the global level using the force plate approach and at the local -regional level by measuring the acceleration of the bone itself. There is a greater than 15% change to the occipital - parietal bone configuration, which is further evidence and confirmation of the fact that the model response is different between the 'inline' and 'out of line' configurations.

4.8.3 Duration of Impact.

From the comparison of the impact time duration between the physical model and present FE model, see Figure 3.26, little variation exists between them, when provided with the same input parameters, represented by 3% at the vertex, 11% at the occiput, 13% at the frontal bones and 10% at the parietal regions at 1.72 m.s^{-1} and by 4% (vertex), 11% (occiput), 10% (frontal) and 8% (parietal) at 2.43 m.s^{-1} ; since both have the same material properties and exhibit the same stiffness.

4.8.4 Head deformation.

During impact, the majority of the strain was produced within the suture and fontanelle areas of the FE head model, as shown in Figures 3.27 and 3.28. Given that the infant head naturally deforms in these areas during birth, this response appears entirely logical [16, 17]. Strains in the suture and fontanelle areas at the impact velocity 1.72 m.s^{-1} and 2.43 m.s^{-1} are of the order of 0.3% and 3%, respectively. The maximum strain percentage of the FE model from the vertex, frontal and occipital impacts were compared to the physical models from the same impact regions at impact velocities of 1.72 m.s^{-1} and 2.43

m.s⁻¹, which show a good correlation with the physical model, see Figure 3.29. There was no significant difference, that is, greater than 15%, between the FE and physical models at both 1.72 m.s⁻¹ and 2.43 m.s⁻¹ impact velocities, as shown in Figure 3.29. The maximum percentage difference between the physical and FE model occipital impacts was 4% at 1.72 m.s⁻¹ and the smallest percentage of difference was 2% at 2.43 m.s⁻¹. Since both models possess the same mass and the same applied material properties, they demonstrate the same material stiffness during impact. During impact, the head was observed to deform, thereby decelerating, followed by a rapid acceleration as the elastic energy from the head deformation was converted to kinetic energy. An example of the head deformation from the physical model is provided graphically in Figure 3.10 and the FE model in Figures 3.27 and 3.28.

4.9 PMHS skull fracture reconstruction.

A fall is one of the commonest causes of head injuries in young children in the UK, however, despite their frequency and significance, it is still difficult for clinicians to discriminate between those fall mechanisms that cause skull fracture and those that do not cause skull fracture. From this study, a novel approach was used to design and manufacture a biofidelic physical head from infant CT datasets. This led to the development of a paediatric physical head model, which was validated against PMHS impact response data. Consequently, it allowed for the unique investigation of the local - regional head impact response from different regions /areas of the paediatric head. To overcome the many of the restrictions of the physical model, including the quality of being easily broken or damaged due to its fragility, resulting in financial and time cost to reproduce a replacement. By implication the physical model cannot be routinely used to

address a paediatric fall representing a “worst-case” scenario. Therefore, a biofidelic FE model was developed to represent the physical model. Global validation of this FE head model was attempted by simulating both the PMHS and physical model experimental tests where the correlation of impact response between each one of them and the FE model shows a good approximation. The FE head model worked successfully as a valid tool to address the regional and local response from different regions of the paediatric skull. Given all of these successes, the FE model was applied as a tool to predict paediatric skull fracture pattern from a low height fall. Thus, the model can be used to improve the biomechanical understanding of head injury for different clinical and forensic cases. To validate the FE model’s ability to predict skull fracture and its ability to show potential skull fracture propagation from impact onto hard surfaces, a computational study of the paediatric PMHS drops onto a hard surface was simulated replicating the experimental study of Weber [80, 81]. Weber dropped fifty PMHS paediatric heads onto the parietal – occipital region of the skull from a supine position from a height 0.82 m onto a range of different surfaces, stone tile, carpet, foam - backed, linoleum, a folded camel hair blank and a 2cm thick foam pad. Whilst the study reporting was limited by its subjective approach, providing a series of drawings of fractures, rather than quantitative response measurements, it does provide the largest experimental PMHS sample size (50 PMHS subjects) of paediatric head impacts of the few paediatric PMHS studies reported in the literature.

All five of PMHSs dropped onto stone tile were observed to sustain a skull fracture. Weber [80, 81], see Figure 1.9. Weber commented that initial propagation of the majority of fractures from impacts onto the stone tile and foam pad initiated at the parieto -

lamboidal suture contours, located on the posterior aspect of the skull, connecting the parietal bones with the occipital bone; and propagated towards the centre of the parietal bone. The FE model shows a high probability of skull fracture, a “hot zone” of high stresses in the right parietal bone. Furthermore, it was observed from the simulation, that a potential initial fracture propagation location was produced at the parieto - lamboidal suture boundary where some of Weber’s fractures occurred, see Figure 3.30. Unfortunately, Weber [80, 81] did not accurately report the fracture length or provide quantitative data to allow a more rigorous comparison.

For justification, the definition of the fracture from the simulation was determined by comparing the skull fracture pattern between Weber’s PMHS test and the FE model prediction. Figure 3.30 (b, c and d) show a high rise in von Mises stress, suggesting a greater risk of skull fracture shown by FE model and the von Mises stress distribution compared to a sketch of the fracture pattern drawing of the right parietal bone of the head from Weber’s study as in Figure 3.30a. It was observed during the computational simulation that when the head impacted the rigid plate, an initial force passed through the head and distributed between both of the parietal bones and the occipital bone. Due to the natural geometry of the paediatric skull, which has a bony curvature located on the upper region of the occipital bone, the impact to the parieto – occipital region strikes this curvature and produces rotation, either to the right or left side of the apex. Consequently, following the head impact, the FE head model displacement is a rotation towards the occipital and right parietal bones. Practically, most of the impact force delivered to the right parietal bone caused it to deform significantly and producing high level of von Mises stress, which in physiological terms could be associated with the breakdown in the cranial

plate fibres at the time of impact and rising the likelihood to fracture in infant. To investigate the phenomenon of shifting to the left or right side of the skull, another FE head model simulation was run, impacting the parieto – occipital region whilst introducing a minor perturbation in fall orientation. It was observed that when the impact region was shifted to the left side of the skull the impact deformation shifted to the occipital and left parietal bones. Given the natural skull curvature and observations from the simulations related to the parieto - occipital impacts it seems extraordinary that the impact force was delivered equally between the left and right parietal bones. Weber’s study diagrams [83, 84] appear to corroborate this point, and occasionally, fractures appeared in both right and left parietal bones, see Figure 1.8. Weber’s study [80, 81] reported that one of the twenty one fractures was bilateral, that is, in the right and left parietal bones. Also, two of the twenty one fractures were in the occipital bone, possibly a result of the uniform allocation of the impact force to both left and right parietal bones.

While Weber [80, 81] used paediatric PMHS to conduct skull fracture experiments, the study did not share detailed experimental information. There was not sufficient information about the experimental setup, the site of head impact and location of fracture initiation or the direction and length of the fracture propagation. Due to these limitations, the FE model impact locations were adapted in this study around the occipito - parietal region until a “hot zone”, a high rise in maximal von Mises stress, appeared to correspond with Weber’s [83, 84] drawings of the skull fracture location and orientation, see Figure 1.8. From the Li et al study [123] , the maximal von Mises stress was reported as a ‘good parameter’ for use in predicting paediatric skull fracture, thus it has been used in this

study to predict skull fracture and compare it with Weber's [83, 84] sketches of the skull fracture location and orientation.

A parametric infant head impact study was conducted, using the FE head model, to address its ability to predict the region of maximum principal stress response and the fracture probability of the parietal and occipital bones based on the study by Coats [71]. Coats commented that if the stress from the FE model exceeds a mean ultimate stress value, from their material property study [66], of 9.4 MPa for occipital and 27.0 MPa for parietal bones, a 50% probability of fracture will be assumed, see Figure 1.10. From Coates et al's study [124], the maximum principal stress was reported as an effective parameter to be used in predicting paediatric skull fracture, thus, it has been applied in this study to predict the fracture probability of the parietal and occipital bones. An FE simulation of parieto – occipital impacts with a stone tile was conducted at four different fall heights, 0.15m, 0.30m, 0.60m, and 0.82m. Maximum principle stresses in the right parietal bone at fall heights of 0.15m, 0.3m, 0.6m, and 0.82m were 22 MPa, 26 MPa, 49 MPa and 68 MPa, respectively, see Figure 3.31. The increases in height from 0.3m to 0.6m and 0.82m did not increase maximum principle stress by greater than 15%. The corresponding parietal bone fracture risks were 28.7%, 48.8%, 79.4% and 92.3%, respectively, using the constructed fracture risk from Coats study [71], see Figure 1.10. At this impact location there were also stresses in the occipital bone, for fall heights 0.15m, 0.3m, 0.6m and 0.82m of 2.0 MPa, 3.2 MPa, 4.5 MPa and 4.8 MPa, respectively. The corresponding occipital bone fracture risks, with reference to Figure 1.10, were 5.2%, 6.6%, 8.5% and 10.7%, respectively. This probability of skull fracture was achieved by

using the ultimate stress values for the parietal and occipital bone reported by Coats [71] for infants less 3-months-old.

From this study, the similarities between the fracture pattern and the maximum stress zone between the Weber cases [80, 81] and the FE simulation highlight the potential for a linear fracture in the parietal bone from the occipito - parietal region.

In a subsequent parametric study, maximum principle stress values from the Coates [71], Hughes [12] and Prange [82] studies were used to assess the FE model's performance. However, further research is required to confirm the potential fracture patterns prior to applying the FE model to predicting skull fracture patterns, based on the site of impact and regional distribution of the load, rather than one single point of impact. Furthermore mechanical characterisation is required during high rate impact tests to inform the FE model with material failure properties.

4.10 Implications and limitations of the coupled physical - computational model.

In recognition of both the potential and limitations of the physical model, a coupled computational infant head model was developed, which in turn was used to analyse the movement of the external and internal structures at the point of impact, since these become increasingly obscured during impacts viewed using the DIC approach. Production of this paediatric head model, using 3D printing and computational modelling worked exceptionally well and showed a good validation with PMHS impact response. Whilst the physical model study only investigated falls from heights up to 0.3m, which is not, if onto a flat surface, generally considered a risk of head injury, it was unrealistic to perform drop tests from greater heights. Heights greater than 0.15 m and 0.30 m, and up

to 0.82 m, were investigated by computational (FE) simulation. The computational model is unconstrained by physical, practical, limitations and is capable of investigating the effects of minor perturbations with respect to different fall heights, angles and surfaces. The FE model was used to predicate the risk of skull fracture by a parametric study investigating the effect of increasing fall height, angle and surface was not investigated.

This study has established that an impact perpendicular to a surface produces significant local and regional translational acceleration at different points on the skull which are up to ten times greater than the measured global acceleration response from a force plate, which provides a global approximation of the entire response of the head. In addition to the local translational acceleration, significant angular accelerations were observed at different regions of the head, deviating from the 'normal', 90 degrees. This highlights that neither form of acceleration (translational and angular) appear to occur in isolation and challenging the reported assumption that traumatic brain injuries can be characterised as either translational or angular in origin [42, 45]. It has become apparent, from the physical model perpendicular impact tests, using the HS-DIC system and from the computational (FE) simulations, that during head impacts with the rigid plate, that significant deformations occurred when the head mass was perpendicular to the point of impact, during reformation, the resultant force (elastic energy) accelerated the head back against the direction of impact. It was noticed that the irregular shape of the head, a result of the natural curvature, produced a non-uniform deformation, which appeared to produce a drift in the mass of the head, causing the resultant force to be offset from the impact point. Thus, producing a moment around the contact point and therefore, significant angular accelerations. A further consideration is that the centre of gravity of the head being at a

different location from the centre of gravity of the massive brain, may also contribute to angular accelerations.

Consequently, initial deformation and curvature of the physical and FE models produced angular accelerations during impact. This observation was also reported by Coats et al. [71], that due to the asymmetrical curvature of the head form, the impact in the parieto - occipital area triggered the head to rotate to the left, thus increasing the risk of fracture on the left side of the headform. It is further noteworthy, that whilst investigating the FE model's ability to predict skull fracture by simulating Weber's studies [80, 81], when impacting the model from 0.82 m onto the parieto - occipital region, the role of this natural curvature at the apex of the head in rotating the head to the right side became apparent. The majority of the force was observed to travel to the right parietal bone where stress was observed to concentrate and a risk of skull fracture was inferred.

A parametric study was conducted to investigate the effects of fall height on head impact response. The studies of Prange et al. [82], Weber [80, 81] and Hughes et al. [12], who reported that skull fractures were absent at heights <0.6m, were used to inform experimental fall heights. This parametric study applied a skull fracture pattern strategy, based on the maximum stress, to predict skull fracture risk from each fall height. A high risk of fracture was said to occur, if the maximum principle stress was greater than the ultimate stress of cranial bone, Coats and Margulies [66], at any time during the simulations. The risk of fracture of the FE head model was estimated based on the fracture probability graph of the parietal and occipital bones created by Coats study [71].

Computationally, the FE head model was impacted onto the parieto – occipital region from four different heights, 0.15 m, 0.3 m, 0.6 m and 0.82 m onto a stone tile and the impact evaluated by using the fracture pattern assessment method based on the maximum stress. A maximum principle stress of 22 MPa, 26 MPa, 49 MPa and 68MPa was produced in the right parietal bone corresponding to fall heights of 0.15 m, 0.3 m, 0.6 m, and 0.82 m, respectively. The maximum principle stress was not raised by greater than 15% during the 0.15 m, 0.3 m, 0.6 m and 0.82 m impacts, respectively. The corresponding parietal bone fracture risks were 28.7%, 48.8%, 79.4% and 92.3%, respectively, using the probability of parietal and occipital fracture graph from Coats study [71]. Stresses were also produced in the occipital bone during the 0.15 m, 0.3 m, 0.6 m and 0.82 m impacts of 2.0 MPa, 3.2 MPa, 4.5 MPa and 4.8 MPa, respectively, see Figure 3.31. The corresponding occipital bone fracture risks were 5.2%, 6.6%, 8.5% and 10.7%, respectively. This investigation gives promising results in terms of skull fracture prediction, even though no injury criteria are presented. The FE model of a newborn child has shown great promise for the study of real world head trauma and is anticipated to be a motivating tool to study child injury mechanisms. This new step in the development of a coupled physical and computational modelling approach provides valuable insight into the biomechanical engineering understanding of how a child's head responds during injurious loading and provides a significant contribution to providing the loading environment for the study of the internal structural complexities of the head, which will subsequently inform clinical and forensic management and injury prevention strategies. Furthermore, the model will be capable of providing a platform for the subsequent development of advanced paediatric models, including skull fracture propagation, the

investigation of the effects of the distribution of grey and white matter and fibre orientation of the brain, cerebral micro and macro vasculature, the cerebrospinal fluid, the foramen magnum, falx cerebri and tentorium cerebelli. Also, the computational domain will be capable of sustaining effective future development of complex internal structures, or techniques, such as reverse engineering, parametric analysis and parameter optimisation.

4.11 Study significance

Research in the area of paediatric head injury has very much concentrated on using PMHS or simple physical or computational models. Each approach has potential, however, each also has many limitations. This study proposed a combined, “coupled” approach, which applied the data derived from PMHS testing with biological materials testing, real world physical testing and validation of physical surrogates and the derivation of matched computational models. The present thesis describes the development, validation and testing/experimentation of the coupled methodology for application to the investigation of the cause and effect relationship between accidental and inflicted head injury scenarios and head injury. The study has produced a significant new approach to characterising and understanding paediatric head impact mechanics by using high resolution computer tomography (CT) scans from which a solid body infant head model has been developed. Applying the solid body model to the subsequent development of a physical model, available infant human tissue response polypropylene polymeric materials, whose responses were matched to published infant human tissue data, the model was printed using a Poly Jet 3D printer. The model replicated the relative stiffness’ of the fibre orientation of immature cranial bone and thus, produced a radially anisotropic

(orthotropic) response for each cranial bone with very fine radial grooves designed into the model, emanating from estimated centres of ossification and in addition, biofidelic fontanelles and sutures. The conducted mechanical study provides much needed data regarding the material properties of PJP at quasi-static strain rates (1 mm min^{-1}) that were used to produce the 3D printed physical model with mechanical/material responses close to human paediatric cranial bone, suture and fontanelles to subsequently test different impact scenarios. These materials constituting the physical skull model, simulated the White material, replicating frontal and parietal bones, the Grey, replicating occipital bone and the Black, replicating the sutures and fontanelles. The 3D printed physical head model was validated against infant PMHS head impact response data using the “gold standard” “global approximation” approach to establish the following key points:

- The physical paediatric head model and PMHS head were in favourable agreement when subjected to experimental impact conditions [82].
- The impact acceleration response of the physical head model, was significantly different for different drop heights but did not vary between impact locations, which is in good agreement with the conclusion of PMHS study [82].

This study, exposed the limitations associated with using a “rigid body approximation” for determining acceleration, for the purpose of investigating head impact response. Due to the flexible nature of the infant skull, a random speckle pattern was applied to the skull surface to enable the performance of a High-Speed Digital Image Correlation (HS-DIC) to measure the impact response of the polypropylene polymer physical surrogate. The experimental DIC approach provides a significant opportunity for producing regional and localised data, with which the “rigid body (“global”) approximation”, could be challenged.

By comparing the physical model impact response with the data from the PMHS impact tests, the following key points were demonstrated:

- The limited global approximation has significant shortcomings for the purpose of determining head response, due to the flexible nature of the infant skull.
- HS-DIC was shown to be highly effective in establishing acceleration data.
- Differential acceleration patterns were observed to be very sensitive to impact location, corresponding to epidemiological findings, that falls from similar heights onto different skull locations result in very varied clinical outcomes.
- Accelerations at certain areas of the skull structure were observed to be 'two to three times greater' than concomitant global acceleration values and significant variation was demonstrated across the surface of the skull.
- Accelerations can be very different at different points on the surface of the skull.
- Surprisingly, significant rotational velocities and accelerations were observed, seemingly as a result of deformational changes within the complex skull geometry.
- Significant differences were observed in the angular acceleration response of the physical model from the same impact views, at different impact heights. Thus, confirming that the infant head significantly deforms during impact, whilst concomitantly producing different angular accelerations in different structures of the head at different times during the impact.
- The angular acceleration data is extremely valuable for quantifying local and regional deformational accelerations of the head, for determining both the nature and risks associated with head impacts.

- The DIC software concomitantly allowed calculation of the angular accelerations at points across the head and comparison between regions, such that the greatest peak angular acceleration for each impact could be quantified.
- The suture and fontanelle regions demonstrated ten times more strain than the bone resulting in significant skull deformations. Given that the infant head naturally deforms in these areas during the quasi-static loading of child birth [16, 17], this response might be expected.
- Strains in the cranial bones have an order of magnitude of approximately 0.3%, for both 1.72 m.s⁻¹ and 2.43 m.s⁻¹ impacts. Strains in the suture and fontanelle areas, for 1.72 m.s⁻¹ and 2.43 m.s⁻¹ impacts were shown to be between 2.5 % and 3.3%, respectively. There is a significant variation in the strain magnitude of the sutures and fontanelles.
- Strain rates in sutures and fontanelles, for 1.72 m.s⁻¹ and 2.43 m.s⁻¹ impacts were between 1000% s⁻¹ and 2000% s⁻¹.
- The physical modelling approach allowed the optical observation and measurement of the response of each individual bone, suture and fontanelle, which is experimentally elegant.
- Different regional acceleration patterns were observed, from which comparisons could be made against epidemiological findings. It is proposed that cases of accident and abuse can be investigated by simulating impact scenarios from similar heights onto different skull locations producing very varied responses, which may, in part, explain the very varied clinical outcomes.

- A very significant advance is the elucidation of regional and localised impact response values, from which correlations, between loading and injury, can be made and computer models can be developed and subsequently validated, which was the physical model's intended primary purpose.

This methodology of combining high resolution scan data with 3D printing technology, response matched polymeric printed materials and PMHS materials and impact response data has been proved to produce a significant new step in characterising and understanding infant head impact injury mechanics. The physical surrogate demonstrates the considerable potential of producing 3D models, with complex geometries and tissue matched materials for head kinematic analyses. However, whilst the physical model provides an excellent opportunity to derive “real world” response data for linear and angular: displacement – time, velocity, acceleration, stress and strain validation of surface structures; it cannot currently, without development of additional technology (instrumentation), be translated to modelling, simulation and measurement of complex internal structures. The physical surrogate's elucidation of regional and localised impact response, however, provides a unique present and future opportunity to develop and subsequently parameterise computer models within which internal structures can be developed.

By recognition of both the potential and limitations of the physical model, a coupled computational infant head model was developed, which in turn was used to analyse the movement of the external and internal structures at the point of impact. This study presents a new geometrically accurate computational FE model of a newborn infant's head, developed from high resolution CT scan images, combined with the generation of

a valid and compatible mesh, giving relatively accurate results and a reduced computational time. Previously developed child head FE models have been used to investigate paediatric head trauma, but none of these have represented the visible fibre orientation appears in the cranial bone, therefore this new FE head model used recently published material property data, successfully implementing the orientation of fibre with different elastic moduli in the tangential and radial directions and recently published material property data, which improved the model's biofidelity.

Infant PMHS head impact data were used to validate the FE head model, in terms of impact acceleration. By computational simulation, the fall impact scenarios onto a hard surface, as reported in Prange's PMHS study, were replicated, using this new FE head model. Global validation of the FE model was achieved by comparing its simulated impact response against the response of the physical model, which was considered a "real world" reference, due to the geometrical and material response similarities between the physical and proposed FE models. The head impact response was calculated using the global approach and the following key points are reported:

- The global kinematic impact response of the FE head model shows a good agreement with the paediatric PMHS drop test data.
- From the sensitivity analysis, the location of the impact at the simulated experimental fall heights has a limited effect on the "global" impact response of the cranial bones. However, this sensitivity analysis was inconclusive, since it did not provide sufficient impact acceleration data, largely as a result of the global approximation proving inadequate and secondly, due to the fact that changing

orientation did not appear to change the impact response, that is, orientation made no difference. This was investigated later using the local and regional approach.

- From the sensitivity analysis, using the global approximation approach, there was a significant influence observed on the impact acceleration response, due to the relative positioning of the occipital bone and parietal bones.

Since this study was conducted using the global approach, adopted in Prange's study, which has been previously shown to be unreliable when orientation has been investigated, a further sensitivity analysis was conducted using the local and regional approach.

- There was no significant variation in the occipital and parietal global impact acceleration response between the FE comparison, study that had an 'out of line' occipital - parietal bone configuration, and the PMHS impact response. Possibly suggesting that Prange's PMHS specimen (3 day old child) had a depressed occipital - parietal bone configuration, as a result of a natural birth.
- From the global validation, the FE model showed a good correlation with the physical model impact acceleration response at different impact locations and impact velocities.
- The impact acceleration responses from both the FE and physical models were different at different fall heights, while the impact time duration was similar. It is evident that the greater impact velocity and kinetic energy, associated with the higher height drops, corresponds with a greater impact force. Accordingly, the peak acceleration of the head also increases with an increasing contact force.

Further, the validated computational model, used to simulate head kinematic responses in a localised area of the head, was applied to investigating different impact scenarios. The results were compared to the individual structural response of the physical model and the following key points were established:

- The local acceleration values from different regions of the FE head model show a good correlation to those of the physical model – HS-DIC study.
- From the sensitivity analysis, location of impact had a significant effect on the impact accelerations response experienced by the skull using the local - regional approach. In contrast, the global approach was insensitive to orientation, which established further the unsuitability of this approach.
- From the sensitivity analysis, the position of the occipital bone in relation to the parietal bones had a significant effect on infant skull response using the local - regional approach. The inline configuration seems to be responsible for the different impact acceleration response between the FE head model 'inline' occipital - parietal bone configuration and the second 'out of line' (depressed occipital - parietal bone configuration) using the local - regional approach. The variation in impact response was confirmed at the global level using the force plate approach and at the regional - local level by observing the acceleration of the bone itself. It is evident that the model response is different 'inline' and 'out of line'. Also, observing the effect of changing the impact velocity (fall distance) provides further evidence that the global validation is relatively insensitive.
- During impact, the majority of the strain was produced within the suture and fontanelle areas of the FE head model. There was no significant variation in the

strain percentage between the vertex, frontal and occipital impacts, compared to the physical model impacted at the same region and impact velocity (1.72 m.s^{-1} and 2.43 m.s^{-1}). As the two models have the same mass and applied material properties they demonstrate the same material stiffness during impact. During impact, the head was observed to deform, thereby decelerating, followed by a rapid acceleration as the elastic energy from the head deformation was converted to kinetic energy.

The FE model was subsequently applied to investigating the fracture occurrence by replicating the PMHS experiments conducted by Weber [80, 81]. A parametric study was conducted to investigate the effects of different fall heights, reported in the literature Prange et al. [82], Weber [80, 81] and Hughes et al. [12] on head impact response, to address the ability of the model to predict the region of maximum stress response and the fracture risk probability. The following key conclusions were made from this study:

- The FE model impact simulation onto the parietal-occipital region, at drop height of 0.82 m onto an impact surface - stone tile, replicated Weber's PMHS head impact experiment. A good qualitative match, was observed compared to a sketch of the fracture pattern drawn at the right parietal bone of the head from PMHS specimen. A "hot zone" was observed, where a high rise in von Mises stress was distributed, suggesting a greater risk of skull fracture.
- The biofidelic FE model showed a good correlation with the fracture pattern of the 3 month old PMHS child reported in the Weber study [80, 81] where the fracture pattern is linear and associated with the margins of a suture.

The parametric study provided maximum principle stress values for the right parietal and occipital bones at a range of fall heights and the corresponding parietal and occipital bones fracture risks were determined using the probability of parietal and occipital fracture graph from Coats study [71].

The investigation of skull fracture response and the subsequent parametric study provides promising results in terms of skull fracture risk prediction, even though no injury criteria are presented. The FE model of a newborn child has shown great potential for the study of real world head trauma and it is anticipated will be a motivating tool for the study child head injury mechanisms. This new step in the development of a coupled physical and computational modelling approach provides valuable insight into the biomechanical engineering understanding of how a child's head responds during injurious loading and provides a significant contribution to providing the loading environment for the study of the internal structural complexities of the head, which will subsequently inform clinical and forensic management and injury prevention strategies.

Further, this study developed only a biofidelic head form, representing the effective mass of the head, thus, the neck was absent. Evidence of unimodal and bimodal loading was reported in [124], showing that the effective mass of the head produces a significant primary acceleration time response followed by the contribution of the neck producing a secondary relatively long time period. To avoid the complex response from the head and neck coupling, only the head was considered in this study, to demonstrate the specific contribution of the head alone. It is an intention to conduct a subsequent analysis of the second impulse response of the neck in due course. This study provides an opportunity to assess head impact variables from the perspective of the head alone. It clearly

demonstrates that the principal force is produced by the head (the effective mass of the head), and quantifies the contribution of the head to the overall loading. Further research is anticipated that will add a neck and the body to make more valid real life comparisons for forensic case investigations. Furthermore, the model will be capable of providing a platform for the subsequent development of advanced paediatric models, including skull fracture propagation, the investigation of the effects of the distribution of grey and white matter and fibre orientation of the brain, cerebral micro and macro vasculature, the cerebrospinal fluid, the foramen magnum, falx cerebri and tentorium cerebelli. This study has acknowledge that TBI is a consequence of both skull and brain mechanics, as a result of both translational and rotational brain motions that produce focal and rotational loading of the brain tissue and associated blood vessels, which all contribute to TBI [42, 44]. However, the modelling framework presented in this study has been used to focus on addressing skull mechanics predominantly in order to assess the skull's contribution to TBI. Also, the computational domain will be capable of sustaining effective future development of complex internal structures, or techniques, such as reverse engineering, parametric analysis and parameter optimisation.

5. Conclusion and Future work

5.1 Conclusion

The objective of this study was to report the development of a modelling framework that can be used to investigate and improve the biomechanical understanding of paediatric head injuries during high impact conditions and the application of this framework to predicting the causal mechanism of a presented injury; helping to distinguish between accidental and non-accidental head injuries in paediatric populations. This framework, was developed by using high resolution computer tomography (CT) scans, to produce a coupled computational and physical infant head model. The physical model was manufactured from available infant human tissue response values, using polypropylene polymers materials whose responses were matched to published infant human tissue data, and printed using a Poly Jet 3D printer, replicated the relative stiffness' of the fibre orientation of immature cranial bone and thus, produced a radially anisotropic (orthotropic) response for each cranial bone with, in addition, biofidelic fontanelles and sutures. Consequently, a geometrically accurate computational FE model of a newborn infant's head was developed from the same CT scan images, combined with the generation of a valid and compatible mesh, giving relatively accurate results, versus reduced computational time. Successfully this new FE head model implemented the orientation of fibers with different elastic moduli in the tangential and radial directions, reported for the infant cranial bone using recently published material property data, which improved the biofidelity of this newborn FE head model. The constitutive properties of the physical model cranial bones, brain, sutures, fontanelles and scalp, all influence the total system response to mechanical loading. Thus, the FE model tissue response

properties must, therefore, be consistent with those of the corresponding areas of physical surrogate, to be appropriately validated against its response. This study subjected the physical model to “global” validation by simulated impacts for comparison with the PMHS study of Prange et al. [82]. Impacts were implemented onto different regions of the head (forehead, parietal, occipital and vertex), at impact velocities of 1.72 m.s⁻¹ and 2.43 m.s⁻¹ onto a ‘rigid surface’. During “global” validation the physical model was subjected to additional measurement by HS-DIC which generated regional and local measurement data. Using ultra high speed cameras and the digital image correlation, the conducted study has been able to monitor the velocity and hence, determine acceleration at different points on a 3D printed skull/suture model during impacts with a force plate. Interestingly, whilst the force plate data, when divided by mass, gives impact acceleration response and curves corresponding with PMHS response in the literature, which is currently supporting the opinion of biomechanics, the acceleration of individual bones, measured directly using DIC approach is very different. The inference of this is that whilst globally the head has an assigned acceleration tolerance (eg 85 g), clearly regions of the head which produce greater accelerations are more tolerant than the assigned global thresholds than is currently claimed.

The computational FE head model was subject to the same “global” PMHS validation. Also, “Global” validation of the FE head model was achieved by a series of impact simulations, conducted in accordance with the physical surrogate head impact experiments. Further, regional and local validation of the computational model was possible from the experimental data of the physical model, since the HS-DIC system provided the translational impact response, including the distribution of the strain

throughout the different structures of the head. From the translational acceleration response of the physical model, a series of computational FE simulations were conducted, replicating the different orientations of the head. A correlation was established between the regional and local impact response, to obtain the important features of the physical model head impact tests and the numerical analyses. So when looking at a regional or localised area of the physical model, being able to manipulate “on screen” the numerical simulation, to focus on regions of interest. The computational analysis was undertaken using Abaqus/Explicit (Simulia, Providence, RI, v.6.12) on the Cardiff University supercomputer cluster.

These experiments and simulations provide justification to the authors to challenge the use of injury thresholds in some cases, as these are based on overall average accelerations of the head, a “black box” approach. Given the wide range of accelerations in individual structures that the study measured, it seems wholly unreasonable to say that an average 60g from a parietal impact should be considered the same as an average 60g from an occipital impact, while the two events may have the same average acceleration, they will cause very different accelerations in the different structures of the head and could therefore be significantly more or less injurious. This appears to be born out in the epidemiological study, which suggests a variation in impact direction vulnerability.

This chapter summarises the conclusions of the physical model impact experiments and the computational impact simulations studies from the coupled physical–computational modelling framework.

- Using the ‘Global’ approximation to determine acceleration was inadequate. These experiments and simulations provide justification to the authors to challenge the use of injury thresholds in some cases, since they are based on overall average accelerations for the head, a “black box” approach. Given the wide range of accelerations measured in the individual structures, it seems wholly unreasonable to say that an average 60g from a parietal impact should be considered the same as an average 60g from an occipital impact, while the two events may have the same average acceleration, they will cause very different accelerations in the different structures of the head and could therefore be significantly more or less injurious. This appears to be born out in the epidemiological study, which suggests a variation in impact direction vulnerability.
- The local acceleration impact response at certain areas of the paediatric skull structure were observed to be two to three times greater than the related global acceleration impact response value.
- The local translational accelerations impact response can be very different at different points on the surface of the skull and it is sensitive to the skull impact location, in contrast to the global translational impact acceleration response.
- The position of the occipital bone in relation to the parietal bones has a significant effect on infant skull impact response.
- There is a different local impact angular acceleration response in different structures of the head at different times during the impact.
- There is a significant variation in the angular acceleration response of the physical model from the same impact views, at different impact heights. Thus, confirming

that the infant head significantly deforms during impact, whilst concomitantly producing different angular accelerations in different structures of the head at different times during the impact.

- The impact angular acceleration data is extremely valuable for quantifying local and regional deformational accelerations of the head for determining both the nature and risks associated with head impacts.
- During impact, the majority of the strain was produced within the suture and fontanelle areas. The suture and fontanelle regions demonstrated ten times more strain than the bone resulting in skull deformations. Given that the infant head naturally deforms in these areas during the quasi-static loading of child birth [16, 17], this response might be expected.
- The presence of a high rise in von Mises stress at the right parietal bone suggested a greater risk of skull fracture, predicted by the computational model compared to 3- month-old PMHS specimen. Further, the computational model provided promising results in terms of skull fracture prediction.
- Provision of regional and local validation of the computational FE model for the first time provided the opportunity to challenge, the ‘Global’, “rigid body approximation”, by measuring the acceleration and deformation at different regions of the head and comparing it with the response of the physical surrogate. Whilst also, overcoming the practical limitations of the physical surrogate and sustaining the effective future investigation of complex internal structures.

5.2 Future work

The coupled physical–computational modelling approach represents a “hook” on approximating how the paediatric head is behaving, how the skull plates move, relative to the sutures and fontanelles, which will facilitate the development of a formal localised environment for modelling the intracranial structures, including brain behaviour that can feedback the understanding of the brain injury cause and effect by the creation of a constitutive model of the brain, looking at the movement of brain in and out of plane, the brain response can be detected from the input, which is the response of the skull so this work a correlation between the physical model and computational model shows a good reasonable approximation that can be used to observe and address different areas of the skull and brain. The main challenge is finding appropriate material response data for the relevant tissues, such that printable materials can be matched for the purpose of mimicking tissue response. Further development, to improve model biofidelity, would require emphasis on material response investigation, in particular the dynamic, rather than quasi static response of the materials. In addition, at present, the brain model is a simple homogenous representation of a heterogeneous regionally anisotropic material, which in addition, does not currently represent intracranial pressure. Subsequent investigation into the effects of this could easily be achieved as a development, by carrying out sensitivity studies into a range of possible brain model materials and intracranial pressures. Furthermore, the FE approach can be used to analyse the movement of the internal structures as these cannot be viewed by the DIC approach. The computational model will facilitate further analyses, considering different heights, angles and impact surfaces. Further, this study developed only a biofidelic head form, thus, the

neck and body were absent. Consequently the effects of the body and neck on the kinematic variables would not have been measured. This uniquely provides an opportunity to assess which variables are influenced solely by the head and further research will measure the effect of the neck and body.

For future work, the surrogates will provide a very significant advance in the current understanding of infant head impact exposure (cause) and primary head injuries (effect); providing data from which injury cause and effect correlates can be established; the computational platform will be capable of sustaining effective future development of complex internal structures, or techniques, such as reverse engineering, parametric analysis and parameter optimisation; establishing coupled physical and computational platforms for further development of skull fracture and brain injury surrogates. Further, subsequent correlations will be derived, from accident data and head impact injury cause and effect relationships, such that secondary pathophysiological outcomes can be predicted and mitigated.

6. References

- [1] National Health Service (NHS). Major trauma centres. 2012. <http://www.nhs.uk/NHSEngland/AboutNHSservices/Emergencyandurgentcareservices/Documents/2012/map-of-major-trauma-centres-2012.pdf> (accessed 20 Feb 2015).
- [2] Trefan, L., Houston, R., Pearson, G., Edwards, R., Hyde, P., Maconochie, I., Parslow, R. and Kemp, A. (2016). Epidemiology of Children with Head Injury: a National Overview. *Archives of Disease in Childhood*, 101, pp.527– 532
- [3] Parslow, R.C., Morris, K.P. and Tasker, R.C. (2005). Epidemiology of Traumatic Brain Injury in Children Receiving Intensive Care in the UK. *Archives of Disease in Childhood*; 90(11), pp.1182-1187.
- [4] Anderson, T., Heitger, M. and Macleod, A.D. (2006) Concussion and Mild Head Injury. *Pract Neurol*, 6, pp. 342–57.
- [5] Hawley, C., Wilson, J., Hickson, C., Mills, S., Ekeocha, S. and Sakr, M. (2013) 'Epidemiology of Paediatric Minor Head Injury: Comparison of Injury Characteristics with Indices of Multiple Deprivation', *Injury*. Elsevier Ltd, 44(12), pp. 1855–1861. doi: 10.1016/j.injury.2013.07.021.
- [6] Warrington, S.A., Wright, C.M., Team, A.S. (2001). Accidents and Resulting Injuries in Premobile Infants: Data from the ALSPAC Study. *Archives of Disease in Childhood*, 85(2), pp.104-107.
- [7] Adelson, P. David, and Patrick, M. Kochanek. (1998). "Head Injury in Children." *Journal of Child Neurology*, 13.2, pp. 2-15.

- [8] Whitwell, H. (2010). "Intentional Head Injury in Infants and Young Children." *Pediatric Homicide Medical Investigation*. Ed. Karen Griest. Boca Raton: CRC Press Taylor & Francis Group, pp. 1-24.
- [9] Kemp, A., Jaspan, T., Griffiths, J., Stoodley, N., Mann, M. and Tempest, V. (2011). Neuroimaging: What Neuroradiological Features Distinguish Abusive From Non-Abusive Head Trauma? A Systematic Review. *Archives of disease in childhood*, 96(12), pp.1103-1112.
- [10] Duhaime, Ann-Christine.(2008). "Editorial Demographics of Abusive Head Trauma." *Journal of Neurosurg Pediatric*, 1, pp. 349-50.
- [11] Kesler, Henry, Mark, S., Dais, Shaffer, M., Rottmund, C., Cappos, K., and Thomas, N. (2008)."Demographics of Abusive Head Trauma in the Commonwealth of Pennsylvania." *Journal of Neurosurg Pediatric*, 1, pp. 351-56.
- [12] Hughes, J., Maguire, S., Jones,M,. Kemp, A.(2016). Biomechanical Characteristics of Head Injuries from Falls in Children Younger than 48 months. *Archives of disease in childhood*, 101(4), pp. 310–5.
- [13] Ruff, R., Osborn, A. (1985). Extraclavicular Soft Tissue in Cranial Computed Tomography: Normal Anatomy and Pathology. *Invest Radiol* , 20, PP. 374-3808
- [14] Young, R. (1959). Age Changes in Thickness of Scalp in White Males. *Hum Bio*, 31, pp. 74-79.
- [15] Scheuer, Louise, and Sue Black. (2004). "The Head and Neck." *The Juvenile Skeleton*, 1st ed. Academic Press, pp. 55-148.

- [16] McPherson, K., and Kriewall, J. (1980). "Fetal Head Molding: an Investigation Utilizing a Finite Element Model of the Fetal Parietal Bone." *Journal of Biomechanics*, 13.1, pp. 9-16.
- [17] Lapeer, R., J., and Prager, R., W. (2001). "Fetal Head Moulding: Finite Element Analysis of a Fetal Skull Subjected to Uterine Pressures During the First Stage of Labour." *Journal of Biomechanics*, 34, pp. 1125-33.
- [18] Crandall, J., Myers, B., Meaney, D., Zellers, S. (2013). *Pediatric Injury Biomechanics*. 1st ed. New York, NY: Springer
- [19] Sinnatamby, S. (2006). "Part Four: Anatomy of the Child." Last's Anatomy: Regional and Applied. Eds. Timothy Horne and Hannah Kenner. *Eleventh ed. Edinburgh: Churchill Livingstone*, pp. 34-37.
- [20] Jasionki, S., C., Reddy, B., D., Louw, K., K. and Chinsamy, A. (2010). "Mechanics of Cranium Sutures Using the Finite Element Method," *Journal of Biomechanics*, 34, pp. 3104-3111.
- [21] Glass, R.,B1., Fernbach, S.,K., Norton, K.,I., Choi, P.,S., and Naidich, T.,P. (2004). "The Infant Skull: a Vault of Information". *Radiographics*, 24(2), pp.507-22.
- [22] Cohen, M. (2000). "Sutural Biology." *Craniosynostosis: Diagnosis, Evaluation, and Management*. Eds. Jr. M. Michael Cohen and Ruth E. MacLean. 2nd ed. *New York: Oxford University Press*, pp. 11-22.
- [23] Opperman, A. (2000). "Cranial Sutures as Intramembranous Bone Growth Sites." *Developmental Dynamics* , 219.4, pp. 472-85.
- [24] Anne, M., R., and Ming, J. (1991). *Grant's Atlas of Anatomy. Ninth ed. Baltimore: William.s & Wilkins.*

- [25] Jaslow, C., R., and Biewener, A., A. (1995b). "Strain Patterns in the Horncores, Cranial Bones and Sutures of Goats (*Capra hircus*) During Impact Loading." *J Zool*, 235, pp. 193-210.
- [26] Herring, W. (2000). "Sutures and Craniosynostosis: A comparative, Functional, and Evolutionary Perspective." *Craniosynostosis: Diagnosis, Evaluation, and Management*. Eds. Jr. M. Michael Cohen and Ruth E. MacLean. 2nd ed. *New York: Oxford University Press*, pp. 3-10.
- [27] Burdi, A., D. Huelke, R. S., and Lowrey, G. (1969) "Infants and Children in the Adult World of Automobile Safety Design: Pediatric and Anatomical Considerations for Design of Child Restraints." *Journal of Biomechanics*, 2, pp. 267-80.
- [28] Prasad, P., J., W., Melvin, D., F., Huelke, A., King, I. and Nyquist, G., W. (1985). "Head." Review of Biomechanical Impact Response and Injury in the Automotive Environment: Task B Final Report. Eds. J. Melvin and K. Weber. *Ann Arbor: Transportation Research Institute*, pp. 1-43.
- [29] Öchsner and Ahmed, W. (2010). *Biomechanics of Hard Tissue*. *WILEY-VCH: Weinheim*.
- [30] Enlow, H. (2000a). "Normal Craniofacial Growth." *Craniosynostosis*. Eds. Jr. M. Michael Cohen and Ruth E. MacLean. 2nd ed. *New York: Oxford University Press*, pp. 35-47.
- [31] Kuffel, Charles W. (2004a). "Orthotic Modeling of the Developing Skull." *Journal of Prosthetics & Orthotics*, 16.4S, pp. 15-17.

- [32] Schaefer, Maureen, Black, S., and Scheue, L. (2009). "The Head and Neck." *Juvenile Osteology: A Laboratory and Field Manual*. Amsterdam: Elsevier, pp.1-66.
- [33] Adeloje, Adelola, Kattan, K., R., and Silverman, F., N. (1975). "Thickness of the Normal Skull in the American Blacks and Whites." *American Journal of Physical Anthropology*, 43.1, pp. 23-30.
- [34] McElhaney, James. (1976). "Biomechanical Aspects of Head Injury." *Mekhanika Polimerov*, 3, pp.465-77.
- [35] McElhaney, James H. (1970). "The Mechanical Properties of the Human Cranium." *Journal of Biomechanics*.
- [36] Yoganandan, Narayan, and Frank, A. (2004). "Biomechanics of temporo-parietal skull fracture." *Clinical Biomechanics*, 19, pp. 225-39.
- [37] Margulies, S., S., and Thibault, K., L. (2000). "Infant Skull and Suture Properties: Measurements and Implications for Mechanisms of Pediatric Brain Injury." *Journal of Biomechanical Engineering*, 122, pp. 364-371.
- [38] Loyd, A., M. (2011). *Studies of the Human Head from Neonate to Adult: An Inertial, Geometrical and Structural Analysis with Comparisons to the ATD Head*. PhD. Duke University
- [39] Ommaya, A., K., Goldsmith, W., and Thibault, L. (2002). Biomechanics and neuropathology of adult and paediatric head injury. *British Journal of Neurosurgery*, 16(3), pp.220–242.
- [40] Goldsmith, W. (1960). *Impact: The Physical Theory and Behaviour of Colliding Solids*. London: Edward Arnold Ltd.; Mineola, NY: Dover Publications; 2001.

-
- [41] Abe, H., Hayashi, K., Sato, M. (1996). Data Book on Mechanical Properties of Living Cells, Tissues and Organs. *New York: Springer.*
- [42] Goldsmith, W.,(1973). In, Fung, YC, Perrone, N, Anliker, M. (eds). Biomechanics of head injury: biomechanics, its foundation and objectives. *Englewood Cliffs: Prentice-Hall*, pp.585–634.
- [43] Gurdjian, E.,S. (1975). Impact Head Injury. *Springfield: C.C.Thomas.*
- [44] Ommaya, A.,K., Grubb, R.,L., Naumann, R.,A. (1971). Coup and Contre-Coup Injury: Observations on the Mechanics of Visible Brain Injuries in the Rhesus Monkey. *J Neurosurg*, 35, pp. 503–16.
- [45] Ommaya, A.,K., Hirsch, A.,E. (1971). Tolerances for cerebral concussion from head impact and whiplash in primates. *J Biomech*, 4, pp. 13–21.
- [46] Caffey, J. (1974). The Whiplash Shaken Infant Syndrome: Manual Shaking by the Extremities With Whiplash Induced Intracranial and Intraocular Bleedings, Linked with Residual Permanent Brain Damage and Mental Retardation. *Pediatrics*, 54, pp. 396–403.
- [47] Hadley, M.,N., Sonntag, V.,K., Rekate, H.,L., Murphy, A. (1989). The Infant Whiplash-Shake Injury Syndrome: a Clinical and Pathological Study. *Neurosurgery*, 24, pp. 536–40.
- [48] Ommaya, A.,K., Faas, F., Yarnell, P. (1968). Whiplash Injury and Brain Damage: an Experimental Study. *JAMA*, 204, pp.285–9.
- [49] Gennarelli, T., A., Thibault, L., E., and Adam.s, J., H. (1982). Diffuse Axonal Injury and Traumatic Coma in the Primate. *Ann Neurol.*, 12, pp. 264–274

- [50] Collants, M. (1990). Evaluation of the Importance of the Using Head Injury Criteria (HIC) to Estimate the Likelihood of Head Impact Injury as a Result of a Fall onto Playground Surface Materials. *US Consumer Product Safety Commission*.
- [51] Lissner, H., Lebow, M., Evans, F. (1960). Experimental Studies on the Relation between Acceleration and Intracranial Pressure Changes in Man. *Surgery, gynecology & obstetrics*, 111, pp. 329-338.
- [52] Cory, C., Jones, M., James, D., Leadbeatter, S., Nokes, L. (2001). The Potential and Limitations of Utilising Head Impact Injury Models to Assess the Likelihood of Significant Head Injury in Infants after a Fall. *Forensic Science International*, 123(2-3), pp. 89-106.
- [53] Versace, J. (1970). A Review of the Severity Index. In *Proceedings of the Stapp Car Crash Conference*, pp.771-796.
- [54] Bandak, F., A. (1996). Biomechanics of Impact Traumatic Brain Injury. *NATO Advanced Studies Institute: Crashworthiness of Transportation System.s*, 1.
- [55] Gadd, C., W. (1962). Criteria for Injury Potential. *Impact Acceleration Stress*. 977, pp.141.
- [56] Mellander, H. (1986). HIC- the head injury criterion- Practical Significance for the Automotive Industry. *Acta Neurochirurgica*, 36, pp.198-220.
- [57] Prasad, P., Mertz, H., J. (1985). The Position of the United States Delegation to the ISO Working Group on the Use of HIC in the Automotive Environment. *SAE transactions*, 94, pp.106-116.
- [58] Mertz, H., J., Prasad, P., and Nusholtz, G. (1996). Head injury risk assessment for forehead impacts. *Soc. Automotive Eng.*, pp. 1–23.

- [59] Eppinger, R., Sun, E., Bandak, F., Haffner, M., Khaewpong, N., Maltese, M. (1999). Development of Improved Injury Criteria for the Assessment of Advanced Automotive Restraint Systems—II. *National Highway Traffic Safety Administration*.
- [60] Melvin, J. (1995). Injury Assessment Reference Values for the CRABI 6-month Infant Dummy in a Rear-Facing Infant Restraint with Airbag Deployment. *SAE*, pp. 950872.
- [61] Goldsmith, W. (1981). Current Controversies in the Stipulation of Head Injury Criteria. *J. Biomech*, 14, pp. 883-884
- [62] McElhaney, J., H., Fogle, J., L., Melvin, J., W., Haynes, R., R., Roberts, V., L., and Alem, N., M. (1970). Mechanical Properties of Cranial Bone. *J. Biomech*. 3, pp. 495–511.
- [63] Wood, J., L. (1971). Dynamic Response of Human Cranial Bone. *Journal of Biomechanics*, 4, pp. 1-12.
- [64] McPherson, G., K., Kriewall, T., J. (1980). The Elastic Modulus of Fetal Cranial Bone: a First Step towards an Understanding of the Biomechanics of Fetal Head Molding. *Journal of Biomechanics*, 13(1), pp. 9-16.
- [65] Kriewall, T., J. (1982). Structural, Mechanical, and Material Properties of Fetal Cranial Bone. *Am J Obstet Gynecol*, 143, pp. 707–714
- [66] Coats, B., Margulies, S. (2006). Material Properties of Human Infant Skull and Suture at High Rates. *Journal of neurotrauma*, 23(8), pp. 1222-1232.
- [67] Wang, J., Zou, D., Li, Z., Huang, P., Li, D., Shao, Y., Wang, H. and Chen, Y. (2014). Mechanical Properties of Cranial Bones and Sutures in 1–2-Year-Old Infants. *Medical Science Monitor Basic Research* , pp. 1808-1813.

- [68] Raposio, E., Nordström, R., E. (1998). Biomechanical Properties of Scalp Flaps and their Correlations to Reconstructive and Aesthetic Surgery Procedures. *Skin Research and Technology*, 4(2), pp. 94-98.
- [69] Margulies, S., Coats, B. (2013). Experimental Injury Biomechanics of the Pediatric Head and Brain. *Pediatric Injury Biomechanics: Springer*, pp. 157-189
- [70] Klinich, K., Hulbert, G., Schneider, L. (2002) Estimating Infant Head Injury Criteria and Impact Response using Crash Reconstruction and Finite Element Modeling. *Stapp car crash journal*, 46, pp.165.
- [71] Coats, B., Ji, S., Margulies, S. (2007) Parametric Study of Head Impact in the Infant. *Stapp Car Crash Journal*, 51, pp.1-15.
- [72] Galford, J.,E., McElhaney, J.,H.(1970). A Viscoelastic Study of Scalp, Brain, and Dura. *Journal of Biomechanics*, 3(2), pp. 211-221.
- [73] Thibault, K., L., Margulies, S., S. (1998). Age-Dependent Material Properties of the Porcine Cerebrum: Effect on Pediatric Inertial Head Injury Criteria. *Journal of Biomechanics*, 31(12), pp.1119-1126.
- [74] Prange, M., Margulies, S. (2002). Regional, Directional, and Age-dependent Properties of the Brain Undergoing Large Deformation. *Journal of Biomechanical Engineering*, 124, pp.244.
- [75] De Santis Klinich, K., D., Hulbert, G., M. (2002). Estimating Infant Head Injury Criteria and Impact Response using Crash Reconstruction and Finite Element Modeling. *Stapp Car Crash J*, 46, pp. 165–194.

- [76] Roth, S., Raul, J-S., Ludes, B., Willinger, R. (2007). Finite Element Analysis of Impact and Shaking Inflicted to a Child. *International journal of legal medicine*, 121(3), pp. 223-228.
- [77] Roth, S., Raul, JS. , Willinger, R. (2010). Finite Element Modelling of Pediatric Head Impact: Global Validation against Experimental Data. *Computer Methods and Programs in Biomedicine*, 99(1), pp. 25-33.
- [78] Chatelin, S., Vappou, J., Roth, S., Raul, J. S., and Willinger, R. (2012). Toward Child versus Adult Brain Mechanical Properties. *Journal of the mechanical behaviour of biomedical materials*, 6, pp. 166-173.
- [79] Margulies, S. S. and Coats, B.(2006). Material Properties of Porcine Parietal Cortex. *Journal of Biomechanics*, 39, pp. 2521–2525.
- [80] Webber, W. (1984). Experimental Study of Skull Fractures in Infants. *Z Rechtsmed*, pp.87-94.
- [81] Weber, W. (1985). Biomechanical Fragility of the Infant Skull. *Z. Rechtmed*, pp. 87-101.
- [82] Prange, M., Luck, J., Dibb, A., Van Ee, C., Nightingale, R., Myers, B. (2004) Mechanical Properties and Anthropometry of the Human Infant Head. *Stapp Car Crash Journal*, 48, pp. 279.
- [83] Irwin, A., Mertz H. (1997) Biomechanical Basis for the CRABI and Hybrid III Child Dummies. *SAE Technical Paper 973317*.
- [84] Prange, M., Coats, B., Duhaime, A., Margulies, S. (2003) Anthropomorphic Simulations of falls, Shakes, and Inflicted Impacts in Infants. *Journal of Neurosurgery: Pediatrics*, 99(1).

- [85] Coats, B., Margulies, S. (2008). Potential for Head Injuries in Infants from Low-Height Falls. *Journal of Neurosurgery: Pediatrics*, 2(5), pp. 321-330.
- [86] Nahum, A., Smith, R., Ward, C. (1977). Intracranial Pressure Dynamics during Head Impact. *Proceedings of the 21st STAPP Car Crash Conference*, pp.339–366.
- [87] Hardy, W., Foster, C., Mason, M., Yang, K., AKing, A., Tashman, S. (2001). Investigation of Head Injury Mechanism.s using Neutral Density Technology and High-Speed Biplanar X-ray. *Stapp Car Crash Journal*, 45, pp. 337–368.
- [88] Yoganandan, N., Pintar, F., Sances, A., Walsh, P., Ewing, C., Snyder, T., Snyder, R. (1994). Biomechanics of Skull Fracture, *in: Proceedings of the Head Injury Symposium, Washington, DC*, pp. 227–236.
- [89] Roth, S., Raul, J., Willinger, R. (2008). Biofidelic Child Head FE Model to Simulate Real World Trauma. *Computer Methods and Program.s in Biomedicine*, 90(3), pp. 262-274.
- [90] Roth, S., Vappou, J., Raul, J., Willinger, R. (2009). Child Head Injury Criteria Investigation through Numerical Simulation of Real World Trauma. *Computer Methods and Program.s in Biomedicine*, 93(1), pp. 32-45.
- [91] Li, Z., Luo, X., Zhang, J. (2013). Development/Global Validation of a 6-Month-Old Pediatric Head Finite Element Model and Application in Investigation of Drop-Induced Infant Head Injury. *Computer Methods and Program.s in Biomedicine*, 112(3), pp. 309-319.

- [92] Li, X., Sandler, H., Kleiven, S. (2017). The Importance of Nonlinear Tissue Modelling in Finite Element Simulations of Infant Head Impacts. *Biomech. Model. Mechanobiol*, 16 (3), pp. 823–840.
- [93] Hughes, J. (2014). *Biomechanics of Skull Fracture and Intracranial Injury in Young Children as a Consequence of a Low Height Fall*. PhD. Cardiff University.
- [94] Juke, A., Baird, D., Weinberg, D., McConnaughey, D., Wilcox, A. (2013). Length of Human Pregnancy and Contributors to its Natural Variation. *Human Reproduction*, 28 (10), pp. 2848-55.
- [95] Tyler, G., Hicks, P., E. (2016). Civil Engineering Formula. Chapter 2. *McGrawHill Companies*. 2sted.[ebook]. Available at: <https://civil24.files.wordpress.com/> [Accessed 31 Apr. 2018].
- [96] Stratasys. (2016b). Objet500 and Objet350 Connex3. [Online]. Available at: <http://www.stratasys.com/3d-printers/production-series/connex3-system.s> [Accessed: 29 March 2016].
- [97] Stratasys. (2016c). PolyJet Technology - How PolyJet 3D Printing Works [Online]. Available at: <http://www.stratasys.com/3d-printers/technologies/polyjet-technology> [Accessed: 29 March 2016].
- [98] British Standards Institution. (2012). BS EN ISO 527-1:2012. Plastics — Determination of Tensile Properties — Part 1: General Principles. *London: BSI*.
- [99] British Standards Institution. (2012). BS EN ISO 527-2:2012. Plastics — Determination of tensile. *London: BSI*.
- [100] British Standards Institution. (2011). BS ISO 37:2011. Rubber, Vulcanized or Thermoplastic. Determination of Tensile Stress-Strain Properties. *London: BSI*.

- [101] McKeen, L., W. (2013). The Effect of UV Light and Weather on Plastics and Elastomers. 3rd ed. *London: Elsevier*.
- [102] Cheng, J., Howard, I., Rennison, M. (2010). Study of an Infant Brain Subjected to Periodic Motion via a Custom Experimental Apparatus Design and Finite Element Modelling. *J. Biomech*, 43 (15), pp. 2887–2896.
- [103] Jones, M., D., Oates, B., Theobald, P., S. (2016). Quantifying the Biotribological Properties of Forehead Skin to Enhance Head Impact Simulations. *Biosurf. Biotribol*, 2(2), pp.75-80.
- [104] Hild, F., and Roux, S. (2006). Digital Image Correlation: from Displacement Measurement to Identification of Elastic Properties – a Review. *Strain*, 42(2), pp.69-80.
- [105] Pullin, R. (2010). Validation of Acoustic Emission (AE) Crack Detection in Aerospace Grade Steel Using Digital Image Correlation. *Applied Mechanics and Materials*, 24-25, pp.221-26.
- [106] Featherstone, C., A. (2010). The Dynamic Buckling of Stiffened Panels – A study using High Speed. *Applied Mechanics and Materials*, 24-25, pp.331-36.
- [107] Bruck, H., McNeill, R., Sutton, M., A. and Peters, W.H. (1989). Digital Image Correlation using Newton-Raphson Method of Partial Differential Correlation. *Experimental Mechanics*, 29(3), pp.261-67.
- [108] Lu, H. and Cary, P., D. (2000). Deformation Measurements by Digital Image Correlation: Implementation of a Second-Order Displacement Gradient. *Experimental Mechanics*, 40(4), pp.393-400.

- [109] Pan, B., Qian, K., Xie, H. and Asundi, A. (2009). Two-Dimensional Digital Image Correlation for In-plane Displacement and Strain Measurement: a Review. *Measurement Science and Technology*, 20(6).
- [110] Luo, P.,F., Chao, Y.,J., Sutton, M.,A., and Peters, W.,H.(1993). Accurate Measurement of Three-Dimensional Deformations in Deformable and Rigid Bodies using Computer Vision. *Experimental Mechanics*, 33(2), pp.123-32.
- [111] Sutton, A.,M., Orteu, J.-J., and Schreier, H.,W. (2009). Image Correlation for Shape, Motion and Deformation Measurements. *Basic Concepts, Theory and Applicaitons*. Columbia: Springer.
- [112] Srinivasan, V. (2005). High Resolution Characterization Of Materials Used In Package Through Digital Image Correlation. In *Proceedings of IPACK2005*. San Francisco.
- [113] Osbourne, N. (2006). High Speed Video Becomes Mainstream. *Reinforced Plastics*, 50(6), pp.48-49.
- [114] Holzreiter, S., Kastner, J., and Wagner, P. (1993). Motion Measurement with High-Speed Video. *Journal of Biomedical Engineering*, 15(2), pp.140-42.
- [115] List, G. (2005). Wear Behaviour of Cemented Carbide Tools in Dry Machining of Aluminium Alloy. *Wear*, 259(7-12), pp.1177-89.
- [116] Kimpara, H., Nakahira, Y., Iwamoto, M., Miki, K. (2006) Investigation of Anteroposterior Head–Neck Responses During Severe Frontal Impacts Using a Brain–Spinal Cord Complex FE Model. *Stapp Car Crash J*, 50, pp.509–544.

- [117] De Lange, R., Van Rooij, L., Mooi, H., Wismans, JS. (2005). Objective Biofidelity Rating of a Numerical Human Occupant Model in Frontal to Lateral Impact. *Stapp Car Crash J*, 49, pp. 457–479.
- [118] ABAQUS (2010) ABAQUS Documentation, Dassault Systèmes. Providence, RI, USA.
- [119] Kleiven, S., Hardy, W., N. (1999). Correlation of an FE Model of the Human Head with Local Brain Motion-Consequences for Injury Prediction. *SAE CONFERENCE PROCEEDINGS (2002)*, pp. 123-144.
- [120] Miller, R., Margulies, S., Leoni, M., Nonaka, M., Chen, X., Smith, D., Meaney, D. (1998). Finite Element Modeling Approaches of Predicting Injury In An Experimental Model Of Severe Diffuse Axonal Injury. Report No.: 0768002931.
- [121] Stalnaker, R., L., Melvin, J., W., Nusholtz, G., S., Alem, N., M., Benson, J. (1977). Head impact response, Biomechanics of Impact Injury and Injury Tolerances of the Head- Neck Complex. *PT*, 43, pp. 425–439.
- [122] Li, Z., Liu, W. Luo, X., Zhang, J., Hu, J. (2015). Prediction of Skull Fracture Risk for Children 0–9 months old through Validated Parametric Finite Element Model and Cadaver Test Reconstruction. *International Journal of Legal Medicine*, 129, pp.1055–1066.
- [123] Hajiaghamemar, M., Lan, I., Christian, C., Coats, B., Margulies, S. (2018). Infant Skull Fracture Risk for Low Height Falls. *International Journal of Legal Medicine*. DOI: 10.1007/s00414-018-1918-1.
- [124] G.S. Nusholtz, D. E. Huelke, P. Lux. N. M. Alem and F. Montalvo. (1983). Cervical Spine Injury Mechanisms. *SAE paper*, 831616.